ON CHIP MICRO POWER SELF GENERATOR

FOR SMART PAVEMENT MATERIAL APPLICATION

By

HASSAN REZAEI HOMAMI

A dissertation submitted to the
Graduate Faculty of Engineering
in partial fulfillment of the requirement
for the degree of Doctor of Philosophy, The City University of New York

2013

This manuscript has been read and accepted for the
Graduate Faculty of Engineering in satisfaction of the
dissertation requirement for the degree of Doctor of Philosophy.

David Crouse, Ph. D
Director of the Center for Advanced Technology in
Photonics Applications
Associate Professor of Electrical Engineering

Date | Chair of Examining Committee

Ardie D. Walser, Ph.D.
Acting Associate Dean of Graduate Studies & Research,
Professor of Electrical Engineering

Date | Executive Officer

Dr. Fred Moshary, Deputy Chairman and Professor of Elec. Engineering, CCNY

Dr. Ali Maher, Director of Center for Advanced Infrastructure for Transportation
and Professor of Civil Engineering, Rutgers University

Dr. Andrew Foden, Senior Supervisor Parsons Brinckerhoff

Dr. Ahmad Sadegh, VP Infrastructure, Schneider Electric
Supervisory Committee

THE CITY UNIVERSITY OF NEW YORK

Abstract

ON CHIP MICRO POWER SELF GENERATOR

FOR SMART PAVEMENT MATERIAL APPLICATION

by

Hassan Rezaei Homami

Advisor: Professor David Crouse

Transportation agencies are spending considerable resources monitoring the status of roadways in many ways. Roadway monitoring is quite often done with low-tech and costly methods and only recently have more sophisticated approaches been implemented. Smart Pavement Material (SPM) is a stand-alone micro node device that can be embedded in the pavement and will operate with a long range life time and will be a highway sensor station. This SPM node will be equipped with its own on chip micro power generator unit and a short range broadband wireless unit. SPM node will operate without external power and wired communication services. SPM deployment will be a large distribution of the nodes along the highway with distances of 3'- 5' apart.

Two main operation duties of a SPM node are (a) sensing/processing that collects the information of the pavement and traffic and (b) interconnection that builds an embedded wireless network providing a communication service between the nodes. Primary applications of SPM will be pavement maintenance and an advanced traffic control system. Under SPM feasibility studies, the system components had been investigated and it was specified that an on chip power generator is the main component of SPM. It was determined that SPM performance and capabilities depend on node self-generating power. The study recognized that the main energy

resource is vehicle mobility energy, which transfers to pavement. This research includes modeling and design of an SPM on chip micro power self generator. The major milestones of the research are: system conceptual planning, simulation and modeling, energy conversion assessment and the microgenerator design. The project results include:

- Traffic mobility simulation model estimated the maximum SPM microgenerator charging/activation rate. In freeway roadway, this maximum is 9.2% of total daily traffic. This value at local collector road estimate is 51%. The mode specified the optimum location for the SPM node that can achieve a maximum charging.
- Pavement response models and macro/ micro simulation models for study of the pavement response were developed. An emulated circuit to simulate the strain and stress of the pavement was presented.
- Roadway pavement energy harvesting alternative analysis and multiple methods were described and analyzed. The results include multiple microstructures, which were proposed for the SPM microgenerator. The results show an electrostatic harvesting approach with multi plate cantilever structure can satisfy the requirement of the SPM node. This microgenerator will have a maximum power of 345 μW with initial 9 Vdc and use a dielectric material permittivity of 2800.
- SPM micro power self generator design (layout, material and control circuits) was completed. The proposed fabrication processes including proposed lithography are included in the design. The design was prepared for a prototype SPM microgenerator element.

.

Preface, Foreword, and /or Acknowledgments

I would like to extend my sincere appreciation to the faculty and staff in The Center for Advanced Technology, particularly Dr. David Crouse for his mentoring and his support throughout the completion of this study because without his constant guidance and encouragement, this project would not have been completed. I would also like to extend my gratitude toward my supervisory committee members, Dr. Fred Moshary, Dr. Ali Maher, Dr. Andrew Foden, and Dr. Ahmad Sadegh for providing guidance, supportive and critical review, and constructive suggestions during the course of this work.

Thanks are also due to George Moglia for his review and technical assistance at different phases of the project. Thanks are due to numerous colleagues, the CAT Laboratory group and Parsons Brinckerhoff members without whose help this project would not have been completed. I also thank Ms. Pamela Smith for her editorial review.

Last but not least, I would like to thank my family and friends who gave support and encouragement throughout the years during this time. There were times when the obstacles seemed insurmountable, but family and friends, near or far, always stood by me, literally or figuratively. I would like to express my love to my family, my wife, Nadereh, my son, Nima, and my sweet daughter, Sonya, who have always been there for me with love and support. I owe them everything.

This thesis is dedicated to the memory of my father, Mohammad R. Homami.

Contents

List of Tables

List of Figures

INTRODUCTION - ON CHIP MICRO POWER GENERATOR

Research and development of the electronic technologies have rapidly enhanced application of the electronic products in the transportation industry. By deploying nano-technologies and passing the boundaries of micro scale in the semiconductor devices, new applications and equipment have been developed in advanced transportation systems. The manufacturing process of the semiconductor industry uses a minimum feature size of 22/20 nm and will support a minimum feature of 14 nm by 2014[1]. These fabrication processes provide chips with higher element density and lower power consumption density. As a result, chip design applications support more integrated circuits such as System On Chip (SOC) and Network On Chip (NOC), which are widely being considered in integrated circuit design. One market for the SOC is the Stand-Alone embedded system, which has a growing demand in industries such as transportation[2]. These embedded systems will require low power components and energy harvesting element design. The SPM node is an example of these embedded systems with additional packaging requirements to be contactless and to have a 3D package. In this study, the feasibility and concept design of a micro power generator element for a highway pavement were investigated and designed. This research is primarily part of the Smart Pavement Material (SPM) project. The SPM project is designing an intelligent sensor embedded system for pavement monitoring and management applications[3].

[1] International Technology Roadmap for Semiconductors (ITRS).
[2] Highway infrastructure monitoring systems
[3] Key word: Intelligent Materials, Sensor Network, SOC, Stand-Alone Systems on Package (SOP) and Intelligent Transportation System (ITS).

The SPM component modules are data collection-sensors, a processing/ microcontroller and micro power supply. The alternatives for the SPM power supply module are either a package micro battery or an on chip energy harvesting module. Micro battery is an SPM power alternative with a short life expectancy because the SPM node packaging limits the capacity of the battery. SPM node size is restricted by: (a) pavement type (asphalt and concrete); (b) pavement materials (aggregate, binder, cement,); (c) pavement structure (fixed, rigid layers); and (d) cost (fabrication, assembly and installation). Based on the feasibility study [1], the SPM node perimeter value is limited to 17 mm with a typical value of 15 mm. This study performed analysis for the available energy source and capability of the micro harvesting methods. The results indicated feasibility of the SPM energy harvesting solution.

This study is focusing on the energy analysis and modeling, and the microgenerator design requirements. These requirements are included on chip/on package power storage and control circuits.

This research includes (a) a description of the project and work breakdown of the research, (b) research work in the micro energy harvesting methodologies for highway pavement, (c) microgenerator integration in the SPM node, and (d) design of the microgenerator structure and fabrication process and proposed materials. This dissertation is submitted to the City University of New York for the Degree of Ph. D. This dissertation research was performed and completed by Hassan R. Homami under the supervision of Professor David Crouse.

DISERTATION CHAPTER REVIEW

The target plan for this research is the microgenerator energy harvesting needed for pavement application. The research plan includes the study of traffic mobility, pavement structure,

microstructure, electronic control and fabrication design of the SPM generator. Fig. 1- 2 represents the research plan flow chart. The main flow process of the research plan includes:

- Vehicle mobility traffic loading study- Energy Source
- Pavement material and response study- Energy Transfer
- Micro scale energy harvesting study-Energy Conversion
- Micro generator analysis
- Micro generator design and proposal

The research plan conducted its first investigation on the energy resource on a roadway pavement. This energy source is the traffic movement on the roadway and the vehicle dynamic loading effect on the pavement. During the research, a simulation method for generating the vehicle distribution, focusing on the loading effect on the pavement, was designed and developed. This stage of the research is called the M-modeling process, which is described in detail in Chapter 2. The main output of the M model is the vehicle dynamic touching point (tire touch) on the roadway surface. This touching point coordinate is used for dynamic estimation of the vehicle loading and the SPM optimum placement for maximum energy availability. The M-modeling process included the simulation algorithms and case studies of this vehicle mobility model also were conducted. As part of the study, the M-models were implemented and results for several roadways in different highway classes were presented. The implementation was done in a Matlab environment. The input parameters for the M-models were designed in a way that data collection and field observation would be minimized. The main information for the M-models are roadway geometry, Annual Average Daily Traffic (AADT) and vehicle classification information (average loads, length, and number of axles). In addition, to more fine-tune the model, a sample data collection, such as car follow method, point speed measurement, and

vehicle offset detection, was considered. M-models provide additional results for the roadway energy distribution plan, which can be used for a future study with pavement and traffic management applications.

Pavement material and response studies include research on the different pavement types used for the roadway and the structure and materials used in different pavement types. This study was necessary to define the vertical placement of the SPM node on the pavement structure and calculate the minimum energy available for the micro generator. The pavement management application required information on the lower layer of the pavement structure, therefore placing the SPM in a lower layer was desirable; however, the availability of the energy on the lower layer was limited when placing the SPM. In addition, this study included a search of the pavement response models for estimating the energy values at a proposed SPM embedded location. The study included the development of micro and macro models. Pavement response modeling can be a complex simulation analysis based on the application of the model. In our research, a solution for SPM deployment was proposed based on an emulation network analysis. This model is used as a pavement unit element, which is adapted from the Kelvin-Voigt/Maxwell material model. The distribution of the pavement unit will provide the complete pavement model in three dimensions. The emulated function for a pavement unit from a micro simulation was studied by using a Comsol simulation model. The micro modeling of the pavement unit depends on the pavement material properties and geometry and distribution pattern of the aggregate materials. The P modeling study is presented in Chapter 3.

After estimating the power source at the pavement and optimizing the SPM placement, the energy harvesting system and the micro structure alternatives were studied in Chapter 4. The applicable energy, harvesting methods including electrostatic, electromagnetic and piezoelectric

approaches, were reviewed and investigated. In addition, different micro structures of a generator were studied. The study showed that electrostatic generators with multi layers in cantilever structures can be capable of generating the minimum power of 50 μw as specified for the SPM. The proposed structure has ten layers of the electrostatic chargers for a total area of 9600 x 9600 $(\mu m)^{2.}$

Chapter 5 includes the design details of the proposed generator. During that design research, the fabrication proposals and the controller circuit with the on chip power storages were studied. The fabrication process research also includes the assembly and packaging plans. The main target for this implementation plan is prototyping the design while mass production design will be considered in future works.

Finally, in Chapter 6, the conclusion of the research results include the main consideration for the micro generator design. Electrostatic micro generator with 10 layers of structure will be able to generate more than 50 μw for a highway class (freeway/expressway). This generator can provide this power with maximum value depending on the roadway class. In local roadway, with low traffic movement, the daily generating time will be less than 6 hours for this generator. Therefore, the SPM node for such local roadways should be considered as a limited functional node, which means the node will be operational at rush hours with a minimum activity (application support) at non rush hours. In future work, power management, dynamic sleeping mode operation, and operation prioritization (in response to the dynamic power) will be proposed. SPM packaging and fabrication alternatives also will be considered in future work for cost effectiveness and improvement of efficiency.

CHAPTER ONE – ON CHIP MICRO POWER GENERATOR CHAPTER OVER VIEW

The research overview and the feasibility resulting conclusions are presented in this chapter. The project overall research work appears in a project implementation plan (PIP) or research work breakdown. The PIP specified the project milestone and the work flow process. PIP includes the requirements of the work, delivery expectations, and staging and time line of the study. The proposed PIP has the following milestones:

1.1 PROJECT DESCRIPTION

Modern stand-alone and portable operational micro-systems like wireless sensor and biomedical implants continue to integrate more functions into smaller devices, which result in low energy levels and short operational lives. To solve the energy resource issue for this operation, system designers consider micro power battery and harvesting energy from the environment as their main options. Even with power efficient designs, low duty-cycle operations, smart power-aware network architectures, and batteries with improved energy density, the stored energy in micro-scale systems is simply not sufficient to sustain extended lifetimes. [2]

In reality, the working environment is primarily surrounded with all kinds of energy resources that can readily be used. As an example, in a roadway pavement monitoring system, forces from moving vehicles, or changing of temperatures on the pavement layers, are sources that more or less can be considered. Other resources such as solar or acoustical noise or different kinds of vibrations are alternative energy resources for different applications.

In this project, we are researching energy self-generation methods and analyzing the feasibility of existing approaches for deployment in a Smart Pavement Material application. The project is looking for a feasible solution that is also a reliable, constructed design, cost effective, and applicable to power usage in the pavement environment. SPM is a proposed Stand-Alone SOC,

equipped with sensor modules, an RF communication module and a data processing module. The power consumption of this chip has been determined based on details from the pavement environment conditions and the application functions.

In this study, analytical methods for the estimation and assessment of the power consumption of SMP chips were developed and form the basis for the main criteria for self-powered generators. The pavement environment study was conducted to provide an analytical picture of power resources. The study followed with conceptual planning and design, which was concluded with a prototype development. Based on this description, the project goal is the "Design of a micro device/ micro system with self-powered generator for pavement application" and project objectives are:

- Power Generation Capacity (50 μW or more)
- Micro Scale final production size limit (less than 17 mm)
- Cost effective production plan (for mass production)
- CMOS or CMOS compatible technologies that minimize design, verification, fabrication, and manufacturing of SPM
- Allowance for micro dynamic power management capability

These preliminary goals and objectives determine the targets for the project; they may be adjusted or modified according to the availability of design tools such as laboratory facilities or physical simulation test beds. However, it will be pursued using multiple facility resources and will not be completely dependent on one facility resource. Based on the preliminary description, the key components of the project will be:

- SPM power load assessment
- Energy harvesting approach investigation

- Conceptual planning
- Design assessment and simulation plans
- Prototype Case Design process

Of the above components, power generation capability assessment, self-power conceptual design and the prototype fabrication plan are three key factors in this study. The project's main expected results are to develop a method to estimate the micro power consumption of SPM components for a pavement sensor network and the development of an innovative design plan for energy harvesting use.

1.2 PROJECT MILESTONE

1.2.1 INVESTIGATIVE MILESTONES

Milestone (01) - Investigative Approach: The microelectronic energy harvesting topics had been researched and found applicable in different applications such as human body harvesting [3]. The investigation includes subsidiary topics such as thin film PZT elements, vibration based micro energy sources, electrostatic micro generator, while thermal power sources had also been found. Main sources of the information data base were IEEE Digital Library (Circuit, VLSI, Low Power VLSI annual conference proceedings).

Milestone (02) - Technology Survey: Paper and publication summaries were reviewed followed by main related references in full paper review. The selected research projects were contacted to update the information and their recent works. After these steps, a revision of the project work was prepared.

Milestone (03) - Similar Project Recognition: MIT Multi Media Lab, University of California Berkley, University of Purdue, University of California San Jose, University of Carnegie Melon, and Arizona State Universities are some of the active centers related to the project.

Milestone (04) - SPM Applications and Specifications: The SPM will be programmable for different applications (as a research target). Each application will require the SPM system specification which requires to be investigated in high level SPM power needs.

Milestone (05) - Technical Practiced Approaches: Power generation in range of 50 microwatt, size less than 17 mm x 17mm area, and compatible CMOS technologies is approached. Implementation approach also depends on the roadway pavement environment and mechanical energy conversion potential. Therefore, the pavement material/structure conditions were evaluated on this milestone. As a result of multiple design methods and different pavement conditions, three invested approaches based on the vibration harvesting methods were considered. However, a combination of these methods is also considered as the favored candidate in the design approach.

Milestone (06) - Research Tools: As part of the investigation milestone, the design tools and materials had been practiced. The SPM is a multi-functions system that includes electronics, mechanics, materials and civil/transportation related subjects. Therefore, different mathematical and simulation tools were used for the planning and design process. Advanced Multi Physics (Comsol), Mathematical modeling (MATLAB), Mechanical (Comsol MEMS), Energy conversion and Circuit design (SPICE/ VERILOG) were used.

1.2.2 PRELIMINARY & CONCEPTUAL PLANNING – DESIGN MILESTONES

Milestone (07) - SPM Deployment Issues: The SPM design, fabrication and deployment key issues had been exercised. These issues limited or directed the entire implementation process. The SPM planning process included investigation and verification of the design limits such as minimum size of the chip, CMOS compatibility, and packaging and SPM integrations.

Milestone (08) - SPM Constructability: What are the fabrication criteria including the format of the design delivery, resolutions and minimum design features, material limitations and fabrication processing time frame? These criteria will be determined after reviewing the existing facilities in CUNY or other outsources party facilities. Different outsource facilities such as University of Cornel Material Lab, MOSIS will be reviewed and considered for future prototyping work.

Milestone (09) - Alternatives Assessments: Multiple conceptual designs alternatives were considered on the assessment process. These designs are based on different approaches, such as, electrostatic, electromagnetic, and piezoelectric harvesting solutions. However, a combination of several methods was considered for physical testing and possible field assessment. Secondary micro power generators for specific applications will not be included in the conceptual plan. This item shall be considered as a future work for the SPM specific application deployment.

Milestone (10) – Conceptual Planning: The conceptual plan includes the SPM micro power generator system and architecture, generator components, the circuit modules, harvesting elements, physical limitations, concepts of operation, fabrication needs, technologies, and the system plan or SPM high level integral package layout plan. The system layout shows the proposed micro power generator modules on the SPM package. The conceptual planning also includes the estimation of the generating power. The estimate was developed based on the mathematical analysis of energy resources (vehicle traffic), conversion efficiency, and generator circuit power consumption.

Milestone (11) – Conceptual Planning: This milestone will specify the level of details needed for the conceptual planning process. The work includes simulation algorithms development, lab work and fabrication or manufacturing investigative efforts. These results are the kind of

customary details that need to be studied to assess the technical merit of the proposed chip in the satisfactory assessment of the proposed microgenerator. The main details should also be useable for the design work. In other words, the results should be easily used in prototype design proposal (fabrication details). The list of the conceptual plan deliveries includes:

- Energy Harvesting System Level Generator module(s), Storages, Controller
- Device Level, Piezo Electric element(s)
- Macro Simulation level, A MATLAB Programming Micro Simulation level, SPICE Simulation
- Engineering cost

1.2.3 PROTOTYPE MILESTONE (FUTURE WORK)

Milestone (12) – SPM Micro Power Generator Prototype Plan: Prototype development will be future work for this project. The prototype device shall be described by: device size, individual device or an integrated device, packaging formats, number of chips, cost and expenses, reviewing process, and the ordering process.

i. **SPM Micro Power Generator Structure/Mechanical Design:** Based on the proposed micro generator proposed vibrator structure, the fabrication design process has been proposed and introduced in this milestone.

ii. **SPM Micro Power Generator Material Design:** The results of the analysis of the material properties and materials selections for the structure and circuits are presented. The proposed materials are based on the fabrication process for the prototype device.

iii. **SPM Micro Power Generator Circuit Design:** Based on the equipment or the proposed tools, what will be the design materials? This was determined after Stage Two, namely after

preliminary design. The design materials, based on the equipment or the proposed tools, were determined after Stage Two, namely after preliminary design.

iv. **SPM Micro Power Generator Design:** The design will be based on the planning needs that will be specified in the preliminary design stage and the selected technology and facilities. One option is using the MOSIS University program which may not be a sub-micron technology.

1.2.4 FIELD TEST MILESTONES (FUTURE WORK)

Milestone (13) – SPM Micro Power Generator Operation Analysis: The proposed micro generator operation analysis will include power generation rate estimates, power storage capacity, worse case operation conditions, the system efficiency factor, and a production cost analysis.

Milestone (14) – SPM Micro Power Generator Goal/Objectives Expectations: During this milestone, the project's goal and objectives have been to compare the expected results of the proposed micro generator with the following:

- Chip efficiency (mechanical and electronic efficiencies)
- Power output voltages and clearance lack of noise of the generating voltage
- Device size
- Fabrication process (integration with other SPM modules)
- Production cost

Milestone (16) –Conclusion and Expansion Works: In this final milestone, future work expected in prototype implementation and design optimization is discussed and described.

1.3 PROJECT BACKGROUND

Stand-alone and modern portable operational micro-systems like wireless sensors and biomedical implants continue to integrate more functions into smaller devices, which result in lower energy levels and shorter operational lives. As a result of these energy usage issues, micro power battery and energy harvesting from the environment are important concerns for system designers. Even with power efficient designs, low duty-cycle operations, smart power-aware network architectures, and batteries with improved energy density, the stored energy in micro-scale systems is simply not sufficient to sustain extended lifetimes. The working environment is often surrounded with energy resources that can be used or harvested. As an example, in roadway pavement monitoring systems, the force or vibration arising from vehicle movement and temperature gradients are energy sources that should be considered.

Other resources, such as solar or acoustic noise or different kinds of vibrations are alternative energy resources for different applications. In this study, we are researching the energy self-generation methods and analyzing the feasibility of the existing approaches for deployment in a Smart Pavement Material application. The project is looking for a feasible solution that will provide a reliable, easily constructed, cost effective design applicable with minimum power usage.

The SPM Micro Power generator project was started in 2008 with the targeting of planning and design of the micro power generator for the roadway pavement environment and traffic movement energy source.

1.4 RESEARCH PLAN

Research and development of electronic technologies are rapidly enhancing the application of advanced electronics in many industries. With the development of nano-technologies and surpassing the boundary of micro scale in semiconductor devices, it is feasible to design an intelligent embedded system on a miniature size package.

The SPM is an embedded system in miniature scale (less than 17 mm). The SPM sensing module will include a variety of sensor type such as: temperature, dry/wet detection, frozen point, dew point, frost point, chemical detector, snow and ice detection, traffic volume, vehicle speed and acceleration, axle loads, axle spacing, vehicle class, and vehicle length. The SPM second module is a microcontroller or processor. This microcontroller shall be of ultra-low power and can be an existing Intellectual Property (IP) circuit, which is customized for the SPM application. SPM third major module is a wireless network interface module. This module provides communication between the SPM nodes and roadside interface units. The wireless unit also is a low power RF system for a short range. This range will be the typical distance between two adjoining SPM nodes. The forth module of the SPM are microgenerator modules, which are investigated and designed in this research. The analyses and design of the SPM sensor, microcontroller and wireless modules are considered as future works. Fig. 1- 1 shows a proposed deployment of SPM on a highway pavement. This deployment includes a large mesh network of the SPM nodes placed along the highway. The SPM will have different applications including:

- New pavement management tools with advanced micro electric sensors,
- Integrating of new monitoring technology for improving the life cycle of roadway pavement, and
- New communication infrastructure for vehicle to vehicle service.

The freedom of SPM distribution along the roadway makes its a smart infrastructure that can provide service to different ITS systems, such as: Pavement Management Systems, Advanced Traffic Management Systems, Freeway Management Systems, Transit Operation Systems, In Vehicle Communication Systems, and Travelers Safety Systems.

1.4.1 SPM RESEARCH PROCESS CHART

The SPM system components and their interconnections are presented in Fig. 1- 2. These system block diagrams were based on (a) the SPM applications (expecting market), (b) the operational concerns, (c) design criteria, and (d) fabrication requirements. Some elements such as actuators or chemical sensors are most likely the focus for advanced generations of the SPM. The verity and functionality of the SPM application are mainly limited by the micro power generator characteristics, such as maximum power, voltage level, efficiency, mechanical limits, and size. This research work is only focused on the micro power generation modules of the SPM.

1.4.2 SPM POWER LOAD ESTIMATES

SPM is a stand-alone, pin/contactless system on package. The power supply will be from the on package battery, which will be recharged by the energy harvesting module. The SPM can be placed in exotic and in large distributed locations along a roadway under the pavement layer.

The power supply in most embedded systems is a conventional battery; however, the finite life span of the battery is a problem for a system with a long expectation of life. In addition, battery voltage drop along the time may not be acceptable for some of the circuits. Because most SPM nodes are being developed in order to be placed in remote locations such as road structures or bridges or in middle of high traffic lanes, battery replacement cannot be an acceptable solution in the matter of maintenance and it can become a very expensive task. Therefore, a rechargeable battery with a micro power generator is the solution for the SPM power source. The

microgenerator is an energy harvesting element that converts pavement energy (stress energy as result of vehicle load) to electricity

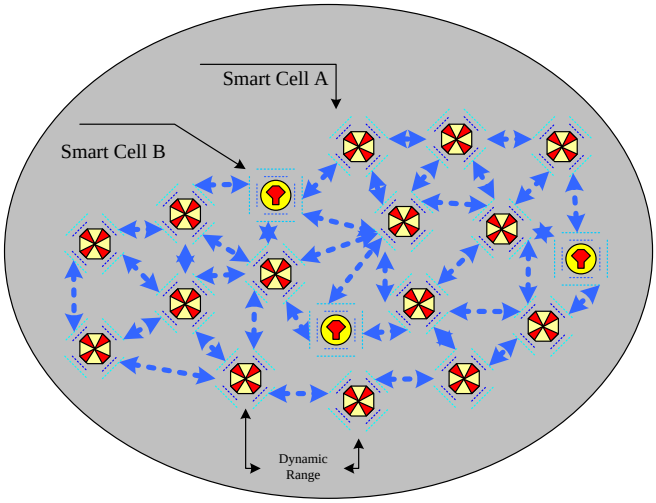

A- SPM Cells random distribution with the communication primary range of 1 to 1.5m

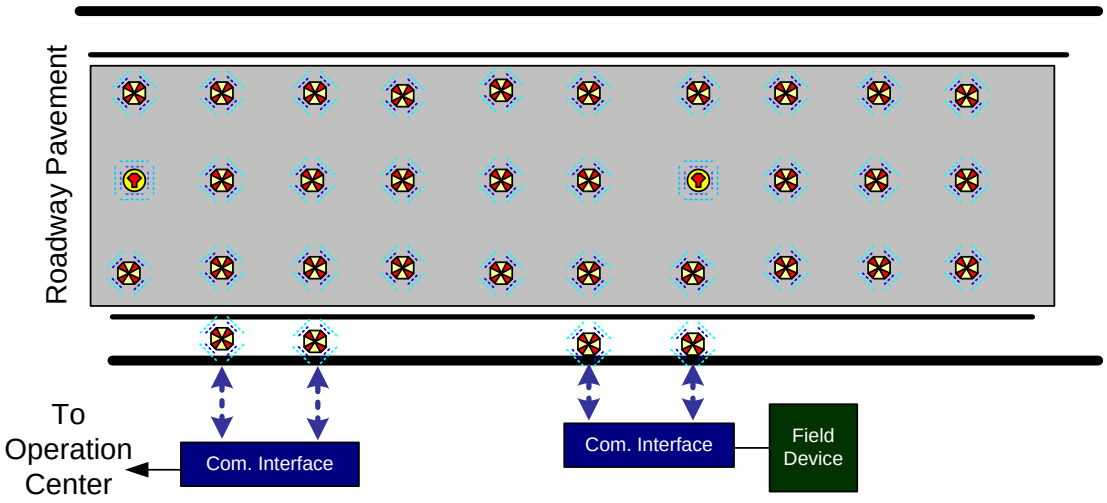

B- SPM uniform distribution with flexible point of access to the SPM network

Fig. 1- 1 SPM deployment - SPM random and uniform distribution with the communication range of 1 to 1.5 m

.

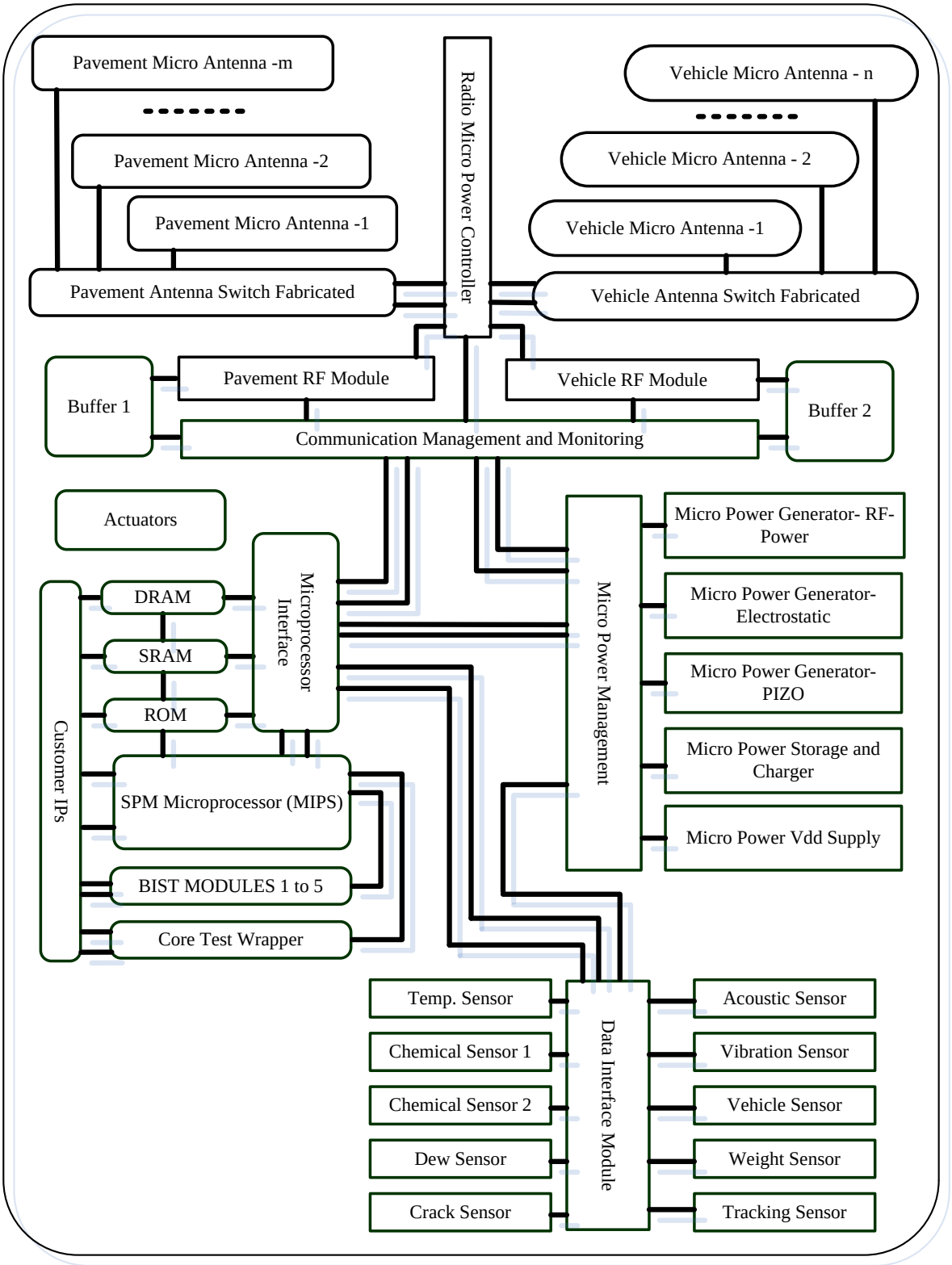

Fig. 1- 2 SPM On-Chip Components

The microgenerator power is limited to the available energy and efficiency of the conversion method. Therefore, power consumption of the SPM components shall be minimized to maintain more application services. For assessment of the capacity of the microgenerator, the SPM power consumption was estimated. A list of considered assumptions on this estimate is as follows:

I. All elements will be managed with a sleeping mode function to reduce the power consumption.

II. Sensors will be managed with variable sampling periods that will be optimized by power consumption and application needs. The sensors will not be a significant consumer of power in the SPM. For example, the PTAT low power temperature sensor proposed by Warneke [4] will use100 nA at the V_{dd} of 1.3 volts. The sensor power is estimated at less than 5 µW.

III. In the VLSI circuit, the effect of the heat transfer and parasitic transistor will be reduced as smaller semiconductor devices with minimum feature size will be used. Using the minimum feature size device increases the chip density and noise effect. The high density circuit will be expected for the SPM core module, which has a microcontroller, some detector circuits and wireless circuits. These effects shall be considered on the core module design. The SPM chip will be expected to be deployed in a 180 nm or 90 nm CMOS technology with less than 3 million transistors on a module.

IV. Low power VLSI circuit design approaches such as dual V_{dd}, variable V_t , adiabatic circuit, reversible logic, clock gating (to avoid changing the state of functional blocks that aren't required for a given operation), and dynamic voltage scaling method. Sub-threshold leakage current is becoming a much more important factor in power consumption of a dense chip than before and needs to be considered on core module design.

V. The leakage current will result in power consumption even when no switching is taking place (static power consumption), and with modern chips, this current is frequently more than 50% of power used by the IC. This loss can be reduced by raising the threshold voltage and lowering the supply voltage. Both of these changes slow the circuit down significantly. Consequently, some modern low-power circuits use dual supply voltages to provide speed on critical parts of the circuit and lower power on non-critical paths. Some circuits even use different transistors (with different threshold voltages) in different parts of the circuit in an attempt to further reduce power consumption without significant performance loss.

VI. In the SPM circuit design, a sleep transistor approach can reduce the power consumption. The transistor would disable entire blocks when not in use. By shutting down a leaky functional block until it is used, leakage current can be reduced significantly. For some embedded systems, that only function for short periods at a time, this can dramatically reduce power consumption. Since systems that are dormant for long periods of time and "wake up" to perform a periodic activity are often in isolated locations, monitoring some sort of activity, they are generally battery or solar powered and power consumption is a key design factor.

VII. The SPM microcontroller/processor is a special low power processor. This processor for fixed operational functions for the SPM can be limited to an ultra-low power micro controller which manages all SPM activities. Thus, we are facing a range of power consumption for this microprocessor that may not completely be applicable for SPM power resources. By considering an ultra-low power microcontroller and optimizing the size of the memory, a good design may be achieved. Therefore, one of the tasks for the

design is to complete the processor requirement details and have a custom design plan for the IP core for the SPM microprocessor.

An example of a microcontroller in wireless sensor devices is Smart Dust mote where the processing unit of a smart dust mote prototype is a 4 MHz Atmel AVR8535 microcontroller with 8 KB instruction flash memory, and 512 bytes RAM and 512 bytes EEPROM [5]. The processing unit of another sensor node prototype, namely the lAMPS wireless sensor node, has a 59–206 MHz SA-1110 micro-processor [6]. A multithreaded l-OS operating system is run on lAMPS wireless sensor nodes. The recent research and available IP design are exceeding these low power controllers. In addition, customizing the SPM controller will reduce the overall power consumption. Therefore, our expectation for power consumption of the SPM controller is lower than these values. The target power for the SPM processor will be 0.5 to 1 PJ/Instruction. This target shall be a special consideration for the SPM microcontroller design. In the study, the average power consumption for a microcontroller is estimated to be 30 µW.

VIII. Antenna modules will be active antennas that provide an optimum impedance matching. As shown in the Fig. 1- 2, multiple antennas will be furnished in the SPM chip to provide a point to point wireless link between SPMs. To minimize the transmission power, the antenna switcher and radio power control will be required.

- SPM system on chip will contain two different RF modules for communication between SPM chips (pavement wireless communication) and communication to the outside (e.g., vehicle wireless communication). The SPM wireless communication is a multi-hop network, which will be formed by radio frequency that eventually should be available worldwide for global interpretability. Thus, industrial, scientific, and

medical (ISM) bands, which have license-free communication frequency is the favorite frequency choice. ISM bans are acceptable in most countries. It will be a secondary goal for the RF radio module to be able to be operated at different frequencies; however it will be a design challenge to design this programmable RF module with minimum power consumption. Some wireless sensor devices are using either 433 MHz ISM band (in Europe) or 915 MHz ISM band (in North America). The SPM node/cell distances are short in the range of 100 to 150 cm. Therefore, a low power transmission will be expected, but we need to take into account the effect of the pavement materials (asphalt or concrete) in our power transmission pictures.

- Several models for power consumption of wireless sensor transmission have been developed which are dependent on the nature of transmitter and transceiver data [6]. The power consumption for the RF pavement transmission is capped at 30 μW. This cap limits the maximum transmission rate of the wireless link, however, it is the design target to have an average power consumption of transmission at less than 100 pw/bit. The RF vehicle power requirement will be different from RF pavement. The RF vehicle module will utilize a passive method, RF-Power via RF-Power Micro Generator. Therefore, the power requirement of that module will not be considered critical.

IX. Communication protocols, besides the hardware and circuit design of the SPM communication system, power efficient communication architecture, and protocol layers should be developed. Shown in Fig. 1- 3 is a communication protocol stack and a wireless sensor network protocol stack. This protocol stack combines power and routing

awareness, integrates data with networking protocols, communicates power efficiently through the wireless medium, and promotes cooperative efforts of sensor nodes [7].

X. Summarizing, the power estimates concludes a minimum of 50 µW, under limiting conditions such as lower data transmission, less programmability, shorter communication range, and the ultra-low power circuit design. However, this minimum power requirement will be useful for specifying the power resources and the methodologies to achieve it which are described in the next section.

Table1. 1 Sample of Wireless Sensor Microcontroller [8]

Mote Type	WeC	Rene	Rene2	Dot	Mica	Mica2Dot	Mica 2	Telos
Year	1998	1999	2000	2000	2001	2002	2002	2004
Type	AT90LS8535		ATmega163		ATmega128			TI MSP43
Program Memory (KB)	8		16		128			48
RAM (KB)	0.5		1		4			10
Active Power (mW)	15		15		8		33	3
Sleep Power (µW)	45		45		75		75	15
Wakeup Time (µS)	1000		36		180		180	6

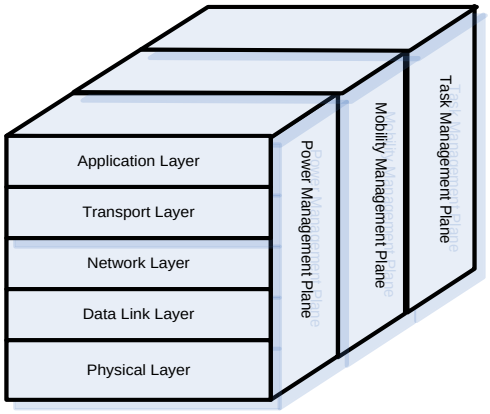

Fig. 1- 3 A communication protocol stack [9]

CHAPTER TWO – VEHICLE MOBILITY MODELING (SPM M MODELS)

2.0 VMM OVER VIEW

Vehicle dynamics is a complicated analytical and experimental technology that is used to study to understand the traffic dynamic loading on a roadway pavement surface. In the SPM research analysis, it is not necessary to deal with full vehicle mobility modeling concepts, but rather with some of the effects related to energy conversion and transferring principles involved in it. The vehicle mobility dynamic modeling was studied and a proposed model(s) was developed to evaluate the force and energy distribution effects on a roadway pavement surface. Based on the results of this modeling process, the energy transferring criteria and SPM node distribution pattern in the pavement were specified. The energy distribution pattern is the energy source information that will be used by a micro generator. That energy will be converted to electricity based on the energy harvesting methods. The vehicle mobility modeling provides the energy distribution pattern along the roadway pavement. This pattern is used to estimate the power generating value and power limits of the SPM node. In this chapter, Vehicle Mobility Model (VMM) for the designing and applications of the SPM node is proposed. The VMM includes a series of sub-models, which were deployed in MATLAB simulation tools, and results for some roadways are presented.

2.1 VMM DESCRIPTION

There are tradeoffs between the number of SPM nodes (SPM network magnitude) and the installation cost of the nodes along the highway. This cost also depends on the roadway construction stage, which will be lower for a new or resurfacing roadway project in comparison with an existing roadway. Therefore, an optimum SPM node distribution should be planned and designed. The vehicle mobility dynamic modeling is a process for this optimization and is a key

process in the SPM installation design. In this section, a review of the modeling approach and the results of simulated cases are concluded. This modeling process is developed based on the SPM needs and does not include all the vehicle mobility aspects which are used in different applications. The modeling process needs some general information, definitions, assumptions and inputs variables in the form of statist or random variables.

VMM contains several sub-models that describe different vehicle mobility aspects. The most important building blocks of VMM are (a) vehicle traffic generation and distribution, (b) vehicle dynamics, and (c) roadway pavement interface. The vehicle chassis is what connects the tires and wheels to the vehicle's body. The chassis consists of the frame, suspension system, steering system, tires, and wheels. In the matter of the SPM study, what is interesting are the vehicle's force effect on the pavement and the tire forces. Tire force variation is a measure of the road holding capability of the vehicle and is directly influenced by shock absorber or strut performance.

Tire loading changes as a vehicle's center of gravity shifts during acceleration, deceleration, and while turning corners. The center of gravity is a point near the center of the car; it is the balance point of the car. The size of the four contact patches of traction at the tires also varies with the changes in tire load. As the vehicle brakes, inertia will cause a shift in the vehicle's center of gravity and weight will transfer from the rear tires to the front tires. This is known as dive. Similarly, weight will transfer from the front to the back during acceleration. This is known as squat. Consistently controlling vehicle weight transfer and suspension movement enhances the road holding capability of the vehicle and ultimately its safe operation [10]. Some of the useful definitions are:

- Track: The side to side distance between the centerline of the tires on an axle.

- Wheelbase: The distance between the centerline of the front and rear tires.
- Road Isolation: The vehicle's ability to absorb or isolate road shock from the passenger compartment.
- Inertia: The resistance to change the direction or velocity of a body, either at rest or in motion. In this case, it is related to changing the heading or direction of a vehicle that is, changing from straight ahead driving to a turn. The importance of inertia and weight distribution as they relate to driving is that they affect the amount of time required to make a transition from straight to turning or vice versa.
- "Poles of inertia" or "center of weight concentration". The "moment" in this concept is determined by the front-to-rear location of the center of gravity.
- Traction: The adhesive friction of the tire to the road surface.
- Pitch: The force felt in acceleration or braking movement around the horizontal axis of the vehicle.
- Roll: The force felt in cornering, side to side movement (lateral axis) of the vehicle.
- Yaw: The force felt in a spin movement around (vertical axis) of the vehicle.
- Road Holding: The degree to which a car maintains contact with the road surface in various types of directional changes and in a straight line.

2.1.1 VMM PROCESS

Vehicle tire dynamic forces damage the roadway pavement with its damping effect. In bridge structure, this force may generate a minimum vibration. Therefore, the topic has been interesting and investigated in transportation research work such as pavement management system (PMS) and bridge structure dynamic loading. Several modeling and simulation researches have been conducted to specify how the effect of the dynamic loading can be measured, monitored and may

be controlled. In addition, pavement or bridge structure response functions to a dynamic force have been investigated for designing more effective pavement or bridge structures. Because the heavy truck vehicle will have significant effected damage, a wide range of studies only focus on the heavy traffic loads. In this study, we analyze the energy conversion/transfer to a pavement and the displacement results which were used for the micro generator design.

These models develop outputs for surface rutting, surface roughness and structural stiffness degradation throughout the life of the pavement. With the SPM vehicle mobility dynamic modeling, our focus is on energy distribution to the surface and depth of the pavement and the effect of vehicle classifications and vehicle placement on traffic lanes. Fig. 2- 3 shows the SPM node parameters and variables.

2.1.2 VMM VARIABLES AND PARAMETERS

The Vehicle mobility modeling process uses several static and dynamic variables and parameters related to the roadway network, traffic conditions, and driving characteristics. One of the main goals in the process is the simplification of the input variables and parameters by easing the data collection system for estimation and evaluation of the input variable or parameters. For organizing these inputs, the following categories are considered:

I. General Vector indicates the general information or selectable case parameters. Table A12. 1 shows these parameters.

II. Dynamic Vehicle Matrix represents the vehicle variables. Table A12. 2 shows the sample of these matrix variables.

III. Force Vector is selected force variables which are calculated based on the input formula. Thus, this vector is not direct input data but the formulas are. Table A12. 3 shows a sample of this vector with formulas describing the models description sub-sections.

IV. Traffic Matrix, as it appears in the vector name, represents the traffic condition variables and the traffic measurement parameters. Table A12. 4 shows a sample of the traffic conditions which are presented in several scalar and vector entities. The traffic parameters are the subject of the field measurements and the number of data collections in the sampling.

V. Roadway Vectors are roadway geometry parameters plus the classification parameters. The values indicated in Table A12. 5 are typical values for the selected roadway for examination of VMM modeling. Fig 2-2 presents typical roadway geometry.

VI. Vehicle Class Vector, or the standard for vehicle classification, includes 12 vehicle classes based on the number of axles, length, and weight. This number of vehicle classes is not applicable for all roadways. City roadways generally have more restrictions for vehicle classes because of congested traffic issues and environment and safety considerations. Table A12. 6 shows the modeling parameters of passenger cars, two axle vehicles, and three and five axle trucks. By using VMM and truck models, the effect of an individual vehicle on the pavement will be specified. In the next Model, we will discuss the effect of traffic flow and the distribution of the vehicle's weight.

VII. Table A12. 6 shows m-Models Vehicle Classification vector which only presents three different classes of the vehicles. It is understandable that most of vehicles are fitted in these three classes. Thus the error of ignoring the other classes will not be significant.

These tables show the modeling parameters of passenger cars, two axle vehicles, and three and five axle trucks. By using VMM and truck models, the effect of an individual vehicle on the

pavement will be specified. In the next Model, we will discuss the effect of traffic flow and the distribution of the vehicle's weight.

2.1.3 VMM SUB-MODELS

The SPM vehicle mobility dynamic modeling structure includes several partner models that describe the process of the energy transformation. These partner models, abbreviated as M-models, have six partner models, as follow:

- VDMM: Vehicle Dynamic Motion Model
- VTGM- Vehicle Traffic Generation Model, which includes Vehicles Generator Module, Vehicle Class Distribution Module, Vehicle Traffic Pattern Module, Vehicle Lane Use Module, Vehicle Lane Change/ Passing Module, and Vehicle Platoon Module
- VWDM- Vehicle Weight Distribution Model
- VLOM - Vehicle Lane Offset Model
- VTCM – Vehicle Tire Contact Model
- VDPAM – Vehicle Parameters Estimation Model

2.1.3.1 SUB-MODEL M01: VEHICLE DYNAMIC MOTION MODEL (VDMM)

Early researchers' works concentrated on the influence that dynamic tire forces generated by vehicles carrying heavy goods in vehicles resulted in road damage and bridge vibration. Several research projects have been performed to understand the mechanisms by which heavy trucks generate dynamic tire forces as they travel along roads and how road surfaces and bridges respond to these applied forces. Sophisticated mathematical models of vehicle dynamics and road and bridge response to moving random wheel loads were developed. Moving vehicles carry their dynamic weight to the pavement and provide dynamic force characteristics over the pavement surface. This dynamic force is the function of vehicle operation and class and dynamic

weight. Federal regulations have been affected to minimize the vehicle dynamic weight effect on the roadways. The regulations define vehicle classes with restrictions for some classes on some roadways. VDMM is a modeling plan for specifying the dynamic motion forces with an approach that can simulate these characteristic over time that depend on the traffic, roadway and vehicle conditions.

Fig. 2- 1 is an example of a truck load stress. Geometry of the vehicle, number and distances of the axles, sizes, and weight all change the stress level over the pavement. As loads are moved from farther to closer distances, the stresses they apply to the pavement structure begin to overlap. In other words, they stop acting as separate loads. While maximum deflection of the pavement surface increases as axle spacing is reduced, maximum tensile stress at the underside of the surface layer will decrease. Tensile stress is a primary cause of fatigue cracking and can decrease as axle spacing is reduced. However, the net effect of changes in axle spacing is very complex and dependent on the nature--flexible versus rigid--of the pavement structure [11]. VDME formulation for a passenger car (a two axle vehicle class) is described in Eq.2.1 to Eq.2.8. The equation parameters and variables are specified in Fig. 2- 3.

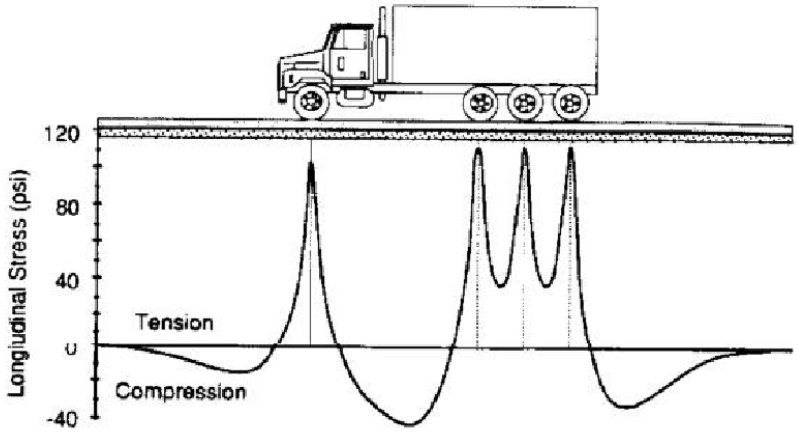

Fig. 2- 1 Tridem-axles are more pavement friendly than split-tandem axles [11]

These equations were developed for a two axle vehicle, passenger car, or truck. Heavy truck or multiple axle vehicles required other modeling for their dynamic effect on the pavement. The dynamic modeling, of the heavy trucks is dependent on the truck classification or axle configuration and regulation, which limits the maximum load of the truck. The heavy truck vehicles are not the majority of traffic flow in most highway networks. However, the dynamic loading effect of these vehicles on the pavement is a significant factor. For simplicity of the simulation run, some of the heavy vehicles with very few traffic densities were not analyzed. This assumption made easy execution of the model which included all vehicle classes. Not all information of the vehicle class traffic volume was available. Only main highways are equipped with vehicle classification monitoring stations.

In pavement operation and maintenance, the one generally used Equivalent Single Axle Load (ESAL) factor estimated from the AASHO Road Test is the basis for designing pavements. However, there is increasing recognition that better relationships between axle load and pavement response are needed. Thus, in this new approach, ESEL is replaced by more axle related load factors which are presented in truck configuration and classification. Therefore, we are using the classification based on the maximum axle load and the number of axles in our study.

The FHWA heavy truck classification is used in this study and the vehicle axle load and distances refer to the FHWA definitions. Fig. 2- 3 shows vehicle interaction with pavement, and SPM activation for charging and communication cycle. Different classes of vehicles with different numbers of axles and weight have different interaction forces and activation cycles, Fig. 2- 5 , Fig. 2- 6 and Fig. 2- 7 show the dynamic force parameters for different classes of vehicles.

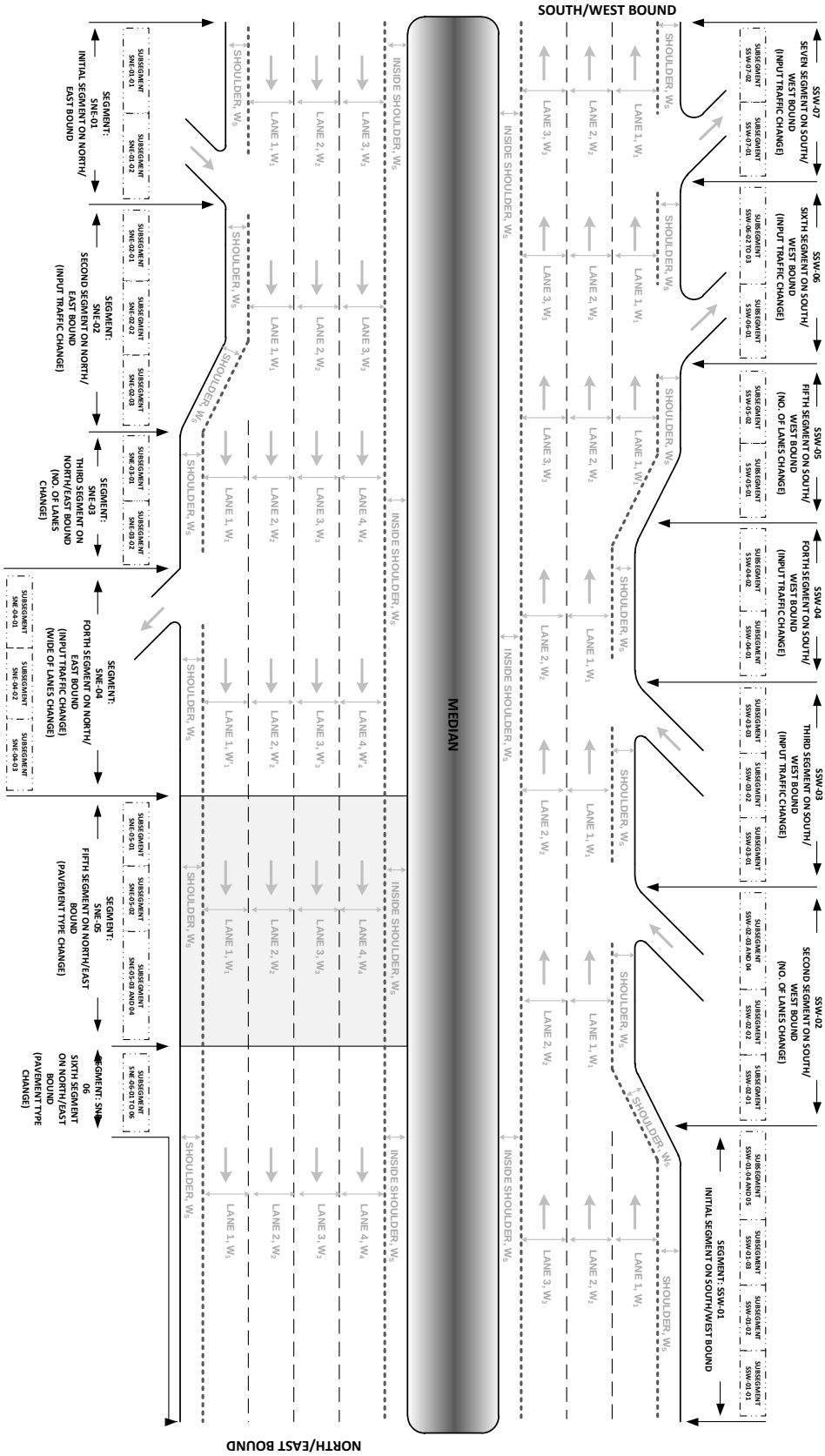

Fig. 2- 2 Example of Roadway Segmentation on SPM VMM Simulation

$$VDME\left(F_z(x_i,y_i,0,t),\bar{F}_z(x_i,y_i,0)\right)=f\left(V_f,V_x,V_a,\vec{V}_c\right) \quad \forall i=0,1 \qquad \text{Eq. 2- 1}$$

$$V_m V_x^{'}(x_0,y_0,0,t)=F_x(x_1,y_1,0,t)+,F_x(x_0,y_0,0,t)+FD_x(x_0,y_0,0,t)+ F_x(x_1,y_0,0,t)+,F_x(x_0,y_1,0,t) \qquad \text{Eq. 2- 2}$$

$$FD_x(x,y,0,t)=\frac{1}{2}C_{d\rho}\cdot V_{efa}\cdot V_x^2(x_0,y_0,0,t)\cdot \text{sgn}\left(V_x(x_0,y_0,0,t)\right) \qquad \text{Eq. 2- 3}$$

$$F_z(x_0,y_0,0,t)=\frac{h.\left(FD_x(x,y,0,t)-V_m.V_x^{'}(x_0,y_0,0,t)\right)+b.V_m.g}{2.(a+b)} \qquad \text{Eq. 2- 4}$$

$$F_z(x_1,y_1,0,t)=\frac{-h.\left(FD_x(x,y,0,t)-V_m.V_x^{'}(x_0,y_0,0,t)\right)+a.V_m.g}{2.(a+b)} \qquad \text{Eq. 2- 5}$$

$$F_z(x_0,y_0,0,t)=F_z(x_0,y_1,0,t) \qquad \text{Eq. 2- 6}$$

$$F_z(x_1,y_1,0,t)=F_z(x_1,y_0,0,t) \qquad \text{Eq. 2- 7}$$

$$F_z(x_0,y_0,0,t)+F_z(x_1,y_0,0,t)+F_z(x_0,y_1,0,t)F_z(x_1,y_1,0,t)=V_m.g \qquad \text{Eq. 2- 8}$$

The illustration of US truck configuration is shown in Appendix 9 US Truck Configuration**.** However, it should be considered that traffic flow rates of these trucks are varied and more common is three or five axles that are shown in Fig. 2- 7.The primary effect of axle spacing on flexible pavement performance is fatigue. Axle spacing is a major parameter for the fatigue study. When widely separated loads are brought closer together, the stresses imparted to the pavement structure begin to overlap and they cease to act as separate entities.

2.1.3.2 SUB-MODEL M02: VEHICLE TRAFFIC GENERATION MODEL (VTGM)

A traffic generation model is a simulation model to generate timely traffic patterns that can be used in real time simulation analyses. Traffic generation models are more than several decades old and several models or available traffic analysis software tools are using them. Examples of these tools are Synchro, Transit 7F, Passer II, and the tools which are familiar to all traffic engineers. In this study, we developed and used a traffic generation model dependent upon the classification of the vehicle. Therefore, the characteristics of a vehicle, classification and some

customary information (such as driver behavior type) were generated and recorded. This information was used as dynamic vehicle identification for the VMM modeling process. By having this information, VMM may be run and characteristics of the surface forces on the pavement were specified. The VTGM Model l describes the vehicle entrance timing function in the simulation system. The model has several sub-models to describe the functional characteristics of time, space, and lane movement of the traffic in the roadway.

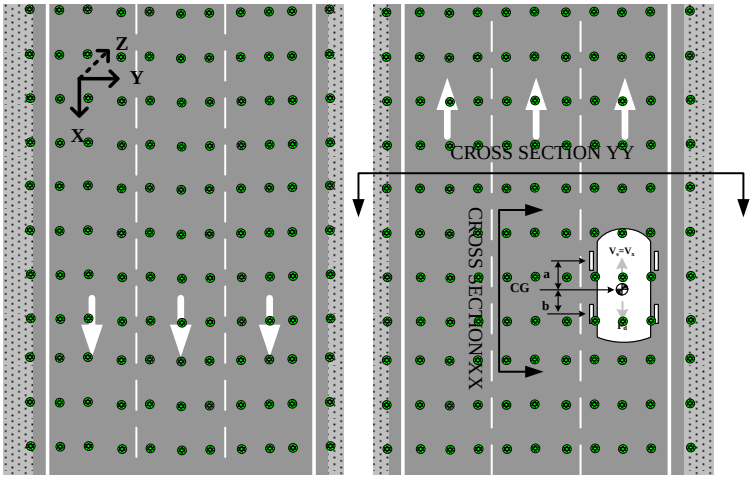

A TYPICAL HIGHWAY SECTION
FURNISHED WITH A GRID SPM NODES. THE SPM GRID NETWORK IS
NOT NECESSARY A UNIFORM NETWORK.

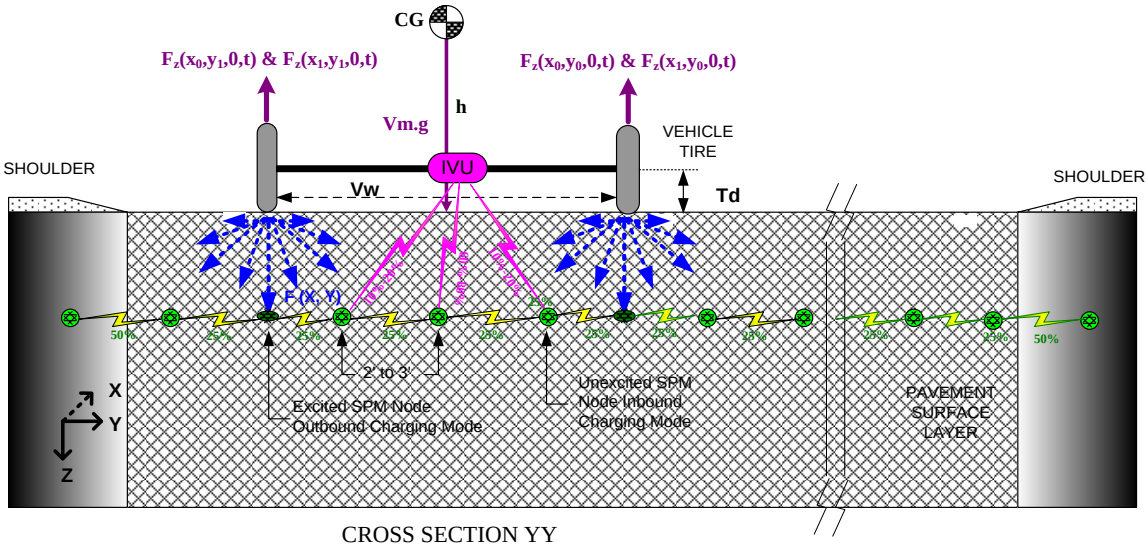

CROSS SECTION YY

Fig. 2- 3 Vehicle Movement and SPM Activation

2.1.3.2.1 VEHICLE GENERATOR

This sub-module generates information on the vehicle for each class of vehicle as objects for the simulation system. A vehicle object has its own fixed parameters such as length, number of axles, base weight, aerodynamic drag force, or variables such as headway, speed, acceleration, which describe the vehicle mobility conditions.

2.1.3.2.2 VEHICLE TRAFFIC PATTERN

A vehicle traffic pattern is the traffic volume on a roadway during each time period of the day. The time periods can be as long as a couple of hours or shorter than a couple of minutes based on the methods of measurement and tools. In our system modeling, the vehicle generator parameters are modified during each period of traffic pattern. As an example, the vehicle headway is changed during each traffic pattern period. The vehicle traffic pattern depends on the classification of the roadway which means the same traffic pattern profile in different roadway classes make different vehicle parameters. Examples of typical daily traffic patterns for a freeway and arterial highways in New York City are shown in Fig. 2- 8 and Appendix 2- VMM Case Study Model Input and Outputs Data, that include additional highway data used in VMM modeling.

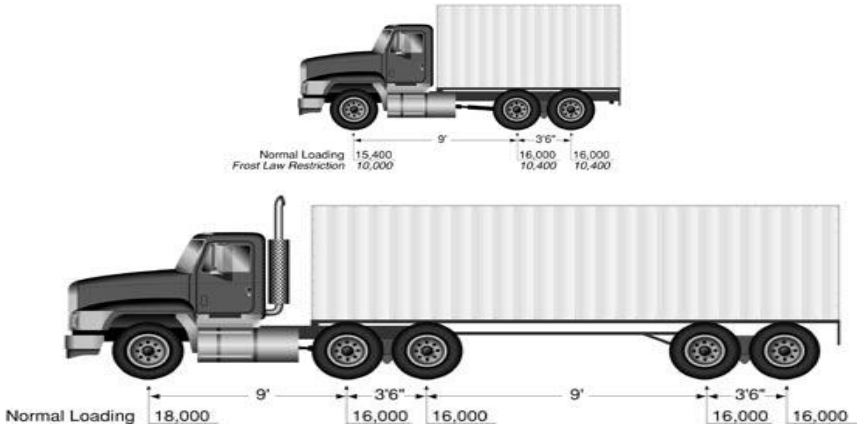

Fig. 2- 4 Three and Five Axle Trucks Parameters

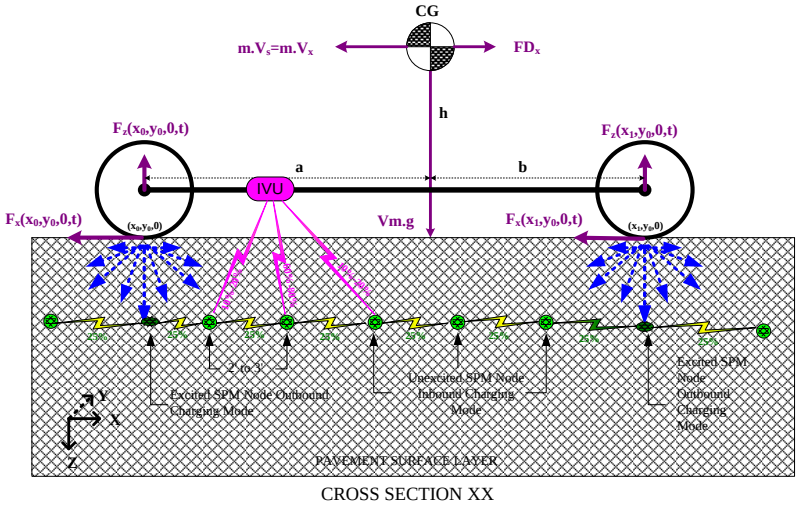

CROSS SECTION XX

Fig. 2- 5 Two Axle Vehicle Force Parameters

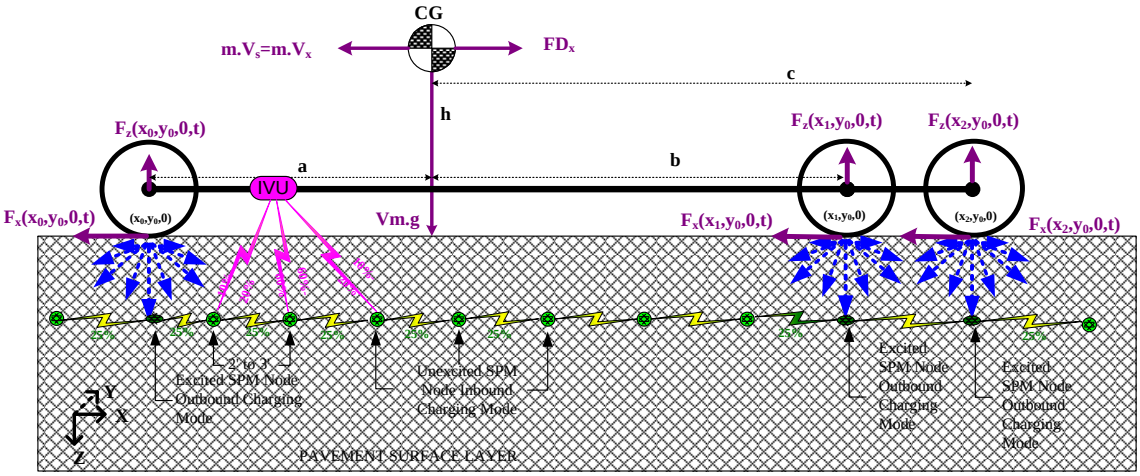

Fig. 2- 6 Three Axle Vehicle Force Parameters

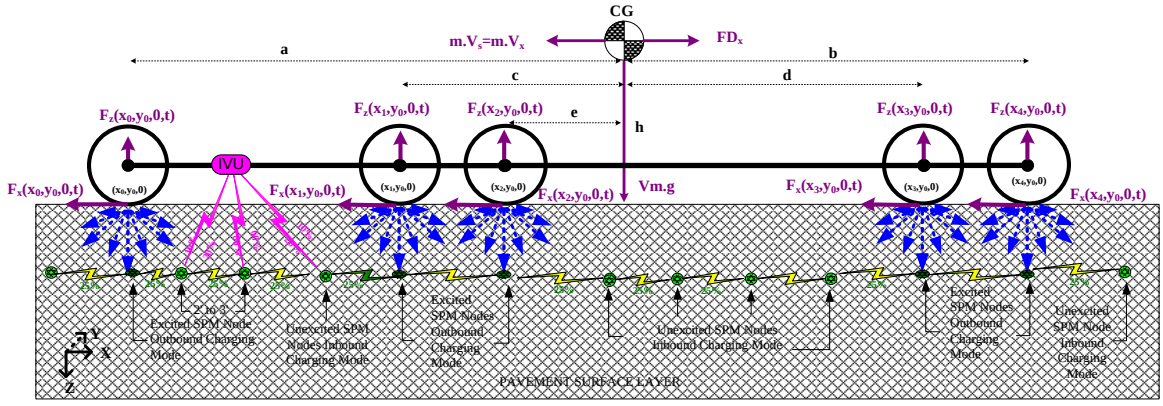

Fig. 2- 7 Five Axle Vehicle Force Parameters

2.1.3.2.3 VEHICLE CLASS DISTRIBUTION

Different vehicle classes will have different effect and pavement responses. Therefore, a vehicle class distribution sub-module is needed. The class distribution sub-model is dependent on the roadway application, the user/driver type, and regulations. In this study, a random process and Poisson Distribution Functions are used. In either case, the average and variances of the vehicle classes in a traffic time window are considered as known parameters. However, these parameters can be varied in a close sensitivity analysis to determine the critical condition of the force/energy transfer to the pavement.

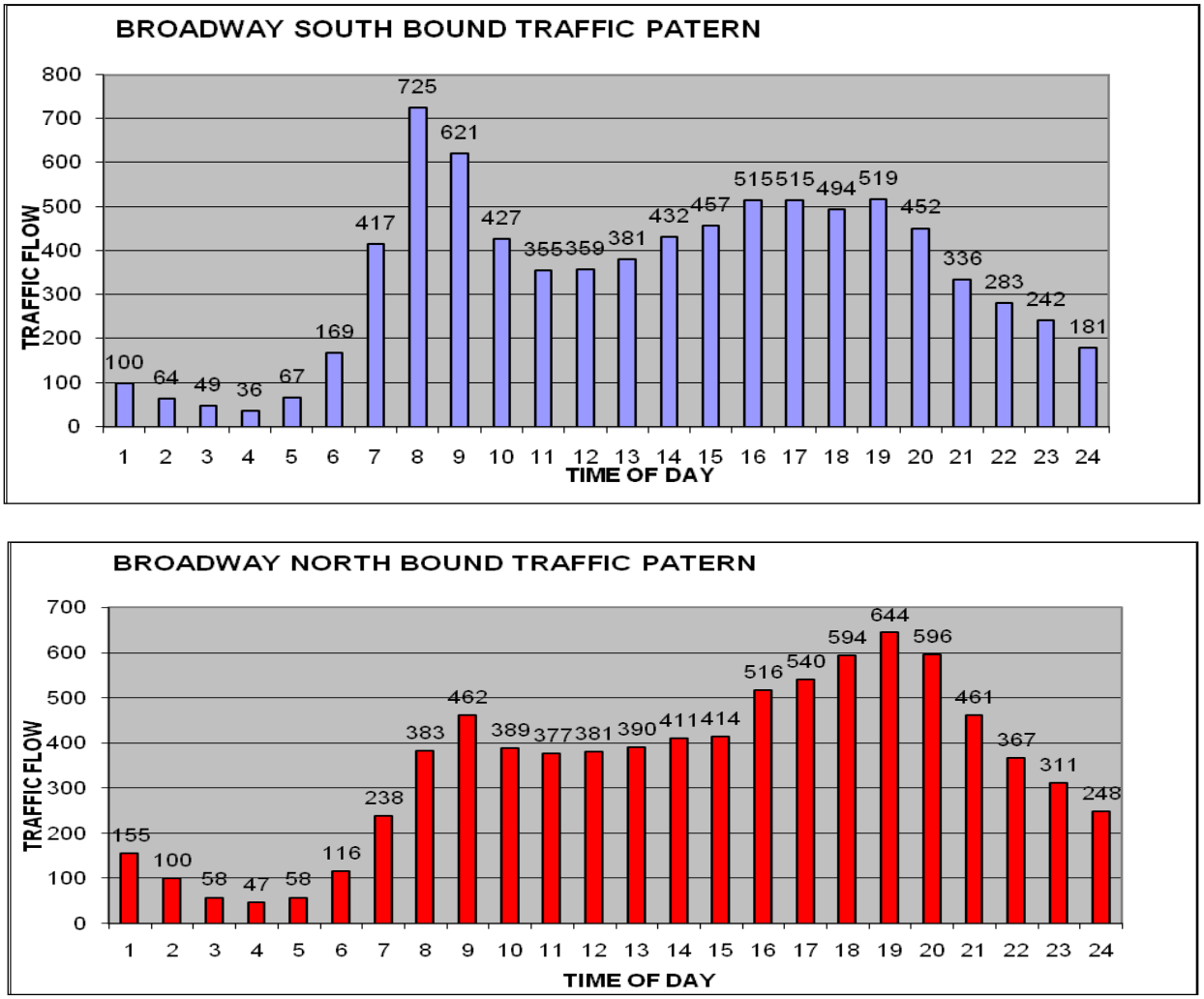

Fig. 2- 8 Typical Traffic Pattern at Broadway Street New York City

2.1.3.2.4 VEHICLE LANE USE

Most of the traffic data is summarized based on roadway approach or direction, which is the total summation of the traffic flow on all traffic lanes. Therefore, a traffic distribution between lanes needs to be specified. Vehicle lane use is considered the estimate of the traffic share in each lane of the roadway. There are several methods for these assignments and each depends on the different roadway statistical information and some driver behavioral factors. In our study, a fixed daily assignment rate for each lane is used. The assignment rate during shorter period is not fixed and is controlled by a random distribution function. A generated vehicle randomly was assigned to a lane where long term total lane use satisfies the fixed rates assigned for the lanes. More sophisticated intelligent and dynamic methods can be used, but more roadway network and driver information would need to be inputted to the model. However, such a complicated model will not significantly change the needs for the SPM application.

2.1.3.2.5 VEHICLE LANE CHANGE/ PASSING

This module describes vehicle lane changes or passing procedures. This procedure includes selection methods for the passing vehicle checking the availability of the next lane and checking the minimum distances and the physical movement of the vehicle into the next lane. The passing vehicle is a complicated entity, but simple rules used are based on the length of the traffic platoon and a random decision point.

2.1.3.2.6 Vehicle Platoon

A group of vehicles with a closed headway make a vehicle platoon. A comprehensive definition of vehicle platoon, which is applied in automated highway systems, can be considered and used in this study. However, to avoid a complexity of the model and because of the target in energy conversion on the critical condition, a simple model was developed.

This model is based on a simple look at the platoon as a group of vehicles on the roadway. This group of vehicles will keep their headway without changing lanes fast and without a lot of passing. In this case, a front vehicle driver in a platoon will be the subject for a passing decision. Thus, tracking the platoon can provide some information for vehicle passing choice. By measuring the headway of the vehicles, a platoon will be recognized and the decision of passing can be shared on the platoon as a group. In our model, the default size of the platoon is five vehicles. The platoon size is an input parameter and can be changed by the user. DTGM is using the above modules and specifying the time space vehicle movement characteristics on the roadway. The output information was used by VDM^2 and the surface forces were specified. However, before complete, reference models need to be developed for the main parameters of vehicles which are important in the energy conversion.

2.1.3.3 SUB-MODEL M03: VEHICLE WEIGHT DISTRIBUTION MODEL (VWDM)

The M- models 1 and 2 describe the vehicle movement and the pavement interface forces. The vehicles are classified based on the number of axles and maximum loads. In real cases, the vehicle loading is different. The different loads for passenger cars, which are the majority of vehicles, may vary between ± 5% e. However, this weight variation may be a wider range as ± 30% for other vehicle classes such as heavy truck classes. Thus, a weight model should be considered in the simulation model especially for heavy vehicle classes.

The vehicle weight is dependent on several factors and in studies such as good transport planning, they will be exercised. However, these studies include some estimation or measurement of goods transport on a network. In other hands, the major highway roads are equipped with a Weight in Motion (WIM) station for measurement of truck load and inspection of its maximum load. Therefore, the truck weight data can be available, however, the data will

not be possible to be used for this study, because the data related a specific roadway section and it cannot be used for a general simulation system. Practically, individual vehicle load modeling is not feasible, thus we are exercising different cases and assumptions in the Vehicle Weight Distribution Model (VWDM). The cases are:

- VWDM Case 1- all vehicles will have a minimum, unloaded weight. Vehicle weight will be a uniform distribution with:

  $$E[V_M(V_{CN}) + V_{DW}(V_{CN})] = V_M(V_{CN}) \quad \text{Eq. 2- 9}$$

  $$V_{DW}(V_{CN}) = 0 \quad \text{Eq. 2- 10}$$

- VWDM Case 2- all vehicles will have a maximum, allowable load. Vehicle weight will be a uniform distribution with:

  $$E[V_M(V_{CN}) + V_{DW}(V_{CN})] = Full \quad Loaded \quad Vehicle \quad \text{Eq. 2- 11}$$

  $$V_{DW}(V_{CN}) = Maximum \quad \text{Eq. 2- 12}$$

- VWDM Case 3- all heavy vehicles will have variable weights. The special case assumed the production of weight to vehicle headway will be constant. This assumption is not a real condition but it is interesting for energy transferring to the pavement as a worse case. Vehicle weight distribution will be a function of vehicle headways random variables.

  $$[V_{DW}(V_c)] \times V_{HEADWAY} = Cons\tan t\ A \quad \text{Eq. 2- 13}$$

- VWDM Case 4- an opposite of the Case 4 that assumed higher dynamic weight under higher headway conditions. Again this case is to study the sensitivity of energy transferring to the pavement in response to the vehicle weight distribution.

  $$[V_{DW}(V_{CN})] \Big/ V_{HEADWAY} = Cons\tan t\ B \quad \text{Eq. 2- 14}$$

- VWDM Case 5- the vehicle weight distribution will be a random distribution. The vehicle dynamic weight will be selected based on the random distribution and the maximum allowable weight of the vehicle class. Values of $\mu_{V_{DW}}$ and $\sigma_{V_{DW}}$ can be estimated from the highway weight station data which are available for heavy vehicles and on the interstate highway.

$$PDF_{V_{DW}}\left[V_{DW}(V_{CN})\right] = N\left(\mu_{V_{DW}}, \sigma_{V_{DW}}\right) \qquad \text{Eq. 2- 15}$$

$\mu_{V_{DW}} = Daily\ Average\ Of\ Vehicle\ dynamic\ weight$

$\sigma_{V_{DW}} = Daily\ Varriance\ Of\ Vehicle\ dynamic\ weight$

2.1.3.4 SUB-MODEL M04: VEHICLE LANE OFFSETMODEL (VLOM)

Vehicle movement or vehicle tire position in a lane is affected by several factors such as driver behavior, speed, traffic volume, and roadway conditions. It is clear a vehicle is not in the center of the lane all the time, and therefore, the pavement surface will be affected inconsistently. This effect will change the force and energy transferring to the pavement surface and eventually affect our SPM placement design plan.

Most of the drivers are controlling their vehicles inside a traffic lane, but the road geometry, passing chance, and careless control, drive the vehicle in the different positions in a lane. To consider these situations in the simulation, a random variable was assigned to each vehicle that describes tires position in the traffic lane. The random variable was specifying with a distribution function that is calculated from field observation. It is important to understand the distribution function is a typical solution and different distribution functions can be proposed based on different observations. However, the mean and variance of the variable should be similar (not necessary exactly the same) and be acceptable with sampling test data. The sampling test data was collected by a video data collection.

To understand these effects, the VLOM model was studied and investigated. As listed above, several factors will be responsible for vehicle position in a lane and we are not intending to include a comprehensive model to describe all factors. But we are intending to have a general model that shows behavior of the vehicles in lanes as typical cases for each roadway class. The VLOM can be branched to subsidiary models based on the traffic patterns. The VLOM model was developed by analyzing field data, video data from highways, and by dispensing with a training or learning process. Fig. 2- 9, Fig. 2- 10 and Fig. 2- 11 show the offset measurements based on the traffic video data of a site (sample data) and the input or training data results are shown in Table 2- 1, and Table 2- 3. [4]

As a result, the vehicle position distribution function was estimated for a roadway class, vehicle class and a traffic period condition. This distribution function specifies the tires' lateral position during the vehicle movement. Number of sampling cases and different roadway classes are required to develop a good training plan and finding the general distribution function for the offset. Because in this study, we are focusing in a placement of the SPM nodes in a range of 1 to 1.5 m, the range of accuracy for the offset is considered as 4 inches (10 cm). Based on this accuracy, an expected value for mean, variance and standard deviation for vehicle offset distribution function is estimated. The field data was collected from traffic video from different roadways collected from a traffic management center surveillance system or car follow video recording system.

[4]Video sources: http://video.dot.ca.gov/asx/d3-mack-99.asx, http://video.dot.ca.gov/asx/D5-Curbaril-Ave-at-101.asx, http://svhqmsmedia.dot.ca.gov/D5-Curbaril-Ave-at-101?.wma

2.1.3.5 SUB-MODEL M05: VEHICLE TIRE CONTACT MODEL (VTCM)

The physical contact of the vehicle to the pavement happens when vehicle tires touch points to the pavement. This physical interface is the function of the tires' parameters such as size, materials, outside shape, and pressure. Tire contact conditions (pressure, formation and area) change the dynamic tire forces dramatically. Their dynamic effects will make some difference to the stresses and strains in the upper pavement layers and probably have negligible influence in the lower layers where the overall dynamic force level will be the most important factor [11].

The tire tread and sidewall elements undergo deformation and recovery as they enter and exit the footprint. Since the rubber is elastomeric, it is compressed during this cycle. As the rubber deforms and recovers, it imparts cyclical forces into the vehicle's tires. These variations are collectively referred to as tire uniformity. Tire Uniformity is characterized by Radial Force Variation (RFV), Lateral Force Variation (LFV), and Tangential Force Variation (TFV). Therefore, tire modeling will be a part of the VPIF. Of course, we do not need a complicated tire model, which has been widely used on the tire or vehicle design. The effect of tire contact interface on a pavement has been studied in several pavement study researches. One main concern is the possibility of accelerated pavement deterioration, particularly a rutting effect caused by increasing tire pressures. The tire structure can be a major factor in the force interfacing with the pavement; however we cannot specify the real distribution function for it.

The physical parameters such as tire width or type will affect the tire footprint over the pavement, which will vary with the concentrate of weight. For example, a radial tire in a heavy truck under 100 pounds per square inch (PSI) inflation pressure in comparison with a standard bias-type tire with inflation pressures between 75 and 80 PSI, has more rutting rate and cracking problems on the pavement. In Appendix 10 Tire Contact Interface, a comprehensive calculation of the tire contact and forces has been collected.

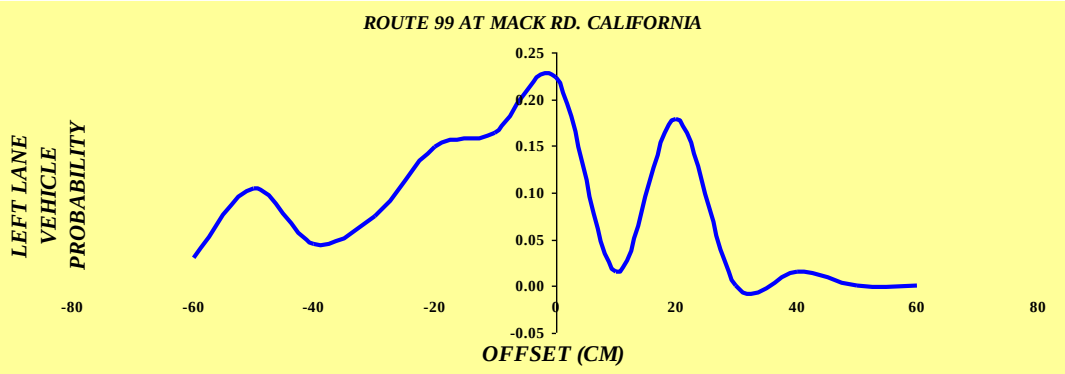

Fig. 2- 9 Vehicle offset distribution function at Left Lane, Speed Lane

Table 2- 1 Sample vehicles offset data- Left Lane

OFFSET (CM)	LEFT LANE	P(X)	X. P (X)	$[X-E(X)]^2$	P(X). $[X-E(X)]^2$
-60	2	0.03	-1.79	3496.05	104.36
-50	7	0.10	-5.22	2413.51	252.16
-40	3	0.04	-1.79	1530.96	68.55
-30	5	0.07	-2.24	848.41	63.31
-20	10	0.15	-2.99	365.86	54.61
-10	11	0.16	-1.64	83.31	13.68
0	15	0.22	0.00	0.76	0.17
10	1	0.01	0.15	118.21	1.76
20	12	0.18	3.58	435.66	78.03
30	0	0.00	0.00	953.11	0.00
40	1	0.01	0.60	1670.57	24.93
50	0	0.00	0.00	2588.02	0.00
60	0	0.00	0.00	3705.47	0.00
	67	1.00	-0.87		55.13
MEAN	**-0.87**	**Case: California Rt. 99 at Mack Rd. Left Lane Sample Data**			
VAR	**55.13**				
STA	**7.42**				

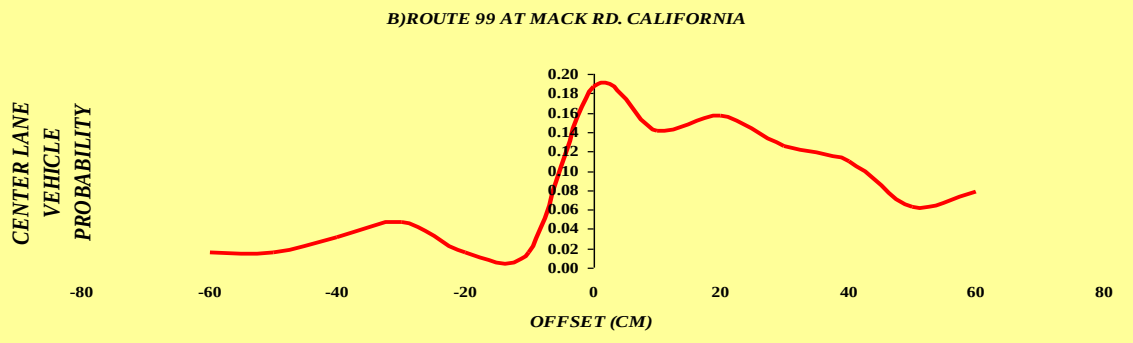

Fig. 2- 10 Vehicle offset distribution function at Center Lane

Table 2- 2 Sample vehicles offset data- Center Lane

OFFSET (CM)	CENTER LANE	P(X)	X. P (X)	$[X-E(X)]^2$	P(X). $[X-E(X)]^2$
-60	1	0.02	-0.94	3745.68	58.53
-50	1	0.02	-0.78	2621.64	40.96
-40	2	0.03	-1.25	1697.60	53.05
-30	3	0.05	-1.41	973.56	45.64
-20	1	0.02	-0.31	449.52	7.02
-10	1	0.02	-0.16	125.48	1.96
0	12	0.19	0.00	1.44	0.27
10	9	0.14	1.41	77.41	10.89
20	10	0.16	3.13	353.37	55.21
30	8	0.13	3.75	829.33	103.67
40	7	0.11	4.38	1505.29	164.64
50	4	0.06	3.13	2381.25	148.83
60	5	0.08	4.69	3457.21	270.09
	64	1.00	1.20		80.06
MEAN	**1.20**	**Case: California Rt. 99 at Mack Rd. Center Lane Sample Data**			
VAR	**80.06**				
STA	**8.95**				

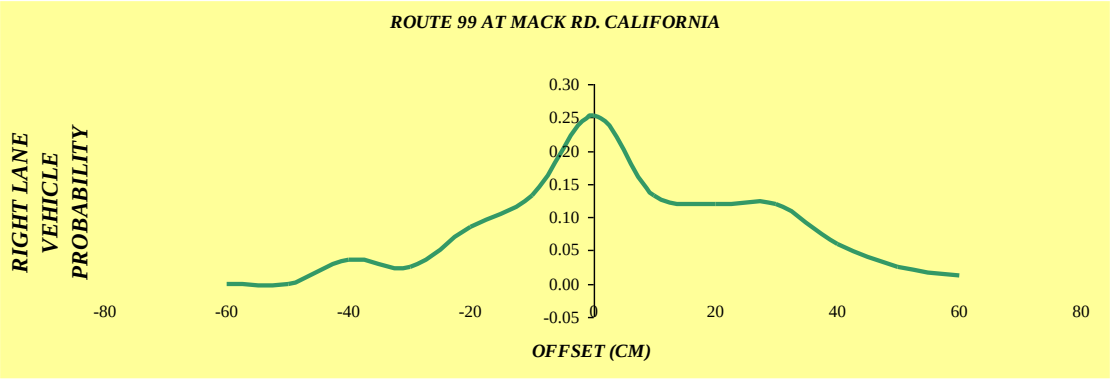

Fig. 2- 11 Vehicle offset distribution function at Right Lane

Table 2- 3 Sample vehicles offset data- Right Lane

OFFSET (CM)	RIGHT LANE	P(X)	X. P (X)	$[X-E(X)]^2$	P(X). $[X-E(X)]^2$
-60	0	0.00	0	3660.31	0
-50	0	0.00	0	2550.30	0
-40	3	0.04	-1.45	1640.29	59.29
-30	2	0.02	-0.72	930.28	22.42
-20	7	0.08	-1.69	420.27	35.44
-10	11	0.13	-1.33	110.26	14.61
0	21	0.25	0	0.25	0.06
10	11	0.13	1.33	90.24	11.96
20	10	0.12	2.41	380.23	45.81
30	10	0.12	3.61	870.22	104.85
40	5	0.06	2.41	1560.21	93.99
50	2	0.02	1.20	2450.20	59.04
60	1	0.01	0.72	3540.19	42.65
	83	1.00	0.50		40.84
MEAN	0.500	**Case: California Rt. 99 at Mack Rd. Right Lane Sample Data**			
VAR	40.844				
STA	6.391				

The comprehensive tire modeling approach will require more vehicles and tire information inputs which will make the model more complicated and expensive because more sampling data needs to be collected. Thus, a simplified solution with uniform conditions will be considered and the comprehensive model will be considered in future work to be integrated in the mobility group models.

VTCM specifies the estimated (average) effective contact point will be specified for each vehicle class. The vertical force at each tire will be shard on the contact points. The number of contact points will be specified based on physical resolution of the overall simulation. Based on the vehicle class, optimum tire pressure, and a random variance, a distribution function for tire contact touch is used in VTCM. The distribution model generates contact touch length bounded from 5 to 20 cm (the range can be adjusted).

2.1.3.6 SUB-MODEL M06: VEHICLE PARAMETER ESTIMATION MODEL (VPEM)

The M-models are proposed to describe the energy and forces on the pavement surface. The results of those models are used by Pavement Response models and energy/force micro distribution patterns will be simulated. As discussed on the previous models, multiple input variables which are not constant values can be described with stochastic variable and different distribution functions.

Because the varieties of factors are involved in these functions, it is difficult to specify the best distribution function for these variables. In other words, any distribution function will not be independent from others. For example, the traffic volume, speed, drivers' behaviors, and lane movement are all dependent on the roadway conditions. Therefore, we did not plan to describe all these variables in an individual dynamic manner. The parameter estimation is not a or linear analysis and was considered as pricewise linear cases. The parameter estimation method is varied

for special cases. The important cases are a highly congested/over saturated roadway, exclusive road, or truck assigned roadway. VPEM is proposing a plan for limiting the variation of the parameters and including the limits on the evaluation and study of the effects of uncertainty of the static parameters in the M- models.

2.1.3.6.1 VEHICLE SPEED PARAMETERS

The vehicle speed, $V_{s.}$, is an input parameter in the M-Models. The speed is the average traffic movement from the data log such as Average Annual Data Traffic, a sampling measurement or from a traffic planning study. A vehicle speed V_s is described in the Eq. 2-16. The term $N_s(t)$ is the dynamic part of speed variation and it will be a function of time and of course traffic congestion and driver behavior. The traffic speed in a roadway is related to the vehicle density variable, $V_{d.}$ The density definition is the number of vehicles per unit length per lane, as follows:

$$V_s(t) = \overline{V}_s + N_s(t) \qquad \text{Eq. 2- 16}$$

$$V_d(t) = {V_f(t)}/{V_s(t)} \qquad \text{Eq. 2- 17}$$

$$V_d(t) = f\{V_f(t), V_s(t)\} \quad \Leftrightarrow \quad V_f(t) = g\{V_d(t), V_s(t)\} \qquad \text{Eq. 2- 18}$$

Eq. 2-18 in a flow traffic movement will be estimated with a linear function as defined in Eq.2-17. The "g" function is replaced with modification of speed by density. By accepting the linear approximation, we can have Eq. 2-19, which is the combination of the above equations. By rearranging the equation, the $N_f(t)$ is calculated and two maximum and minimum values are estimated for as defined in Eq. 2-20 and Eq. 2-21. These estimates are functions of headway, which is more interesting for energy conversion studies. The Eq. 2-19 is our reference for estimating the $N_s(t)$. However, it is reasonable that other methods for estimation of $N_s(t)$ may be

more suitable but they require a more complicated solution with additional input data or parameters.

$$\overline{V}_s + N_s(t) = {V_f(t)}\big/{V_d(t)} \qquad \text{Eq. 2- 19}$$

$$N_s(t)\big|_{\min} = \overline{V}_f \times h_{\min} - \overline{V}_s \qquad \text{Eq. 2- 20}$$

$$N_s(t)\big|_{\max} = \overline{V}_f \times h_{\max} - \overline{V}_s \qquad \text{Eq. 2- 21}$$

In the above equation, $\overline{V}_s$ is the average speed for the traffic time window, which is a dial. A daily traffic pattern is specified with several traffic dials. The number of dials is set based on the source of the collection data.

2.1.3.6.2 VEHICLE TRAFFIC FLOW PARAMETERS

Traffic flow rate, V_f is the main variable in our M-Models, which has a dynamic range depending on network dynamic demand, driver behaviors, and roadway geometries. This dynamic range can be the result of accuracy of the estimated V_f value and it can vary between $\pm v_{f\max}$. Because of the variety of parameters and input data for V_f modeling, it is out of our target and will be a later subject for traffic simulation and modeling. However, we limit the definition of the V_f changes to a shifting of the traffic between some traffic patterns/windows and describe it in:

$$v_{f\max}\big|_{window\,(n)} = abs\{\frac{\overline{V}_f\big|_{window\,(n-1)} + \overline{V}_f\big|_{window\,(n+1)}}{\overline{V}_f\big|_{window\,(n-1)} + \overline{V}_f\big|_{window\,(n)} + \overline{V}_f\big|_{window\,(n+1)}}(\overline{V}_f\big|_{window\,(n-1)} - \overline{V}_f\big|_{window\,(n+1)})\}$$

Eq. 2- 22

2.2 VMM DEPLOYMENT

The deployments of the M-Models were executed in the MATLAB environment. This deployment process was dependent on the static and traffic parameters of the roadway and vehicle classes as the input information to the system, which are detailed on the following:

- Table A12. 1 VMM General Vector
- Table A12. 2 VMM- Dynamic Vehicle Matrix
- Table A12. 3 VMM- Force Vector
- Table A12. 4 VMM- Traffic Matrix
- Table A12. 5 Roadway Vector

These tables show the modeling parameters of passenger cars, two axle vehicles, and three and five axle trucks. By using VMM and truck models, the effects of an individual vehicle on the pavement were specified. In the next model, we discuss the effect of traffic flow and the distribution of the vehicles' weights. These tables show the modeling parameters of a passenger car, a two axle vehicle, and a three and a five axle truck. By using VMM and truck models, the effect of an individual vehicle on the pavement was specified. In the next Model we discuss the effect of traffic flow and the distribution of the vehicles' weights.

- Table A12. 6 Vehicle Classification Vector

The roadway static information depends on the roadway geometry and physical condition. In a typical roadway, the geometrical conditions can be considered stable or constant for a roadway segment. A segment can be as short as a couple of hundred meters to as long as several kilometers in different roadways. Also, the roadway network configuration and geometry will affect the input data variation that is required to update more of the input data for the M-model simulation over a roadway network. In this stage of the study, the M-Model simulates a segment

for different completed roadways. The selected roadways are served in different levels of service with different traffic profiles as described in Appendix 4.

The traffic information was organized for collection and input into the model/program. A sample of the traffic data information and data collection form, which was developed for the VMM modeling, is shown in Appendix 4. The table presents input data for two segments for a 15 minute sampling time period. The number of segments and sampling periods were adjusted based on the source of the traffic data. A downside of longer segment and longer sampling data will affect the micro simulation results of the Model. As referenced above, MATLAB was used as the model simulation tool. Because of the long processing time, in this simulation experience, the number of vehicle classes was limited to three vehicle classes. The vehicles in classes 4 to 14 represent a smaller portion of the highway traffic. In the upcoming stage of this study, all classes will be included. The VMM modeling program codes are attached in Appendix 1- VMM Modeling Program. The outputs of the M-models are framed to be used on the P-Models. The results of the M-Models are presented in the section.

2.3 VMM SIMULATION RESULTS

The results of the simulation of M-Models include the dynamic movement of the vehicles and the dynamic force matrix in the roadway cross section. An interpolation of force matrix in the time domain provides the force matrix mesh that covers the roadway segment/sub-segment. In a high traffic roadway such as the Major Deegan Expressway (NY), more than 160,000 vehicle axles will be simulated and significant dynamic information will be recorded. The output results include large matrixes of the pavement tire force placement in a resolution set by the VMM minimum length (5 CM). The full simulation results are included in Attachment 3. Based on the simulation, the SPM charging activation characteristics are evaluated. The SPM charging activation characteristics are functions of time and placement of the SPM. Table 2- 4 is shown as an example of VMM output data. The complete table may have more than 300,000 vehicle axles' output data.

Fig. 2- 12 A Cross Section of Dynamic Force on the Henry Hudson Parkway, NY shows a cross section of dynamic force over one traffic lane (lane 1) on the Henry Hudson Parkway. The characteristic of force over time for a cross section of this lane shows in the Figure. More analysis and simulation of the dynamic forces inside the pavement are studied in the P-Model development stage. The results of the simulation can be used for other applications including the Pavement Management System which will be part of a future work for expansion of M-model applications in other transportation fields. Traffic input data, AADT, and average hourly rate were included in Appendix 2- VMM Case Study Model Input and Outputs Data. This data was collected from the New York City Department of Transportation, 2005 Screen Line Traffic Flow data publication.

Table 2- 4VMM outputs data example

AXCLE NO.	ORIGINAL LANE	LANE OFFSET	TIME	DYNAMIC TIME	DISTANCE	DYNAMIC DISTANCE	VEHICLE TRACK	VEHICLE AXCLE NO.	FINAL LANE	VEHICLE CLASS	POSITION Y=01	POSITION Y=02	POSITION Y=03	POSITION Y=04	POSITION Y=05	POSITION Y=06	POSITION Y=07	POSITION Y=08	POSITION Y=09	POSITION Y=10	POSITION Y=11	POSITION Y=12	POSITION Y=13
AXL-000001	1	0	0	0	0	0	1	1	1	1	0	0	0	0	0	0	0	0	0	0	0	0	1419
AXL-000002	1	0	0.037	0	3	0	1	2	1	1	0	0	0	0	0	0	0	0	0	0	0	0	1031
AXL-000022	1	0	3	0	7863.98	18	3	1	1	2	0	0	0	0	0	0	0	0	0	0	0	0	0
AXL-000046	1	0	3.082	0	7867.98	18	3	2	1	2	0	0	0	0	0	0	0	0	0	0	0	0	0
AXL-000051	1	0	3.103	0	7868.98	18	3	3	1	2	0	0	0	0	0	0	0	0	0	0	0	0	0
AXL-000098	1	0	8	0	8180.73	36	5	1	1	3	0	0	0	0	0	0	0	818	818	818	818	818	0
AXL-000103	1	0	8.092	0	8183.73	36	5	2	1	3	0	0	0	0	0	0	0	364	364	364	364	364	0
AXL-000138	1	0	8.123	0	8184.73	36	5	3	1	3	0	0	0	0	0	0	0	364	364	364	364	364	0
AXL-000139	1	0	8.215	0	8187.73	36	5	4	1	3	0	0	0	0	0	0	0	364	364	364	364	364	0
AXL-000148	1	0	8.246	0	8188.73	36	5	5	1	3	0	0	0	0	0	0	0	364	364	364	364	364	0
AXL-000267	1	0	139.4	0	26109.7	12	9	1	1	1	0	0	0	0	0	0	0	0	0	0	0	0	0
AXL-000268	1	0	139.4	0	26112.7	12	9	2	1	1	0	0	0	0	0	0	0	0	0	0	0	0	0
AXL-000314	1	0	202.3	0	38300.5	12	11	1	1	1	0	0	0	0	0	0	0	0	0	0	0	709	709
AXL-000315	1	0	202.4	0	38303.5	12	11	2	1	1	0	0	0	0	0	0	0	0	0	0	0	516	516

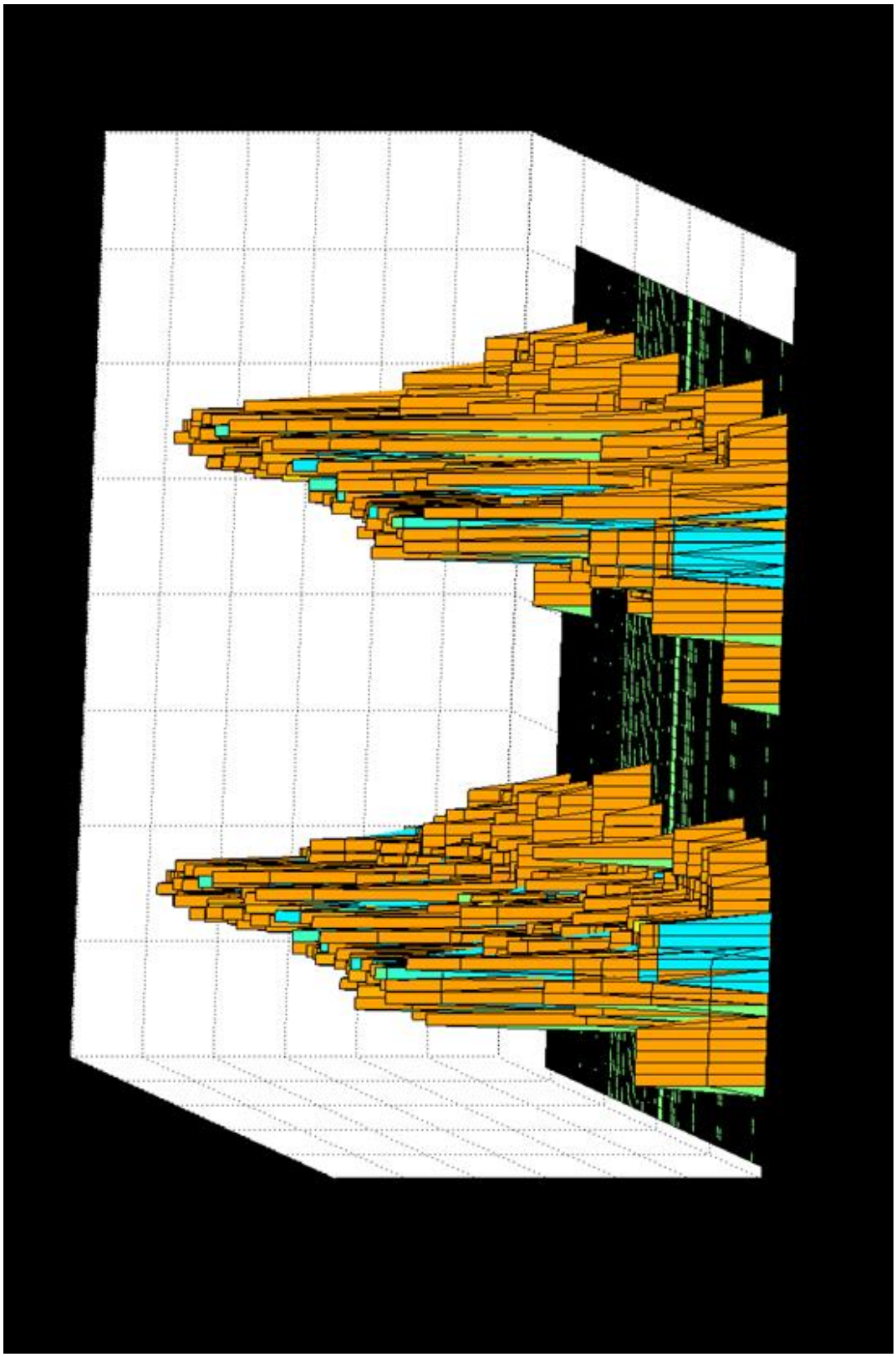

Fig. 2- 12 A Cross Section of Dynamic Force on the Henry Hudson Parkway

2.4 VMM RESULTS

The VMM simulation for Henry Hudson Parkway showed a distribution of 126,286 and 108,769 axles in the south and north bound lanes. The distribution specified the tire load at a time and at a vertical offset from the right edge of the traffic lane. Based on this distribution, the position of the SPM for maximum charging activation will be specified. In this example for a cross section of the pavement, the average charging activation rate data is shown in Table 2- 5 and Fig. 2- 13. The activation rates are based on (1) the traffic data, (2) vehicle class, (3) roadway geometry, and (4) tire information. VMM results of the HHP north bound lane include distribution and assignment of more than 130,000 vehicle axles in different vehicle classes.

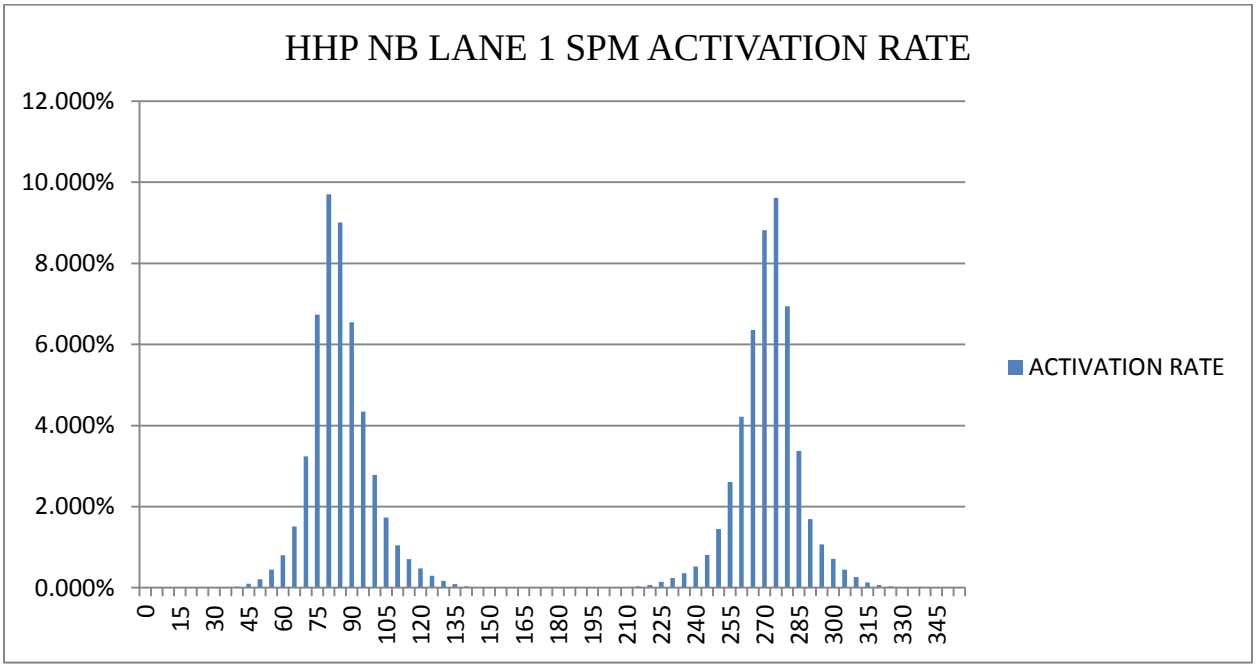

Fig. 2- 13 HHP North Bound Lane 1 SPM Activation Rate Distribution per Vertical Offset

VMM assessment requires a monitoring capability of the roadway segments for long time periods. In this study, a sample method for the model assessment was used for simplicity and constructability of the assessment. The car fallow video system was used for the data resources.

Table 2- 5 HHP North Bound Lane 1 SPM Daily Activation Average Data in a Cross Section

OFFSET (CM)	*0*	*5*	*10*	*15*	*20*	*25*	*30*
FORCE (N)	**0**	**0**	**0**	**0**	**0**	**0**	**0**
PERCENTAGE	**0.000%**	**0.000%**	**0.000%**	**0.000%**	**0.000%**	**0.000%**	**0.000%**
OFFSET (CM)	**35**	**40**	**45**	**50**	**55**	**60**	**65**
FORCE (N)	**3323**	**65976.5**	**223683.5**	**501192**	**1052190**	**1900848**	**3578971**
PERCENTAGE	**0.001%**	**0.028%**	**0.094%**	**0.212%**	**0.444%**	**0.803%**	**1.511%**
OFFSET (CM)	**70**	**75**	**80**	**85**	**90**	**95**	**100**
FORCE (N)	**7670676**	**15959128**	**22973893**	**21325266**	**15497831**	**10293496**	**6580945**
PERCENTAGE	**3.239%**	**6.738%**	**9.699%**	**9.003%**	**6.543%**	**4.346%**	**2.778%**
OFFSET (CM)	**105**	**110**	**115**	**120**	**125**	**130**	**135**
FORCE (N)	**4099680**	**2466090**	**1673746**	**1122151**	**706402.7**	**404828.7**	**206388**
PERCENTAGE	**1.731%**	**1.041%**	**0.707%**	**0.474%**	**0.298%**	**0.171%**	**0.087%**
OFFSET (CM)	**140**	**145**	**150**	**155**	**160**	**165**	**170**
FORCE (N)	**90514.67**	**31546.67**	**0**	**0**	**0**	**0**	**0**
PERCENTAGE	**0.038%**	**0.013%**	**0.000%**	**0.000%**	**0.000%**	**0.000%**	**0.000%**
OFFSET (CM)	**175**	**180**	**185**	**190**	**195**	**200**	**205**
FORCE (N)	**0**	**0**	**0**	**0**	**0**	**1213.333**	**7280**
PERCENTAGE	**0.000%**	**0.000%**	**0.000%**	**0.000%**	**0.000%**	**0.001%**	**0.003%**
OFFSET (CM)	**210**	**215**	**220**	**225**	**230**	**235**	**240**
FORCE (N)	**40586**	**79048.67**	**166621**	**352989**	**573011**	**851174**	**1238396**
PERCENTAGE	**0.017%**	**0.033%**	**0.070%**	**0.149%**	**0.242%**	**0.359%**	**0.523%**
OFFSET (CM)	**245**	**250**	**255**	**260**	**265**	**270**	**275**
FORCE (N)	**1908337**	**3435834**	**6176222**	**9985956**	**15055561**	**20877202**	**22776269**
PERCENTAGE	**0.806%**	**1.451%**	**2.608%**	**4.216%**	**6.356%**	**8.814%**	**9.616%**
OFFSET (CM)	**280**	**285**	**290**	**295**	**300**	**305**	**310**
FORCE (N)	**16428697**	**7983521**	**4001123**	**2539508**	**1685873**	**1049476**	**623124.8**
PERCENTAGE	**6.936%**	**3.371%**	**1.689%**	**1.072%**	**0.712%**	**0.443%**	**0.263%**
OFFSET (CM)	**315**	**320**	**325**	**330**	**335**	**340**	**345**
FORCE (N)	**303181.7**	**166469.3**	**80959.67**	**30818.67**	**10313.33**	**0**	**0**
PERCENTAGE	**0.128%**	**0.070%**	**0.034%**	**0.013%**	**0.004%**	**0.000%**	**0.000%**

The video reference for HHP North bound[5] used and the tire distribution was measured. Table 2-6 and Fig. 2- 14 include this result. The collected data was collected from manual analysis of the car following the video and the accuracy was subject to the video resolution. The maximum tire activation measured 70 centimeters offset for the right tire. The activation offset for the left tire

[5] http://www.youtube.com/watch?v=R-fG_I04-fo&feature=player_embedded and http://www.youtube.com/watch?v=vR7TO5mrZbg&feature=player_embedded

was estimated as 70+w, which is the vehicle width. The maximum activation rate was 11.43%. Comparing the case measure results with VMM indicates:

- The offset with maximum activation has a difference of 100 mm (12.5%)
- Maximum activation rate has a difference of 1.8%
- The measurement was a sample method for a short period of observation time

VMM application for SPM will specify the different roadway activation zoning placement. This placement is used for SPM large system mesh energy resource. VMM will have additional applications for pavement management systems and traffic modeling which can be considered for future work for expansions of VMM applications.

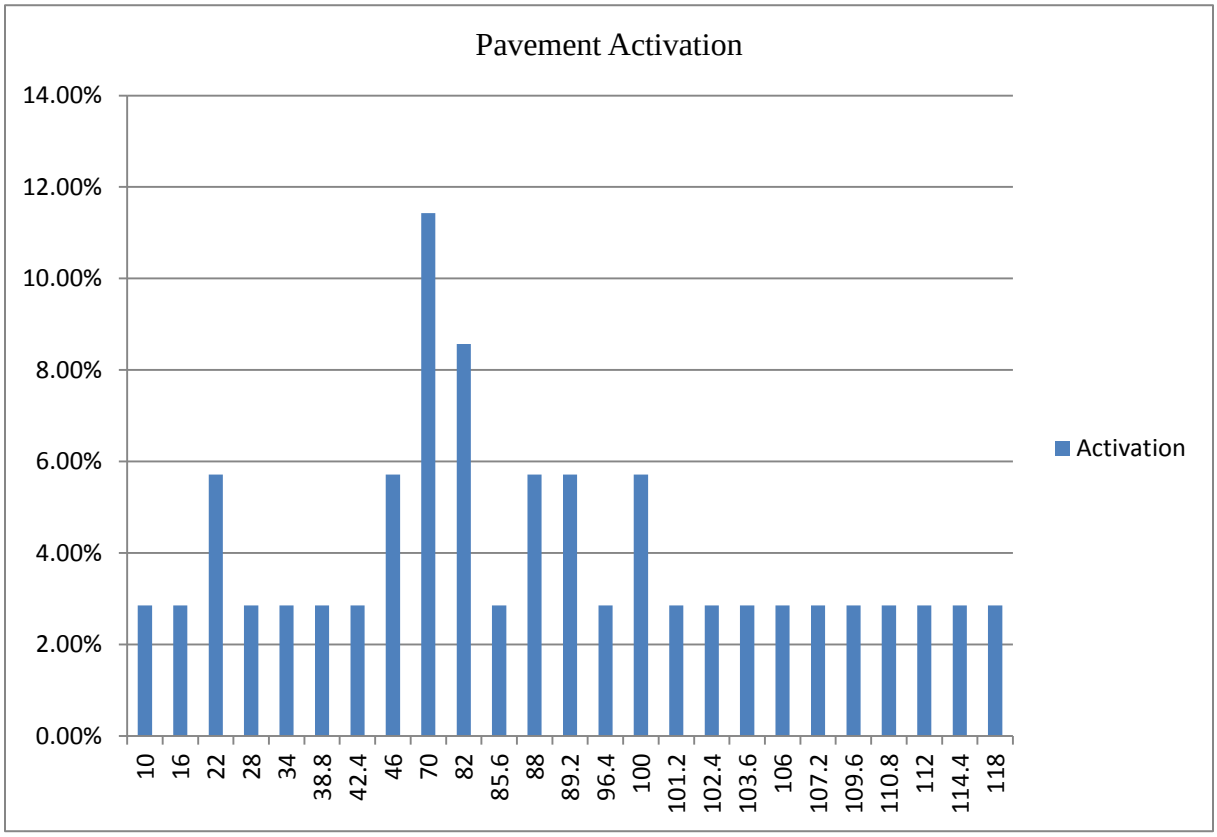

Fig. 2- 14 HHP North Bound Sample Data- A Tire Activation

Table 2- 6 HHP North Bound Sample VMM Assessment[6]

No.	*TIME (Sec)*	*OFFSET (Cm)*	*LANE No.*	*Vehicle Class*	*No.*	*TIME (Sec)*	*OFFSET (Cm)*	*LANE No.*	*Vehicle Class*
1	8	24	1	1	28	218	30	2	1
2	22	50	2	1	29	218	90	3	1
3	23	10	1	1	30	230	50	1	1
4	34	50	2	1	31	230	50	2	1
5	44	27	2	1	32	235	66	1	1
6	52	85	3	1	33	235	90	2	1
7	57	83	2	1	34	240	100	1	1
8	57	60	3	1	35	242	90	2	1
9	66	50	2	1	36	247	60	2	1
10	66	76	3	1	37	247	95	3	1
11	73	84	2	1	38	253	85	1	1
12	73	63	3	1	39	253	65	2	1
13	89	77	3	1	40	253	30	3	1
14	95	75	2	1	41	267	84	2	1
15	95	81	3	1	42	270	100	2	1
16	103	20	1	1	43	270	75	3	1
17	103	66	3	1	44	275	90	3	1
18	108	78	1	1	45	279	92	2	1
19	108	65	2	1	46	295	0	2	1
20	108	109	3	1	47	295	5	3	1
21	119	75	2	1	48	302	5	2	1
22	119	87	3	1	49	310	10	2	1
23	128	72	3	1	50	326	0	2	1
24	162	15	2	1	51	340	100	1	1
25	162	83	3	1	52	342	90	1	1
26	183	80	2	1	53	342	60	2	1
27	183	90	3	1					

[6] Some cells were not considered due to the video quality.

CHAPTER THREE – ROADWAY PAVEMENT MODELS (P – MODELS)

Roadway Pavement Modeling includes an analytical process to describe the design, operation, and performance of roadway pavement. This modeling process was developed for the SPM needs, which includes the SPM nodes placement and energy calculation. The pavement modeling process has been widely used in different applications (generally on a pavement management and design system) and with different approaches (typically finite element or discrete element methods). This study included both flexible and rigid pavements, which are main types of the roadway pavement. Approximately 90% of the highways and roads in the U.S. are paved by hot mix asphalt (HMA). Example of an existing pavement design tool is SuperPave (Superior Performing Asphalt Pavements), which was developed through the TRB program as a set of optimized mix designs and analysis [12].Over the past three decades, many studies and research programs have been investigating the micromechanical behavior of pavement materials and response. Martin et al presented a numerical macro modeling scheme for asphalt concrete based on micromechanical simulation using the finite element method. Their model first incorporates an equivalent lattice network approach whereby the local interaction between neighboring particles is modeled with a special frame type finite element [13]. F. Aragao presented his research work in the microscopic modeling of pavement for developing a computational microstructure modeling framework for evaluating the effects of constituents and mix design characteristics (the key factors directly affecting the quality of the pavement structures) on the mechanical responses of asphalt mixtures [14].During these studies, other pavement modeling, including macro simulation modeling, was investigated. In all cases, the complexity and wide range of the inputs' parameters are noticed. Therefore, it was decided to develop a new modeling approach, which will be more applicable for the SPM. Because of a

variety of the parameters in a roadway pavement, we were considering a hybrid (macro and micro simulation) method that includes (1) pavement classification, (2) pavement layer/structures, (3) a pavement unit and unit distribution, (4) a pavement unit macroscopic model and (5) a microscopic multi-physic modeling for pavement stress/strain physical characteristics.

Under this approach, the Roadway Pavement Modeling design was deployed. In this modeling process, the concepts of the SPM physical placement inside the pavement and analytical results of energy and force transferring to the SPM were evaluated. Advances in micro simulation and multi-physic computational mechanics have led to the development of more accurate modeling, which allow the analyst to account for material gradients and to simulate pavement operational behaviors including fatigue, fracture, and permanent deformation.

3.0 ROADWAY PAVEMENT MODELING CHAPTER OVER VIEW

In this chapter, the base information about the roadway pavement system will be discussed. The purpose of the discussion will be the understanding of the pavement system regarding the SPM applications, operation, maintenance and design. This chapter includes:

- General review of the roadway pavement structure
- General review of the roadway pavement materials
- General review of the roadway pavement design and construction
- General roadway pavement modeling
- SPM and pavement modeling

A typical pavement design process includes (1) review and analysis of the roadway proposed sub-grade competency, (2) traffic analysis including forecasting loads, (3) pavement materials, (4) climate/drainage effects, (5) environmental condition effects, and (6) construction

considerations. For special roadway conditions such as roadway owner's requirements, other factors may be included in that process. The main design factors on a pavement project are sub-grade protection, smoothness, surface friction (skid resistance), and drainage. The application of the SPM can manage operation and maintenance of the pavement by monitoring these factors. The SPM pavement simulation is labeled as P-Modeling work in this report and the results of these models are presented.

3.1 ROADWAY PAVEMENT FOUNDAMENTALS

Pavement modeling is a group of analytical processes for understanding the fundamentals of the pavement in different concepts for design, performance, operation, and maintenance. These modeling efforts have been interesting topics for highway and transportation researchers. Pavement modeling systems use simulation tools and field data measurement for the calibration. These modeling systems apply to the pavement design process for better selection/ control of the material and the construction work. One of the main pavements modeling topics is the pavement materials and their properties' evaluation. The pavement material property characteristic changes are caused by (1) environmental and weathering, (2) pavement aging, (3) traffic loading, and (4) temperature effects. Behavior studies of those factors are interesting topics in the pavement design work.

Pavement materials are generally produced using specific blends of aggregates and quarry fines. Products will vary in terms of grading and often properties depend upon the designated specifications. The two main types of pavement materials are base and sub-base. Base materials are generally covered with a wearing surface comprising of either a sprayed bituminous seal or asphaltic concrete. Base materials are typically 20mm in nominal size. A sub-base layer is

generally below the base course and sub-grade layer of the pavement design. Sub-base materials are generally 40mm-75mm in nominal size.

In this section, we are presenting a description of the major foundation of the roadway pavement modeling. These foundations are a combination of inputs, outputs or process modules of a pavement modeling system. Based on interesting points for SPM, these items are presented. One main pavement modeling foundation that is not discussed here is the modeling related to the pavement deformation and maintenance work which is an actively engrossing research topic today. As part of the future work and part of the SPM application development sub-project, an enhancement of P-Models will be applicable and will be well thought out.

3.1.1 PAVEMENT CATEGORIES

Paved road, with more than 2.5 million lane lines, is one of the main highway infrastructures in the United States. Generally, all hard surfaced pavement types can be grouped into three categories, as, Flexible, Composite, and Rigid Pavement. A Flexible Pavement type (FP) consists of one or more layers of asphalt supported by a granular sub-base. A Composite Pavement type (CP) consists of a flexible surface layer supported by a stiff Portland Cement Concrete (PCC) base. A Rigid Pavement type (RP) consists of a layer of PCC on a granular foundation. The RP category is classified further according to its arrangement of steel reinforcement and joints. [15]

Asphalt concrete surfaced pavements are categorized as being flexible or semi-rigid. A Flexible Pavement is a relatively thin surface of Asphalt Concrete Pavement (ACP) over a base and sub-base resting on a sub-grade. The semi-rigid pavement has a higher modulus of elasticity than a flexible pavement. The elements contributing to the higher modulus may be the increased thickness in asphalt, chemical stabilization of the base, sub-base, and/or sub-grade layers and asphalt stabilization of the base course.

The higher modulus adds to the structural capacity of the pavement layers. The load is thereby distributed over a wider area of the sub-grade. The fundamental differences between a flexible, semi-rigid, and rigid pavement are the load distributions over the sub-grade. In Flexible Pavements, layers of bituminous (or asphalt) materials are surfaced. These can be either in the form of pavement surface treatments (such as a Bituminous Surface Treatment (BST) generally found on lower volume roads), or, Hot Mix Asphalt (HMA) surface courses (generally used on higher volume roads such as the interstate highway network). These types of pavements are called "flexible" since the total pavement structure "bends" or "deflects" due to traffic loads.

A flexible pavement structure is generally composed of several layers of materials which can accommodate this "flexing". Flexible pavements comprise about 93% of US paved roads. Flexible pavements are so named because the total pavement structure deflects, or flexes, under loading. A flexible pavement structure is typically composed of several layers of materials. Each layer receives the loads from the above layer, spreads them out, and then passes on these loads to the next layer below. Thus, the further down in the pavement structure a particular layer is, the fewer loads (in terms of force per area) it must carry. Fig. 3- 1 illustrates a load distribution pattern in a FP.

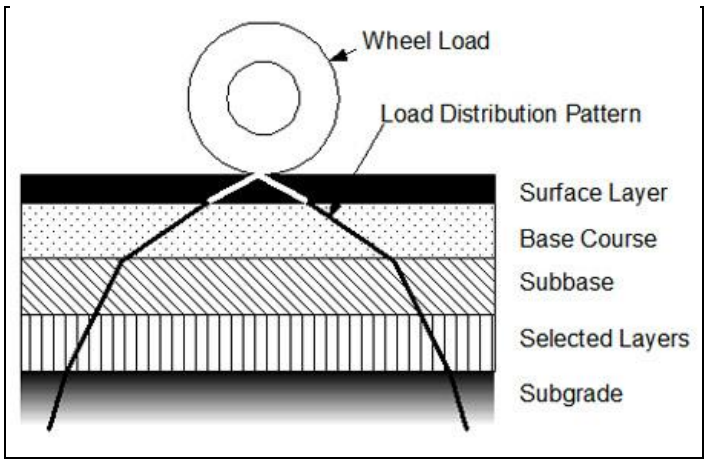

Fig. 3- 1 A Load Distribution Pattern in a Flexible Pavement [**16**]

Hot Mix Asphalt (HMA), which is referred above, is a bituminous concrete made principally from asphalt binding agents and aggregate. It is distinguished from other bituminous products by its constituent materials (asphalt and aggregate), mixture design methods and elevated mixing temperature (thus the term "hot mix"). Although it is known by many different names such as hot mix, asphalt concrete (AC or ACP), asphalt, blacktop or bitumen, it is referred as HMA in this report. The six types of HMA defined as asphalt surfaced pavements are:

- Tin HMA concrete (< 2 inches) above granular base
- Intermediate HMA concrete (5 to 15 cm) above granular base
- Thick HMA concrete (> 15 cm) (semi-rigid)
- Surface HMA treated above granular base
- Thin HMA concrete above chemically stabilized base or sub-base (semi-rigid)
- Thin HMA above asphaltic bound base (semi-rigid)

Stabilization of the sub-grade layer can apply to any of the above pavement types. Typical stabilizers include asphalt cement (for base only), lime, and fly ash.

Rigid Pavements (RP) are composed of a PCC surface course. Such pavements are substantially "stiffer" than flexible pavements due to the high modulus of elasticity of the PCC material. RP may or may not incorporate underlying layers of stabilized or unsterilized granular materials. Since PCC is quite stiff, rigid pavements do not flex appreciably to accommodate traffic loads. Further, these pavements can have reinforcing steel which is generally used to reduce or eliminate joints. Rigid pavements comprise 7% of US paved roads.

Rigid pavements are so named because the pavement structure deflects very little under loading due to the high modulus of elasticity in their surface course. A rigid pavement structure is typically composed of a PCC surface course built on top of either (1) the sub-grade or (2) an

underlying base course. Because of its relative rigidity, the pavement structure distributes loads over a wide area with only one, or at most two structural layers. Each of these pavement types distributes its load over the sub-grade in a different fashion. Rigid pavement, because of PCC's high elastic modules (stiffness), tends to distribute the load over a relatively wide area of sub-grade. The concrete slab itself supplies most of the rigid pavement's structural capacity. Flexible pavement uses more flexible surface course and distributes loads over a smaller area. It relies on a combination of layers for transmitting the load to the sub-grade. [17]

The increased rigidity of concrete allows the concrete surface layer to bridge small weak areas in the supporting layer through what is known as beam action. This allows the placement of rigid pavements on relatively weak supporting layers, as long as the supporting layer material particles will not be carried away by water forced up by the pumping action of wheel loads. Fig. 3- 2 illustrates a load distribution pattern in an RP.

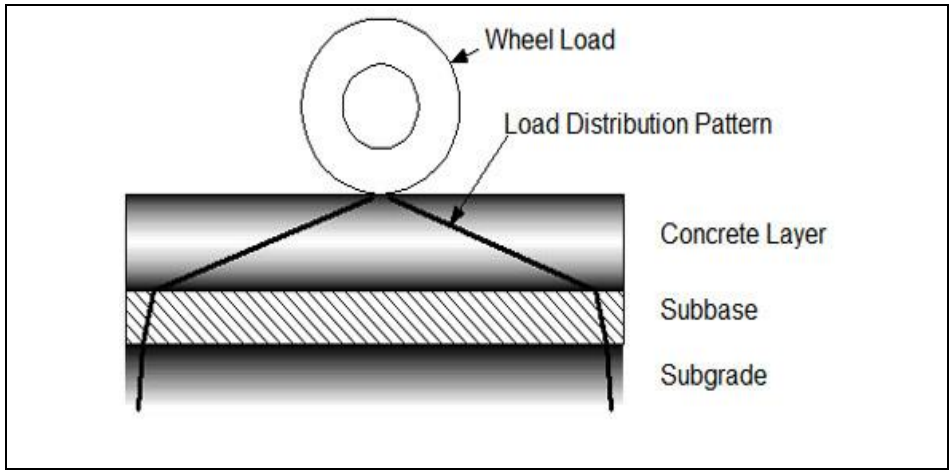

Fig. 3- 2 A Load Distribution Pattern in a Rigid Pavement [16]

Pavements selection can be divided into two different categories, depending on the traffic loading from a low volume road to an extremely heavy traffic road. Flexible and rigid pavements are constructed to accommodate these wide traffic ranges. The main traffic factors for the

selecting a pavement classes are (1) Average Daily Traffic (ADT), (2) Annual Average Daily Traffic (AADT), and (3) Annual Average Daily Truck Traffic (AADTT) or percent of trucks. Based on the current traffic data, the future traffic will be projected. The traffic projection will depend on the traffic planning study and rate of traffic growth. The projected data will be used for pavement design.

3.1.2 PAVEMENT STRUCTURE

3.1.2.1 FLEXIBLE PAVEMENT STRUCTURE

The general description of Flexible Pavement structure was described in this section. In Fig. 3- 3, an example of flexible pavement (FP) is shown with 6 different layers of materials. It is our expectation that most SPM will be placed in the surface layer of the pavement structure on the existing roadway. The cost of installation of the SPM nodes at lower layers (base and sub-base) will be extremely expensive. However, few installations of the SPM node at lower layers of the pavement may be applicable. These nodes will sense the structure information that will be used for pavement rehabilitation. For a new roadway, placement of the SPM at lower layers (base and sub-base) can be considered.

3.1.2.1.1 FP-SUBGRADE

Sub-grade soil conditions vary widely across roadway networks. The soil can be classified according to different types of pavement design, a soil classification with three broad categories based on strength and stiffness. The sub-grade materials' physical properties are typically characterized by the resistance to deformation under load, (stiffness), and the bearing capacity, (strength). In general, the more resistant to deformation a sub-grade is the more loads it can support before reaching a critical deformation value. Although there are other factors involved when evaluating sub-grade materials (such as shrink/swell in the case of certain clays and ash),

stiffness is the most common parameter. The main physical sub-grade classes in the US are CBD[7], R-Value[8], M_R[9] and are listed in Table 3- 1. A sub-grade should be categorized based on its strength or stiffness and not its soil type alone. Thus in the modeling process, a sub-grade soil primarily classified in the Unified Soil Classification (USC) system is described as the strength and stiffness of the soil which are also required as input parameters. The "Poor" classification shown in the table, below, is meant to describe sub-grades with low strength and stiffness values and/or high fines content.

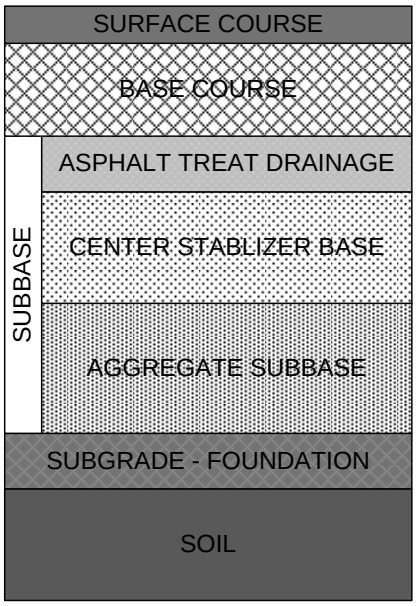

Fig. 3- 3 Example of Flexible Pavement Structural Layers

[7] California bearing ratio (CBR). A simple test that compares the bearing capacity of a material with that of a well-graded crushed stone (thus, a high quality crushed stone material should have a CBR of about 100%). CBR is basically a measure of strength. It is primarily intended for, but not limited to, evaluating the strength of non-stabilized cohesive materials having maximum particle sizes less than 0.75 inches (AASHTO, 2000).

[8] Resistance value (R-Value). A test that expresses a material's resistance to deformation as a function of the ratio of transmitted lateral pressure to applied vertical pressure. It is essentially a modified triaxial compression test. Materials tested are assigned an R-value. The R-Value is basically a measure of stiffness.

[9] Resilient modulus (M_R). A test used to estimate elastic modulus (a material's stress-strain relationship). The resilient modulus test applies a repeated axial cyclic stress of fixed magnitude, load duration and cycle duration to a cylindrical test specimen. Resilient modulus is basically a measure of stiffness.

3.1.2.1.2 FP-AGGREGATE BASE

Aggregate base refers to crushed aggregate untreated base. The minimum recommended crushed aggregate base thickness is 10 cm, however lower is possible.

Table 3- 1 Design Catalog Sub-grade Classification [17]

Classification	CBR	R-Value	M_R (psi)	Typical Description (by USC)
Good	10 or greater	25 or greater	20,000	Gravels, crushed stone and sandy soils. GW, GP, GM, SW, SP, SM soils are often in this category.
Fair	5 - 9	12 - 24	10,000	Clayey gravel and clayey sand, fine silt soils. GM, GC, SM, SC soils are often in this category.
Poor	3 - 5	5 - 12	5,000	Fine silty sands, clays, silts, organic soils. CL, CH, ML, MH, CM, OL, OH soils are often in this category.

3.1.2.1.3 FP-CEMENT STABILIZED BASE

The term stabilized base refers to a class of paving materials that are mixtures of one or more sources of aggregate and cementations material(s) blended with a sufficient amount of water that result in a mixture having a moist, non-plastic consistency that can be compacted to form a dense mass and gain strength. This class of base or sub base materials is not meant to include the stabilization of soils or aggregates using asphalt cement or emulsified asphalt. Soil-cement (or cement-treated base) is probably the earliest example of a stabilized base material. Roller-compacted concrete, which is similar to, but more granular than soil-cement, is another type of stabilized base product. Probably the most frequently used type of stabilized base materials are the basic lime (and/or cement) fly ash-aggregate family of mixtures which can use many different combinations of reagents(s) and aggregate(s) together with coal fly ash. Calcium chloride has also been used to a lesser degree in some of the warmer regions of the country for mechanical stabilization of densely-graded aggregate base courses. [18]

The purpose of a stabilized base or sub-base layer is to provide transitional load-bearing strata between the pavement layer, which directly receives the wheel loadings of vehicular traffic and

the underlying sub-grade soil. Stabilized base or sub base materials may be used to provide support for either flexible or rigid pavements, but are more frequently used with flexible pavements. Stabilized base or sub-base materials are either mixed in place at the job site or are mechanically combined in a mixing plant and transported to the site. These materials are spread evenly in loose layers on a prepared sub-grade or sub-base using either a blade-grader bulldozer, spreader box, or paving machine. Once the material has been spread, it will be compacted by means of conventional rollers of compaction equipment. [18]

3.1.2.1.4 FP-BBASE MIX

The base mix layer is the layer immediately beneath the surface course. It provides additional load distribution and contributes to drainage. Base courses are usually constructed out of crushed aggregate or HMA. The base course provides the strength of the pavement and typically has an aggregate top size of 3/4 to 1 inch. Base mix course applications may involve multiple layers, with the maximum layer thickness being largely determined by practical placement considerations taking into account the total asphalt thickness and ability to achieve the required finished shape and riding qualities. For most applications, 20 mm is selected as the largest nominally sized mix [19]. A guide to typical layer thickness is shown in Table 3- 2.

Table 3- 2 Typical Asphalt Layer Thickness as a Function of Nominal Mix Size [20]

Nominal Mix Size (mm)	Compacted Layer Thickness (mm)
5	15-20
7	20-30
10	25-40
14	35-55
20	50-80
28	70-110
40	100-160

Notes: (1) The minimum thickness may need to be increased when placing thin layers in cool conditions or using less workable mixes. (2) Minimum thickness may not apply to some ultra-thin asphalt applications. (3) Maximum thickness may be exceeded provided that asphalt surface shape requirements can be adequately achieved.

3.1.2.1.5 FP-SURFACE MIX / SURFACE COURSE

The surface or wearing course is the top course of the pavement that acts as the riding surface and protects the underlying pavement structure. The surface course is usually, but not always designed to be impervious to the ingress of water, has an even, running surface that is durable, has a high resistance to skidding, and be chosen so as not to deform under the weight of traffic appropriate to the road. In wearing and intermediate course applications, the maximum compacted layer thickness is generally limited to around four times the nominal mix size. Greater thicknesses may be used to achieve practical placing thickness, for example a requirement for 50 mm of 10 mm asphalt is better achieved with one 50 mm layer than with two 25 mm layers. Where the layer thickness exceeds four times the nominal size, it may be more cost effective to use a larger nominal size mix, although larger sized mixes are also more prone to segregation and may not necessarily provide the surface finish that is required.

3.1.2.2 RIGID PAVEMENT STRUCTURE

A Rigid Pavements structure deflects very little under loading due to the high modulus of elasticity of its surface course. A rigid pavement structure is typically composed of a PCC [20], surface course built on top of either the sub-grade or an underlying base course. Because of its relative rigidity, the pavement structure distributes loads over a wide area with only one, or at most two, structural layers. Fig. 3- 4 shows the basic layers in a RP roadway. Besides the sub-grade layer described before, the three main layers in RP structure are described [20]:

- **Surface course**, the top layer consists of the PCC slab.
- **Base course**, the layer directly below the PCC layer, generally consists of aggregate or stabilized sub-grade.
- **Sub-base course**, the layer/s under the base layer is not always needed and therefore may often be omitted.

A typical rigid pavement structure similar to Fig. 3- 4 consists of the surface course and the underlying base and optional sub-base courses. The PCC surface course is the stiffest and provides the majority of strength. The underlying layers are orders of magnitude less stiff but still make important contributions to pavement strength as well as drainage and frost protection.

3.1.2.2.1 RP SURFACE COURSE

The surface course is the layer in contact with traffic loads and is made of PCC. It provides characteristics such as friction, smoothness, noise control, and drainage. In addition, it serves as a waterproofing layer to the underlying base, sub-base and sub-grade. The surface course can vary in thickness but is usually between 150 mm (six inches) (for light loading) and 300 mm (12 inches) (for heavy loads and high traffic).

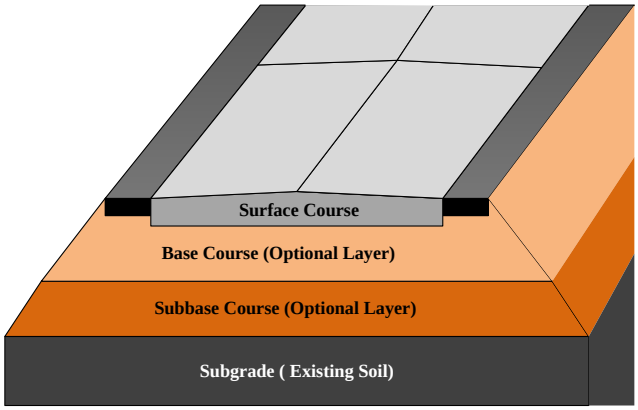

Fig. 3- 4 General Rigid Pavement Structure Layers

3.1.2.2.2 RP BASE COURSE

The base course is immediately beneath the surface course. It provides (1) additional load distribution, (2) drainage and frost resistance, (3) uniform support to the pavement. and (4) a stable platform for construction equipment. Bases also help prevent sub-grade soil movement due to slab pumping. Base courses are usually constructed out of:

- Aggregate base. A simple base course of crushed aggregate has been a common option since the early 1900s and is still appropriate in many situations today.

- Stabilized aggregate or soil. Stabilizing agents are used to bind otherwise loose particles to one another, providing strength and cohesion. Cement treated bases (CTBs) can be built to as much as 20 - 25 percent of the surface course strength (FHWA, 1999).
- Densely-graded HMA. In situations where high base stiffness is desired, base courses can be constructed using a densely-graded HMA layer.
- Permeable HMA. In certain situations where high base stiffness and excellent drainage is desired, base courses can be constructed using an open graded HMA.
- Lean concrete. A lean concrete contains less Portland cement paste than a typical PCC and is stronger than a stabilized aggregate. Lean concrete bases (LCBs) can be built to as much as 25 – 50% of the surface course strength (FHWA, 1999).

3.1.2.2.3 RP SUB-BASE COURSE

The sub-base course is the portion of the pavement structure between the RP-Base Course and the RP-sub-grade Course. It functions primarily as structural support but it can also minimize the intrusion of fines from the sub-grade into the pavement structure, improve drainage, minimize frost action damage, and provide a working platform for construction. The sub-base generally consists of lower quality materials than the base course but better than the sub-grade soils. A sub-base course is not always needed or used.

3.1.3 PAVEMENT MATERIALS

The performance of asphalt in service significantly depends on the mechanical or physical properties of the materials and, to a lesser extent, the chemical constitution of the asphalt bitumen. To understand these behaviors, it is best to describe the material classification and their modeling which would describe the behavior of all types of asphalt concrete with the input data and experimental field test data. This section is a collection of roadway pavement material

descriptions. The section includes two main sub-sections for flexible and rigid pavement. The information in this section is the pavement foundational information gathered from references. Pavement material information was used in the SPM macro modeling process for development of pavement unit emulation circuit, which is described in next sections.

3.1.3.1 FLEXIBLE PAVEMENT AGGREGATE

Aggregate is a collective term for the mineral materials such as sand, gravel and crushed stone that are used with a binding medium (such as water, bitumen, Portland Cement, lime, etc.) to form compound materials (such as asphalt concrete and PCC). By volume, aggregate generally accounts for 92% to 96% of HMA and about 70% to 80% of PCC. Aggregate is also used for base and sub-base courses for both flexible and rigid pavements. Aggregates can either be natural or manufactured. Natural aggregates are generally extracted from large rock formations in an open excavation (quarry). Extracted rock is typically reduced to usable sizes by mechanical crushing. Manufactured aggregate is often the byproduct of other industries. Aggregate physical properties are the most readily apparent aggregate properties and they also have the most direct effect on how an aggregate performs as either a pavement material constituent or by itself as a base or sub-base material.

3.1.3.2 FLEXIBLE PAVEMENT ASPHALT BINDER

Asphalt binders are produced mainly by petroleum refiners and, to a lesser extent, by formulators who purchase blending stock from refiners. Until recently, binder specifications were relatively lenient and gave refiners a high level of production flexibility. Therefore, refiners tended to view asphalt as a simple, convenient way to use the residual material from the refinery operation. As a result of the new super-pave specification, asphalt refiners increasingly perceive asphalt as a value-added product. It also has caused many refiners to reevaluate their commitment to asphalt

production; some have made a strategic decision to de-emphasize or cease asphalt production, though others have renewed their efforts to produce high-quality binders. Understanding the chemistry and microstructure of asphalt is critical in the development and improvement of performance-based specifications. The environmental factors that cause asphalt oxidation and moisture-associated effects, for example, vary across the United States. The conditioning schemes used in the specifications need to reflect the environment more accurately. Therefore, existing oxidation models must be modified and new models must be developed to reflect the effects of moisture on asphalt pavements. [21].

3.1.3.3 RIGID PAVEMENT MATERIALS

In section 3.1.2.2 RIGID PAVEMENT STRUCTURE, the structure of typical RP was described. A RP main material is PCC at the surface course. The American Concrete Institute (ACI)'s PCC mix materials are discussed here. The ACI method is a widely accepted method in the US and continually updated by the ACI. As discussed before, RP protect the surface load defect due to its high value of modules of elasticity. Elastic modulus is sometimes called Young's Modulus after Thomas Young who published the concept in 1807. An elastic modulus (E) can be determined for any solid material and represents a constant ratio of stress and strain (stiffness).

A material is elastic if it is able to return to its original shape or size immediately after being stretched or squeezed. Almost all materials are elastic to some degree as long as the applied load does not cause it to deform permanently. Thus, the "flexibility" of an object or structure depends on its elastic modulus and geometric shape. The modulus of elasticity for a material is basically the slope of its stress-strain plot within the elastic range. It is important to remember that a measure of a material's modulus of elasticity is not a measure of strength. Strength is the stress

needed to break or rupture a material, whereas elasticity is a measure of how well a material returns to its original shape and size. Some typical Elastic modules are shown in Table 3- 3.

3.1.3.4 RIGID PAVEMENT AGGREGATE

The aggregate particle size distribution or gradation is one of the most influential aggregate characteristics in determining how it will perform as a pavement material. Maximum aggregate size will be the PCC parameters in the amount of cement paste and will affect PCC properties including its strength. In general, ACI recommends that maximum aggregate size be limited to 1/3 of the slab depth and 3/4 of the minimum clear space between reinforcing bars. Aggregate larger than these dimensions may be difficult to consolidate and compact resulting in a honeycombed structure or large air pockets. PCC maximum aggregate sizes are on the order of 25 mm to 37.5 mm[10].

Table 3- 3 some typical materials' Elastic Modules

	Elastic Modules	
Materials	**Mpa**	**Psi**
Diamond	1,200,000	170,000,000
Steel	200,000	30,000,000
Aluminum	70,000	10,000,000
Wood	7,000-14,000	1,000,000-2,000,000
Crushed Stone	150-300	20,000-40,000
Silty Soils	35-150	5,000-20,000
Clay Soils	35-100	5,000-15,000
Rubber	7	1,000

[10]ACPA, 2001

Table 3- 4 Volume of Course Aggregate per Unit Volume of PCC

Nominal Max Aggregate Size	***Fine Aggregate Fineness Modulus***			
	2.40	**2.60**	**2.80**	**3.00**
9.5 mm (0.375 inches)	0.50	0.48	0.46	0.44
12.5 mm (0.5 inches)	0.59	0.57	0.55	0.53
19 mm (0.75 inches)	0.66	0.64	0.62	0.60
25 mm (1 inches)	0.71	0.69	0.67	0.65
37.5 mm (1.5 inches)	0.75	0.73	0.71	0.69
50 mm (2 inches)	0.78	0.76	0.74	0.72

Notes: (1) These values can be increased by up to about 10 percent for pavement applications. (2) Coarse aggregate volumes are based on oven-dry-rodded weights obtained in accordance with ASTM C 29.

Thus, even a small amount of particles passing the 0.075-mm (#200) sieve results in very low permeability. Fine aggregate is other parameters in the PCC volume content, which is described as gradient and falls mostly above the 0.45 power maximum density line when plotted on the 0.45 power gradation graph[11]. The graph shows some typical aggregate.

Table 3- 4 shows ACI recommended values of the gradations and their associated permeability.

[11] **0.45 Power Maximum Density Curve,** In the early 1960s, the FHWA introduced the standard gradation graph used in the HMA industry today. This graph uses n = 0.45 and is convenient for determining the maximum density line and adjusting gradation (Roberts et al., 1996). This graph is slightly different than other gradation graphs because it uses the sieve size raised to the n^{th} power (usually 0.45) as the x-axis units.

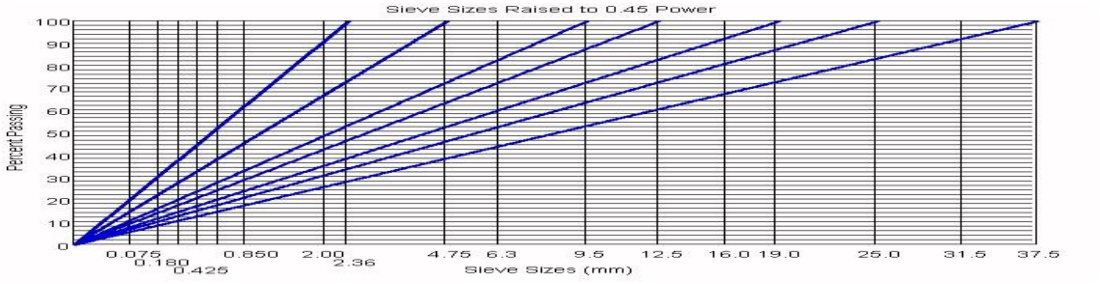

3.1.3.5 RIGID PAVEMENT CEMENT

Cement content is determined by comparing the following two items: Item one, the calculated amount, based on the selected mixing water content and water-cement ratio, and Item two, the specified minimum cement content, if applicable. Most state transportation agencies specify minimum cement contents in the range of 300 - 360 kg/m^3 (500 - 600 lbs/yd^3). The water-cement ratio is a convenient measurement, the value of which is well correlated with PCC strength and durability. In general, lower water-cement ratios produce stronger, more durable PCC. If natural pozzolans are used in the mix (such as fly ash), then the ratio becomes a water-cementitious material ratio (cementitious material = Portland cement + pozzolonic material). The ACI method bases the water-cement ratio selection on desired compressive strength and then calculates the required cement content based on the selected water-cement ratio. Table 3- 5 provides a general estimate of 28-day compressive strength vs. water-cement ratio (or water-cementitious ratio). Values in this table tend to be conservative (ACI, 2000). Based on the ACPA 2001, most state DOTs tend to set a maximum water-cement ratio between 0.40 - 0.50.

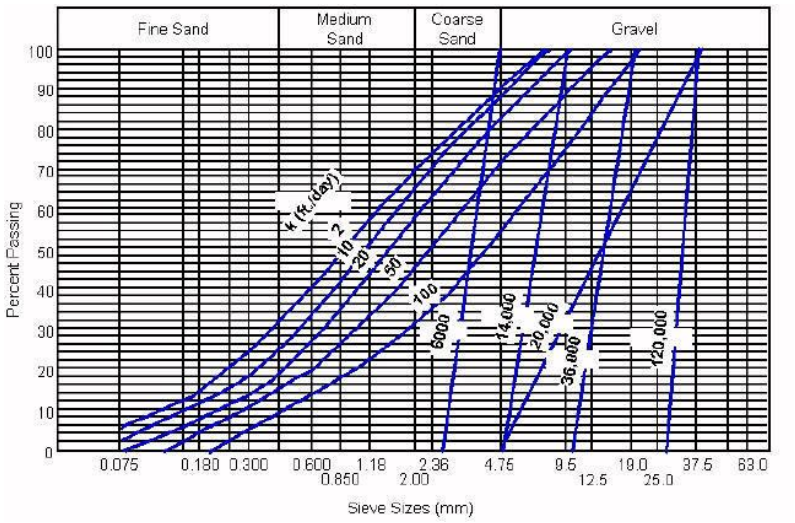

Fig. 3- 5 Typical Aggregate Gradations and Permeability (after Ridgeway, 1982)

3.1.3.6 WATER AND AIR CONTENT

Water is one of the factors affecting the dynamic slump. Also, pavement PCC is almost always air-entrained, so air-entrained values are most appropriate. Based on the ACPA 2001 data, state agencies specify between four and eight percent air by total volume. Note that the use of water-reducing and/or set-controlling admixtures can substantially reduce the amount of mixing water that is required to achieve a given slump.

Table 3-6 is adapted from ACI 2001. At this point, all other constituent volumes have been specified (water[12], Portland cement, air and coarse aggregate). Thus, the fine aggregate volume is just the remaining volumes of mixing water, air, Portland cement, coarse aggregate and fine aggregate.

Table 3- 5 Water -Cement Ratio and Compressive Strength Relationship

28-Day Compressive Strength psi)	***Water-cement ratio by weight***	
	Non-Air-Entrained	**Air-Entrained**
41.4 (6000)	0.41	-
34.5 (5000)	0.48	0.40
27.6 (4000)	0.57	0.48
20.7 (3000)	0.68	0.59
13.8 (2000)	0.82	0.74

[12] Unlike HMA, PCC batching does not require dried aggregate. Therefore, aggregate moisture contain must be accounted for. Aggregate moisture affects the following parameters:

1. **Aggregate weights**. Aggregate volumes are calculated based on oven dry unit weights, but aggregate is typically batched based on actual weight. Therefore, any moisture in the aggregate will increase its weight and stockpiled aggregates almost always contain some moisture. Without correcting for this, the batched aggregate volumes will be incorrect.
2. **Amount of mixing water**. If the batched aggregate is anything but saturated surface dry it will absorb water (if oven dry or air dry) or give up water (if wet) to the cement paste. This causes a net change in the amount of water available in the mix and must be compensated for by adjusting the amount of mixing water added.

Table 3- 6 Approximate Mixing Water and Air Content Requirements for Different Slumps and Maximum Aggregate Sizes [6]

	Mixing Water Quantity in kg/m^3 (lb/yd^3) for the listed Nominal Maximum Aggregate Size							
	9.5 mm	12.5 mm	19 mm	25 mm	37.5 mm	50 mm	75 mm	100 mm
Non-Air-Entrained PCC								
25 - 50 (1 - 2)	207 (350)	199 (335)	190 (315)	179 (300)	166 (275)	154 (260)	130 (220)	113 (190)
75 - 100 (3 - 4)	228 (385)	216 (365)	205 (340)	193 (325)	181 (300)	169 (285)	145 (245)	124 (210)
150 - 175 (6 - 7)	243 (410)	228 (385)	216 (360)	202 (340)	190 (315)	178 (300)	160 (270)	-
Typical entrapped air (percent)	3	2.5	2	1.5	1	0.5	0.3	0.2
Air-Entrained PCC								
25 - 50 (1 - 2)	181 (305)	175 (295)	168 (280)	160 (270)	148 (250)	142 (240)	122 (205)	107 (180)
75 - 100 (3 - 4)	202 (340)	193 (325)	184 (305)	175 (295)	165 (275)	157 (265)	133 (225)	119 (200)
150 - 175 (6 - 7)	216 (365)	205 (345)	197 (325)	184 (310)	174 (290)	166 (280)	154 (260)	-
Recommended Air Content (percent)								
Mild Exposure	4.5	4.0	3.5	3.0	2.5	2.0	1.5	1.0
Moderate Exposure	6.0	5.5	5.0	4.5	4.5	4.0	3.5	3.0
Severe Exposure	7.5	7.0	6.0	6.0	5.5	5.0	4.5	4.0

3.2 PAVEMENT RESPONSE MACRO/MICRO MODELS: P-MODELS

P- Models are a family of the simulation models describing the pavement energy absorption/ conversion/transfer response for the SPM feasibility study. These models also are the guide line tools for SPM placement and furnishing design. The descriptions here are general algorithmic layout of models and the actual deployed models maybe slightly different due to the simulation software limits.

3.2.1 P-MODEL REVIEW

Pavement type, structure, materials and mixing properties are the key components of the pavement behavior actions study. P-models describe the pavement displacement responses due to real traffic conditions or traffic information from M-models. P-models analysis includes other effects such as stress, strain, and response time, which depend on the field of study and its application. In the SPM project case, we are interested in the displacement and energy transferring impact of the pavement response on the different pavement layers (surface and base layers).

The P-Models are described in two stages, Macro and Micro modeling procedures. The macro modeling includes a multi series of modeling steps. Pavement unit (PU) is a small physical geometry of pavement. An array of these PUs will make a pavement layer. Each layer of a pavement structure will be represented with a different array of the PU. Each PU is modeled separately and emulated with a macro model and a transfer function. Based on the pavement material distribution, All PUs are grouped into a limited number of PU classes at each layer. One emulation function represents each PU class. The second modeling step is a pavement PU assembly model. The pavement assembly model uses a random distribution function to assign the PU classes to the pavement PU array (see Fig. 3- 6). Each PU class has a specific transfer

function with variables such as (a) displacement, (b) strain, and (c) stress. The main benefits of these models are less complexity and a faster solution. However it should be considered that these P-models are developed for the SPM application and further works for generalizing them to other applications shall be considered as a future work. P-models for other applications may require different assembly models and different macro emulation models. The second P modeling procedure is a micro simulation with Finite Element analysis. The existing multi physics simulation tools such as Comsol or Ansys are considered. The micro modeling is used to specify the emulated function. The main challenge in this method is the complexity of the model that will limit the simulation tools.

3.2.2 MACRO P-MODEL DESCRIPTION

Complexity and large size of the simulation environments are the main problems for the simulation of the pavement. A better review of the complexity is provided by looking at some dimensions of the pavement simulation. In typical pavement RP or FP, the minimum size of the aggregate may be in the range of several millimeters (2 to 20 mm) and its shape has (a) random shaping, (b) non symmetric and (c) multiple faces (more than 6). A small pavement simulated segment may have a length equal to four or more vehicle lengths. This segment will have a length from 30 m to 100 m. SPM structure will utilize the multiple layers of micro structure from different semiconductor materials such as silicon, oxide, polymers or a piezoelectric. These device layers will have a thickness of micron or sub-micron[13] size. Therefore the size of a finite element simulation that meshes will be significantly large.

Macro modeling approach was proposed to simplify the simulation process in two levels of the sub-simulation process. Fig. 3- 6 presents the overall viewing of a pavement structure. Each

[13] Dependence on the proposed SPM charger structure and technology used will be described in chapter 4.

pavement layer is partitioned into a smaller unit, which is called a PU. PU is our macro simulated element. The dimensions of a PU depend on (a) pavement layer, (b) materials type, (c) the sizes of the material components or maximum aggregate sizes, (d) material distribution, and (e) the simulation accuracy. A pavement with a uniform constructed layer will require less number of PUs with larger sizes. Each PU has carried a class of emulated function. A simulated pavement section has an array of PU, which are distributed randomly. Fig. 3- 6 shows an example of such a segment. The material components are varied for each layer of the pavement structure, thus the different PU elements are considered for each pavement layer. The process of Macro P-Modeling will include the following procedures:

- Material Determination
- Roadway Segmentation
- Pavement Unit Determination
- Roadway Segment Meshing
- Pavement Unit Element Simulation
- Pavement Unit Element Transfer Function Determination
- Pavement Unit Element Boundary Determination
- Pavement Unit Element with SPM Simulation
- Pavement Unit Element with SPM Transfer Function Determination
- Pavement Unit Element with SPM Boundary Determination
- Roadway Segment Pavement PU Assembly
- Assemble PU Mesh Network Simulation
- SPM Boundary Force/Strain/Stress Determination

In most cases, the input parameters for the model are roadway geometry and material. This information is used for roadway segmentation and mesh assembly, as listed above. The shape and geometry of the material components and their properties are used for pavement unit (PU) simulation and specifying the PU emulated function. Appendix 11 PAVEMENT GEOMETRY PARAMETERS presents pavement material and geometry input information.

The P-Modeling outputs determine the estimate of the mechanical energy for the SPM micro charger. The mechanical function is time dependent and its effect on the SPM charger will depend on the SPM placement orientation. The following sections will discuss (a) the description of the models parameters, (b) the definition of sub-models and the algorithms, (c) discussion of the models operation, and (d) some case study results. The P-Model modules are identified by a unique calling number and are referenced in the design.

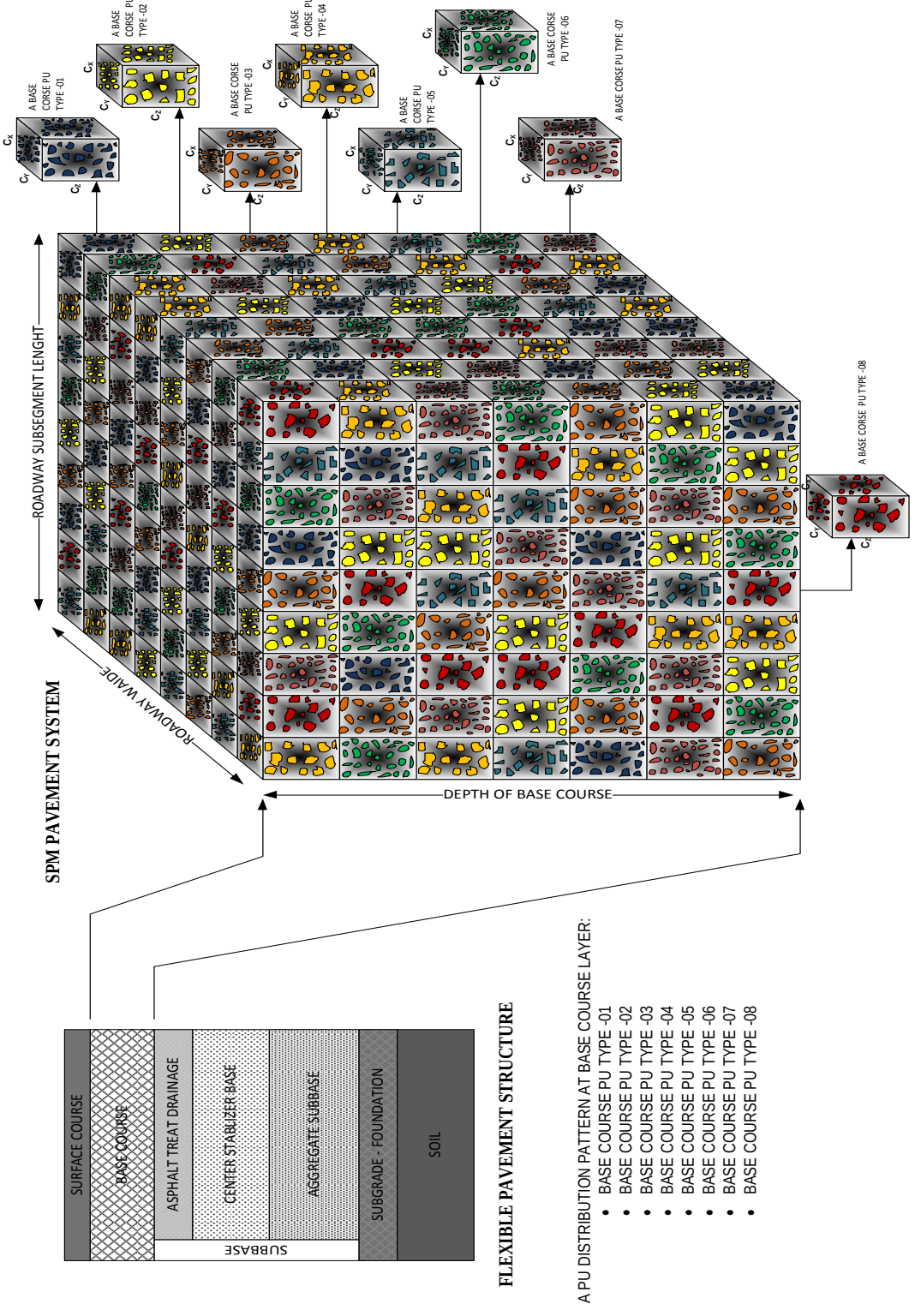

Fig. 3- 6 Pavement Surface Layer simulated of the Pavement Unit mesh network (Four Pavement Unit Distribution Pattern)

3.2.3 P-MODEL-00: PAVEMENT ASSEMBLY MODULE (PAM)

PAM is the core calling process for P-modeling. This model is the main interface with the user. PAM includes the collection of subroutines related to (a) filtering the inputs, (b) the internal flow chart, and (c) output analysis of the P-models. The PAM components are:

- Input Data Recall (Dynamic Axles Time Traveling Data) and the resulting M-Model will be needed for interfacing (inputs) to P-Model series. The M-Model provides the dynamic force movement transition data. This input data will be dependent on the time and position (X and Y dimensions). M- Models are MATLAB models developed as part of M-Model[14]
- Input Pavement Static Information, that is, pavement classified data including type, materials, distribution and structures were developed in an input library to be used by the P-Model series. The pavement information has been processed to convert into simple form data.
- Output Data assembly includes interfaces for conversion of the P-Models outcome to the specific applications. There are two main applications for P-Models outcome, which are the design for SPM (used in S- Model Simulation) and pavement management (to be used in a future application).

3.2.4 PAVEMENT GEOMETRY MODELING

This Section is a description of all geometry modeling for the complete pavement simulation. The geometries in a large view start with a roadway segmentation process. For a roadway with specific alignment, this information includes (a) segment length, (b) number of lanes, (c) lane widths, (d) slope, (e) cross section slop, (f) in and off ramp, and (g) carve. The geometry not only inputs to the P-models but also affects the traffic profile in the M-models. The roadway

[14] See SPM Report 4- Vehicle Mobility Models for details of the M-Models

geometry is modeled and the segmentations are generated. The geometry parameters of each segment are uniform which means the length of segments will not be constant.

The segmentation model is followed with a sub-segmentation model. The sub-segmentation is considered to reduce the simulation processing time. In addition, some secondary geometry parameters can be modified in the sub-segmentation model. Secondary parameters are less important geometry information, which are estimated with an average during the segmentation modeling. The segmentation and sub-segmentation inputs can be imported by local or state roadway information systems such as existing GIS database or the Roadway Straight Line Diagram Data.

After completion of the sub-segmentation modeling, the Pavement Unit distribution model will be executed to distribute the PU classes' assignment. As discussed, number of PU classes defined by: (a) pavement type (rigid or flexible), (b) pavement courses (surface, base, sub-base) and (c) material type. For a faster simulation process, it is important to optimize the number of PU classes. The optimum PU classes are a tradeoff between simplicity and accuracy of the modeling. The next geometry sub-model defined the PU dimensions. This sub-model specified the PU that can be simulated with a finite element tool such as Comsol. Finally, roadway assembly model will be used to link the PU emulated transfer functions together based on the PU placements at a sub-segment The P-Model-01 to 05 present in the Pavement Geometry Modeling.

3.2.4.1 P-MODEL-01: PAVEMENT SEGMENTATION MODULE (PSM)

Most roads have different geometry profile and cross sections that vary based on the land use, geotechnical condition of the road, and the design requirement of the road. The major parameters in our study are:

- Number of lanes
- Major increase/decrease of lanes wide
- Entry ramp
- Exit ramp
- Highway interchanges
- Pavement type changes
- Vertical slope (a future factor for the model)
- Horizontal curve (a future factor for the model)
- Intersection junction (arterial or local road)
- Shoulder changes (a future factor for the model)

Fig. 2- 2 is an example showing the segmentation model expectations' outcome. Each road segment will be specified with starting and ending references along with segment geometry information. The description of the geometry parameters are:

- SEG_{NO}: Segment Number, segment ID
- SEG_{SMP}: Segment Start Point Mile Post, mile marker of the roadway
- SEG_{EMP}: Segment End Point Mile Post, mile marker of the roadway
- SEG_{WIDE}: Segment Average Wide, the constant roadway segment wide value
- SEG_{LENGHT}: Segment Length, the constant roadway segment length value
- SEG_{TYPE}: Segment Type, segment pavement type; rigid or flexible pavement (composite pavement to be included in the future)
- SEG_{IFAF}: Segment Input Flow Adjustment Factor, a factor for adjustment of the traffic flow change in response to on/off ramp (exit or entrance ramp) at the segment starting point

- SEG_{OFAF}: Segment Output Flow Adjustment Factor, a factor for adjustment of the traffic flow change in response to on/off ramp (exit or entrance ramp) at the segment end point
- SEG_{SAF}: Segment Speed Adjustment Factor, a factor for adjusting the traffic average speed in the segment in response to the geometric change or on/off ramps (exit or entrance ramps)

3.2.4.2 P-MODEL-02: PAVEMENT SUB-SEGMENTATION MODULE (PSSM)

In a uniform segment such as a long corridor between two exits or entrances, a sub-segment process will not be necessary. However, in a shorter segment, the nonlinear effect of the traffic movement will change the uniform conditions. A non-uniform condition means the modeling process is more sensitive to the road geometry parameters and average parameters shall be replaced with actual parameter values. In a segment, all parameters have average values but in a sub-segment, the parameters have constant values. The sub-segment will have a very short length. Example of such locations where sub-segment processes will require are (a) ramps, (b) underpass or (c) overpasses. .

3.2.4.3 P-MODEL-03: PAVEMENT UNIT DISTRIBUTION (PUD)

In this model, PU will be distributed along a roadway segment or sub-segment. The PU geometry will be determined in P-Model-05 for each layer of the pavement. The distribution process is specified with a random distribution function, which is embedded, as default, or will be an input to the model.

The PU placement for each pavement structure layer will be an independent process. The PU sizes are the same for each pavement layer as a default, but P-model 05 may generate different PU geometry for each layer.

Table 3-8 shows several pavement structures that are considered for SPM placement. However, the general pavement structure for the SPM modeling will be one layer (surface course) or two

layers (surface and base or resurface and surface course). Either of the pavement layers will have different material particles. These particles will have different geometry, distribution and properties factors, which will affect the PU micro model and the emulated transfer function. The default size of a PU is 50 mm x 50 mm x 50 mm.

3.2.4.4 P-MODEL-04: PAVEMENT UNIT GEOMETRY MODULE (PUGM)

PU is a small block of the pavement which depends on the pavement type and its materials. For example, in a surface course of flexible pavement aggregate and binder, fillers are the main components of the pavement. In addition, the air voids also distribution volume in the surface course. Based on the percentage of the different aggregate sizes, the PU geometry will be defined. If a pavement layer has a larger size aggregate with higher percentage, the size of PU will be larger than the default values. Therefore, the information of physical material distribution needs to be considered for PU modeling. The material distribution information for PUGM are:

- Asphalt Binder (at Flexible Surface or Resurface Layers)
- Filler (at Flexible Layers)
- Aggregate (at Flexible or Rigid Layers)
- Fine Aggregate (at Flexible or Rigid Layers)
- CCP (at Rigid Layers)
- Air Void (at Flexible or Rigid Layers)

Table 3- 9 has some practical data of component values for a surface layer PU. Aggregate materials have a wide range of dimension and are non-symmetric in shape. However, in a practical pavement design, the parameters such as maximum aggregate size or nominated size are used. We considered this fact and PUGM uses these two parameters. As we can see, to develop a micro geometry model for these aggregate materials, unlimited possibility and

distribution of materials will be expected. To simplify the process the following assumptions are proposed:

PUGM Assumption 1. Total Average Aggregate Volume will be granted by the PUGM for each PU with a variance from 0 to a%[15]

PUGM Assumption 2. Total Average Aggregate Weight will be granted by the PUGM for each PU with a variance from 0 to b%[16]

PUGM Assumption 3. Maximum Aggregate Size will be granted by the PUGM; as favored aggregate size, the maximum particle size will be used that complies with Assumptions 1 and 2.

PUGM Assumption 4. Geometry of an Aggregate will be cubic, rectangular cubic and as lower option Spheris types. The size will be selected by complying with Assumption 1 to 3.

PUGM Assumption 5. Total Area of Aggregate particles will be a new parameter for optimization of the aggregate geometry, size, and quantities. This parameter will be considered in an advanced deployment of PUGM.

Table 3- 7 Example of Rigid Pavement Structure ID (RGID-PSID)

LAYERS NAME	*S*	*S, B*	*S, B, SB*	*S,B, SB, SG*
NO. OF LAYERS	1 LAYER	2 LAYERS	3 LAYERS	4 LAYERS
PSID	11000	11100	11200	11210

[15] a% will be set by user.
[16] b% will be set by user.

Table 3- 8 Examples of Flexible Pavement Structures ID (FLEX-PSID)[17]

LAYERS NAME	*S*	*S,B*	*RS1, S*	*S,B,SB*	*RS1,S,B,*
NO. OF LAYERS	1 LAYER	2 LAYERS	2 LAYER	3 LAYER A	3 LAYER B
PSID	01000	01100	02000	01200	02100
LAYERS NAME	RS2, RS1,S	S,B,SB,SG	RS3, RS2, RS1,S	RS2, RS1,S, B	RS1,S, B, SB
NO. OF LAYERS	3 LAYER C	4 LAYER A	4 LAYER B	4 LAYERS C	4 LAYERS D
PSID	03000	01210	04000	03100	02200
LAYERS NAME	S, B, SB1,SB2	RS1, S,B,SB,SG	RS2,RS1, S,B,SB	RS3, RS2,RS1, S,B	S,B, BS1,SB2,SG
NO. OF LAYERS	4 LAYERS E	5 LAYERS A	5 LAYERS B	5 LAYERS C	5 LAYERS D
PSID	01300	02210	03200	04100	01310
LAYERS NAME	RS1, S, B, SB1, SB2	S, B, SB1, SB2, SB3	S,B, SB1, SB2, SB3, SG	S,B, SB1, SB2, SB3, SB4	RS1, S,B, SB1, SB2, SB3,
NO. OF LAYERS	5 LAYERS E	5 LAYERS F	6 LAYERS A	6 LAYERS B	6 LAYERS C
PSID	02300	01400	01410	01500	02400
LAYERS NAME	RS1, S,B, SB1, SB2, SG,	RS2, RS1, S,B, SB1, SB2,	RS2, RS1, S,B, SB, SG,	RS3, RS2, RS1, S,B, SB	S,B, SB1, SB2, SB3, SB4, SG
NO. OF LAYERS	6 LAYERS D	6 LAYERS E	6 LAYERS F	6 LAYERS G	7 LAYERS A
PSID	02310	03300	03210	04200	01510
LAYERS NAME	RS1, S,B, SB1, SB2, SB3, SG	RS1, S,B, SB1, SB2, SB3, SB4	RS2, RS1, S,B, SB1, SB2, SB3	RS2, RS1, S,B, SB1, SB2, SG	RS3, RS2, RS1, S,B, SB1, SB2
NO. OF LAYERS	7 LAYERS B	7 LAYERS C	7 LAYERS D	7 LAYERS E	7 LAYERS F
PSID	02410	02500	03400	03310	04300
LAYERS NAME	RS3, RS2, RS1, S,B, SB, SG	RS1, S,B, SB1, SB2, SB3, SB4, SG	RS2, RS1, S,B, SB1, SB2, SB3, SB4	RS2, RS1, S,B, SB1, SB2, SB3, SG	RS3, RS2, RS1, S,B, SB1, SB2, SB3
NO. OF LAYERS	7 LAYERS G	8 LAYERS A	8 LAYERS B	8 LAYERS C	8 LAYERS D
PSID	04210	02510	03500	03410	04400
LAYERS NAME	RS3, RS2, RS1, S,B, SB1, SB2, SG	RS2, RS1, S,B, SB1, SB2, SB3, SB4, SG	RS3, RS2, RS1, S,B, SB1, SB2, SB3, SB4	RS3, RS2, RS1, S,B, SB1, SB2, SB3, SG	RS3, RS2, RS1, S,B, SB1, SB2, SB3, SB4, SG
NO. OF LAYERS	8 LAYERS F	9 LAYERS A	9 LAYERS B	9 LAYERS C	10 LAYERS
PSID	04310	03510	04500	04410	04510

[17] Proposed Pavement Layers Naming: S≡ Surface ; RS1≡ First Re-Surface; RS2≡ Second Re-Surface ; RS3≡ Third Re-Surface; B≡ Base ; SB≡ Sub-Base ; SB1≡ Sub-Base 1; SB2≡ Sub-Base 2 ; SB3≡ Sub-Base 3 ; SB4≡ Sub-Base 4 ; SG≡ Sub-Grade

PUGM Assumption 6. The following inputs specified for the model:

- MMD_i: PAVEMENT UNIT I; MESH MASS DENSITY
- MVD_i: PAVEMENT UNIT I; MESH VOLUME DENSITY
- MGF_i: PAVEMENT UNIT I; MESH GEOMETRY FACTOR
- MDF_i : PAVEMENT UNIT I; MESH DISTRIBUTION FACTOR
- $PMAS_i$: PAVEMENT LAYER I; MAXIMUM AGGREGATE SIZE[18]
- $PNAS_i$: PAVEMENT LAYER I; NOMINAL AGGREGATE SIZE[19]

Table 3- 9 Flexible Pavement Surface Course Pavement Unit

PAVEMENT UNIT DIMENSIONS	*CX*	*CY*	*CZ*	
MM	50	50	25	
	GRAMS			MM3
PU MASS	130.125	PAVEMENT UNIT VOLUME		62500
AGGREGATE MASS	97.59375	AGGREGATE VOLUME		40625
FINE MASS	23.4225	FINE VOLUME		4375
ASPHALT MASS	9.10875	ASPHALT VOLUME		13750
CHECK PAVEMENT UNIT MASS	130.125	AIR VOLUME		3750
SPHARE AGGREGATE		CHECK PAVEMENT UNIT VOLUME		62500

[18] The smallest sieve through, which 100 percent of the aggregate sample particles pass through. Super pave defines the maximum aggregate size as "one sieve larger than the nominal maximum size.

[19] The largest sieve retains some of the aggregate particles but generally not more than 10 percent by weight. Super pave defines nominal maximum aggregate size as "one sieve size larger than the first sieve to retain more than 10 percent of the material aggregate size as "one sieve larger than the nominal maximum size.

Table 3- 10 A sphere aggregate placement in FP Surface Course Pavement Unit 00

SIZE (mm)	*VOLUME*	*%*	*MAX NO.*	*MAX FILLING*		***FP-SC-00***
19	2019.118	3.23%	4	8076.473	12.9%	4
18	1716.795	2.75%	4	6867.18	11.0%	0
17	1446.264	2.31%	4	5785.058	9.3%	0
16	1205.76	1.93%	9	10851.84	17.4%	0
15	993.5156	1.59%	9	8941.641	14.3%	0
14	807.765	1.29%	9	7269.885	11.6%	0
13	646.7419	1.03%	9	5820.677	9.3%	0
12	508.68	0.81%	32	16277.76	26.0%	14
11	391.8131	0.63%	32	12538.02	20.1%	0
10	294.375	0.47%	50	14718.75	23.6%	0
9	214.5994	0.34%	50	10729.97	17.2%	0
8	150.72	0.24%	108	16277.76	26.0%	0
7	100.9706	0.16%	147	14842.68	23.7%	0
6	63.585	0.10%	256	16277.76	26.0%	0
5	36.79688	0.06%	500	18398.44	29.4%	25
4	18.84	0.03%	864	16277.76	26.0%	0
3	7.948125	0.01%	2048	16277.76	26.0%	2466
2	2.355	0.00%	7500	17662.5	28.3%	1736
1	0.294375	0.00%	62500	18398.44	29.4%	2781
		NO. AGGREGATE OBJECTS				7026
		VOLUME OF AGGREGATE OBJECTS				40624.93
		VARRIATION				0.00%

At the following step, each aggregate particle will be placed inside the PU block. This placement process will also limit the number and sizes of the aggregate particles to limit the size of the PU block and non-overlapping layers between each aggregate. After placement of the aggregates, the final aggregate will be distributed in a uniform way. The total of aggregates and fine aggregates shall be the average values inputted to the modeling.

In this example, for cubit aggregate size with a volume percentage of 65%, the Flexible Pavement Surface Course Pavement Unit (FPSC-PU-06) has the minimum number of 24 aggregates.

Table 3- 11 Cubic Aggregate Placement in Flexible Pavement Surface Course PU 01 to 06

SIZE	*VOLUME*	*%*	*MAX NO.*	*MAX FILLING*		***FP-SC-01***	***FP-SC-02***	***FP-SC-03***	***FP-SC-04***	***FP-SC-05***	***FP-SC-06***
19	6859	10.97%	4	27436	43.9%	4	4	4	3	2	2
18	5832	9.33%	4	23328	37.3%	0	0	0	0	0	0
17	4913	7.86%	4	19652	31.4%	0	0	0	0	0	0
16	4096	6.55%	9	36864	59.0%	0	0	0	1	4	3
15	3375	5.40%	9	30375	48.6%	0	0	0	0	0	0
14	2744	4.39%	9	24696	39.5%	0	0	0	0	0	0
13	2197	3.52%	9	19773	31.6%	0	0	0	0	0	4
12	1728	2.76%	32	55296	88.5%	0	0	0	0	0	0
11	1331	2.13%	32	42592	68.1%	0	0	0	0	0	0
10	1000	1.60%	50	50000	80.0%	0	0	0	0	0	4
9	729	1.17%	50	36450	58.3%	0	8	4	0	0	0
8	512	0.82%	108	55296	88.5%	0	11	20	24	10	1
7	343	0.55%	147	50421	80.7%	0	0	0	0	0	0
6	216	0.35%	256	55296	88.5%	0	0	0	0	0	0
5	125	0.20%	500	62500	100.0%	105	13		29	43	10
4	64	0.10%	864	55296	88.5%	0	0	0	0	0	0
3	27	0.04%	2048	55296	88.5%	0	0	0	0	0	0
2	8	0.01%	7500	60000	96.0%	0	0	0	0	0	0
1	1	0.00%	62500	62500	100.0%	0	0	0	0	0	0
		NO. AGGREGATE OBJECTS				109	36	28	57	59	24
		VOLUME OF AGGREGATE OBJECTS				40561	40525	40592	40586	40597	40556
		VARRIATION				0.05%	0.08%	0.03%	0.03%	0.02%	0.06%

3.2.5 PAVEMENT UNIT MODELS

In previous Sections, roadway segmentation, sub-segmentation and Pavement Unit generation were discussed. As part of those models, a roadway or a network of roadway pavement models will be directed to PU multi-physic modeling to specify the pavement response to the vehicle loading. This approach reduces the complexity of the modeling. Based on the SPM application, the proposed PU models are divided in two processes. The first model, Pavement Unit Micro Module (PUM^2), is a multi-physic PU model based on a Finite Element analysis. The effects of different physics are analyzed in this model. PUM^2 will be used for assessment of the SPM micro generator performance and its efficiency estimation for different pavement layers. PUM^2 is presented in the following sub-section. Second modeling class is a macro simulation that includes material strain and stress models.

Energy Model (PEM) is designed to describe the energy transformer behavior between vehicle traffic flow and the roadway pavement layers (Surface and Base Courses). PEM is a macro simulation model for describing the traffic movement loading, energy effect over the pavement. This model has three main components: vehicle mobility, pavement response, and vibration to electrical conversion. These components are replaced with an equivalent nonlinear circuit network. The equivalent circuit network has parameters, which depend on the traffic characteristic, vehicle class distribution, pavement's physical characteristics and its materials.

The vehicle mobility model depends on its main vehicle parameters which are the vehicle and its operation parameters, vehicle weight, suspension system, tire type, number, pressure, and geometric sizes. The operation parameters are speed and traffic flow rates. The Mechanical Model and equivalent Circuit Network are shown in Fig. 3- 7.

This model is revised from the Quarter Car Model. NT, NSC and NBC are virtual noise sources, which represent the uncertainly of the material properties estimates. Eq. 3-1 described the

vehicle motion in contact with the pavement surface. The pavement surface interface was simulated with the Kelvin-Vogit model, which is represented by a purely viscose damper and purely elastic spring connected in parallel as shown in the Fig. 3- 8. The figure also shows the Maxwell representative model. In these models, the following notations were used (a) stress = σ and (b) strain=ε and their relationship is described by equation Eq. 3-3.

The mechanical model has a damper with C_S as the equivalent coefficient of viscosity in the range of 4 KNs/m to 40 KNs/m, with K_S as equivalent to the elastic coefficient in range of 50 KN/m to 500 KN/m, and K_T is the equivalent to an elastic coefficient of a vehicle spring system approximate as 2 MN/m. Based on the strain and elasticity relationship equation at the mechanical model, we will have:

$$M_S \times Z_S^{"} + K_S \times (Z_S - Z_U) + C_S \times (Z_S{}' - Z_U{}') = 0 \qquad \text{Eq. 3- 1}$$

$$M_U \times Z_U^{"} + K_T \times (Z_U - Z_P) + C_T \times (Z_U{}' - Z_P{}') - K_S \times (Z_S - Z_U) - C_S \times (Z_S{}' - Z_U{}') + N_T = 0 \qquad \text{Eq. 3- 2}$$

Pavement layers and courses have different configurations depending on the pavement types. Generally, all hard surfaced pavement types can be grouped into three categories, Flexible, Composite and Rigid Pavement. A Flexible Pavement (FP) consists of one or more layers of asphalt supported by a granular sub-base. A Composite Pavement (CP) consists of a flexible surface layer supported by a stiff Portland Cement Concrete (PCC) base. And Rigid Pavement (RP) consists of a layer of PCC on a granular foundation. The RP category is classified further according to its arrangement of steel reinforcement and joints. FP is a more common pavement on the highway system on an estimated 90% of the roadways. Fig. 3- 3 and Fig. 3- 4 show the typical pavement structures plans, which are considered in this modeling. Based on the SPM goal

for a cost effective installation deployment, Surface Course and Base Course are two layers that will be of interest in this simulation.

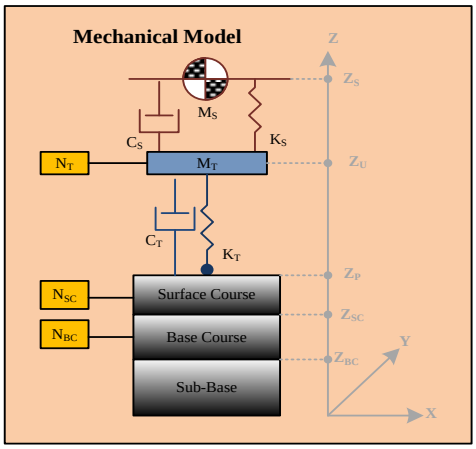

Fig. 3- 7 Vehicle Forces Model over Pavement

$$\sigma(t) = E\varepsilon(t) + \eta\frac{d\epsilon(t)}{dt}$$ Eq. 3- 3 (Kelvin-Voigt Model)

$$\frac{1}{E}\frac{d\epsilon(t)}{dt} + \frac{\sigma(t)}{\eta} = \frac{d\epsilon(t)}{dt}$$ Eq. 3- 4 (Maxwell Model)

Where *E* is a modulus of elasticity and η is the viscosity[20].

Based on the type of geometry (pavement structure type), the equivalent material model will be placed in the simulation. In a simple structure modeling, a surface course materials PU will be represented with a Kelvin-Voigt material model. We discuss the details of these modes in the sub-section 3.2.5.2 P-MODEL-06: PAVEMENT ENERGY MODULE (PEM)

[20] Viscosity is a measure of the resistance of a fluid which is being deformed by either shear stress or extensional stress. [Wikipedia]

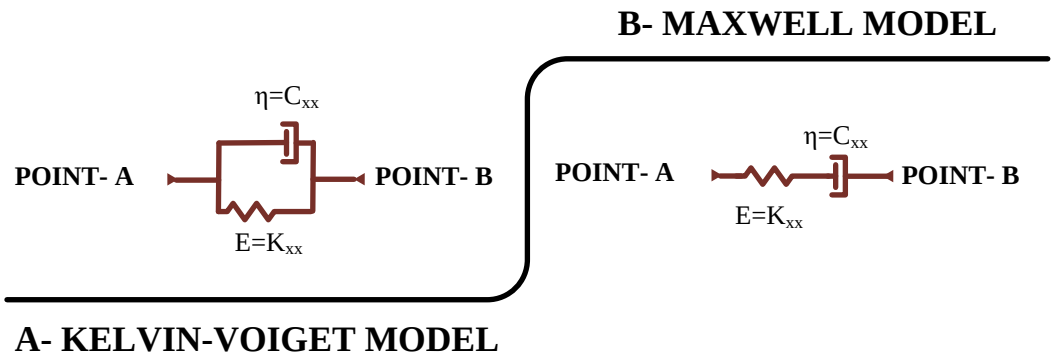

Fig. 3- 8 Stress- Strain representative models

3.2.5.2 P-MODEL-05: PAVEMENT UNIT MACRO MODULE (PUM^2)

Pavement Macro Modeling is a process for distribution of the PU along a sub-segment/segment of the roadway. The modeling is based on a random or specific distribution of PU based on the user's defined inputs. A long sub-segment of a roadway is divided into small blocks of PUs. Each PU type will be analyzed independently. The boundary conditions of each PU will be the function of other neighboring PUs and vehicle movement. Therefore, in a sequential process, the whole transition and steady state condition of pavement response can be analyzed. In practice, the construction of the roadway segment attempts to be uniform, however, depending on material sizes, overall distribution will not be possible. In conclusion, we will use random PU distribution. The main benefit for this approach is the simplicity of the pavement material distribution in a small PU instead of the complete micro level simulation of a pavement sub-segment.

Fig. 3- 10 is a proposed algorithm process for this model. In this way, the distribution of PU and the geometry of PU will determine the pavement structure and its materials. Of course, the methods still need a significant amount of processing memory and time, which are the practical limits for exercising the model and needs to be considered. PPU3 execution process requires a

long processing time and a large volume of the processing memory. Based on the simulation environment, tools of the complexity of the process varied.

3.2.5.2 P-MODEL-06: PAVEMENT ENERGY MODULE (PEM)

PEM is a model for presenting the responses of multi layers of the pavement courses (see Fig. 3-7). The PEM process replaces each layer of the pavement course with an emulated Kelvin-Voiget Strain/Stress model. The Kelvin-Voiget model may be enhanced with temperature, dependent on random variables regarding the material properties' variation. Therefore, the PEM is dependent on the pavement structure type, material properties, temperature, and the overall size of the road segments. Material modeling is represented for each PU in the pavement layer, and, to perform it in three dimensions, uniform arrangements are proposed. A PU representative material model, as shown in Fig. 3- 9, is a PU on a Base Course layer in a symmetrical PU and means:

$C_X=C_Y=C$ or

$C_{BCX}=C_{BCY}=C_{BC}$ and Eq. 3- 5

$K_{BCX}=K_{BCY}=K_{BC}$

The symmetric assumption is not a fully realistic condition, but for different thicknesses of pavement layer C value, needs to be adjusted.

As we discussed in 3.2.4.3 P-MODEL-03: PAVEMENT UNIT DISTRIBUTION (PUD), there will be a distribution of PU type in each layer, and therefore the values of spring and dumper not only change by layer but also will be changed by PU type. This provides an additional degree of freedom in this model. By putting the PUs and quarter car model together, we will have a comprehensive system model. Fig. 3- 11 shows such a comprehensive model for pavement structure PSID=01200. The size of this model geometry can be unlimited in the size of the

roadway sub-segment, however, it will not be practical and it may be limited to a fraction or multiplier of vehicle length. This assumption will require the model to be repeated for different lengths which is related to the different traffic flow rate.

The tire contact area is one of other factors that will affect this model. The tire area is estimated based on the vehicle class and a simple tire pressure expected in the M-Model. Therefore, the contact size can be read from M-Model input for each vehicle in the model.

The PEM model diagram is faced with a familiar network, a circuit network, which can have linear or non-linear components. The power sources, vehicle dependent, are time variant emulated power sources. The effect of uncertain parameters is activated by a noise power source. This noise source can simplify the rest of network elements to linear components. However, it is not necessary to challenge the non-linear elements, since, noise power source is specified to the model. An alternative to a non-linear element can be specified in the model. Of course, nonlinear components will increase the complexity of the network solution. In our work, the linear elements are used. In addition a probability distribution function is specified for use with the PEM and the emulated circuit network.

The Pavement response component of the model explains that a vehicle is at a position on a road. Vehicle speed is the parameter that affects the equivalent power source Vs (t). c (t), l(t), and r(t) in our model. These sources are time dependent functions, however, that relationship can be considered in a linear zone for small time periods. In such a period, the vehicle speed and other time dependent parameters will be considered time independent.

The second component, pavement response, describes the deformation caused by stress and strains of the pavement layer materials in response to the vehicle loading. The distribution of the different material particles in the pavement layer affects the model parameters.

Solution of the emulated network of the pavement and vehicle such as the network in Fig. 3- 11 requires the pavement materials and vehicle details information. Such a solution determines more the vehicle ride and its suspension performance (by exercising different suspension modules). However, more input information about the vehicle suspension parameters, tires, and engine will be required. Thus, in the matter of a pavement response study, dynamic loading on the pavement surface is emulated at a dynamic force affected on the tire contact area.

This force will be shown with an emulated power supply at each contact tire. Thus, the revised network will be used as shown in Fig. 3- 12. Prior to examining the solution to this network, we need to list the parameter and inputs of the emulated circuits. These parameters are dependent on the pavement structure and materials. Thus typical variance values can be considered. The typical pavement parameters are:

i. FP Surface materials equivalent Damping parameter " C_{SCZ} " and " C_{SC} " equal to random variables.
ii. FP Surface materials equivalent String parameter "K_{SCZ} "and "K_{SC} "equal to random variables.
iii. FP Base materials equivalent Damping parameter " C_{BCZ} "and " C_{BC} " equal to random variables.
iv. FP Base materials equivalent String parameter "K_{BCZ} "and "K_{BC} "equal to random variables.
v. FP Sub-Base materials equivalent Damping parameter " C_{SBCZ} "and " C_{SBC} " equal to random variables.
vi. FP Sub-Base materials equivalent String parameter "K_{SBCZ} "and "K_{SBC} "equal to random variables.

vii. FP Sub-Grade materials equivalent Damping parameter " C_{SGCZ} "and " C_{SGC} " equal to random variables.

viii. FP Sub-Grade materials equivalent String parameter "K_{SGCZ} "and "K_{SGC} "equal to random variables.

These variables are as shown in Table 3- 12. In addition, the following assumptions and parameters were made:

ix. Soil layer is emulated as a ground level.

x. Vehicle dynamic load is imported from M-Model. These forces are time, and space (x,y,0) dependent functions.

xi. Tire contact area is imported from M-Model. These areas are changed, based on the vehicle class and type. M-Model generates these values which are a function of time.

xii. Pavement material information or sample data Non Destructive Testing (NDT) is data for direct evaluation of the damping and string parameters.

To solve this emulated network, PSPICE is used. This network in the inside pavement has a 3D symmetric schematic plan. However, the elements' values are varied in a random process. To identify each pavement unit's elements, a PU with placement of IDs was proposed. Also, the size of material in the Kelvin-Voiget model shall be set as a minimum value for better results and model conversion.

The minimum size for C_X and C_Y are specified the same as the length resolution value used in the M-Model, 50 mm in this study. Also the minimum element length in z direction is set shorter, 25 mm, for a more detailed model, but with a more computational process. These coordinate IDs are based on the pavement geometry coordination.

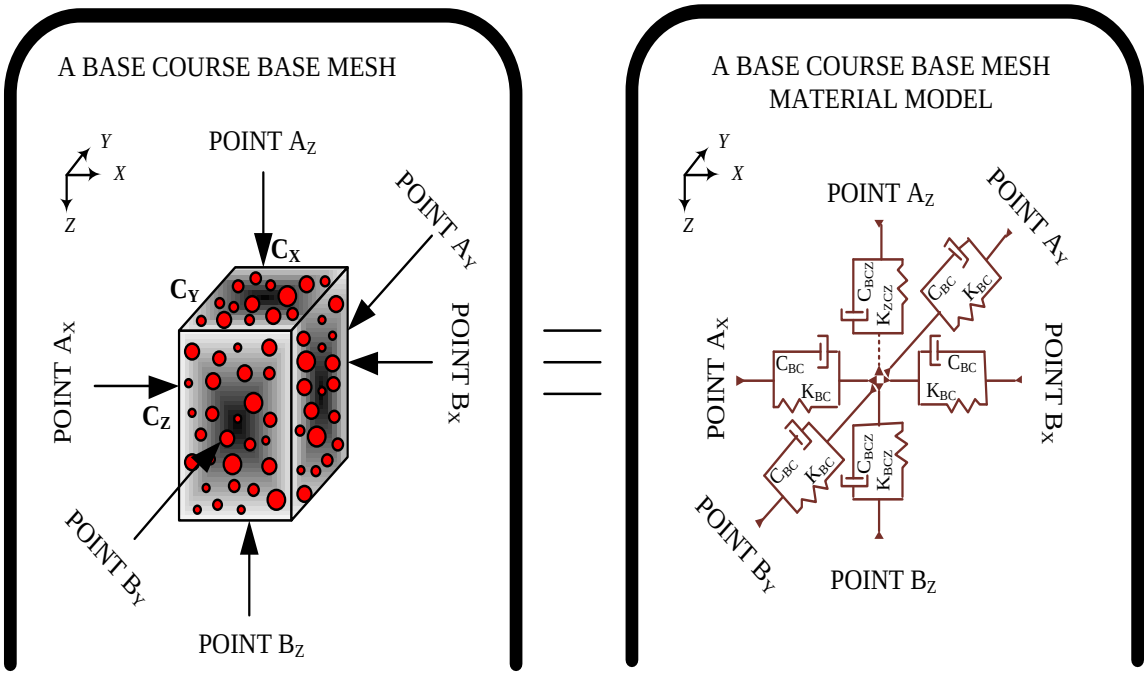

Fig. 3- 9 a Base Course Pavement Unit and Material Model

PEM Model Parameters to be estimated: (C_{SCZ} , $C_{SC,}$ K_{SCZ} , K_{SC} , C_{BCZ} , $C_{BC,}$ K_{BCZ} , K_{BC}, C_{SCZ} , $C_{SC,}$ K_{SCZ} , K_{SC})

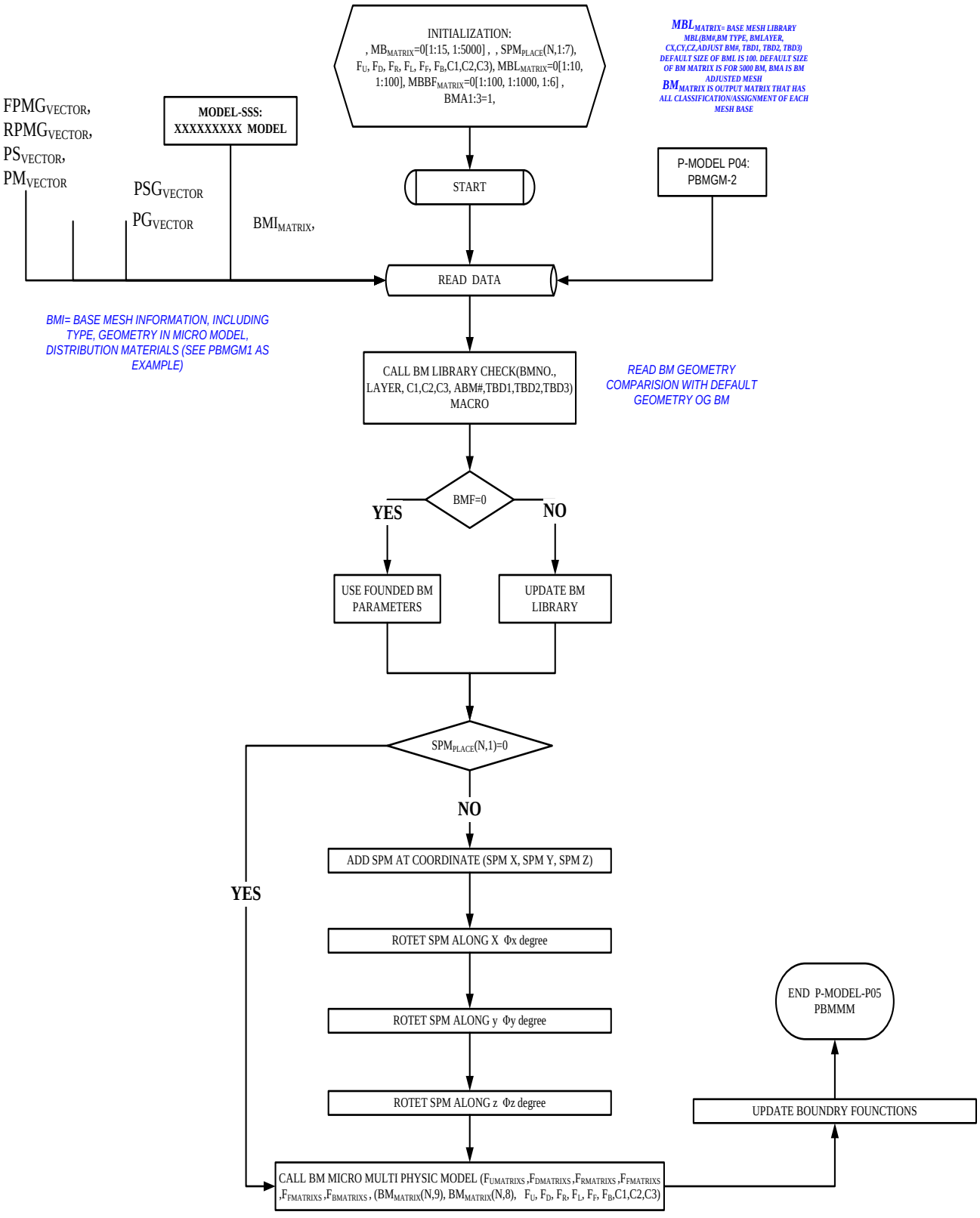

Fig. 3- 10: PUM^2- PAVEMENT UNIT MACRO MODEL PROCESS

Table 3- 12 A PEM - Example Pavement Parameters [21]

A Surface Layer			*A Base Layer*		
Parameter	**Example**	**Variance**	**Parameter**	**Example**	**Variance**
C_{SCZ}	7.1E+04	1.1E+04	C_{BCZ}	5.2E+01	7.9E+00
$C_{SC}=C_{SCX}=C_{SCY}$	1.0E+04	5.0E+03	$C_{BC}=C_{BCX}=C_{BCY}$	7.4E+00	3.7E+00
K_{SCZ}	7.7E+09	1.2E+09	K_{BCZ}	2.1E+06	3.1E+05
$K_{SC}=K_{SCX}=K_{SCY}$	3.9E+09	1.9E+09	$K_{BC}=K_{BCX}=K_{BCY}$	1.0E+06	5.2E+05
A Sub-Base Layer			**A Sub-Grade Layer**		
Parameter	**Example**	**Variance**	**Parameter**	**Example**	**Variance**
C_{SBCZ}	5.2E+01	7.9E+00	C_{SGCZ}	3.0E-06	4.5E-07
$C_{SBC}=C_{SBCX}=C_{SBCY}$	7.4E+00	3.7E+00	$C_{SGC}=C_{SGCX}=C_{SGCY}$	4.2E-07	2.1E-07
K_{SBCZ}	2.1E+06	3.1E+05	K_{SGCZ}	2.2E-08	3.3E-09
$K_{SBC}=K_{SBCX}=K_{SBCY}$	1.0E+06	5.2E+05	$K_{SGC}=K_{SGCX}=K_{SGCY}$	1.1E-08	5.6E-09

Assumptions			**Surface Layer**			**Sub-Base**	**Base**	**Sub-Grade**
Description	**Parameter**	**Unit**	**Asphalt 1**	**Asphalt 2**	**Asphalt 3**	**Typical**	**Typical**	**Typical**
Viscosity Rate	**z**	NA	1.90E-01	1.05E-01	2.75E-02	8.50E-03	8.50E-03	5.00E-03
Length Size (Pavement Unit)	l	m	5.00E-02	5.00E-02	5.00E-02	5.00E-02	5.00E-02	5.00E-02
Width Size (Pavement Unit)	w	m	1.00E-02	1.00E-02	1.00E-02	1.00E-02	1.00E-02	1.00E-02
Elasticity (Z direction)	E_Z	Pascal	7.70E+09	1.20E+10	2.10E+10	2.07E+06	2.07E+06	2.22E-08
Elasticity (X and Y directions)	$E_{x,y}$	Pascal	3.85E+09	6.00E+09	1.05E+10	1.03E+06	1.03E+06	1.11E-08
Density	**r**	Kg/m3	1.80E+03	2.00E+03	2.30E+03	1.84E+03	1.84E+03	1.60E+03
Estimated								
Viscosity Factor (Z direction)	$\mathbf{h_z}$	Pa x Sec	**7.07E+04**	**5.14E+04**	**1.91E+04**	**5.24E+01**	**5.24E+01**	**2.98E-06**
Viscosity Factor (X and Y direction)	$\mathbf{h_{x,y}}$	Pa x Sec	**1.00E+04**	**7.27E+03**	**2.70E+03**	**7.42E+00**	**7.42E+00**	**4.22E-07**

[21] Subject of the materials and pavement type

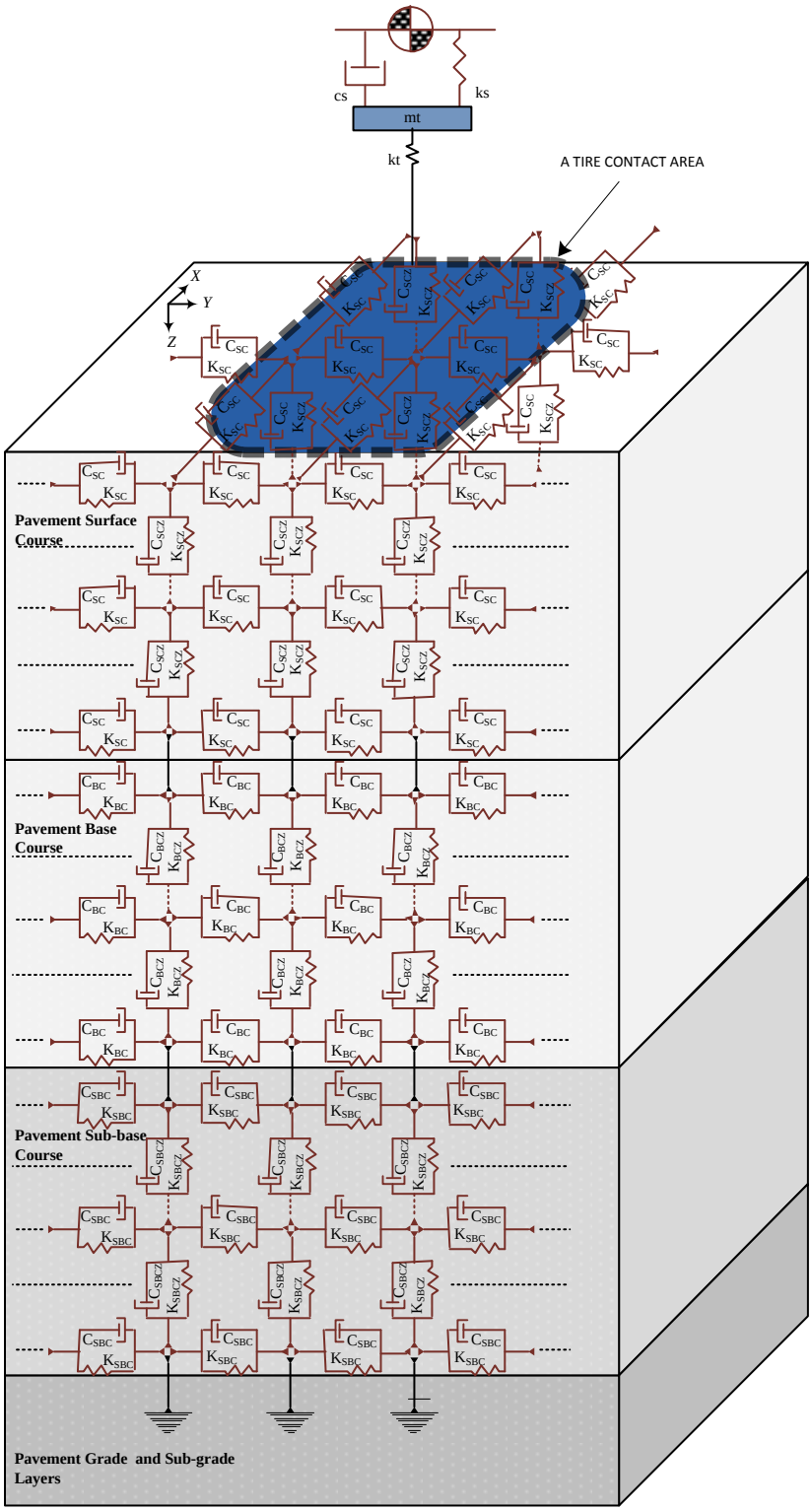

Fig. 3- 11 Example of PEM
($C_{SCX} = C_{SCY} = C_{SC}$, $K_{SCX} = K_{SCY} = K_{SC}$), ($C_{BCX} = C_{BCY} = C_{BC}$, $K_{BCX} = K_{BCY} = K_{BC}$), ($C_{SCX} = C_{SCY} = C_{SC}$, $K_{SCX} = K_{SCY} = K_{SC}$)

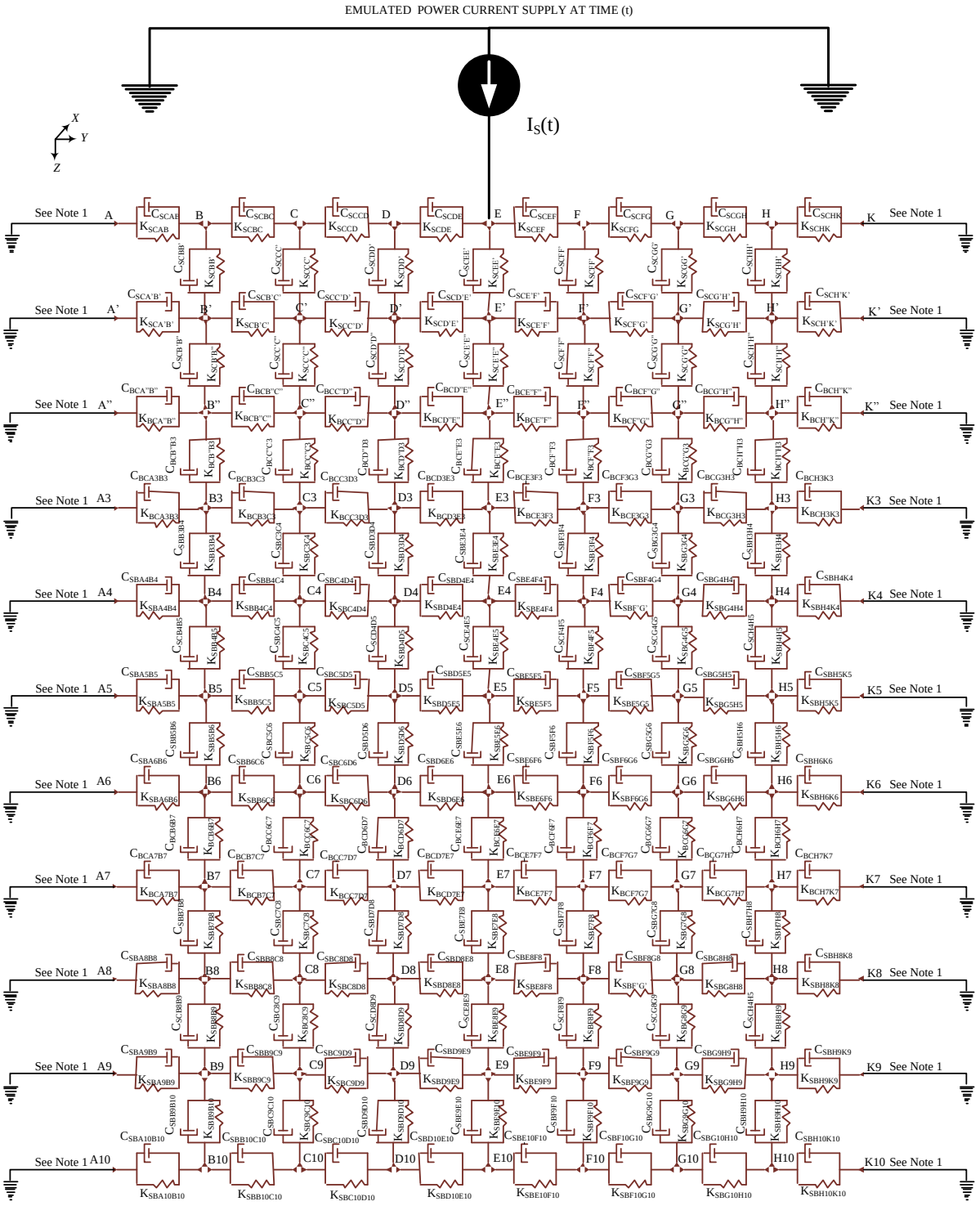

NOTE:
1) FOR SIMPLISITY OF THE NETWORK THIS NODE CONSIDERED AS GROUND POINT. IN A DETAIL COMPERHENSIVE ANALYSIS A LARGER NETWORK WITH EQUIVALENT AREA OF ROADWAY WIDE- Y DIMENTION x THREE TIME OF VEHICLE LENGTH – X DIMENTION x FULL PAVEMENT STRUCTURE-Z DIMENTION WILL BE PROPOSED.
2) THE PRESENTATION IS TWO DIMENTIONS PLAN (Y,Z) . A THREE DIMENTIONS NETWORK

Fig. 3- 12: PEM REVISED EXAMPLE CIRCUIT

3.3 PAVEMENT RESPONSE MODELING PROCESS

In this Section, a summary result of the P-Models is presented. As discussed previously, pavement response modeling also has applications in pavement design and pavement management systems; however, we are only focusing on the requirement of the model for an SPM application. This Section starts with a model's parameters' definition and estimate reviews. The analysis of the PEM macro modeling and micro modeling are presented.

3.3.1 PAVEMENT RESPONSE MODEL PARAMETERS

This Sub-Section includes the review of the estimations of the modeling parameters' values' based on field assumptions and conditions. The parameters were projected from sample cases because not all parameters have a systematic measurement. Example of a systematic measurement is AADT or WIM station information. Regarding the existing pavement materials, the existing data may not have detail information that we need for the model and sampling and data parameters estimation will be necessary. In this proposed sampling routine, each projected parameter will present with a random variable. The parameter expected value and variance are projected from sampling data. The default probability distribution functions for these random variables are uniform, Poisson or Gaussian distribution functions. The PEM macro modeling results depend on the roadway class and the pavement type being the same as the material properties. P-Model parameters and variables are:

a) Force/Loading Parameters, M-Models' results generate the following inputs:
    i. Tire Contact Position ("X" and "Y" index): x and y coordinates of a tire touching point
    ii. Tire Contact Time ("T" index): time of tire touching

iii. Vehicle Force/Load per Tire (“F” index): Average load per class per axle and per each tire

b) Pavement Geometry, input parameters based on existing pavement structure and, proposed layer for the SPM placement and the aggregate geometries information generate the following inputs:

i. Pavement Type (“0 as FP” or “1 as RP”)

ii. Pavement Layer (“0 as SL” or “1 as SBL” or “2 as BL” or “3 as SGL”)

iii. Pavement Depth (“SL_D, SBL_D, BL_D, SGL_D)

iv. Pavement Unit Codes such as “FP-SC as Flexible Pavement Surface Course” or “FP-BC as Flexible Pavement Base Course” or “FP-SBC as Flexible Pavement Sub-Base Course” or “FP-SGC as Flexible Pavement Sub-Grade Course” or “RP-SC as Rigid Pavement Surface Course” or “RP-BC as Rigid Pavement Base Course” OR “RP-SGC as Rigid Pavement Sub-Grade Course”)

See

Table 3- 10 for example of FP-SC-00 to 06 cases)

c) Material Properties Parameters, physical properties of the pavement layers components or the layer average values: These parameters depend on environment conditions such as temperature and compounding process. The pavement material information generate the following inputs:

i. Flexible Pavement Surface Layer Inputs

1) Pavement Surface Density (PS-D)

2) Pavement Surface equivalent Poisson Ratio (PS-PR)

3) Pavement Surface equivalent Module of Elasticity/ Young Module (PS-ME)

4) Pavement Surface equivalent Module of Rigidity/ Shear Module (PS-MR)

5) Pavement Surface Dynamic Viscosity / Absolute Viscosity (PS-DV)

6) Pavement Surface Shear Viscosity / Viscosity (PS-SV)

ii. Flexible Pavement Base Layer Inputs

7) Pavement Base Density (PB-D)

8) Pavement Base equivalent Poisson Ratio (PB-PR)

9) Pavement Base equivalent Module of Elasticity/ Young Module (PB-ME)

10) Pavement Base equivalent Module of Rigidity/ Shear Module (PB-MR)

11) Pavement Base Dynamic Viscosity / Absolute Viscosity (PB-DV)

12) Pavement Base Shear Viscosity / Viscosity (PB-SV)

iii. Flexible Pavement Sub-Base Layer Inputs

13) Pavement Sub-Base Density (PS-BD)

14) Pavement Sub-Base equivalent Poisson Ratio (PSB-PR)

15) Pavement Sub-Base equivalent Module of Elasticity/ Young Module (PSB-ME)

16) Pavement Sub-Base equivalent Module of Rigidity/ Shear Module (PSB-MR)

17) Pavement Sub-Base Dynamic Viscosity / Absolute Viscosity (PSB-DV)

18) Pavement Sub-Base Shear Viscosity / Viscosity (PSB-SV)

iv. Flexible Pavement Sub-Grade Layer Inputs

19) Pavement Sub-Grade Density (PSG-D)

20) Pavement Sub-Grade equivalent Poisson Ratio (PSG-PR)

21) Pavement Sub-Grade equivalent Module of Elasticity/ Young Module (PSG-ME)
22) Pavement Sub-Grade equivalent Module of Rigidity/ Shear Module (PSG-MR)
23) Pavement Sub-Grade Dynamic Viscosity / Absolute Viscosity (PSG-DV)
24) Pavement Sub-Grade Shear Viscosity / Viscosity (PSG-SV)

v. Rigid Pavement Concrete Layer Inputs

25) Pavement Concrete Density (PC-D)
26) Pavement Concrete equivalent Poisson Ratio (PC-PR)
27) Pavement Concrete equivalent Module of Elasticity/ Young Module (PC-ME)
28) Pavement Concrete equivalent Module of Rigidity/ Shear Module (PC-MR)
29) Pavement Concrete Dynamic Viscosity / Absolute Viscosity (PC-DC)
30) Pavement Concrete Shear Viscosity / Viscosity (PC-SV)

In Table 3- 13, default values for these parameters are listed. The actual values of the parameters are subject to (a) the existing pavement information, (b) field sampling data, (c) mixed material properties, and (d) materials distribution. In addition, the environmental condition, primarily the temperature, will also affect real inputs parameters. Therefore, some of the generating inputs shall have an environmental correction factor.

Direct testing and measurement of the pavement are used for pavement condition or response assessment. Example of this testing can be: (a) repeated road triaxial testing, (b) Falling Weight Deflectometer (FWD), (c) Heavy Weight Deflectometer (HWD), (d)

Ground Penetrating Radar (GPR) and (e) AASHTO[22] test methods such as T-48, T-44, T-202, T-240 parameters. Such tests will be used for sampling and model validation access.

Table 3- 13 Default Pavement Parameters

FP/PS	FROM	TO	FP/PB	FROM	TO	FP/PSB	FROM	TO	UNIT
PS-D	1.67E+03	2.50E+03	PB-D	1.47E+03	2.21E+03	PSB-D	1.47E+03	2.21E+03	KG/M3
PS-PR	2.40E-01	3.60E-01	PB-PR	2.00E-01	3.00E-01	PSB-PR	2.00E-01	3.00E-01	
PS-ME	2.72E+00	4.08E+00	PB-ME	4.16E+00	6.24E+00	PSB-ME	4.80E+00	7.20E+00	GPa
PS-MR	5.44E-01	2.04E+00	PB-MR	8.32E-01	3.12E+00	PSB-MR	9.60E-01	3.60E+00	GPa
PS-DV	1.53E+01	8.48E+01	PB-DV	2.62E-02	1.05E-01	PSB-DV	2.62E-02	1.05E-01	KPaS
PS-SV	2.16E+00	1.20E+01	PB-SV	3.71E-03	1.48E-02	PSB-SV	3.71E-03	1.48E-02	KPaS
FP/PSG	**FROM**	**TO**	**RP/PC**	**FROM**	**TO**	**UNIT**	**NOTE**		
PSG-D	1.28E+03	1.92E+03	PC-D	1.84E+03	2.76E+03	KG/M3	Subject: material mix & construction		
PSG-PR	3.36E-01	5.04E-01	PC-PR	1.50E-01	2.50E-01		Subject: material & mixture process		
PSG-ME	5.60E+00	8.40E+00	PC-ME	2.67E+01	3.34E+01	GPa	Subject: material mix & construction		
PSG-MR	1.12E+00	4.20E+00	PC-MR	5.34E+00	1.67E+01	GPa	Subject: material mix & construction		
PSG-DV	1.49E-09	5.96E-09	PC-DV	2.32E+00	9.28E+00	KPaS	Subject: material mix & Temperature		
PSG-SV	2.11E-10	8.43E-10	PC-SV	3.28E-01	1.31E+00	KPaS	Subject: material mix & Temperature		

[22] See Appendix 5 for list of the AASHTO testing

3.3.2 PAVEMENT RESPONSE MODELING RESULTS

Finite Element analysis is a core base for pavement micro modeling. In this modeling plan, the pavement structure is analyzed with an FE tool, Comsol. Several PU cases are modeled in this study. The main assumption in this modeling is the uniform pavement material geometry distribution that allows unique parameters for each pavement structure layer. The resolution of the FE mesh is in the range of micro millimeter depending on the limits of the tools and simulation computer.

In this Section, we are reviewing the results of the micro modeling of a very small pavement section or a pavement unit (PU). As mentioned before, several limitations included (a) the overall physical size of the model, (b) processing time, and (c) the system memory did not allow us to use a microscopic simulation approach over a large section of a pavement. The simulation was done by using Comsol multi-physic simulation tool version 4.3. The comprehensive simulation results are included in the Appendix 6 – PEM Micro Simulation Reports, but the summary is presented here with a conclusion.

In a previous Section, a definition and application of PU were discussed. The PU sizes were determined by P-model 03, which can provide different PU dimensions for different roadway or layers. The physical geometries of PU in this study are the default values, which are: $L_{|x}$ =50 mm, $W_{|y}$ =50 mm and $D_{|z}$ =50 mm. A surface layer PU has typical properties' values as listed in Table 3- 13. The traffic loads of two axle vehicles were presented in the study but other heavy vehicle loads were also studied in the project. A two axle vehicle will have two SPM single activation stages. The Comsol PU models were simulated for the following cases:

3.3.2.1 CASE 1- PU AT SURFACE LAYER WITHOUT SPM.

Fig. 3- 13 PU Geometries in Case 1 show the model geometry and activated force.

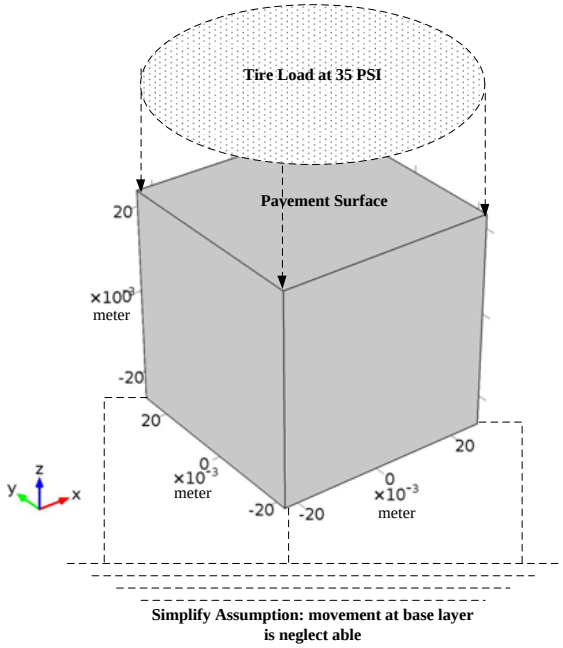

Fig. 3- 13 PU Geometries in Case 1

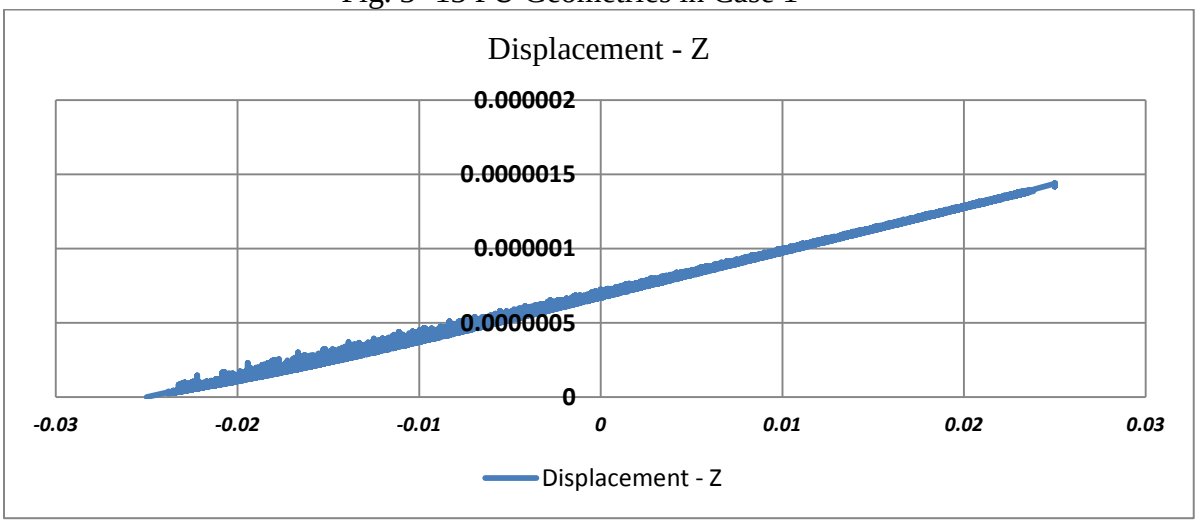

Fig. 3- 14 PU z Displacement Plot 1

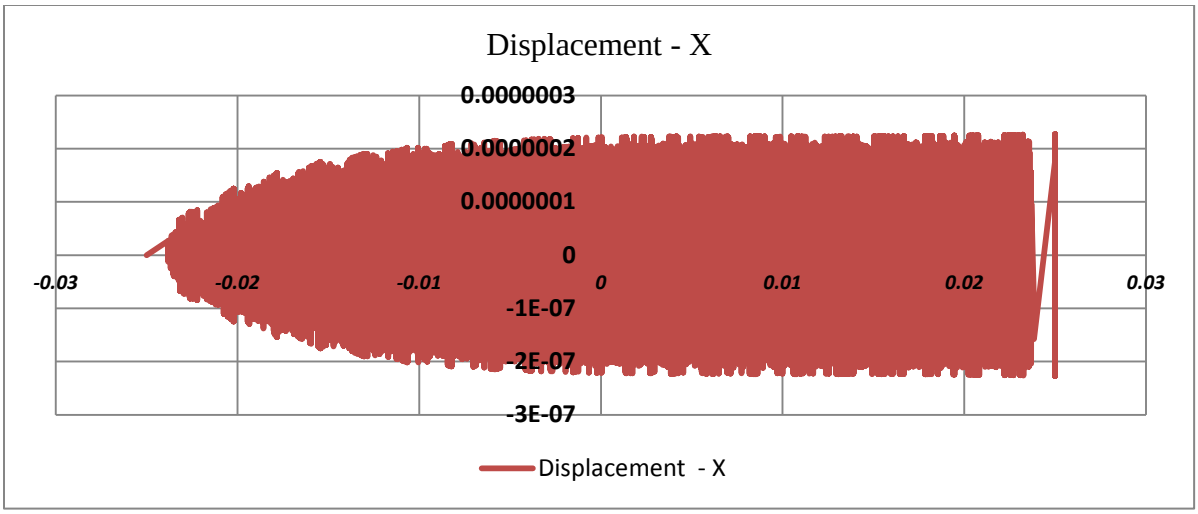

Fig. 3- 15 PU x Displacement Plot 1

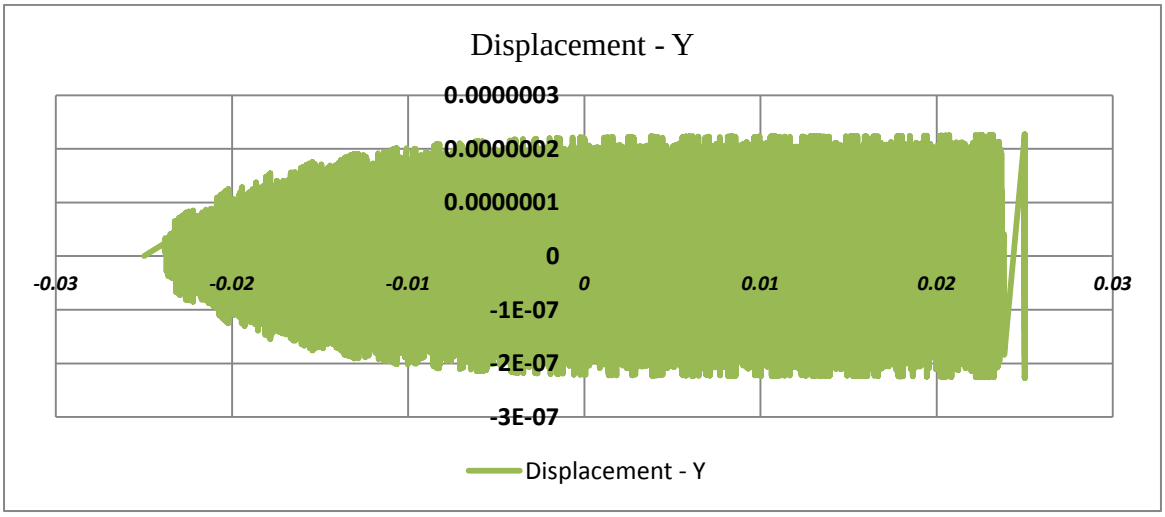

Fig. 3- 16 PU y Displacement Plot 1

This case is a base case in our study. The pavement base course and other layers under it are considered as fixed layers with zero movement. Fig. 3- 14 and Fig. 3- 15 show the deformations in z and x / y directions. The deformations are dependent on the depth of the pavement position; Z therefore with the symmetric x and y deformation values is expected. A maximum displacement is 1.5 μm.

The next output is the time dependent response function of the displacement. The total displacement time response function is shown in Fig. 3- 17 PU Total displacement time response function. The time response function were used for the determination of the emulation circuit elements (see Fig. 3- 9) and validation of the values (see Table 3- 12). The discussion for the emulation circuits' parameters is in Section 3-4-4. The displacement ratios for different directions are:

- D_{XZ}= (Displacement-X/ Displacement-Z)=% 14.2
- D_{YZ}= (Displacement-Y/ Displacement-Z)=% 14.2

Most displacement and strain energy is in z direction, which is our source for energy harvesting. The x and y movement may considered in the case of a 3D microgenerator. In chapters 4 and 5, more discussion of the micro-generator and its packaging are included. Study of a 3D microgenerator will be a future work.

For review, different tire contact points (touching area) or tire pressure affect different cases with different PU sizes were tested. For a single dimension emulated circuit model, the displacement rates will be used as a factor on the parameters' validation.

Another result is the density of strain energy, which is 1.58 J/m3. This density is used for estimating the available power for the micro-generator, which is discussed in Chapter 4.

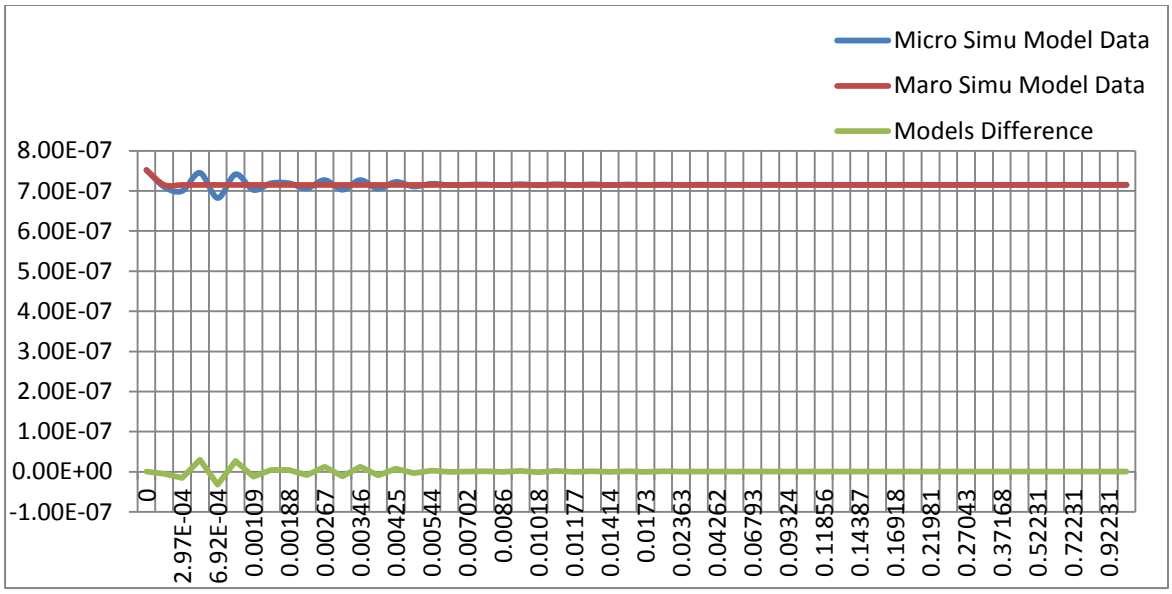

Fig. 3- 17 PU Total displacement time response function

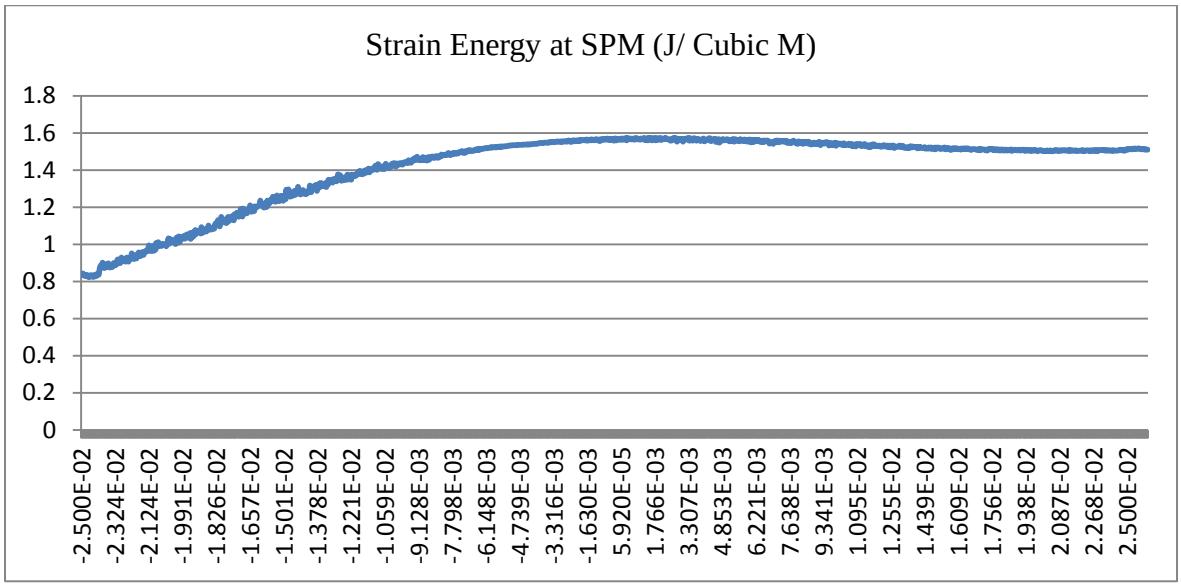

Fig.3- 18 Strain Energy Plot 1

3.3.2.2 CASE 2- PU AT SURFACE LAYER WITHOUT SPM BUT WITH NEW LENGTH AND WIDTH DIMENSIONS

This case is an exercise of the PU with smaller dimensions. The physical geometries of PU in this case are: $L_{|x}$ =10 mm, $W_{|y}$ =10 mm and $D_{|z}$ =50 mm. See Fig. 3- 19 PU Geometries in Case 2. The material properties are the same as Case 1.

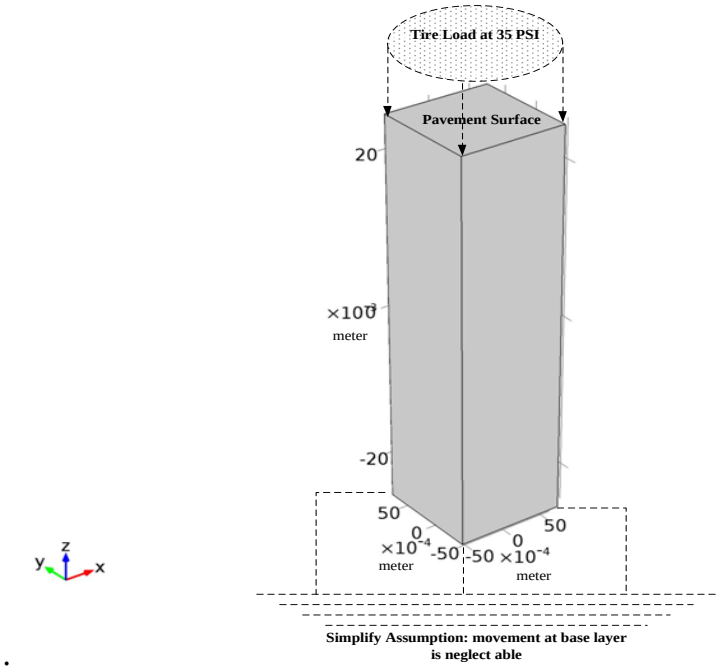

Fig. 3- 19 PU Geometries in Case 2

Fig. 3- 21, Fig. 3- 22 and Fig. 3- 23 show some plot results of the PU Case 2. The results are similar to Case 1, and the maximum displacement in Z direction is less than 1.5 μm. The displacement at x and y direction is smaller because of the bindery conditions (zero displacement on side faces). The displacement ratios for different directions are:

- D_{XZ}= (Displacement-X/ Displacement-Z)=% 4.1
- D_{YZ}= (Displacement-Y/ Displacement-Z)=% 4.1

In a practical case, the sizes of the aggregate have a maximum of more than 10 mm. Thus this PU case is not used in P-Model macro modules. For a single dimension emulated circuit, the effects of the displacement rate will not be significant.

The density of strain energy is 1.5 J/m^3.

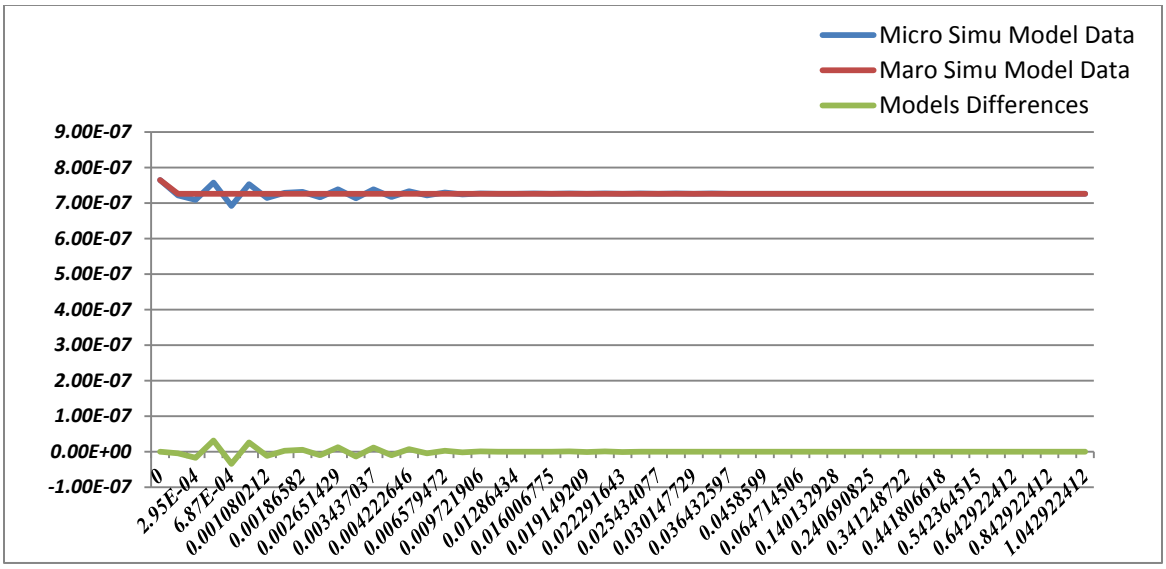

Fig. 3- 20 PU Total displacement time response function Plot 2

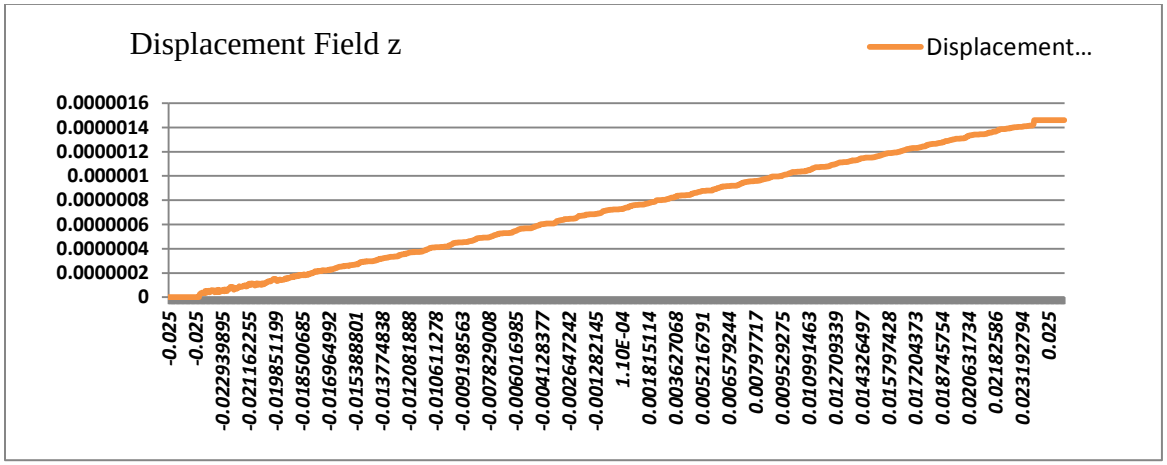

Fig. 3- 21 Z Displacements in PU Plot 2

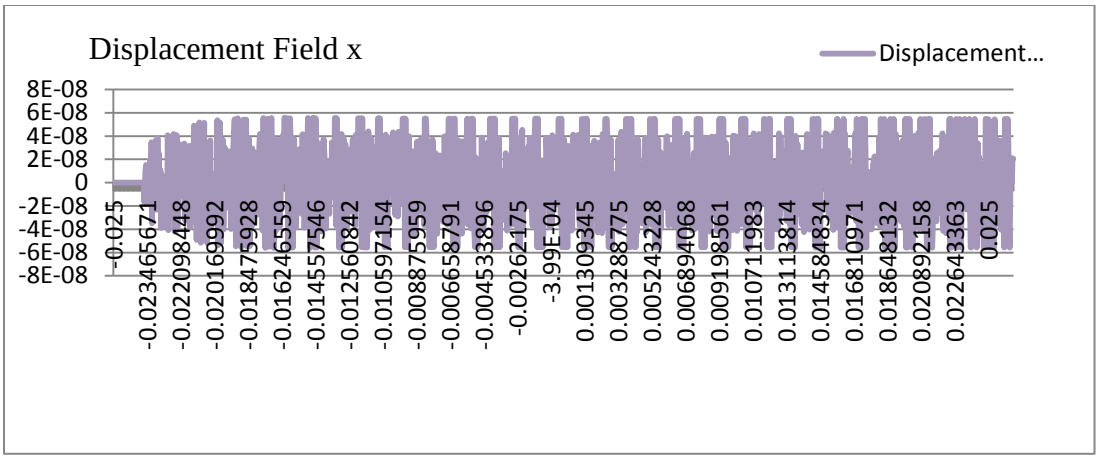

Fig. 3- 22 X Displacements in PU Plot 2

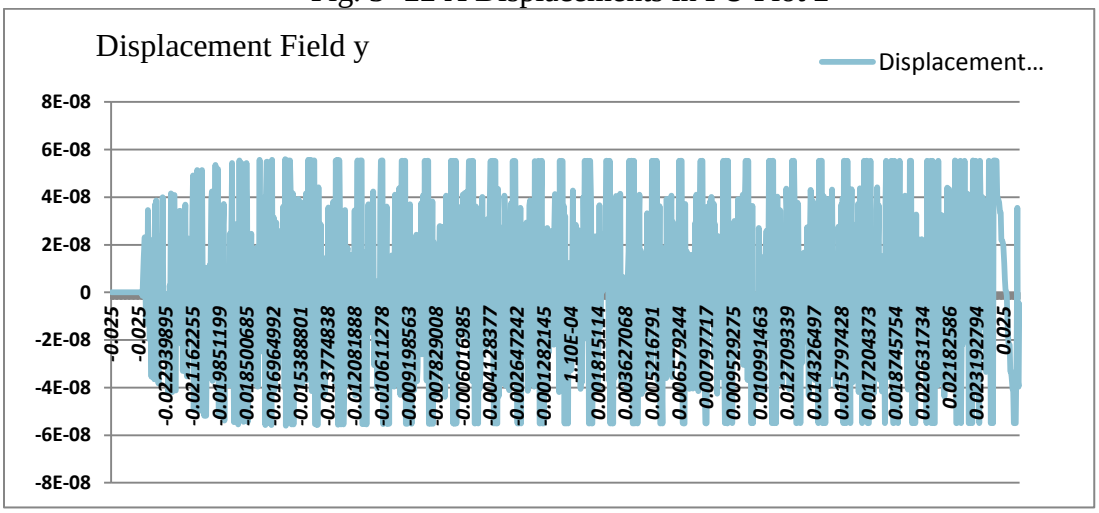

Fig. 3- 23 Y Displacements in PU Plot 2

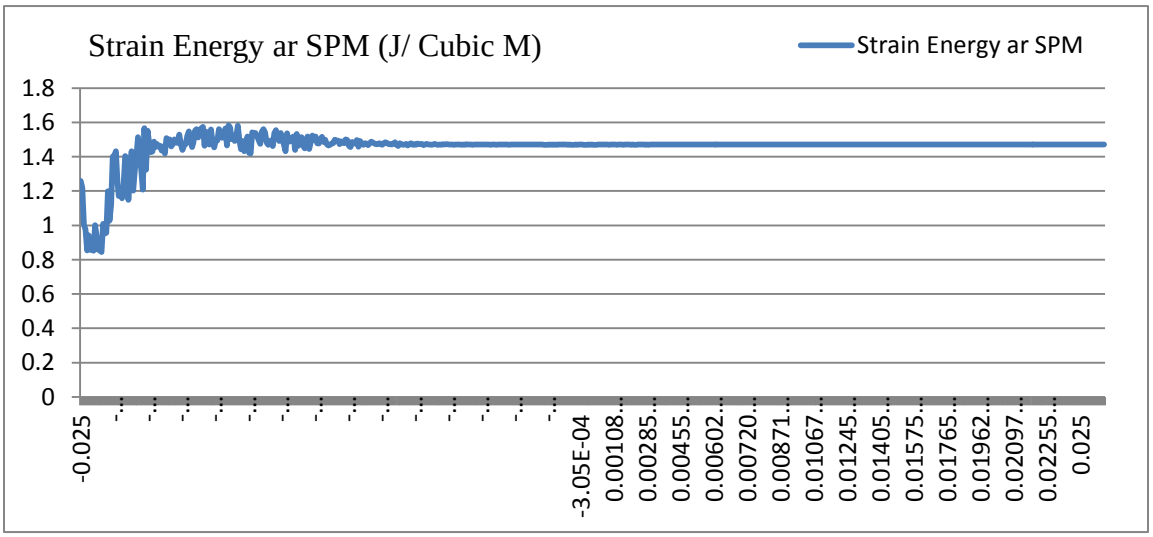

Fig. 3- 24 Strain Energy Plot 2

3.3.2.3 CASE 3 - PU AND BASE LAYER WITHOUT SPM

In this case study, the effects of the pavement multi layers (base and sub-base) are also included in the model simulation.

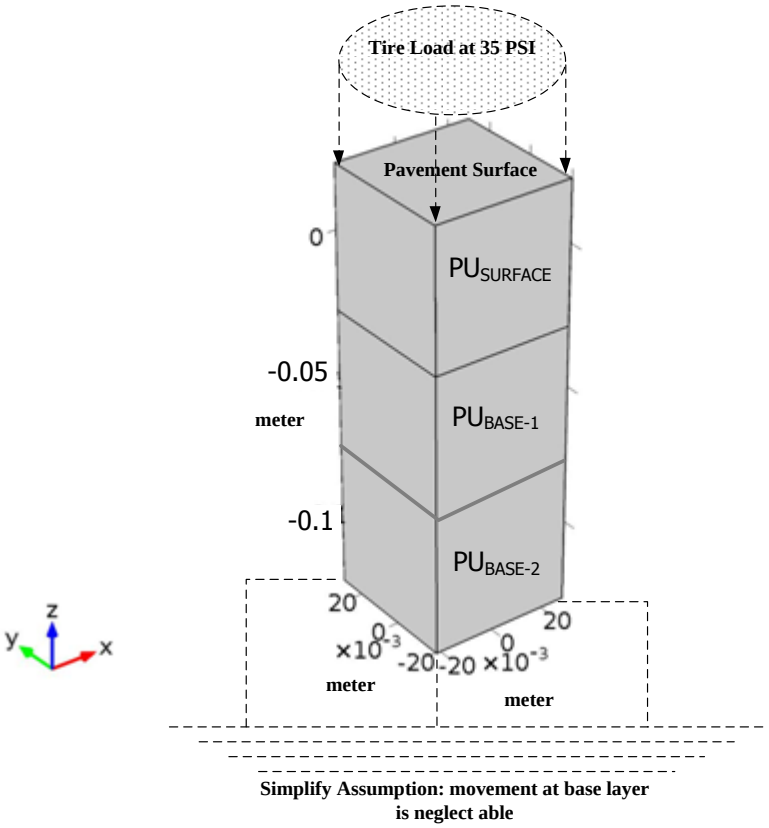

Fig. 3- 25 PU Geometries in Case 3

A stack of three PU in pavement layers is modeled. The physical geometries of each PU are:

- $PU_{Surface}$: $L_{|x}$ =50 mm, $W_{|y}$ =50 mm and $D_{|z}$ =50 mm,
- PU_{Base-1}: $L_{|x}$ =50 mm, $W_{|y}$ =50 mm and $D_{|z}$ =50 mm, (PU in interface with the Surface layer)
- PU_{Base-2}: $L_{|x}$ =50 mm, $W_{|y}$ =50 mm and $D_{|z}$ =50 mm, (PU in interface with Sub-Base or Grade layer)

The displacement results at each PU position are shown in Fig. 3- 26 to Fig. 3- 34. In this case, we are looking for displacement assessments on three different layers.

The displacement ratios for different directions are:

- $D_{XZ\text{-}Surface}$= (Displacement-X/ Displacement-Z)=% 5.9
- $D_{YZ\text{-}Surface}$= (Displacement-Y/ Displacement-Z)=% 5.9
- $D_{XZ\text{-}Base}$= (Displacement-X/ Displacement-Z)=% 6.5
- $D_{YZ\text{-}Base}$= (Displacement-Y/ Displacement-Z)=% 6.5
- $D_{XZ\text{-}Sub\text{-}Base}$= (Displacement-X/ Displacement-Z)=% 13.2
- $D_{YZ\text{-}Sub\text{-}Base}$= (Displacement-Y/ Displacement-Z)=% 13.2

Most displacement and strain energy are in z direction. Averages of strain energy in the PU are 1.46, 1.009 and 0.957 J/m^3. This density indicates the possibility for the SPM placement in each of these layers; however, the preferred layer will be the surface course. The calculation of the available energy for the SPM node depends on the SPM volume and number of activations. As discussed earlier, the heavy trucks will generate more loading, which provide more strain energy. For a single dimension emulated circuit model, the displacement rates will be used as a factor on the parameters validation.

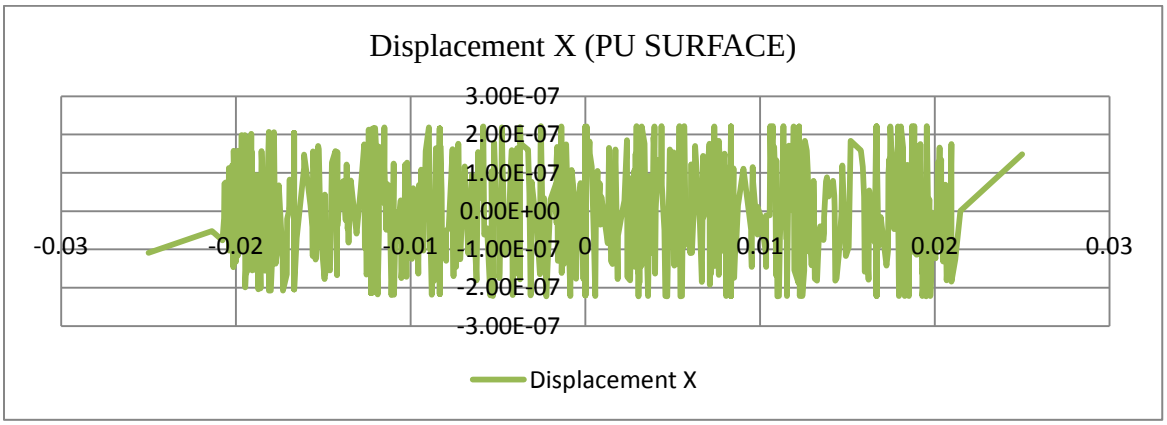

Fig. 3- 26 X displacements at z elevation in PU- Surface Plot 3

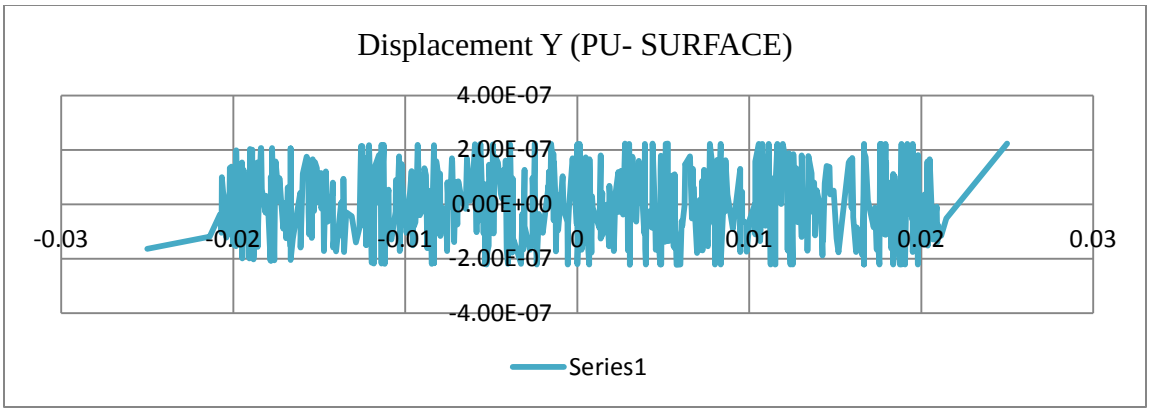

Fig. 3- 27 Y displacements at z elevation in PU- Surface Plot 3

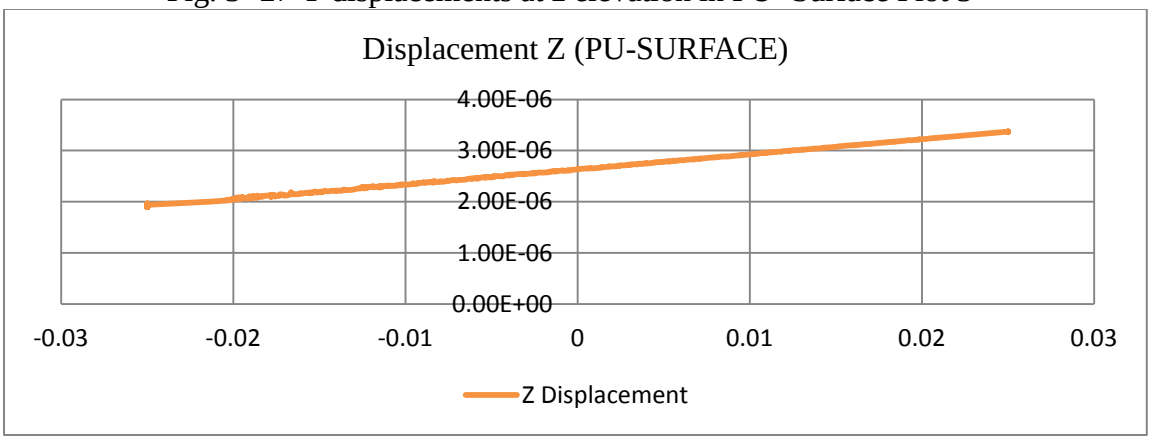

Fig. 3- 28 Z displacements at z elevation in PU- Surface Plot 3

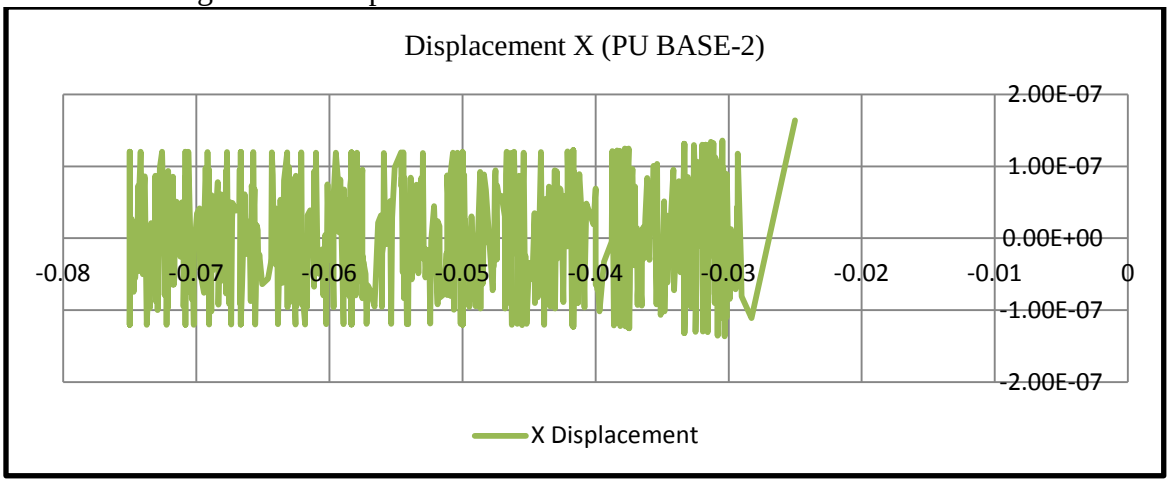

Fig. 3- 29 X displacements at z elevation in PU- Base 1Plot 3

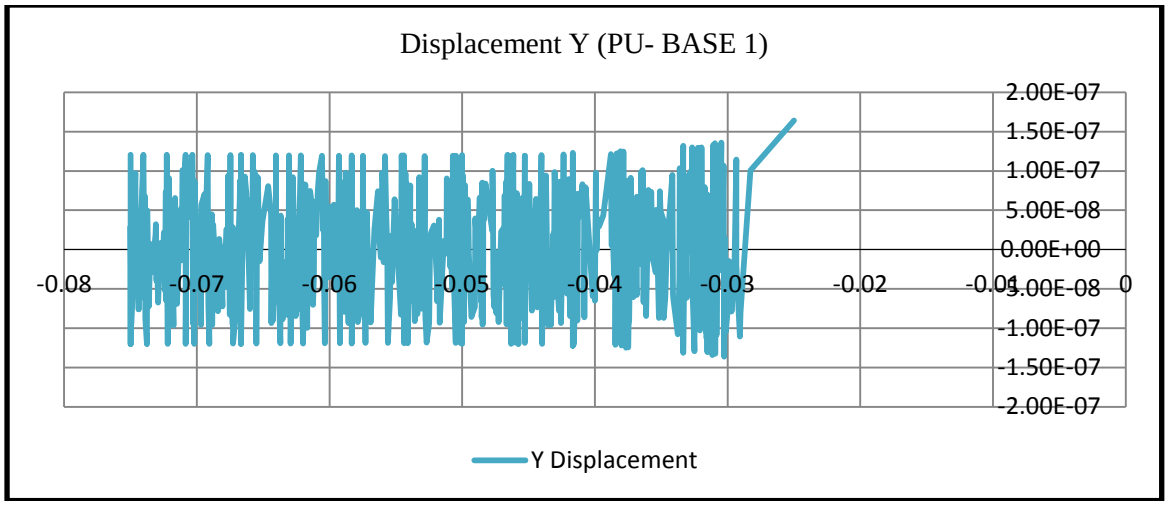

Fig. 3- 30 Y displacements at z elevation in PU- Base1 Plot 3

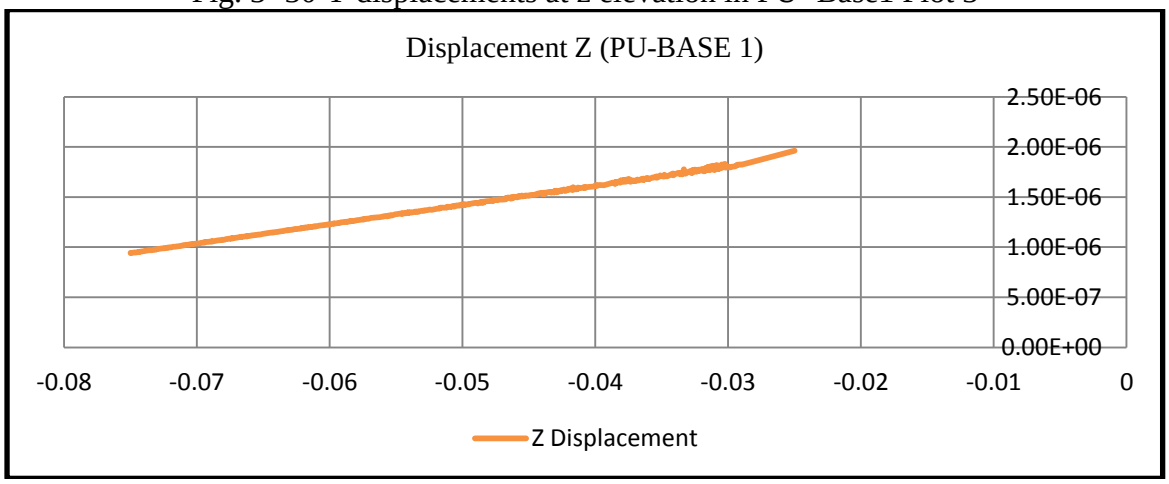

Fig. 3- 31 Z displacements at z elevation in PU- Base1 Plot 3

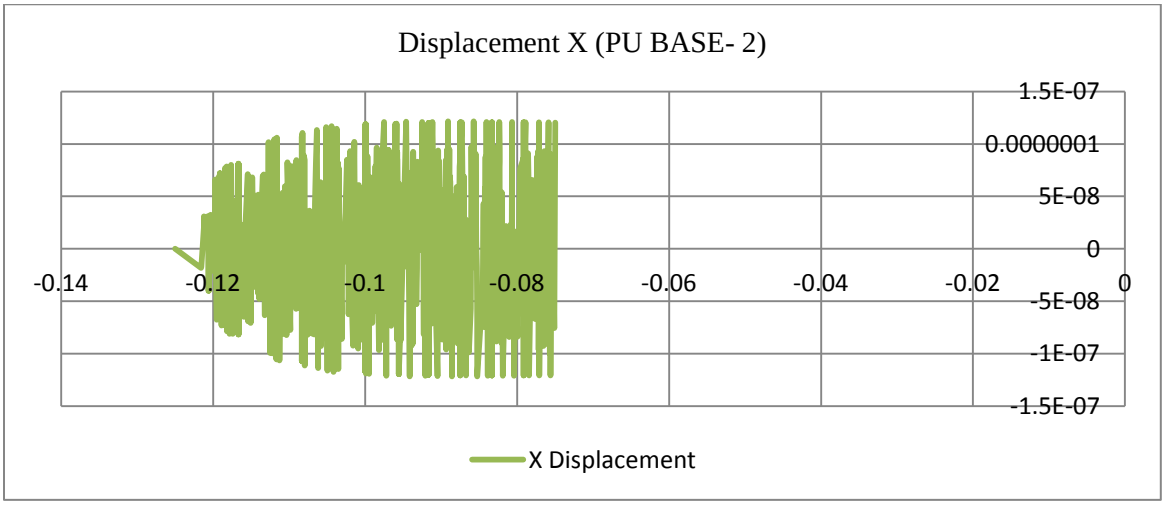

Fig. 3- 32 X displacements at z elevation in PU- Base2 Plot 3

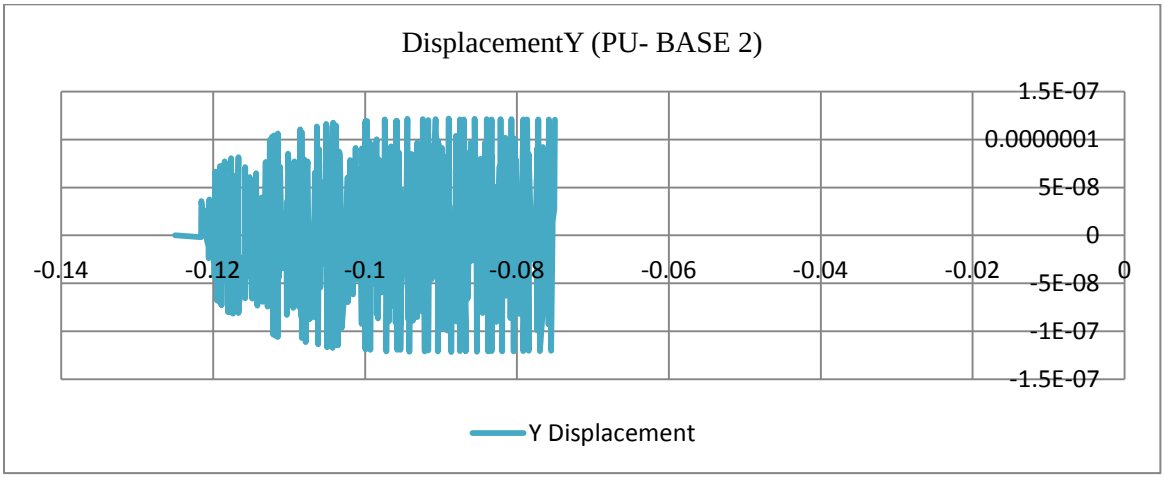

Fig. 3- 33 Y displacements at z elevation in PU- Base2 Plot 3

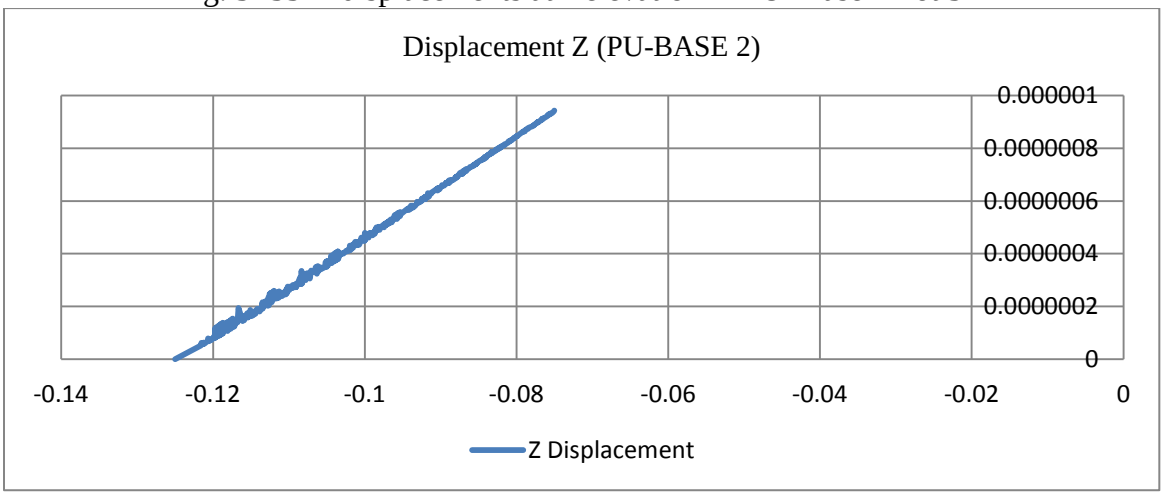

Fig. 3- 34 PU X, Y AND Z displacements at z elevation in PU- Base2 Plot 3

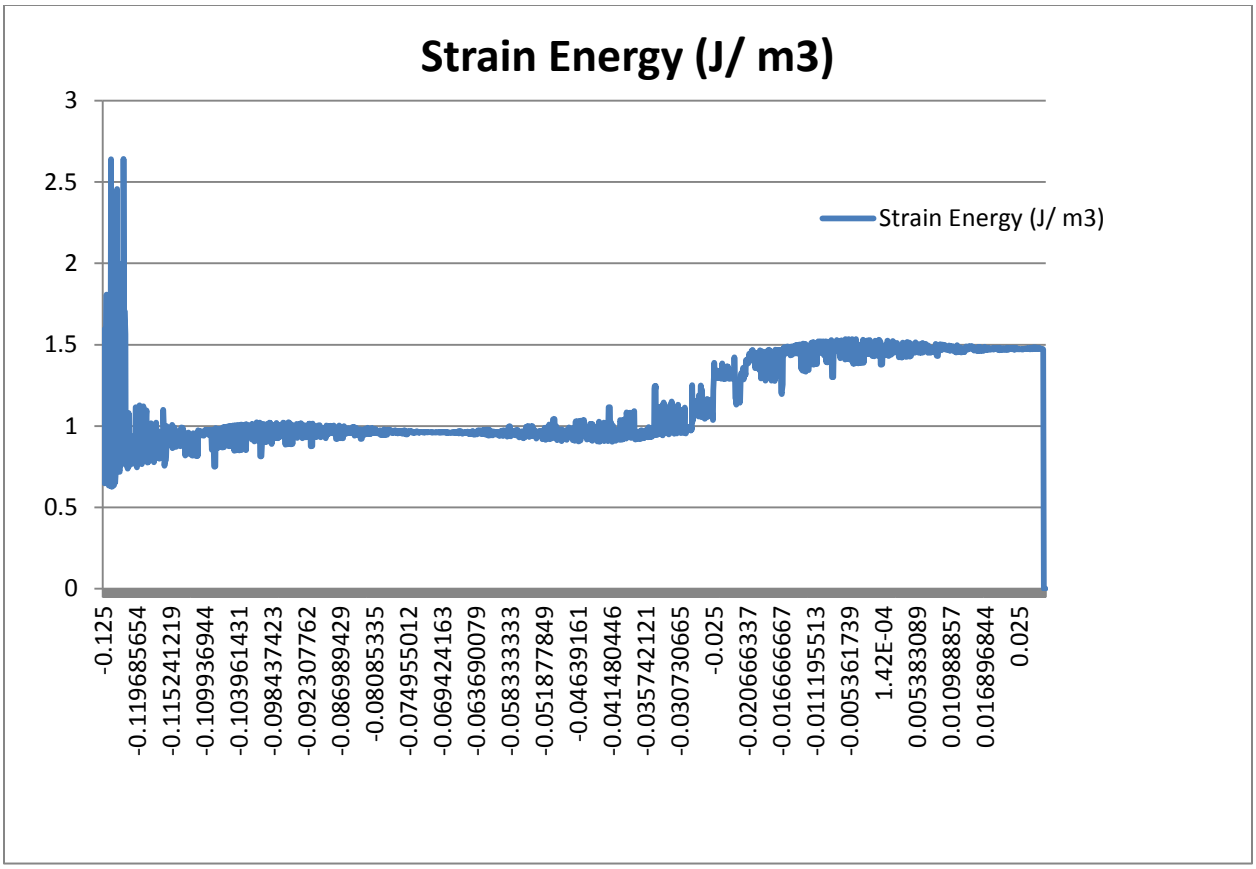

Fig. 3- 35 Strain Energy Plot 3

3.3.2.4 CASE 4- PU AT SURFACE LAYER WITH AN SPM

In this case, a surface PU characteristic is modeled with a semi SPM object. The semi SPM is a globe shaped object with polymer materials (majority materials of SPM). Because the limitations of the Comsol, exact SPM design structure details and materials did not appear in the micro modeling. Therefore, a simple form, semi SPM, was considered on this model. The physical geometries of the pavement unit are: Surface PU; $L_{|x}$ =5 mm, $W_{|y}$ =50 mm and $D_{|z}$ =50 mm, and the semi SPM has a radius of R=5 mm placed in the center of the PU. Fig. 3- 19 PU Geometries in Case 2 shows the geometries of this case. The size of SPM radius will be the subject of the SPM design and may be varied. In addition, the semi SPM placed in the center of PU in this case and other arrangements were tested.

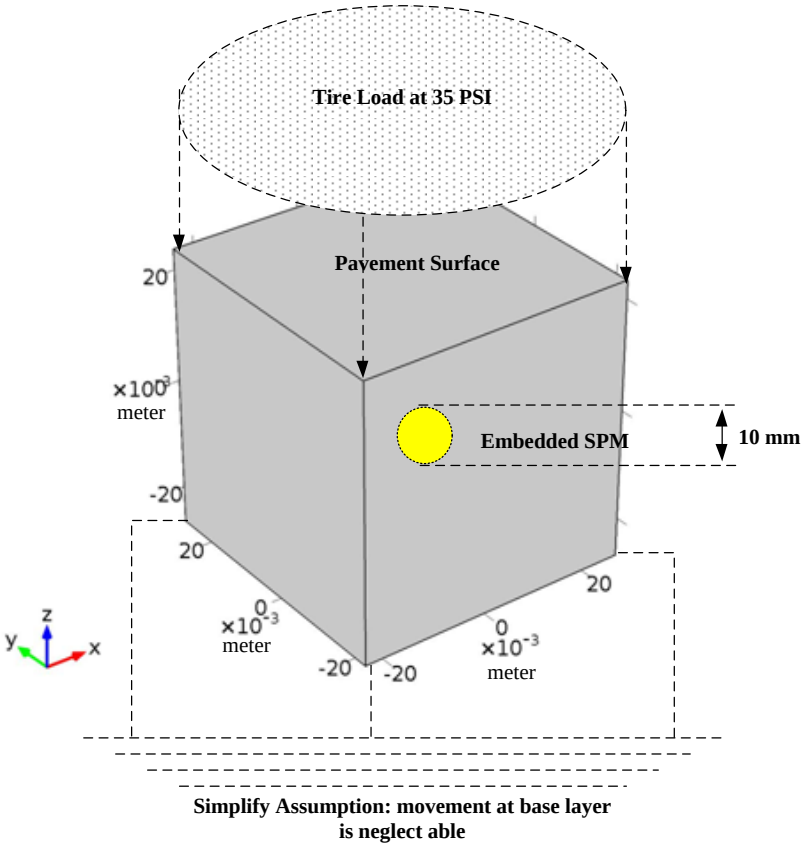

Fig. 3- 36 PU Geometries in Case 4

Displacement and the strain energy density profiles are shown in Fig. 3- 37, Fig. 3- 38 and Fig. 3- 39. In the energy density, the effect of SPM at the center of PU is clear.

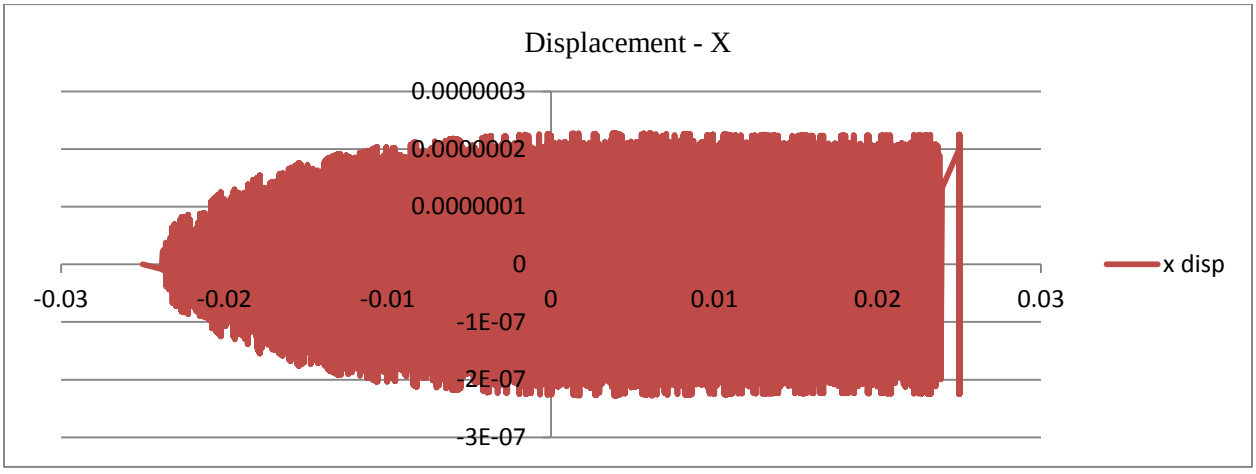

Fig. 3- 37 X displacements at z elevation in PU- Surface Plot 4

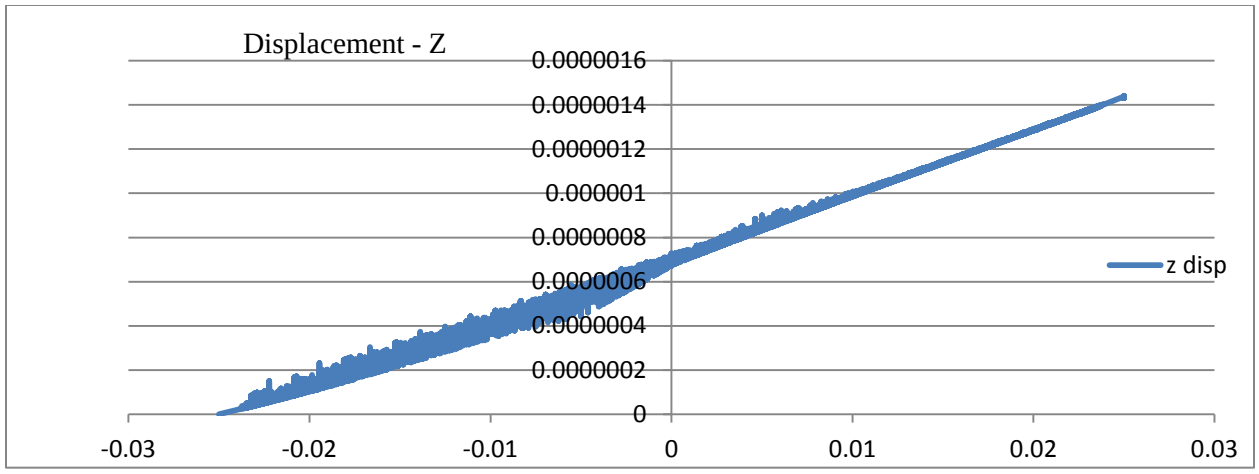

Fig. 3- 38 Displacement at z elevation in PU-Surface Plot 4

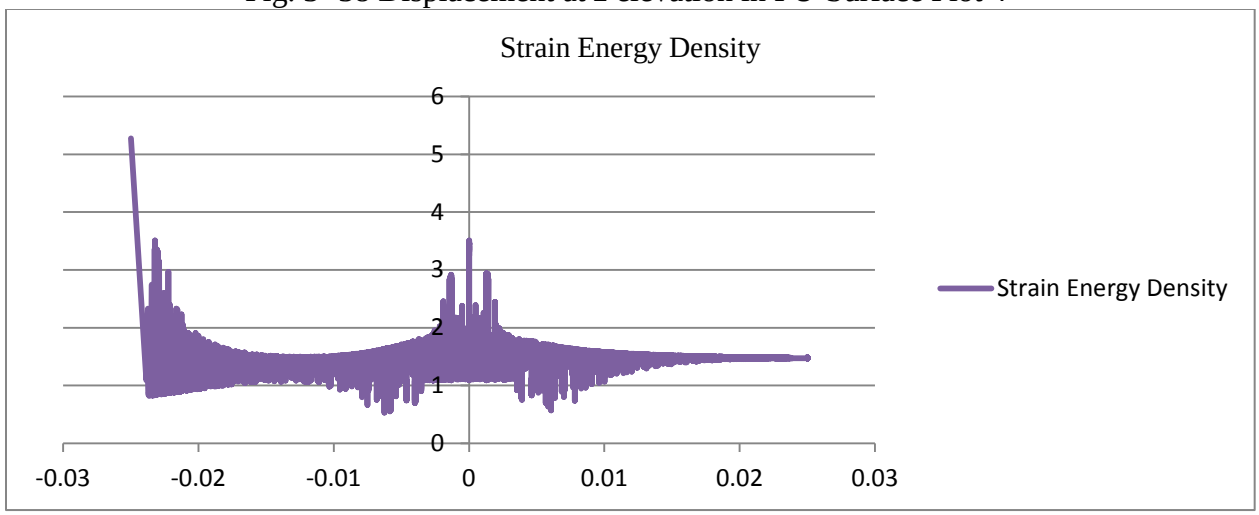

Fig. 3- 39 Strain Energy Density (J/ m^3) at z elevation in PU-Surface Plot 4

3.3.3 MULTI PU SECTION PAVEMENT RESPONSE REVIEW

In the last Section, individual PU cases were simulated and discussed. The complexity of the micro simulation mesh network makes the simulation of a large pavement sector impractical for the SPM study, but a small mini-section with multiple PU and multi semi SPM objects was modeled. In Fig. 3- 40, a small pavement section with four SPM objects in the pavement layer are presented as the geometry model. The X and Y distances between the SPM nodes are 800 mm. The SPM nodes are placed in the surface course layer.

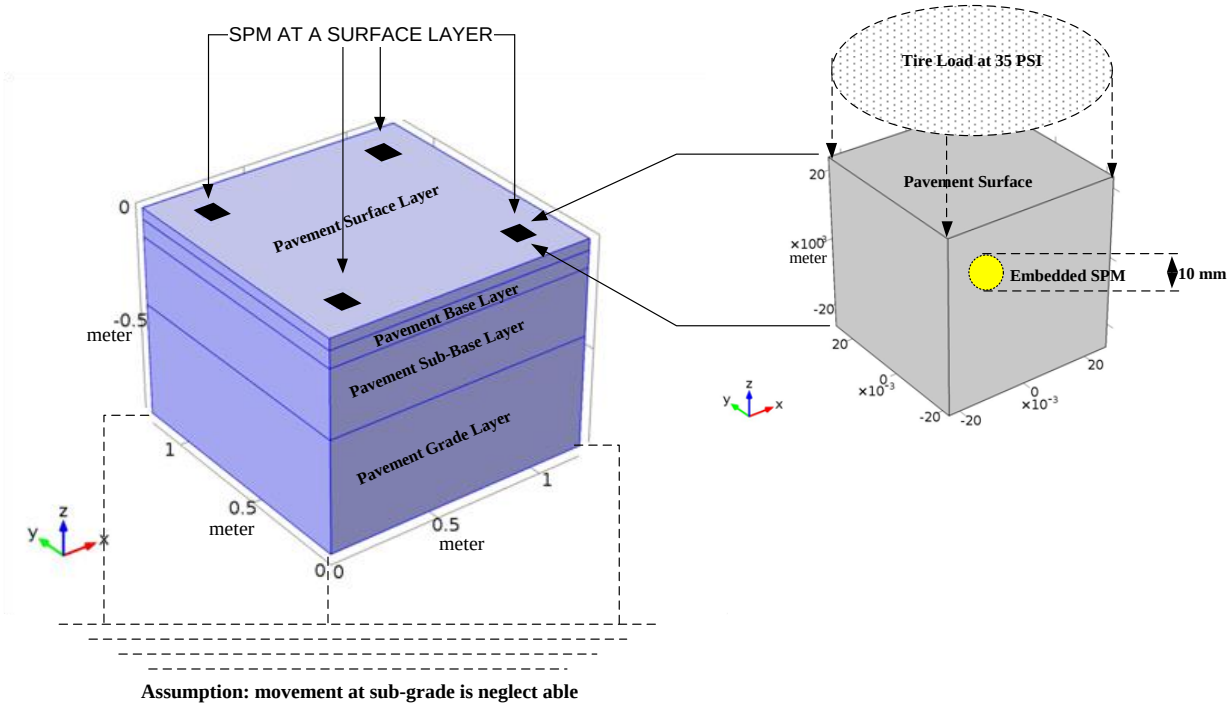

Fig. 3- 40 Small mini section Pavement with multi PUs Geometries in Case 5

The overall physical geometric information of this model is:

- Small Mini Section Pavement Length: $P_{L|x}$= 1.2 m, Small Mini Section Pavement Width: $P_{W|y}$= 1.2 m, Small Mini Section Pavement Depth: $P_{D|z}$= 0.95 m,
- Surface layer thickness: 50 mm
- Base layer thickness: 75 mm
- Sub-base layer thickness: 300 mm
- Sub-grade layer thickness: 500 mm
- PU geometries are: $L_{|x}$ =50 mm, $W_{|y}$ =50 mm and $D_{|z}$ =50 mm.

The PU at the surface pavement layer will have typical property values as listed in Table 3- 13 Table 3- 13 Default Pavement Parameters. The traffic loads are from a two axle vehicle (two SPM single activation stages). Other vehicle class with different axles and loads will have more SPM activation stages. The Comsol simulated model results are as follow:

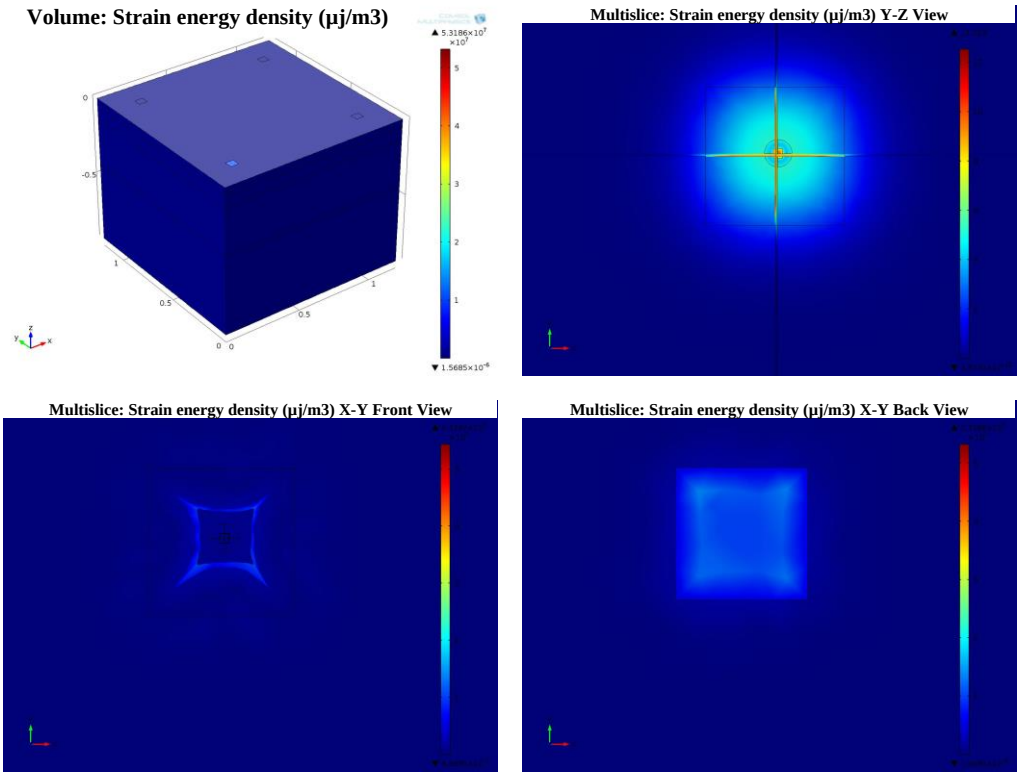

Fig. 3- 41 Strain energy density (µj/m^3), Plot 5

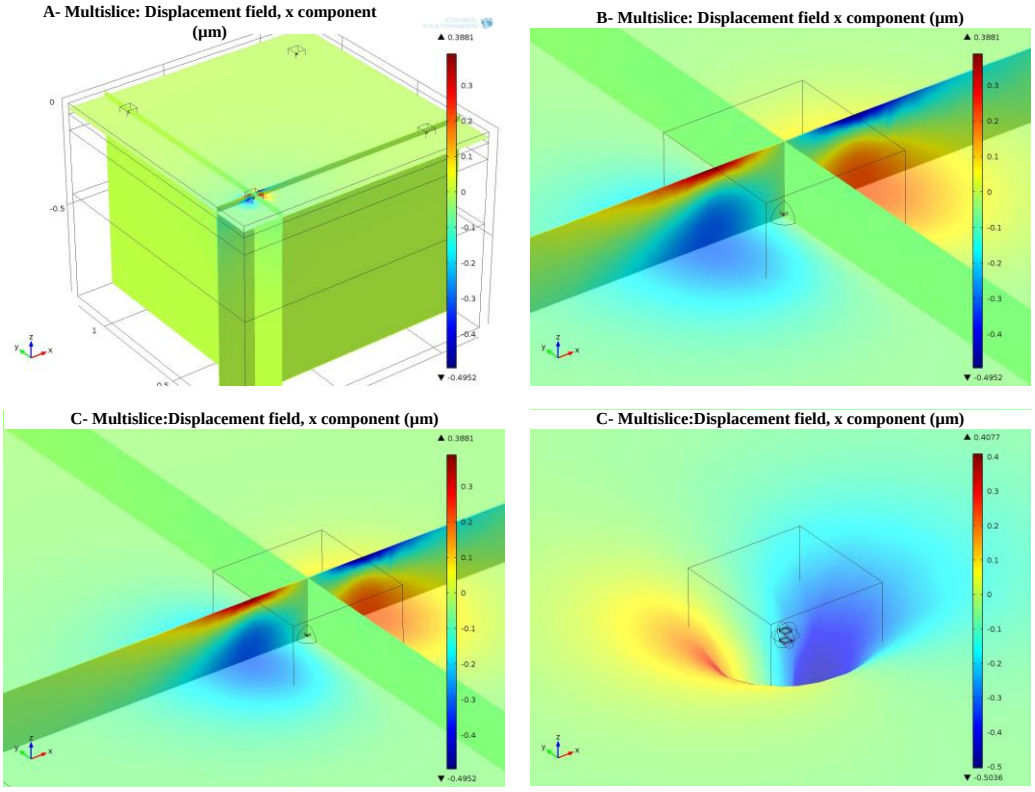

Fig. 3- 42 Displacement field x component (µm) Plot 5

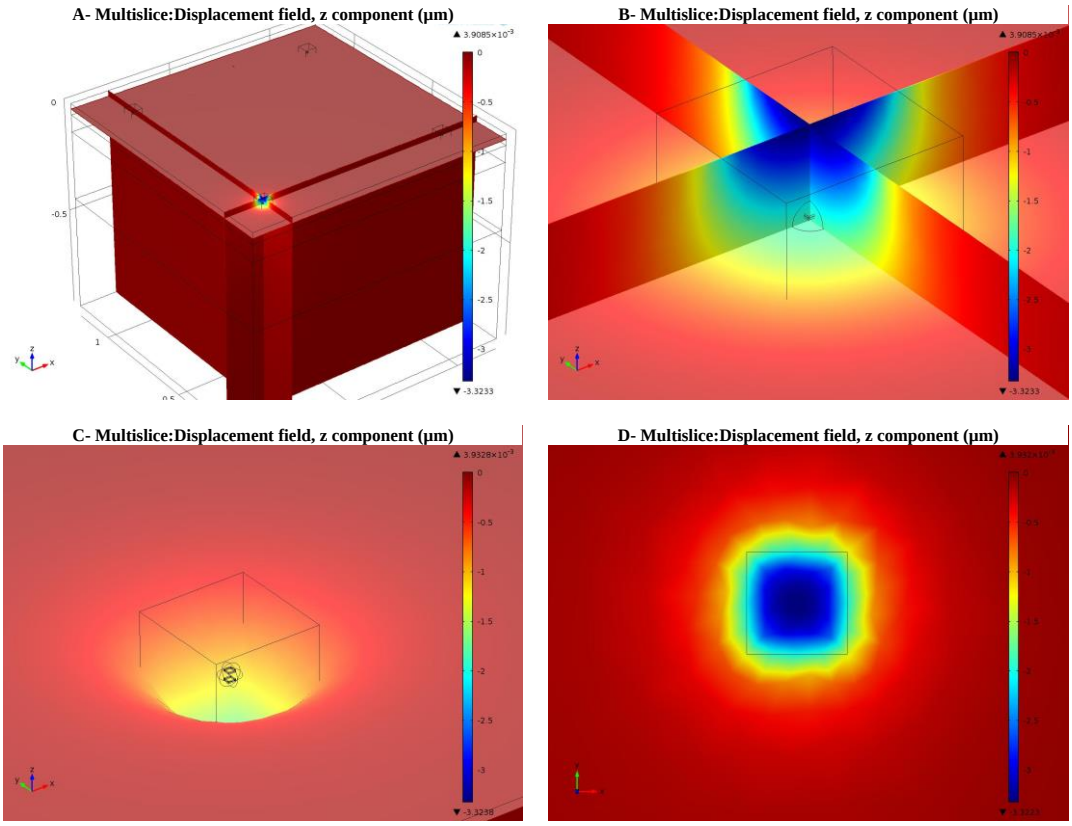

Fig. 3- 43 Displacement field, z component (µm) Plot 5

The proposed distances between the SPM nodes made the node activations independent from each other. The density of the strain energy will be less than 1% on the neighboring nodes. These results are valid for most vehicle classes, however for the heavy truck with double tires, a minor coloration is observed. For comparative analysis, the displacement characteristics are presented in Fig. 3- 44, Fig. 3- 45 and Fig. 3- 46. The displacements data are from a position of the active PU. As we can see and expect, the symmetry in X and Y displacements are assessed. In addition, we can conclude that the activated PU is only affecting the neighboring PUs. The displacement ratios for different directions are:

- $D_{XZ\text{-}Surface}$= (Displacement-X/ Displacement-Z)=% 4.5
- $D_{YZ\text{-}Surface}$= (Displacement-Y/ Displacement-Z)=% 4.5

These rates were calculated based on the maximum displacements of $5x10^{-2}$, $5x10^{-2}$ and 1.1 μm for X, Y and Z directions. Most displacement and strain energy are in the z direction. Averages of strain energy densities in each layer are: 1.84 (surface layer), $1x10^{-2}$ (base layer), $6.49x10^{-5}$ (sub-base layer), and $1.21x10^{-5}$ (sub-grade) J/m^3.These densities indicate the possibility for the SPM placement in the surface and top of the base layer. Fig. 3- 47 shows these energy densities for each layer. As a result, we conclude that the SPM operation at a sub-grade of deep sub-base layers shall be extremely limited to minimize the power consumption of the node. Such node shall only work as a sensor with no data processing function. This requirement shall be addressed in the SPM core module design.

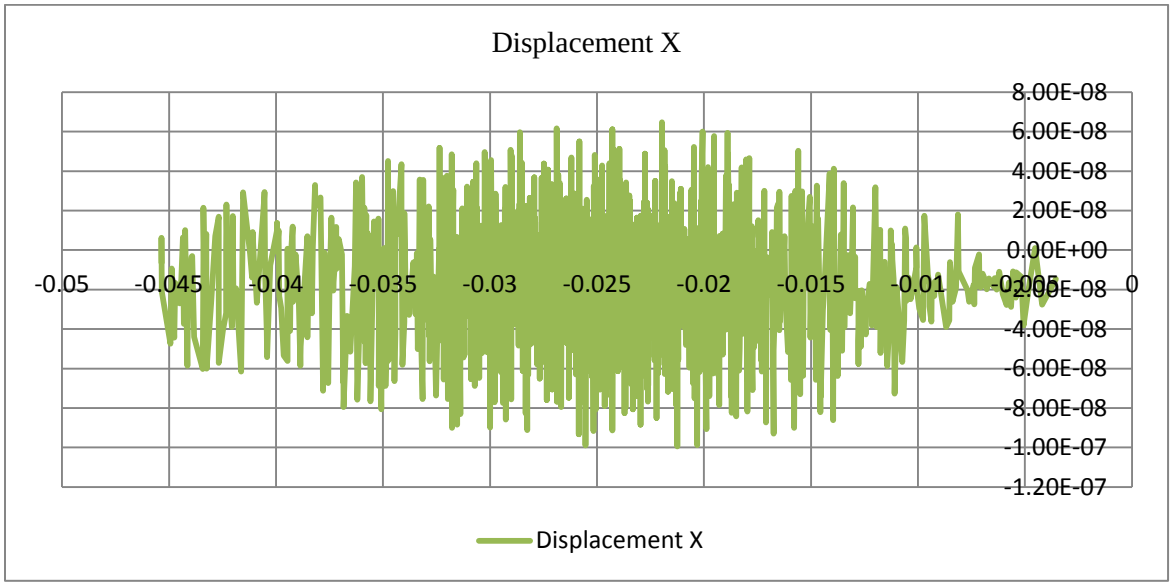

Fig. 3- 44 X displacement at z elevation in PU-Surface Plot 5

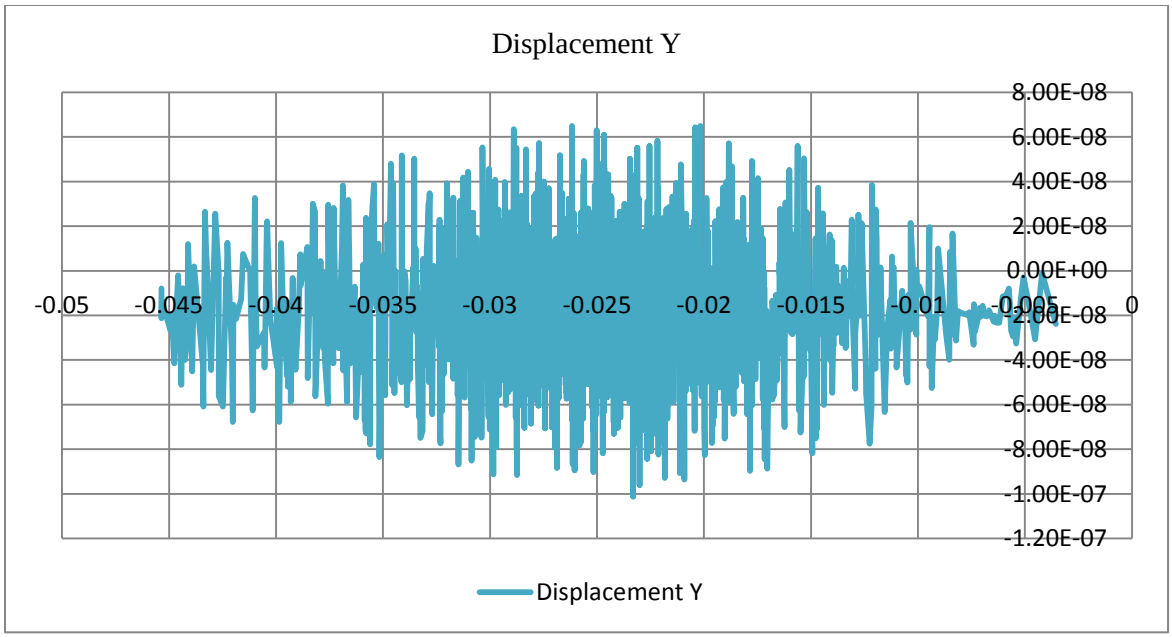

Fig. 3- 45 Y displacement at z elevation in PU-Surface Plot 5

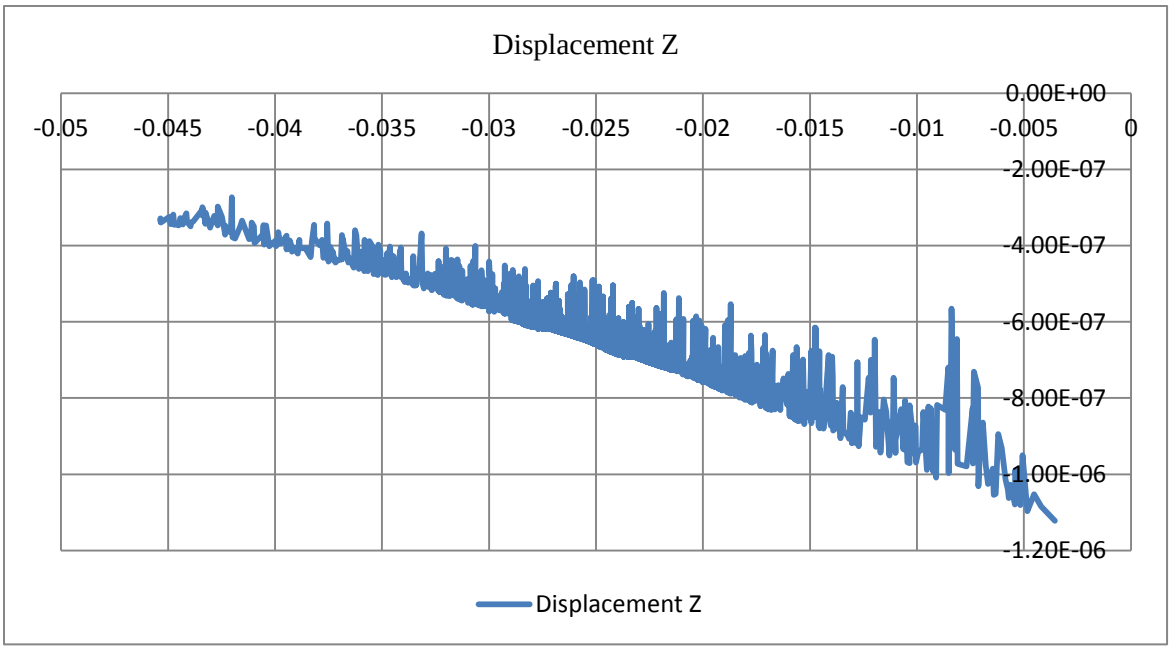

Fig. 3- 46 Z displacement at z elevation in PU-Surface Plot 5

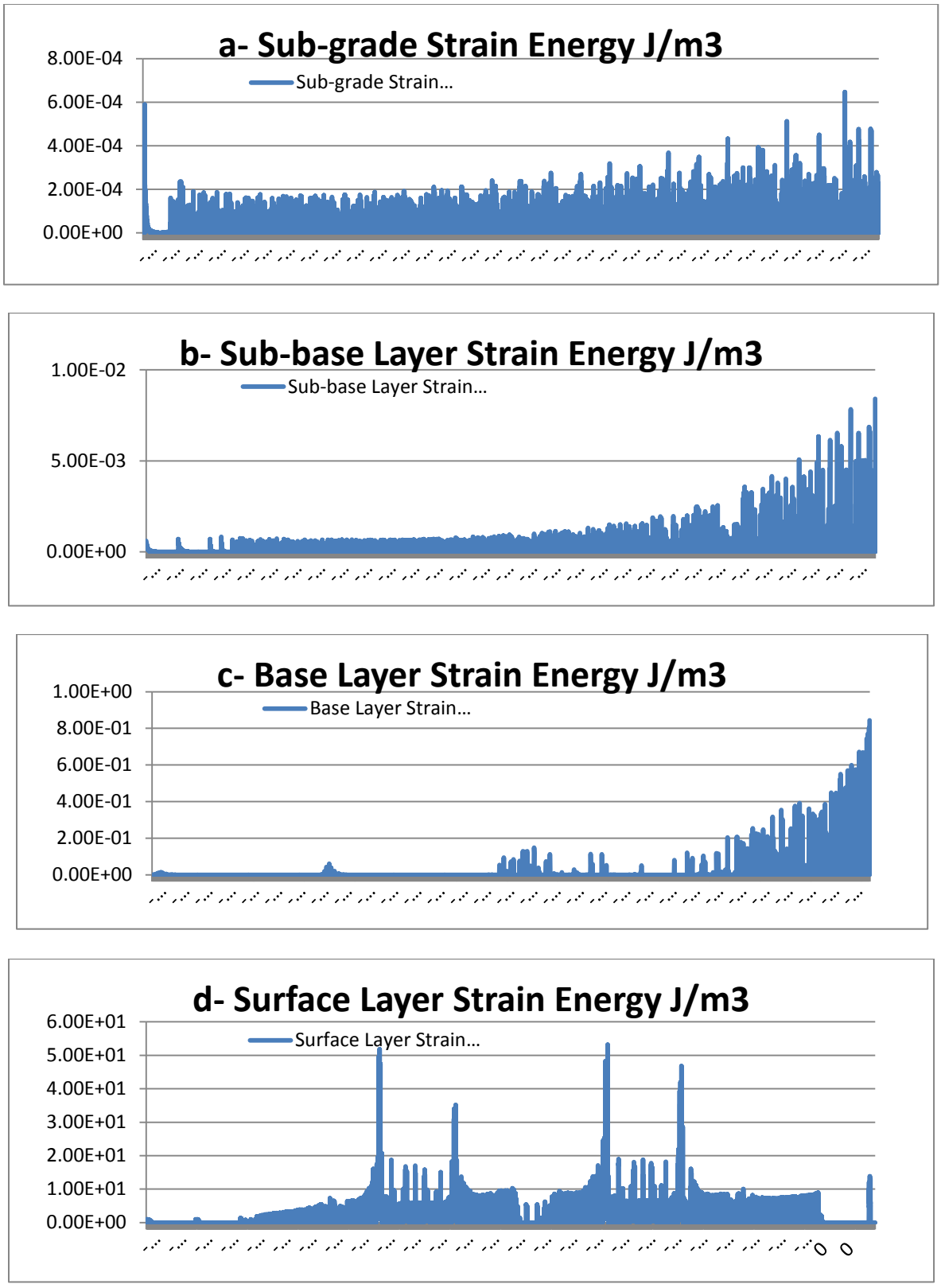

Fig. 3- 47 Small pavement section simulation, strain energy density at different layers (a,b,c,d)

3.3.4 PAVEMENT RESPONSE MODELS CONCLUSION

In this Section, we will review and propose a modeling process for pavement response for an SPM application. The SPM application looks for a method for designing the placement of the SPM nodes along the roadway pavement. This placement shall be designed to maximize the node energy absorption and increase the SPM microgenerator power output. In addition, the models also can be used for estimating some characteristic of the pavement response that can be used in other applications, such as a pavement management system or traffic operation system. The first modeling effort was based on a full micro simulation model. The traffic information was generated by M-Model outcomes. The micro model was only proposed for the pavement unit because of the complexity of the modeling and the computing limits for a large pavement section. Therefore, macro modeling was proposed for simulation of a large pavement section with a multi layered pavement structure. The macro model used a revised version of the Kelvin – Voiget material strain-stress model, which we discussed earlier in this Chapter.

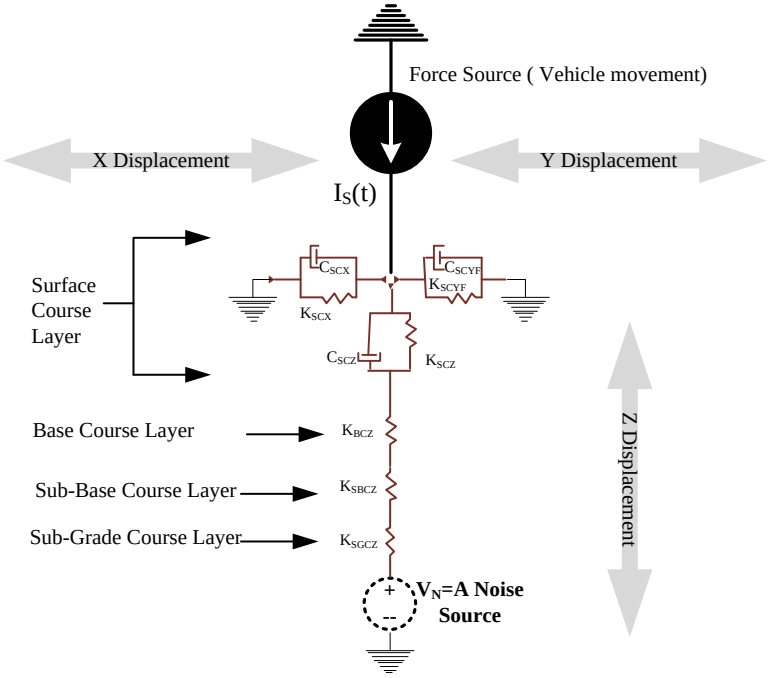

Fig. 3- 48 PEM Validated Model

Several cases were studied and PU simulations results were presented. Results of the PU micro simulation has been used for a validation of the PU emulated mode. Fig. 3- 48 shows a simplified emulated model for a PU at surface layer. A more comprehensive emulated circuit is shown in Fig. 3- 11, however, based on the displacement rate, the effects of X and Y movements are not significant (≃ %5) for the SPM application. All the model parameters considered as random variables with default values are included in Table 3- 12 A PEM - Example Pavement Parameters The model comparison with micro simulation results is shown as a variation less than 5% for the study's stated condition. The assessment data for the PU case 1 is shown in Fig. 3- 49 PEM Assessment Data. The model difference shows a mean of 2.866E-08 and a standard deviation of 9.18334E-09. In this PEM model, the V_n noise source was ignored and by considering it on the model, better results can be calculated. We will use the PEM simplified model in Fig. 3- 48 PEM Validated Model in analysis of the micro generator energy in CHAPTER 4 – ENERGY HARVESTING SYSTEM MODELING (S – MODELS).

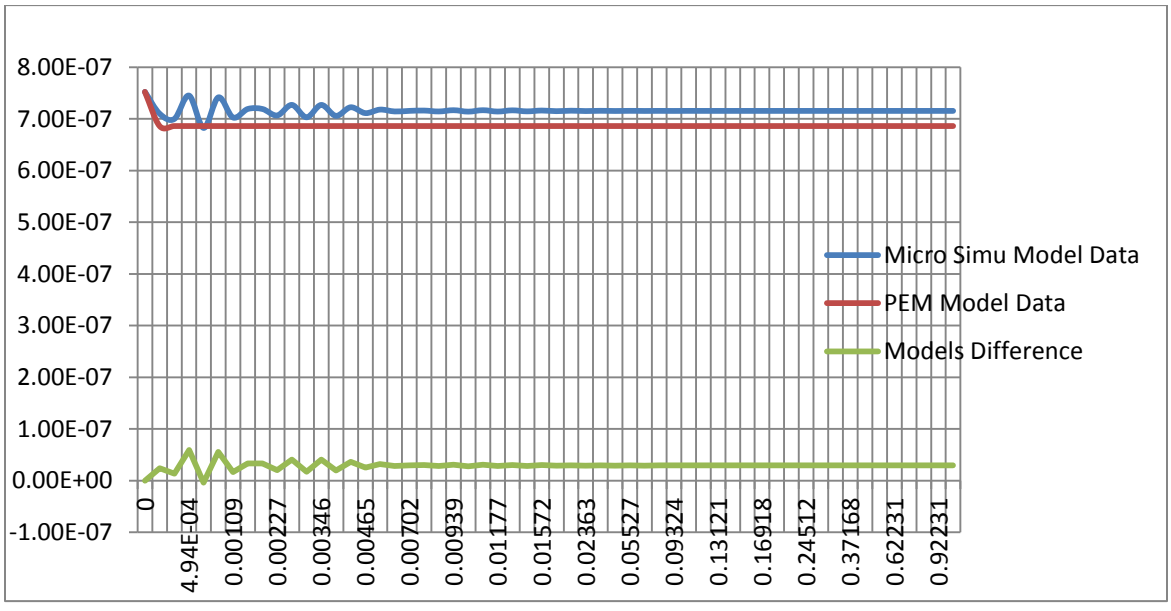

Fig. 3- 49 PEM Assessment Data

CHAPTER 4 – ENERGY HARVESTING SYSTEM MODELING (S – MODELS)

In the previous Chapters, we discussed and analyzed the environmental conditions of roadway pavement regarding the SPM application. Traffic and pavement response models provide information of the potential energy source, which is used for the SPM microgenerator design. In this Chapter, we analyze the SPM power system based on (a) the system component, (b) the energy conversion, and (c) the efficiency. The Chapter also includes the review and analyzes of harvesting methods for constructing the SPM micro power generators. The sub-components of the micro power generator also was reviewed and explored in this Section.

4.0 S-MODELS' CHAPTER OVER VIEW

This Chapter begins with the description of the SPM power system. The description covers the components of the proposed SPM as it is related to (a) the micro power generation, (b) power storage, (c) power distribution, and (d) power estimation.

The Chapter continues with the review and investigation of the energy harvesting methods. The explored methods are (a) Electrostatic, (b) Piezoelectric, (c) Electromagnetic and (d) a hybrid approach. This discussion also includes the energy conversion calculation and the microstructure alternatives analysis. The energy resource is calculated, based on the M and P series model results. The calculation was prepared for different roadway classes with typical pavement conditions. The study also includes the review of an SPM hybrid micro-generator alternative for the harvesting method.

In addition to calculating the energy resource, the energy conversion expectation was also presented. The study results are dependent on the materials and the generator structure that were conceptually reviewed and upon which a selected alternative was focused.

The chapter reviews several proposed micro structure alternatives. The structure selection is completely dependent upon (a) the fabrication process, (b) deposition and etching, (c) the material properties, and (d) the geometry limits of the micro generator. The fabrication process for the selected alternative is discussed and designed in CHAPTER 5 – PAVEMENT ON-CHIP MICRO GENERATOR DESIGN.

4.1 MICRO ENERGY HARVESTING REVIEW

In a large scale ITS deployment project, the power and communication distribution systems will be the main and most costly elements of the project implementation. In addition, when the mobility service will require complexity of the power service, distribution will be more essential. In micro system and sensor networks, the energy harvesting is a key technology for reduction of the power distribution and enables long-term operation. This solution has been used in low-power electronic devices such as human wearing items. By capturing waste energy from the environment sources such as (a) lighting, (b) heating/temperature differentials, (c) vibrations, (d) radio waves (RF energy) and (e) roadway traffic, a low power device can be powered.

In this study, we were focusing on the feasibility of the harvesting methods for absorbing waste energy on the roadway pavement. As discussed in the previous Chapters, traffic movement is a source of energy that transfers to the roadway pavement. This energy damages the pavement and reduces its performance. In the last Chapter, we simulated a pavement unit and showed the results of strain energy density on the pavement layers. We showed a surface layer PU can have a density of more than **1.5 J/m^3** at each activation time. Based on traffic distribution data from M-Models, the average energy can be more than a **150 µW** (potential energy source). This value for more congested roadway and truck roads will increase to **350 µW.** Of course, not all PUs will reach this potential energy source, but with optimum placement of the SPM node, the energy can

be available for the micro-generator. In the next Section, details of the energy resource analysis are presented. Based on the energy source, different types of harvesting methods are feasible and applicable for the SPM. In the case of a roadway pavement, the following methods were reviewed and considered:

- Electrostatic Energy Harvesting Method
- Piezo Energy Harvesting Method
- RF Energy Harvesting Methods
- Electromagnetic Energy Harvesting Method
- Thermal Energy Harvesting Method

4.1.1 SPM ENERGY HARVESTING SOURCE-VEHICLE WEIGHT DAMPING

Calculation of the expected energy source in pavement layers requires a review of the M and P model results as presented in Chapters 2 and 3. As discussed before, there are a large number of factors that will affect pavement modeling, primarily related to(a) the pavement material, (b) material distribution, (c) material size (aggregate material), (d) construction and quality of the installation work, and (e) level of complexity of the modeling as a single layer or full pavement structure. Therefore, this analysis is dependent on these factors and the assumptions in each step of the modeling process. The SPM energy source estimation conducted the following steps:

Step 1- Traffic Distribution: Based on the M-Model simulation, three input functions for the energy estimate are predicted as follows:

- Daily vehicle movement for all simulated traffic on a segment. This pavement dynamic function is called: Time Distribution Characteristic (TDC)
- Tire contacting placement for all simulated traffic on a segment. This pavement dynamic function is called: Space Distribution Characteristic (SDC)

- Vehicle classification for all simulated traffic on a segment. This pavement dynamic function is called: Loading Distribution Characteristic (LDC)

Based on the roadway class and geometry of the roads, these functions may generate a very large input matrix; however, we only include the inputs that are used for our targets. Additional parameters can be added to these inputs for other applications (future work). Table 4- 1 shows the summary of the TDC, SDC and LDC for five case studies in Section 2.3 VMM SIMULATION RESULTS.

Table 4- 1 TDC, SDC, LDC Examples-Summaries

	ROADWAYS	***BOSTON RD.***		***BROADWAY RD.***		***BRONX RIVER PARKWAY***		***HUTCHINSON RIVER PARKWAY***		***MAJOR DEEGAN EXPRESSWAY***	
	DIRECTION	NB	SB	NB	SB	NB	SB	NB	SB	NB	SB
TDC	**NO OF AXCELS**	28,900	29,530	19,899	19,792	106,703	112,991	104,346	106,035	128,568	123,504
TDC	**AVE. SAMPLE TIME (s)**	70.52	68.97	102.8	161.3	19.0	17.9	19.4	19.0	15.7	16.3
TDC	**AADT**	12,251	12,527	8,401	5,356	45,572	48,260	44,640	45,446	55,136	52,975
SDC	**NO. OF X POINT**	144	144	144	144	216	216	288	288	288	288
SDC	**NO. OF Y POINT**	2000	2000	2000	2000	2000	2000	2000	2000	2000	2000
SDC	**RESOLUTION (cm)**	5	5	5	5	5	5	5	5	5	5
LDC	**MIN LOAD (kg)**	303	303	303	303	303	303	303	303	303	303
LDC	**MAX LOAD (kg)**	2097	2125	1972	1972	2272	2272	2045	2045	1972	1978
LDC	**NO. OF CLASSES**	4	4	4	4	4	4	4	4	4	4

Step 2- Pavement unit energy estimate, in this step the available energy to a PU is estimated. The estimate value depends on the activation type.

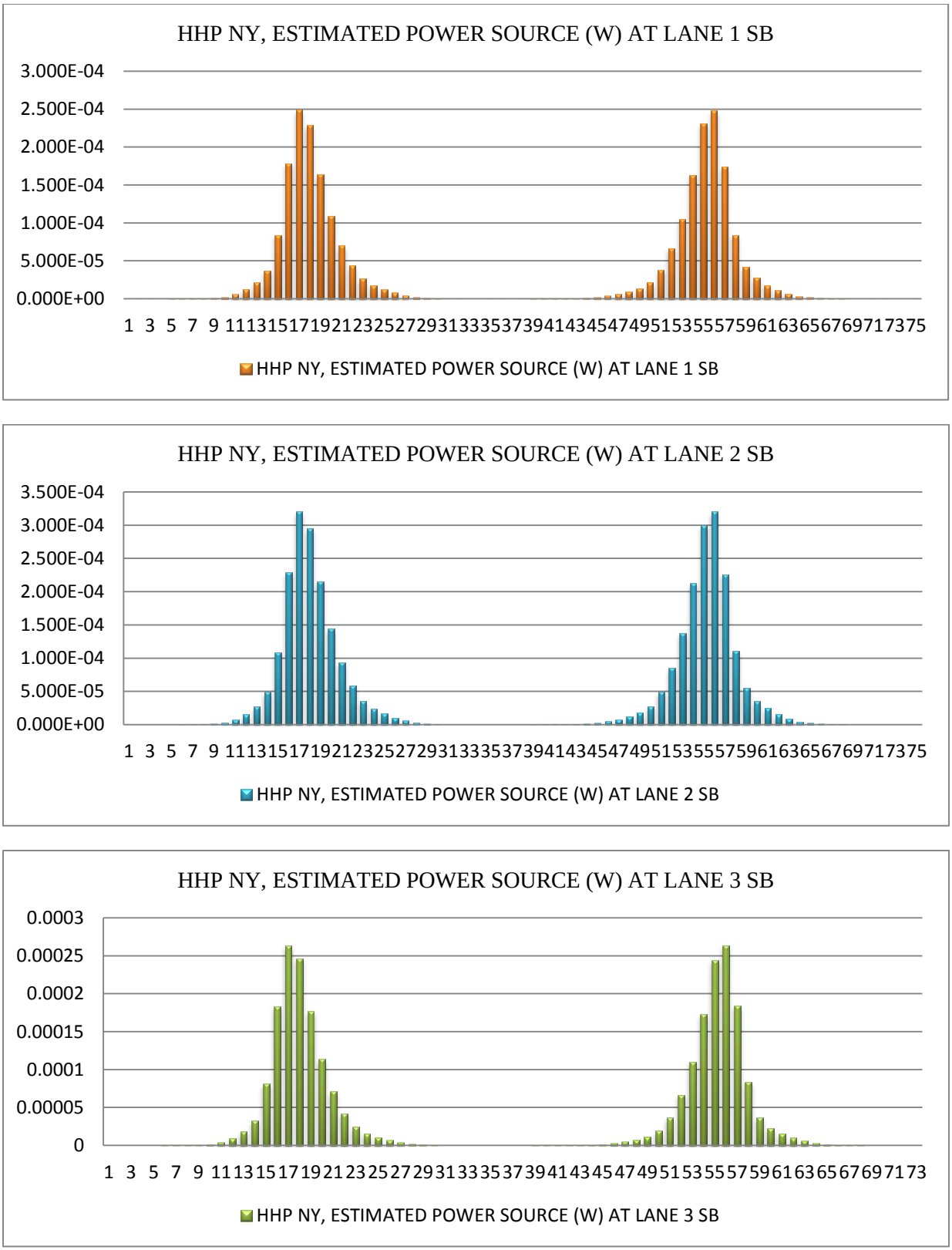

Fig. 4- 1 Henry Hudson Parkway NY, Estimated Power Source (Watt) at Lanes 1 to 3 south bound direction

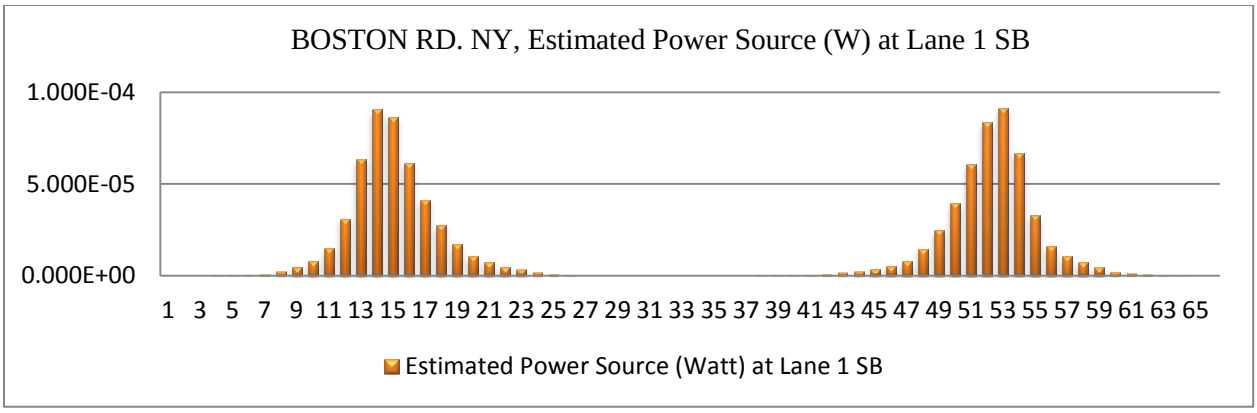

Fig. 4- 2 Boston Rd. NY, Estimated Power Source (Watt) at Lane 1 to 3 south bound direction

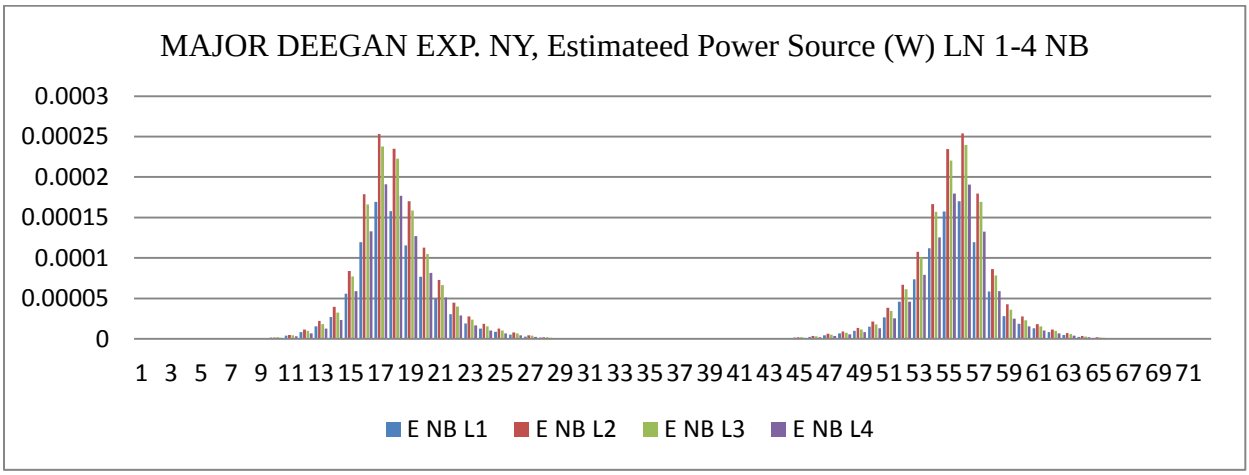

Fig. 4- 3 Major Deegan Exp. NY, Estimated Power Source (Watt) at Lanes 1 to 4 north bound direction

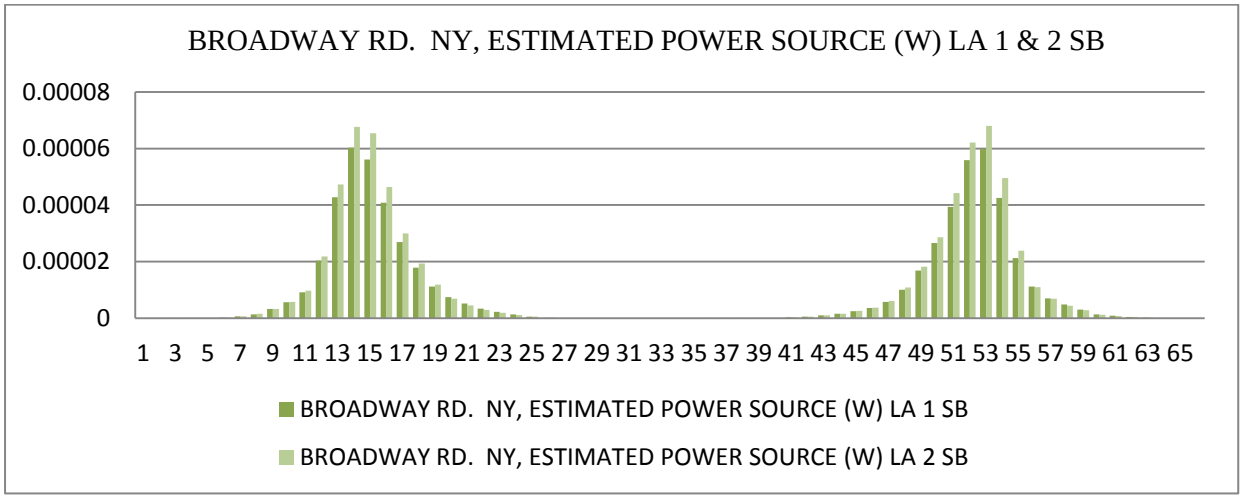

Fig. 4- 4 Broadway Rd. NY, Estimated Power Source (Watt) at Lanes 1 & 2 south bound direction

The activation type is referred to tire loading and tire offset from the PU. Based on the results of P-Model, the energy density of a PU with zero offset is estimated as:

PU Average Energy Density under Load = (LDC Load/250) x 1.5 J/m^3 Eq. 4- 1

In this equation, the constant density rate is measured from Fig.3- 18 Strain Energy Plot 1. Integrating the equation on the SDC chart with the average of TDC, the energy source of PU was calculated. That energy estimate is for typical pavement lane geometry (standard lane). As examples, the results for Henry Hudson Parkway, Boston Road and Major Deegan Expressway are presented in Fig. 4- 1, Fig. 4- 2, Fig. 4- 3, and Fig. 4- 4.

Step 3- Estimate PU average daily power; By calculating the number of daily activation and the tire offset over a PU we calculated the average daily power. If the SPM only placed on a zero offset PU (the PU that has maximum possibility of the tire contact), the maximum power source at the PU was predicted. In a heavily used roadway, such as Henry Hudson Parkway, the estimated power source reaches more than 300 µW. In the typical expressway or freeway roadway, this power will be expected. The AADT value is an index to be used for recognizing heavy loaded traffic conditions (with number of lanes)[23]. With the addition of heavy traffic, a high percentage of heavy vehicles also directly affects the power sources estimate. In the above examples, three classes of traffic were included (the density of other vehicle classes were neglected). In our design process, M-Model results specified the detail estimate not only for the power source but also for the most activated PU placement.

Qualify PU is a pavement unit proposed for housing a SPM node. A qualify PU should have the number of daily activations that can provide a minimum threshold power source for the SPM node. For 150 µwas the threshold value, we found the following qualify PUs:

[23] In other words, the highway traffic classification can be used.

Highway	Direction	Lane	PU
HHP	SB	1	16, 17, 18, 19, 54, 55, 56, 57
HHP	SB	2	16, 17, 18, 19, 54, 55, 56, 57
HHP	SB	3	16, 17, 18, 19, 54, 55, 56, 57
MDE	NB	1	17, 18, 55, 56
MDE	NB	2	16, 17, 18, 19, 54, 55, 56, 57
MDE	NB	3	16, 17, 18, 19, 54, 55, 56, 57
MDE	NB	4	17, 18, 55, 56

For 50 μwas the threshold value, we can find the following qualify PUs:

Highway	Direction	Lane	PU
Boston	SB	1	13, 14, 15, 16, 51, 52, 53, 54
Boston	NB	1	13, 14, 15, 16, 51, 52, 53, 54
Broadway	SB	1	14, 15, 52, 53
Broadway	SB	2	14, 15, 16, 52, 53, 54
Broadway	NB	1	14, 15, 52, 53
Broadway	NB	2	13, 14, 15, 16, 52, 53, 54

The threshold of 150 μW for a typical local road is not achievable and no qualify PU can be found. As for results, we should categorize the SPM charging capability based on the roadway class and limit the SPM application for each class. This estimation analysis directly depends on traffic volume, but the above thresholds of 150 μW for freeways and expressways, and 50 μW for local/access roads, are acceptable estimates based on our study. It is necessary that the SPM power management module balances the running applications to comply with the power limits.

4.1.2 SPM ENERGY HARVESTING SOURCE-ACOUSTIC/NOISE

Roadway traffic is a source of the noise. This noise as an environment pollution has been controlled by noise barriers naturally (trees) or by manmade noise walls around the major roadways. This source of energy will be very small in comparison with traffic loading. Noise level at a roadway can be measured and estimated based on traffic information. The traffic data are:

- Both Direction Vehicle Traffic per Hour- Day Time: 4000
- Both Direction Vehicle Traffic per Hour- Night Time: 1000
- Both Direction Truck Traffic per Hour- Daily: 400
- Average Vehicle Speed, Mile/Hour: 50
- Average Truck Speed, Mile/Hour: 50

The level of noise will be in a range of:

- Ldn[24]= 71 (in distance of 10 m)
- Ldn= 87 (in distance of 2 m)
- Ldn= 90 (in distance of 1 m)

The noise power range will be 0.0015 to 0.24 µW/ cm^3, which means the estimated acoustic power source, will be 0.187 to 30 µW. This range, compared with 50 to 300 µW of the traffic damping source, is a much smaller source. As a result, we did not consider this source for SPM microgenerator design. However, a hybrid generator with acoustic and damping harvesting

[24] **Ldn:** The Day-night Average Sound Level (Ldn) is the level of noise expressed (in decibels) as a 24-hour average. Nighttime noise, between the hours of 10:00 p.m. and 7:00 a.m. is weighted; that is, an additional 10 decibels is added to compensate for sleep interference and other disruptions caused by nighttime noise.

methods could be considered in some future work. More details for a Traffic Noise Model[25] may be found on the FHWA site.

4.1.3 SPM ENERGY HARVESTING SOURCE- THERMAL

Thermal conductivity and thermal expansion are physical effects which have been used for an energy harvesting method. Micro thermal generators based on the Seebeck effect do have widespread future applications as a micro energy source. A thermal generator does need a temperature difference, which depending on the application, is generated by different elements.

In the SPM node, a weak temperature difference will be the pavement temperatures at different pavement depths. We called it a weak source because it is a significant temperature difference. However, we can have more temperature differences at surface layers and micro thermo generators can be considered. The thermal generator is now capable of supplying the appropriate sensors and microprocessors with energy and with the storing of the measured data in the microprocessor [22].

The important requirement for the generator environment is the rate of the temperature difference. In the pavement layers with an SPM node size as little as a few centimeters, it is difficult to reach a good temperature difference for the thermal generator. We did not find specific research in this topic for pavement applications but other applications and micro systems with thermal harvesting were investigated. In a study reported by Tan and Panda [23], it was estimated:

- 60 $\mu W/cm^2$ at 5º C gradient
- 135 $\mu W/cm^2$ at 10º C gradient

[25] http://www.fhwa.dot.gov/environment/noise/traffic_noise_model/

These numbers indicate high generation but not for pavement condition/applications. The temperature gradient in the pavement elevation structure is smaller and the maximum operation temperature also is lower, 50º C, in comparison with other applications. The efficiency of a thermal generator in gradient less than 5º C may cap to 1% [23]. This generating efficiency will be more when higher temperature operations will be granted. In Fig. 4- 5, power generating of an available thermo generator device component, TEG[26] is shown.

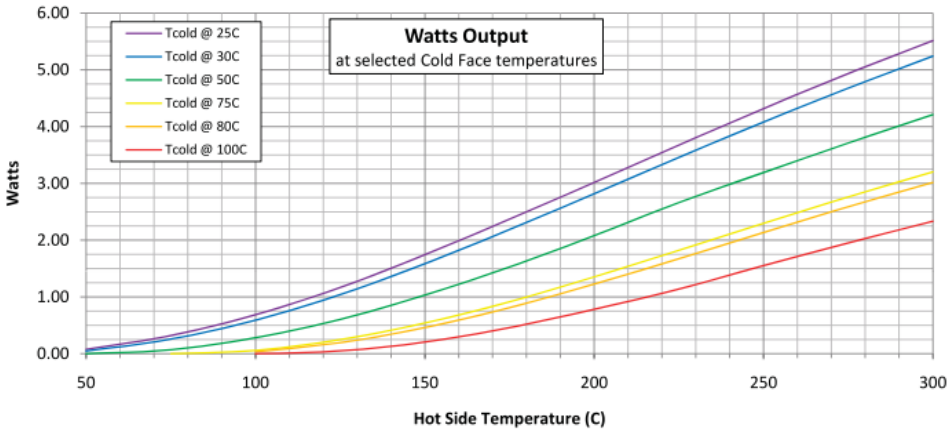

Fig. 4- 5 Example of an Eexisting Thermo Generator Device Component [24]

The temperature difference expected in the pavement layer can be estimated with different models such as in versions of the SHRP[27] models (Mohseni and Symons). The maximum temperature of roadway pavement in a depth d for an annual predication is expressed as [25]:

$$T_{Pavement\text{-}Max} = [T_{Surface\text{-}Max} + 17.8] \times [1 - 2.48 \times 10^{-3} d + 1.1 \times 10^{-5} d^2 - 2.4 \times 10^{-8} d^3] - 17.8 \qquad \text{Eq. 4- 2}$$

For SPM at the depth of 30 mm to 45 mm, the upper limit size for the SPM structure, the $T_{Pavement\text{-}Max}$, values are:

- $T_{Surface\text{-}Max}$ =40 º C Depth=30 mm $T_{Pavement\text{-}Max}$= 35.610 º C
- $T_{Surface\text{-}Max}$ =40 º C Depth=45 mm $T_{Pavement\text{-}Max}$= 33.774 º C

[26] Seebeck Thermoelectric Generator from Custom Thermoelectric Part No. 1261G-7L31-04CL
[27] SHRP: Strategic Highway Research Program; http://www.shrp2nds.us/

- $\Delta T_{Surface\text{-}Max} = 1.836\ ^{o}C$

This temperature gradient is not large enough for producing power required by the SPM. It is noticeable that when the above temperature is annually predicted, the daily estimate will be expected to be lower. Diefenderfer's research [25] proposed a predication model based on field investigation in the Virginia Smart Road program as follows:

$y = 0.6861x_1 + 5.6736x10^{-4} x_2 - 27.8739x_3 + 2.78752$ Eq. 4- 3

- y = predicted pavement temperature (°C);
- x_1 = daily minimum ambient temperature (°C);
- x_2 = calculated daily solar radiation (kJ/m 2 day); and
- x_3 = depth from the surface (m)

Changing the depth from 30 mm to 45 mm will show a temperature difference of 0.418°C.

Thus, pavement $\Delta T < 2°C$ and thermal micro generator will not be the prime approach.

As a conclusion, we did not consider a thermo generator as a primary micro-generator for the SPM node, but, it is considered for as a secondary generator. It is also important to know that a temperature sensor is a necessary sensor for the SPM node; therefore, designing of a sensor with a power generating option can be considered for future work. An example of existing micro thermo generator devices in the market is Micro Pelt Thin Film microgenerator and sensor device "MPG-D751". This device has an area of 4248 x 3364 $(\mu m)^2$ and thickness of 1096 μm. The Seeback voltage of the generator is 140 mV/K [26]. The device layout and the output power are shown in Fig. 4- 6.

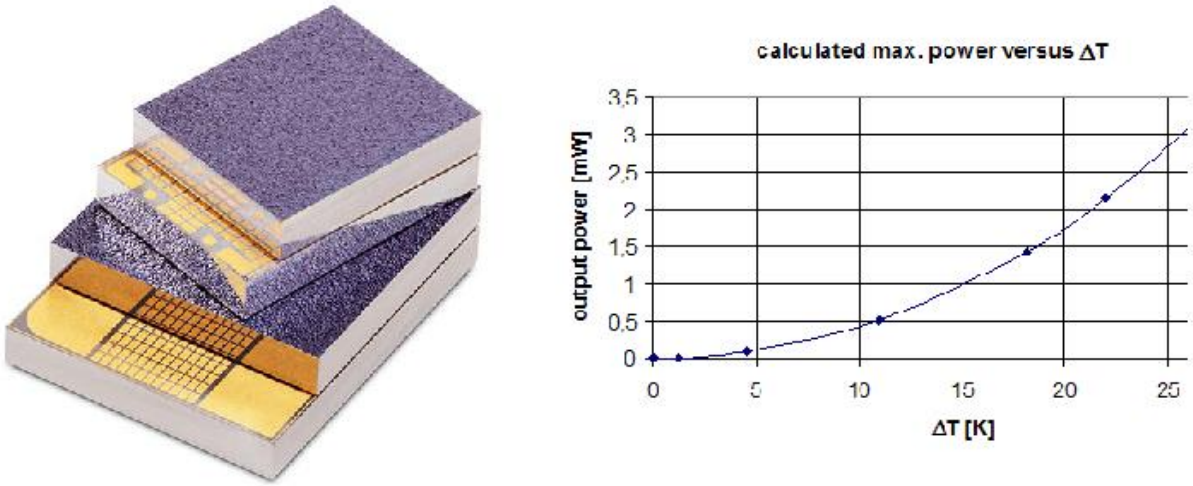

Fig. 4- 6 Micro Pelt MPG-D751 thermo microgenerator layout and power output

4.2 PAVEMENT ENERGY HARVESTING METHODS

By focusing on the SPM application and analysis provided in 4.1 MICRO ENERGY HARVESTING REVIEW, several harvesting methods are described and discussed in this Section. The methods of selections are mainly based on the pavement energy source, technology comparability with integrated circuit design, and materials which include feasibility and fabrication cost. In this Chapter, the base review of these approaches was presented. The fabrication and design details are presented in next Chapter.

4.2.1 PAVEMENT ELECTROSTATIC ENERGY HARVESTING

An electrostatic device such as a capacitor can be an energy conversion element that converts mechanical energy (vehicle load force) to the electrical energy. This conversion can be a reversible and electrical energy that can be converted to a mechanical movement or vibrator (an Actuator). The electrostatic conversion method was not used in a large generator because of the difficulty and lack of efficiency for the large capacitor, but the electrostatic methods will be more desirable for a micro scale generator and for a micro scale power resource. The electrostatic

generator concept is called Coulomb-Damped Resonant Generators (CDRG). Fig. 4- 7 shows charging and discharging stages of a simple electrostatic generator.

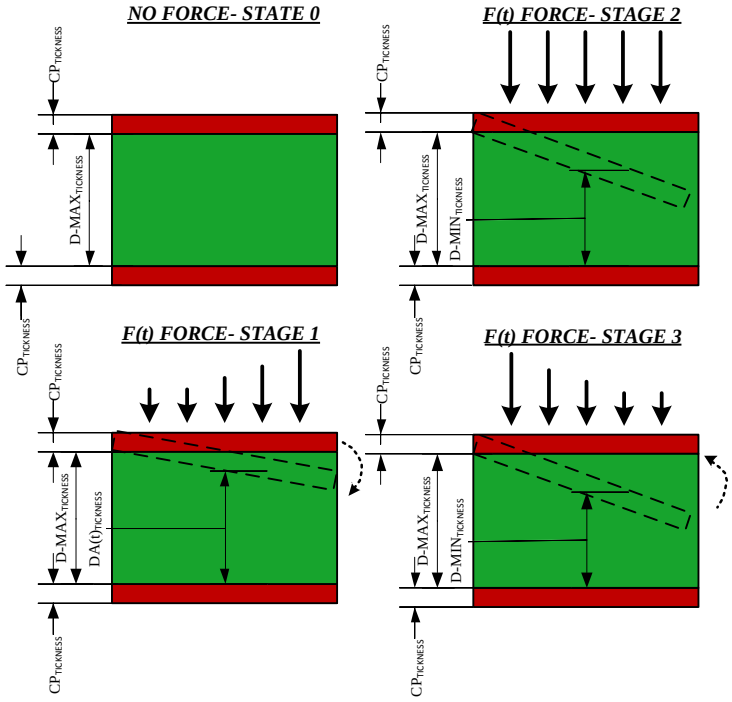

Fig. 4- 7 Electrostatic Generator Simple Operation Stages

The concept of the generator is that of a capacitor unit having two conductance layers (metal) and a dielectric layer. An input force with a characteristic function of F (t) activates the generator and the capacitor shows a dynamic behavior. This process has four stages with the following definition:

Stage -0: Initial Stage

This is the initial stage or steady stage of the process. In this stage, no external force affects the unit and the capacitor has its initial voltage source, V_s. The capacitor value, C_{min} and initial energy of E_{min} are:

$$C_{min} = \frac{\epsilon A}{D_{max}} \qquad \text{Eq. 4- 4}$$

$$E_{min} = \frac{\epsilon A}{D_{max}} V_s^2 \qquad \text{Eq. 4- 5}$$

Stage -1: Force Activation

Vehicle cross over in an SPM node will activate a SPM micro generator. The tire contact over pavement will force the vehicle weight to the capacitor unit. In an actual SPM case, it is not a direct force to the micro-generator. The tire pressure force is carried to the pavement surface layer, and through the SPM package and the microstructure, activates the generator. The input force will be affective in a short period of the time determined by the crossing vehicle speed. It is noticeable that a force from other close crossing vehicles will affect the SPM node generator but with much less amplitude. A characteristic of the simple force function for the SPM analysis is drafted in Fig. 4- 8. The assumptions for proposing force function are:

I. T_{max} is factor of the vehicle speed. This parameter will be a random variable. A default for a freeway is 1,875 μs. An M-Model vehicle speed distribution was developed and assigned speed for each vehicle.

II. F_{max} is the factor of the vehicle weight, vehicle class, tire pressure and pavement structure. This parameter will be a random variable. A default for passenger vehicle is 20 N.

III. The actual pavement force function is not a piecewise linear function.

IV. Time T_2 is the time that second vehicle axle crosses over the SPM node. This time is estimated in Eq. 4-6.

V. The force function characteristic will depend on the vehicle class, weight and number of axles.

$$T_2 = \frac{V_{Lenght}}{V_{Speed}} + \frac{T_{max}}{2} \qquad \text{Eq. 4- 6}$$

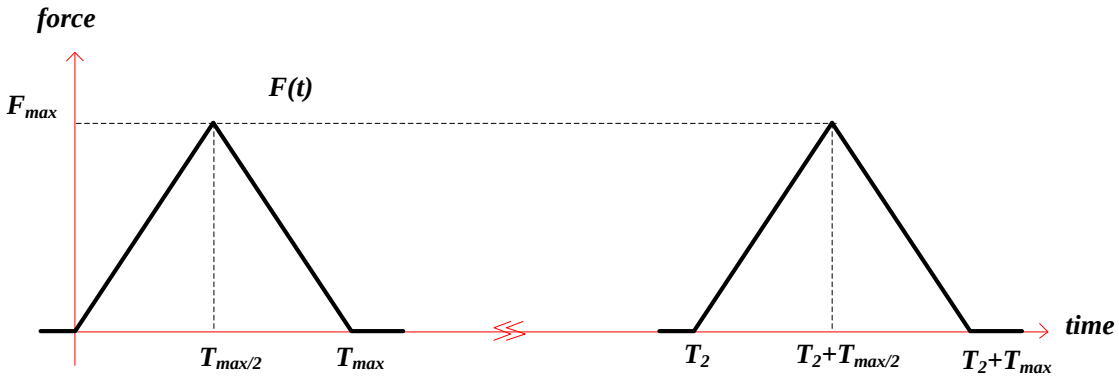

Fig. 4- 8 a Force Input Function over SPM Node

Input force will change the capacitor thickness and increase the capacitance value. Mateu and Mole [27] illustrated an energy cycle process and a V-Q characteristic (an adaption version from Meninger, et al [28]). A revision of this cycle is shown in Fig. 4- 9. The charging control will be done with two different methods called Charge Constrain and Voltage Constrain methods. The potential energy for each method is the area covered with each cycle (Charge Constrain in Blue and Voltage Constrain in Yellow). The control circuits, structure and material selection are involved in each method of deployment.

Stages -2 and -3: Force Released

In the Charge Constrain method, the capacitor will be charged during stage 1 and 2 input forces. The controlling circuit floats and by charging the voltage will be increased in response to the input force. This increase (path A to B) is not linear but close. At point B, the control circuit will keep the charge stable and further input force will only increase the voltage. The charge in a practical sense will not be constant but the approximation will be a constant. At the transition point, force is removed and the capacitor decreased to the initial value (C_{min}). At point D, additional charge will be sent to the storage circuit and micro generator back to stage 0 at point A. The Cycle Energy is the area of ABD.

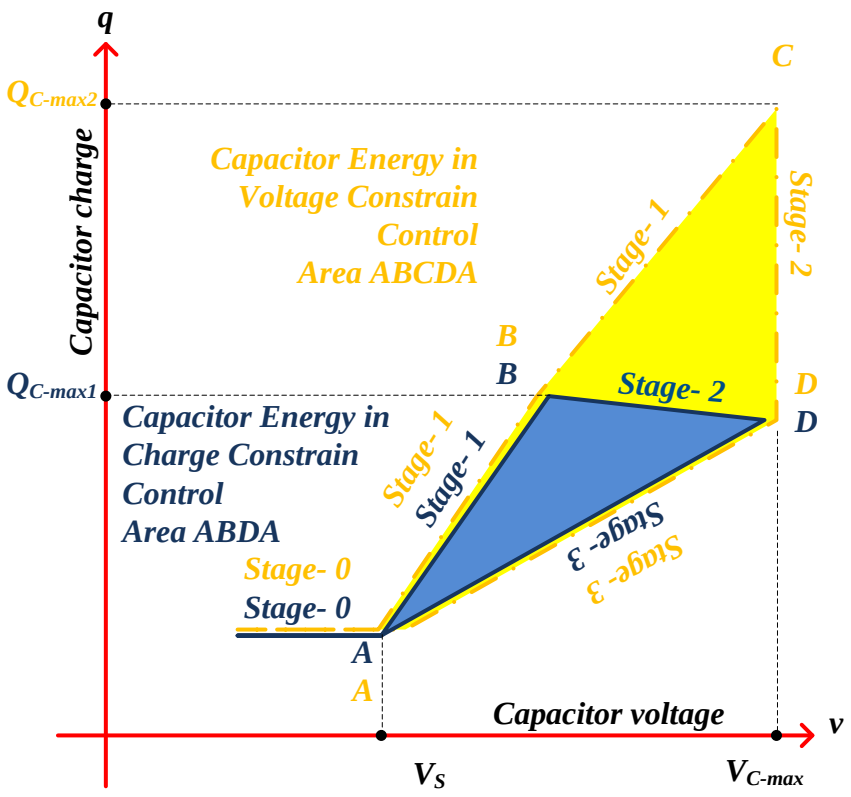

Fig. 4- 9 Electrostatic Generator Charge and Discharge

The energy cycle process in voltage constrain control has a similar start. The capacitor voltage and charge increase as results of the input. The initial voltage source of the circuit controller charges the capacitor to V_{max} at point C. At that point, the transition will be placed and the capacitor changed from the maximum value to the minimum. This is the point when additional charges will be sent to the circuit storage. At Point D in stage 3, the capacitor is decreased to the initial value (C_{min}). The energy cycle will be the ABCDA path. The energy amount will be higher in this approach, but the initial voltage source value will be at its limit for the approach [27]. In the next Sections, as part of the proposed SPM micro charger, we discuss this matter further.

4.2.2 PAVEMENT PIEZO ENERGY HARVESTING

The piezoelectric effect was discovered by the Curies in 1880. Piezoelectric material crystal structure exhibits electrical charges under mechanical forces. In a larger scale, detection high input impedance is needed to sense this signal. In a micro scale device, the effect can be used in a sensor and a micro-generator. Piezo crystals, or piezoelectric crystals, are unique mineral structures that have very useful electric properties. When physical stress is applied to these crystals, especially a certain pressure or pressure waves in the form of sound, the crystal responds to the vibrations by producing an electrical current. The piezoelectric materials are generating electricity in response to a stress. The generated charges are dependent on the material property, geometries, and the volume reduction. The volumetric changes may reach in the range of 4%.[28]

The piezoelectric effect occurs only in non-conductive materials. Piezoelectric materials can be divided into two main groups: crystals and ceramics. Originally, crystals made from quartz were used as a material for piezoelectric transducers. In the early 1950s, quartz crystals began to give way to piezoelectric ceramic as the primary transducer material. The ceramic piezo materials are common products for a piezo actuator, sensor and micro-generator. Table 4- 2 has some examples of the piezoelectric materials.

Table 4- 2 Piezoelectric Material Examples

Material	*Name*	*Structure*	*Density- Kg/m^3*
Quartz	SiO2	Hexagonal Crystal	2,650
Aluminum orthophosphate - Berlinite	AlPO4	Rhombic Crystal	2,560
Gallium orthophosphate	GaPO4	Tetrahedrons Crystal	3,570
Lead zirconate titanate	PZT	Symmetry Uniaxial Class Crystal	7,750
Zinc oxide	ZnO	Hexagonal Wurtzite and cubic Zinc blend Crystal	5,606
Aluminum nitride	AlN	Hexagonal Crystal	3,260
Polyvinylidene fluoride	PVDF	Trans (t) and Gauche$^{\pm}$ (g$^{\pm}$)	1,760

[28] http://www.piezomaterials.com/

Piezoelectric ceramic as individual material or packaged devices can have few hundred microns or more thickness from a variety of the vendors. In the case of the piezoelectric, thin film polymer solution is more common for sensor applications. Piezoelectric has two mode of the operation. When a mechanical stress is applied to a layer of piezoelectric material in the longitudinal direction (parallel to polarization), a voltage is generated which tries to return the piece to its original thickness. That operation mode called as d31 mode. Similarly, when a stress is applied to the layer in a transverse direction (perpendicular to polarization), a voltage is generated which tries to return the piece to its original length and width. The layer bonded to a structural member, which is stretched or flexed will induce electrical generation. This will be the piezoelectric operation mode d33. Fig. 4- 10 shows longitudinal and transverse generators operational modes.

Typical properties of a piezoelectric film[29] are included in the Appendix 7 – Piezoelectric Materials Film Typical Properties.

4.2.2.1 PIEZOELECTRIC MATHEMATIC DESCRIPTION

$D = \varepsilon \times E$ Eq. 4- 7

$S = s \times T$ Eq. 4- 8

Where: "D" is Electric Displacement, "E" is applied Electric Field (V/m) and "ε" is Permittivity (F/m), "S" is the Strain, "s" is mechanical compliance (m^2/N) and "T" is the stress (N/m^2). A description of the piezoelectric parameters is included in Appendix 8 – Piezoelectric Parameters Description[30] . Based on the ANSI/ IEEE 176 notation, the equations with coupling effect are:

$\{S\} = [s]^E \times \{T\} + [d^t] \times \{E\}$ Eq. 4- 9

[29] Measurement Specialties, Inc., www.msiusa.com
[30] PI Ceramic PmbH. www.piceramic.com

$$\{D\} = [d] \times \{T\} + [\varepsilon^T] \times \{E\} \qquad \text{Eq. 4- 10}$$

Where: "[d]" is the matrix for the direct piezoelectric effect ($C/m^2/N/m^2$); the superscript "*E*" indicates a zero, or constant, electric field; the superscript "*T* " indicates a zero, or constant, stress field; and the superscript "*t* "stands for transposition of a matrix[29].

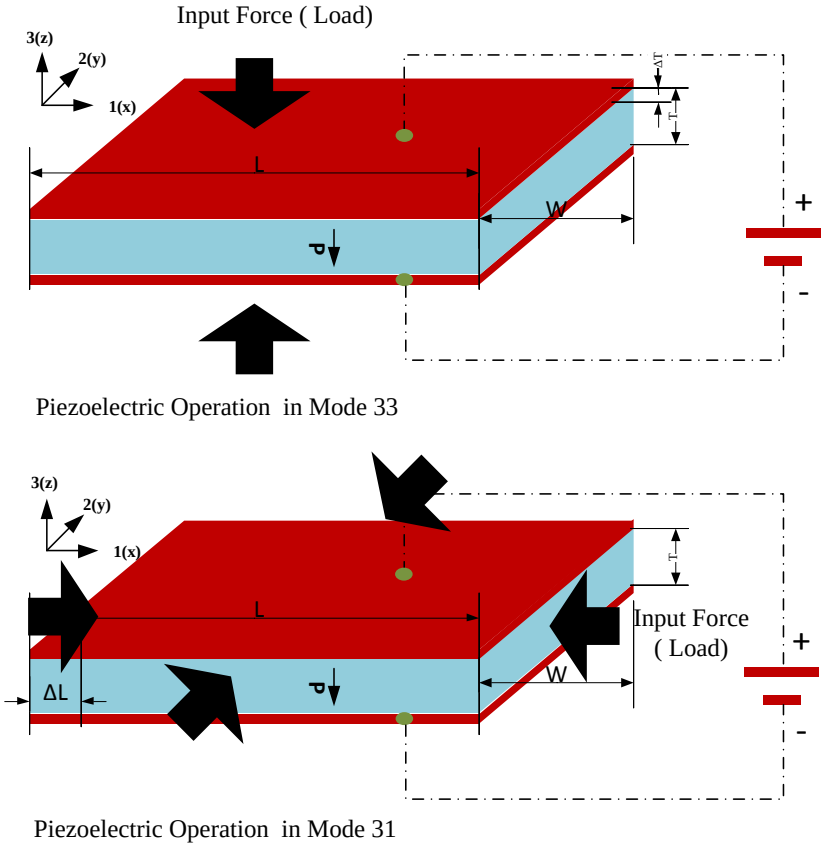

Fig. 4- 10 Piezoelectric Material Common in Operation Modes

4.2.2.2 PIEZOELECTRIC EMULATION CIRCUIT

Piezoelectric operation can be described by an emulation circuit. This circuit has two parts, a mechanical and an electrical equivalent circuit. We also consider the assumption that we have a very low frequency input force. For a component of the stress, for instance, longitudinal in z direction, differential equation of a simple scalar form of the piezoelectric above equation can be written and modeled as:

$S_i' = s_{i3} \times T_3' + d_{i3} \times E_3'$ Eq. 4- 11

$D_i' = d_{i3} \times T_3' + \varepsilon_{i3} \times E_3'$ Eq. 4- 12

It is assuming that T_1, T_2, T_4, T_5, T_6, E_1, E_2 are zero. In roadway pavement, force/stress source will be in z direction, but the pavement layer will provide other stress based on the geometry of the layer and the position of the SPM (piezo charger) inside the pavement. We will consider these assumptions in a more detailed analysis that will be referred to as a micro pavement response modeling. The general form of the emulated circuit of the piezo generator is shown in Fig. 4- 11 that presents the mechanical and electrical circuits. Based on the position of SPM, the stress input to the micro generator can be calculated with the PEM modeling approach. Thus, a complete modeling picture of the system can be presented, as follows:

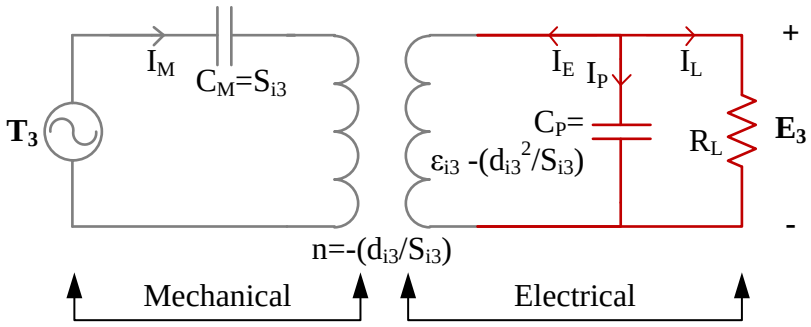

Fig. 4- 11 An emulated piezoelectric circuit

S is the piezoelectric material compliance, which is the inverse of its stiffness. This parameter depends on the material in the Young module. By notion of Y_C as the Young module tensor (N/m^2), "e" as permittivity tensor (F/m) and "d" as piezo strain tensor (m/v, the circuit variables are:

$C_M = \frac{1}{Y_c}$ Eq. 4- 13

$$n = -dY_c \qquad \text{Eq. 4- 14}$$

$$C_P = \varepsilon^T \left(1 - \frac{d^2 Y_C}{\varepsilon^T}\right) \qquad \text{Eq. 4- 15}$$

$$K = \sqrt{\frac{d^2 Y_C}{\varepsilon^T}} \qquad \text{Eq. 4- 16}$$

The coupling factor "K" is described as the mechanical to electrical or electrical to mechanical conversion rate. Materials with higher K can have higher conversion rates. The common modes of piezoelectric material operation, m_{31} and m_{33}, have different values of coupling factors. The m_{33} K factor is higher than m_{31} in typical cases. In the case of the Open load (R_L=0), the piezoelectric charge and voltage for each mode can be formulated as shown in Table 4- 3[31]. In the pavement environment, the SPM orientation may not be uniform and may be a random case depending on the SPM installation proposal.

SPM Random Placement Distribution (SPM-RPD) is a simple, low cost approach. The SPM will only distribute based on the distances and offsets from the roadway. The actual orientation of SPM is random. However, as we discuss in the next Section, the SPM structure will be a 3D structure with a symmetry related to the different directions.

SPM Oriented Placement Distribution (SPM-OPD), in this approach, the SPM node will be pre-assembled in a mesh net. The net will be placed in the placement during the pavement construction or re-surfacing work. The net will keep the SPM node in almost uniform orientation. The large aggregate material can affect the SPM placement and orientation but that will not cause significant changes. As we can see, the voltage and charges in mode 31 are greater than in mode 33 with a rate of "L/T". In other words, d_{33}, d_{31}, g_{33} and g_{31} are not

[31] Note: see Fig. 4- 10 Piezoelectric Material Common in Operation Modes for the piezo dimensions notation.

significant factors to change the rate of voltages or charges between modes. Example of piezoelectric material is PVDF thin film product[32], the operation coefficient values are d_{31}=18 to 20 (pC/N), d_{33}=-20 (pC/N), g_{31}=0.15 (Vm/N) and g_{33}=-0.15 (Vm/N).

Table 4- 3 Piezoelectric Operation Modes Formulations

	Mode 33	*Mode 31*
Voltage	$V = \frac{g_{33} \times F \times T}{W \times L}$	$V = \frac{g_{31} \times F}{w}$
Charge	$q = d_{33} \times F$	$q = \frac{d_{31} \times F \times L}{T}$
Displacement	$\Delta T = d_{33} \times V$	$\Delta L = \frac{d_{31} \times L \times V}{T}$ $\Delta W = \frac{d_{31} \times W \times V}{T}$

4.2.3 PAVEMENT ELECTROMAGNETIC ENERGY HARVESTING

This harvesting approach is a micro scale of the electromagnet generator. The generator operation is based on the Faraday Law. A moving magnet or fixed magnet with a moving coil will provide a variable magnetic flux through an electrical circuit and an electrical field. A device that employs this type of conversion, designed by Amirtharajah and Chandrakasan [30] is shown in Fig. 4- 12. An electromagnetic structure will not be as easy and as simple as for the electrostatic or piezoelectric micro generator.

[32] http://www.goodfellowusa.com/A/Polyvinylidenefluoride.html

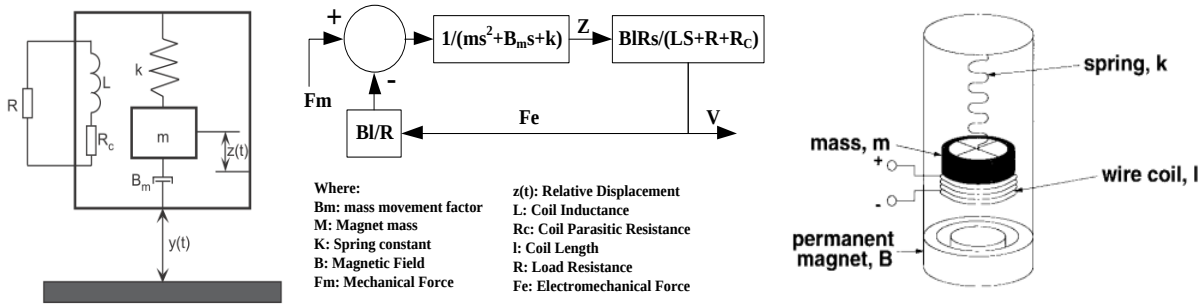

Fig. 4- 12 Magnetic induction transducer model, (Amirtharajah and Chandrakasan)

The transfer function of the Amirtharajah and Chandrakasan proposed generator is:

$$\frac{V(s)}{F_m(s)} = \frac{B \times l \times R \times s}{(m \times s^2 + B_m \times s + k)(L \times s + R + R_C) + (B \times l)^2 \times s}$$

Eq. 4- 17

If the parasitic resistance is small and the assumption that electrical time constant is much smaller than mechanical, we can simplify the transfer function to one with order of two. The Laplace transform of the input tire force shown in Fig. 4- 8, is:

$$F_m(s) = \frac{2 \times F_{MAX}}{T_{MAX}}\left(1 + e^{-s \times T_{Max}} - 2 \times e^{s \times T_{Max}/2}\right) \qquad \text{Eq. 4- 18}$$

As a result, the generating voltage in an SPM node can be estimated below. The parameter default values are in Table 4- 4.

Assumptions and Notations:

$$V(t) = \left(2 \times \frac{F_{MAX}}{T_{MAX}} \times \frac{(B \times l)}{m}\right) \times \left\{\left\{\frac{u(t)}{{\omega_n}^2} - \frac{e^{-\zeta \times \omega_n \times t}\cos(\omega_n \times \sqrt{1-\zeta^2}) \times t}{{\omega_n}^2} - \frac{\zeta \times e^{-\zeta \times \omega_n \times t}\sin(\omega_n \times \sqrt{1-\zeta^2}) \times t}{\omega_n \times \sqrt{1-\zeta^2}}\right\} - \right.$$

$$2 \times \left\{\frac{u\left(t-\frac{T}{2}\right)}{{\omega_n}^2} - \frac{e^{-\zeta \times \omega_n \times \left(t-\frac{T}{2}\right)}\cos(\omega_n \times \sqrt{1-\zeta^2}) \times \left(t-\frac{T}{2}\right)}{{\omega_n}^2} - \frac{\zeta \times e^{-\zeta \times \omega_n \times \left(t-\frac{T}{2}\right)}\sin(\omega_n \times \sqrt{1-\zeta^2}) \times \left(t-\frac{T}{2}\right)}{\omega_n \times \sqrt{1-\zeta^2}}\right\} +$$

$$\left.\left\{\frac{u(t-T)}{{\omega_n}^2} - \frac{e^{-\zeta \times \omega_n \times (t-T)}\cos(\omega_n \times \sqrt{1-\zeta^2}) \times (t-T)}{{\omega_n}^2} - \frac{\zeta \times e^{-\zeta \times \omega_n \times (t-T)}\sin(\omega_n \times \sqrt{1-\zeta^2}) \times (t-T)}{\omega_n \times \sqrt{1-\zeta^2}}\right\}\right\} \qquad \text{Eq. 4- 19}$$

$$\omega_n = \sqrt{\frac{K}{m}} \qquad \text{Eq. 4- 20}$$

$$\zeta = \frac{B_m}{2\times\sqrt{K}\times m} + \frac{B\times l}{2\times R\times\sqrt{K}\times m} = \zeta_m + \zeta_e \qquad \text{Eq. 4- 21}$$

In Fig. 4- 13, the voltage and power generation of one vehicle (passenger car) is presented. The maximum voltage of 50 mV and 2000 µW can be estimated. The average of the generating power will not be significant. This power will be less than 8 µW, which is not sufficient for the SPM application. More power can be generated with other vehicle classes such as trucks or heavy vehicles; however, the traffic density of those vehicles is less than passenger cars.

Table 4- 4 SPM default parameters for Electromagnetic Generator

Parameter	*Time*	*Time step*		*Size*		*Mass*	*EM Field*
Unit	Sec	Sec		M	N/M	KG	TESLA
Symbol	***t***	**Δ*t***	***BM***	***l***	***K***	***m***	***B***
Value	3.62E-01	2.50E-05	1.68E+00	1.00E-02	1.74E+02	5.00E-03	5.00E-01
Parameter	**Period**	**Tire Force**	**Damping**	**Damping**	**Damping**	**an**	**Load**
Unit	Sec	N	Factor Elect	Factor Mesh	Factor Overall	Radia/Sec	OHM
Symbol	T	FMAX	ζe	ζm	ζ	ωn	***R***
Value	2.81E-03	3.7728E+00	1.3401E-06	9.01E-01	9.01E-01	1.87E+02	1.00E+01

The Electromagnetic structure and fixed electric field are some of the issues for this generator in an SPM and CMOS process fabrication. Therefore, the electrostatic and piezo electric approaches are considered the prime approaches for the SPM generator.

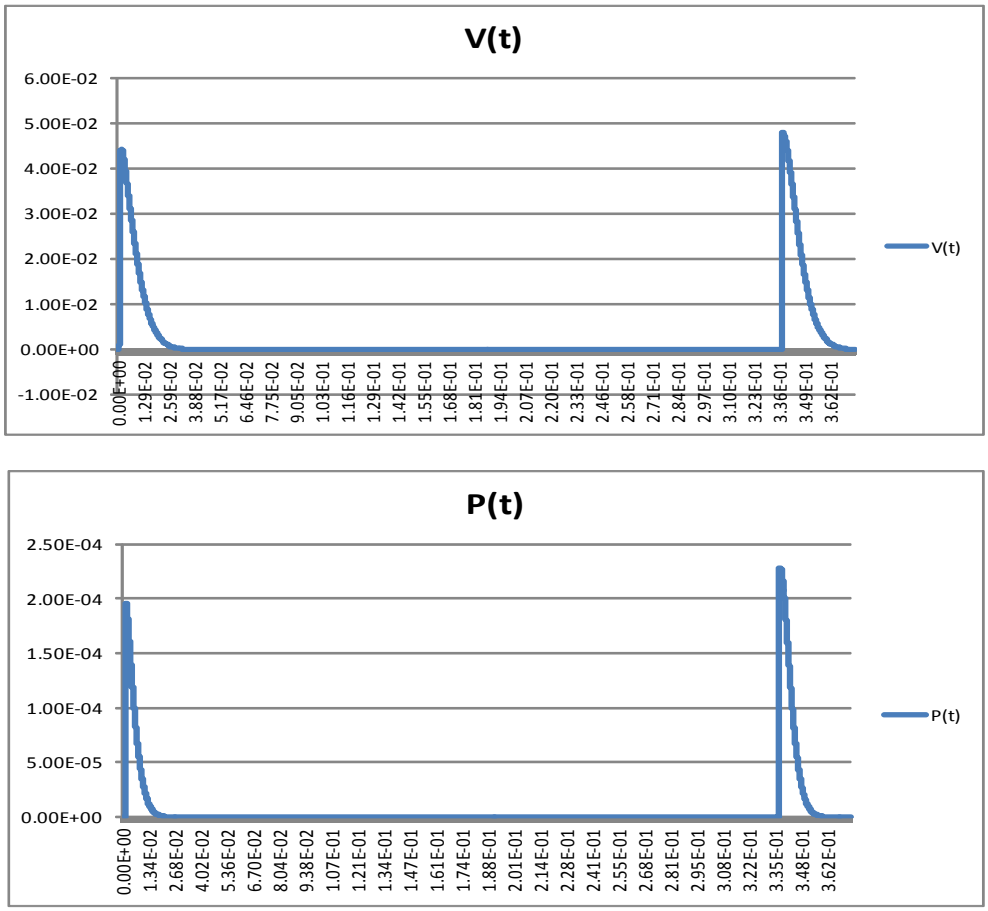

Fig. 4- 13 Voltage and Power Estimates for a SPM Electromagnetic generator

4.3 SMP MICRO GENERATOR STRUCTURE PLAN

In this Section, the micro structure for the SPM micro-generator is discussed and the proposed alternatives for the micro structure are proposed. The micro-generator structure depends on the methods of the energy harvesting that we discussed in the last Sections. A single structure, multi layered, and, partitioned structures are alternatives to be considered. The details of a fabrication plan and materials are in the next Chapter. The SPM packaging will include multiples of the micro-structure assembly to core SPM SOC and SPM frames.

4.3.1 OPERATION CONDITIONS

General conditions of the SPM in pavement systems and resources of the energy were described in previous Chapters. These conditions will depend on pavement type and daily traffic status. Average conditions may be:

I. SPM will be a pavement surface layer in a depth of 5 mm under the surface.

II. Pavement Type will be Flexible Pavement or Rigid Pavement with typical parameters as shown in Table 3- 12.

III. Each vehicle class has a tire loading and tire touching area. The vehicle class will follow the FHWA classification. Average values for three vehicle classes are, as follows:

- Passenger Car: Tire Pressure 30 PSI
- Light Truck: Tire Pressure 58 PSI
- Heavy Truck: Tire Pressure 115 PSI

IV. SPM placement will be at a location with maximum activation expectation. The orientation of the SPM will be in a random position.

V. Typical Tire Input force is as shown on Fig. 4- 8.

VI. Average Vehicle speed: 50 MPH. However, the maximum speed of 80 MPH is considered for timing plan, and T=2800 μs is considered for tire touching time.[33]

4.3.2 GENERATOR MICRO STRUCTURE

Cantilever shape is one of the common structure types for a micro-generator. This type of structure with one supporting point has been fabricated in MEMS devices. In the vibration mechanical environment, the operation may be more symmetric. As an alternative, a structure with two support points will offer more symmetrical mechanical movement than a structure with

[33] It is subject of vehicle type, axle arrangement (truck classes), tire type and pressure and vehicle loading.

only one support point. In addition, the number of layers on the micro structure is another design criterion in competition with a simple fabrication process. Fig. 4- 14 shows a simple concept of the micro structure with two capacitor layers. The structure variable capacitance will increase with the external load. The capacitor dielectric materials need to be selected that have higher relative permittivity and optimum Young module and Poisson ratio parameters. The harvesting energy will depend on the capacitor total change during the activation process. To design a larger capacitance and larger capacitor changes, the structure area needs to be larger or the number of layers increased. In addition to the energy capacity in multi-layer structures, we also need to account for the non-linearity of the structure movement that affects the efficiency and characteristic of the generating signal. Three structures in Fig. 4- 14 represent horizontal multi-layer and comb or vertical electrostatic micro structure alternatives. In case 1, the variation of the capacity will be from a minimum to maximum in response to the force. The dielectric layer will be a material with a high dielectric constant (K) such as Strontium titanate ($SrTiO_3$) that has typical K of 300 or Barium titanate ($BaTiO_3$) that has K in range of 1200 to 10000.[34] Of course, the selection of this material depends on the compatibility with the fabrication process of the generator. Strontium titanate with properties including high dialectic value has been interesting in resent research and development. One method for depositing Strontium titanate thin films over high aspect ratio structures is Atomic Layer Deposition (ALD). This method of deposition

34

Molecular formula	dielectric constant	Molar mass g/mol	Density g/cm^3	Melting point	Solubility water	Refractive index (n_D)	Crystal structure
$SrTiO_3$	100-2000	183.49	5.11	2080 °C	insoluble	2.394	Perovskite
$BaTiO_3$		233.192	6.02 solid	1625 °C	insoluble		Tetragonal tP5

will place layer-by-layer growth results on high-quality layers and have an excellent step coverage characteristic. [31]

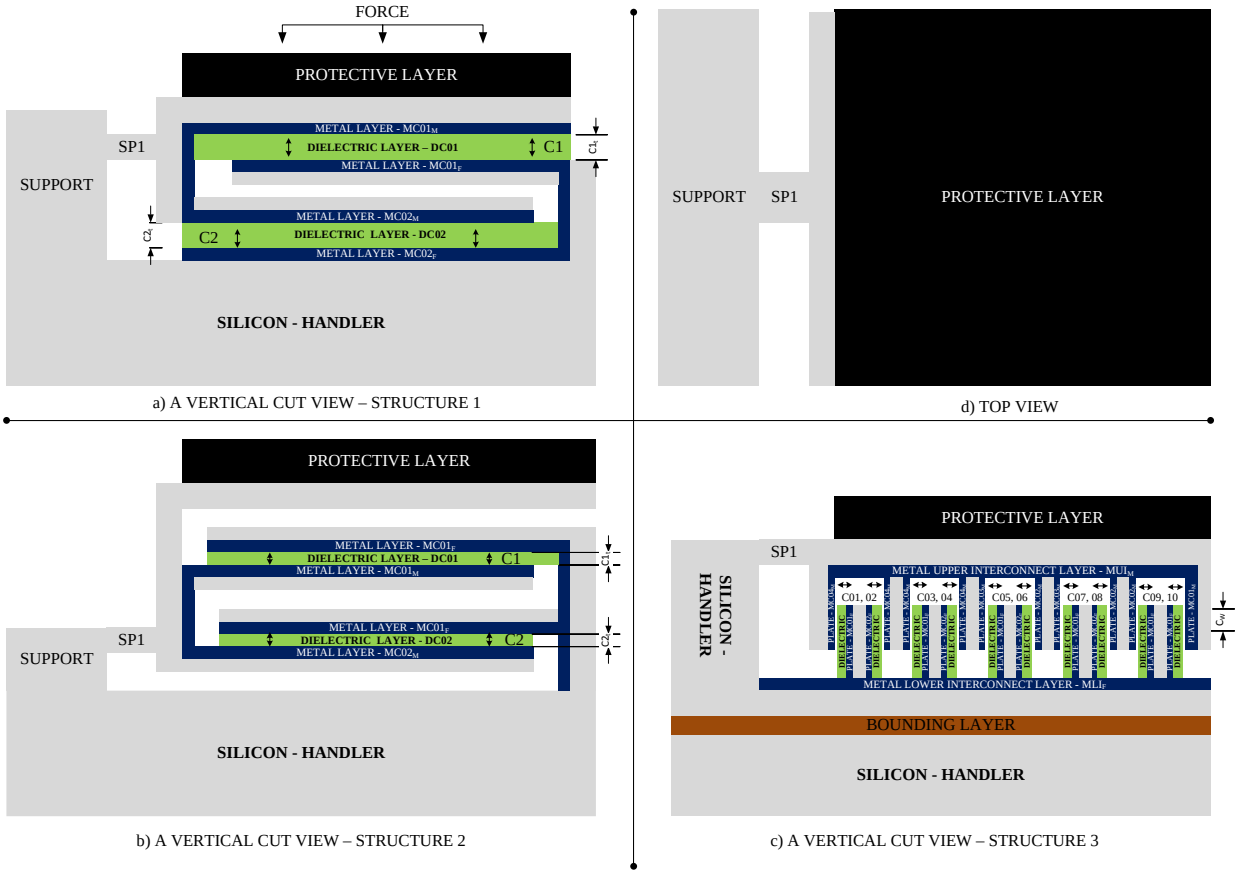

Fig. 4- 14 a simple Cantilever structure with two capacitor layers

The comb/vertical structure required an additional bonding process for assembly of the structure over the main silicon bulk substrate. The bonding process is described in the packaging section for all modules of the SPM. The other notice on the microstructure operation is the direction of the force. The activation force may not be perpendicular to the generator surface and as a result, a fraction of loading force may affect the generator. However, we should also notice that this random positing of the SPM may result in more than one SPM generator module being active.

Above structures are general concepts and the actual design also depends on the details of the layers' thickness and the 3D fabrication process. In addition, the capacitor's plate shape or

numbers on the layer should be considered. Three typical electrostatic micro generator structure design cases are shown in Fig. 4- 15. In this design, the fabrications are based on etch and depositing cycle, which may require a large number of sequences of work. The large fabrication process will be an issue not only for cost effectiveness of the SPM design but also for prototype implementation.

The other structure cases can be designed in similar geometric sizes. The tolerance of the shape and sizes can be factors of harvesting method, material type/properties, fabrication process, and cost. An estimate of the micro-generator structure sizes is presented in Appendix 15. For six generator modules assembled on the SPM faces, the maximum volume occupancy will be 10%. This estimate will be changed on other structure types, but we used this volumetric ratio value, 10%, as the scaling requirement for other micro-generator structure designs.

It is also noticeable that a higher value for the volumetric ratio will increase the cost of SPM node because the generator module will be fabricated in separate processes. In addition, the maximum wafer dimension is another criterion for sizing the micro-generator structure. To analyze this plane structure element, the plate theory [32] and its formulation are used here. Fig. 4- 16 shows the analyses parameters and their descriptions. Freund proposed assumptions for the film substrate layers system analysis [33], which we considered for our analysis. The governing equations for bending a rectangular thin plate are:

$$\frac{\partial^4 w}{\partial x^4} + 2 \times \frac{\partial^4 w}{\partial x^2 \partial y^2} + \frac{\partial^4 w}{\partial y^4} + \frac{q(x,y,t)}{D} + 2 \times \rho \times \left(h_s + h_f\right) \times \frac{\partial^2 w}{\partial t^2} = 0 \qquad \text{Eq. 4- 22}$$

$$D = \frac{2 \times (hs+hf)^3 E}{3 \times (1-\nu^2)} \qquad \text{Eq. 4- 23}$$

$$U^0 = u_x^0 e_x + u_y^0 e_y + w^0 e_z \qquad \text{Eq. 4- 24(Mid-Surface Point)}$$

$$u_x = u_x^0(p_x, p_y) - p_z \times \frac{\partial w^0}{\partial_x} \qquad \text{Eq. 4- 25}$$

$$u_y = u_y^0(p_x, p_y) - p_z \times \frac{\partial w^0}{\partial_y} \quad \text{Eq. 4- 26}$$

$$u_z = w^0(p_x, p_y) \quad \text{Eq. 4- 27}$$

In these equations, the new displaced location for each point will be determined by the original coordinate of the points, (p_x,p_y,p_z), mid-surface point, w^0 (t) and its gradients in x and y directions. If simplified, the solution and dynamic parts ignore ($\frac{\partial^2 w}{\partial t^2} = 0$) the internal moments and force equations are [34]:

$$M_x = -D \times \left\{\frac{\partial^2 w}{\partial x^2} + \nu \times \frac{\partial^2 w}{\partial y^2}\right\} \quad \text{Eq. 4- 28 X direction bending moment}$$

$$M_y = -D \times \left\{\frac{\partial^2 w}{\partial y^2} + \nu \times \frac{\partial^2 w}{\partial x^2}\right\} \quad \text{Eq. 4- 29 Y direction bending moment}$$

$$M_{xy} = -D \times (1 - \nu) \times \frac{\partial^2 w}{\partial x \partial y} \quad \text{Eq. 4- 30 Torsion moments}$$

$$Q_x = -D \times (1 - \nu) \times \frac{\partial(\frac{\partial^2 w}{\partial x^2} + \frac{\partial^2 w}{\partial y^2})}{\partial x} \quad \text{Eq. 4- 31 X direction shear force}$$

$$Q_y = -D \times (1 - \nu) \times \frac{\partial(\frac{\partial^2 w}{\partial x^2} + \frac{\partial^2 w}{\partial y^2})}{\partial y} \quad \text{Eq. 4- 32 Y direction shear force}$$

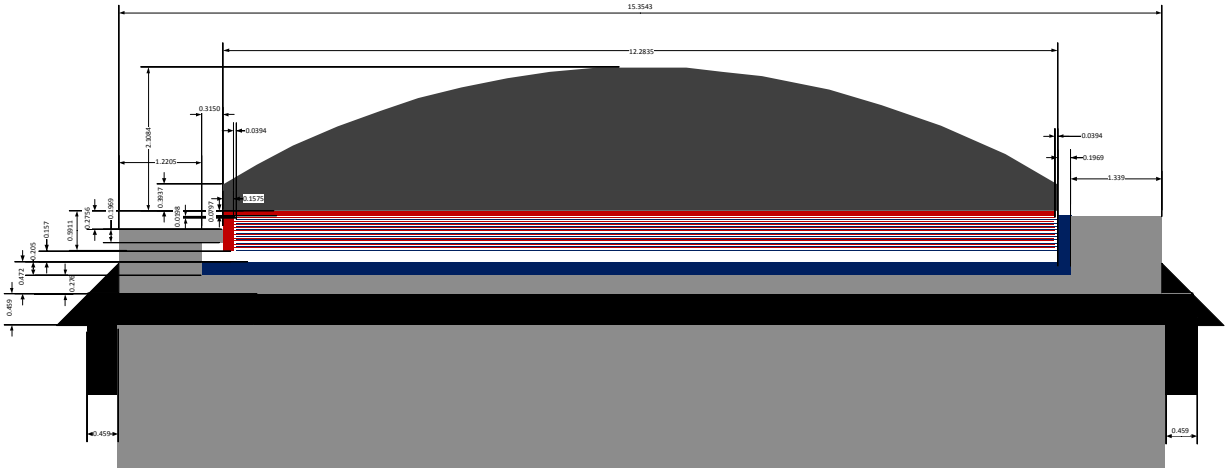

SPM CASE 01- ONE CHARGER STRUCTURE (SCALE IS 30000 μM)

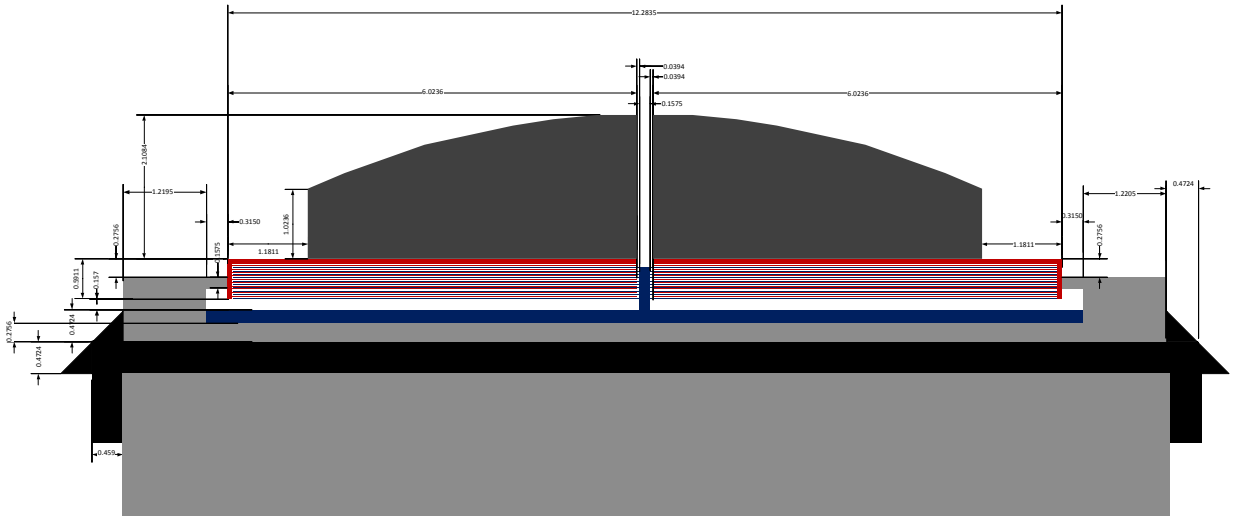

SPM CASE 2- ONE CHARGER STRUCTURE (SCALE IS 30000 μM)

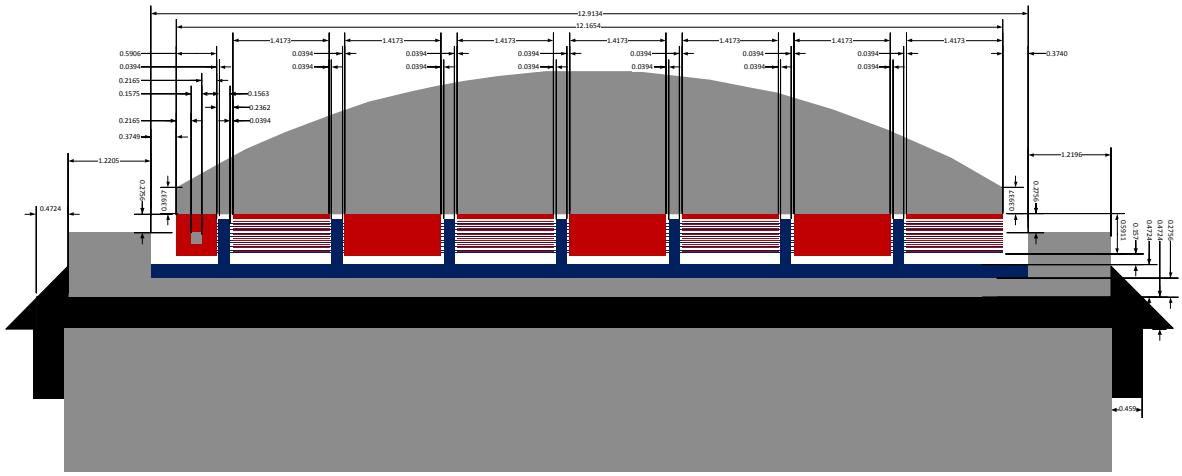

SPM CASE 3- ONE CHARGER STRUCTURE; (SCALE IS 30000 μM)

Fig. 4- 15 SPM Electrostatic Designed Micro Structures

$$V_x = Q_x + \frac{\partial M_{xy}}{\partial y}$$ Eq. 4- 33 X direction effective shear force

$$V_y = Q_y + \frac{\partial M_{xy}}{\partial x}$$ Eq. 4- 34 Y direction effective shear force

Based on the SPM micro structure shown in Fig. 4- 16, the boundary conditions for solving the Eq. 4-22 are:

$$W|_{(x=\frac{-a}{2},-\frac{c}{2}\le y\le\frac{c}{2})} = 0 \; and \; \left.\frac{\partial W}{\partial x}\right|_{(x=\frac{-a}{2},-\frac{c}{2}\le y\le\frac{c}{2})} = 0$$ Eq. 4- 35 (Support clamped)

$$M_x\Big|_{\substack{(x=\frac{-a}{2},-c\le y\le-\frac{c}{2})\\(x=\frac{-a}{2},\frac{c}{2}\le y\le c)\\x=a}} = -D\left(\frac{\partial^2 W}{\partial x^2} + \nu\times\frac{\partial^2 W}{\partial y^2}\right)\Big|_{\substack{(x=\frac{-a}{2},-c\le y\le-\frac{c}{2})\\(x=\frac{-a}{2},\frac{c}{2}\le y\le c)\\x=a}} = 0$$ Eq. 4- 36 (Free)

$$V_x\Big|_{\substack{(x=\frac{-a}{2},-c\le y\le-\frac{c}{2})\\(x=\frac{-a}{2},\frac{c}{2}\le y\le c)\\x=a}} = -D\left(\frac{\partial^2 W}{\partial x^2} + (2-\nu)\times\frac{\partial^2 W}{\partial y^2}\right)\Big|_{\substack{(x=\frac{-a}{2},-c\le y\le-\frac{c}{2})\\(x=\frac{-a}{2},\frac{c}{2}\le y\le c)\\x=a}} = 0$$ Eq. 4- 37 (Free)

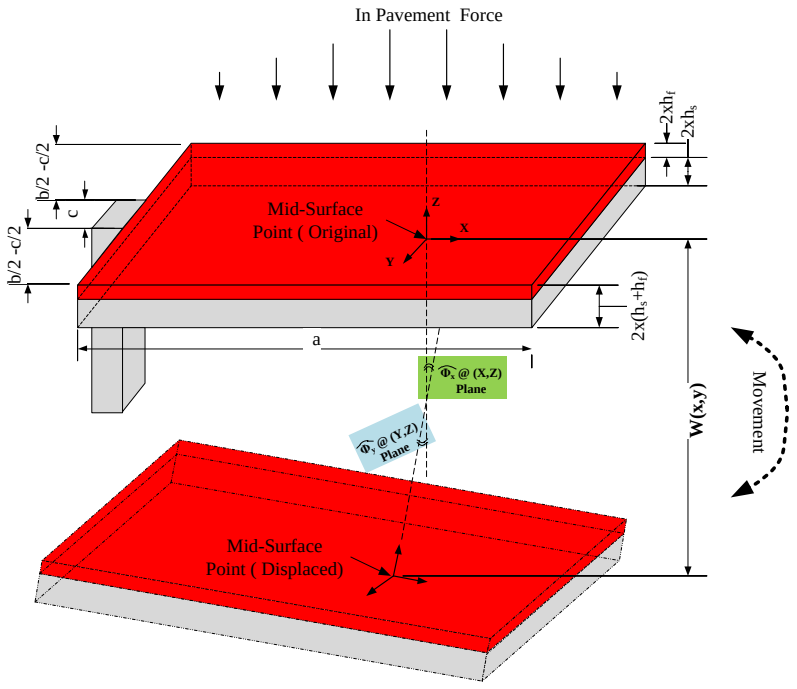

Descriptions:
1) Φ_y is the angle between new Normal vector to the Z axle @ (Y,Z) Plane
2) Φ_x is the angle between new Normal vector to the Z axle @ (X,Z) Plane
3) W (x,y) is the mid point displacement vector
4) Film layer is the moveable metal layer of the capacitor (in Electrostatic generator) or piezoelectric layer (in piezo generator). The metal layer

Assumption:
1) The layers are considered Thin means h_f and h_s <0.1 x lateral dimension
2) The film thickness is much smaller than substrate layer thickness
3) The substrate material is homogeneous, isotropic and linearly elastic, and the film material is isotropic
4) Edge effects near the periphery of the substrate are inconsequential and all physical quantities are invariant under change in position parallel to the interface
5) All stress components in the thickness direction vanish throughout the material;
6) The strains and rotations are infinitesimally small

Fig. 4- 16 Micro structure movement parameters

$$M_y\Big|_{\begin{cases} y=\frac{-b}{2} \\ y=\frac{b}{2} \end{cases}} = -D\left(\frac{\partial^2 W}{\partial x^2} + \nu \times \frac{\partial^2 W}{\partial y^2}\right)\Big|_{\begin{cases} y=\frac{-b}{2} \\ y=\frac{b}{2} \end{cases}} = 0 \qquad \text{Eq. 4- 38 (Free)}$$

$$V_y\Big|_{\begin{cases} y=\frac{-b}{2} \\ y=\frac{b}{2} \end{cases}} = -D\left(\frac{\partial^2 W}{\partial x^2} + (2-\nu) \times \frac{\partial^2 W}{\partial y^2}\right)\Big|_{\begin{cases} y=\frac{-b}{2} \\ y=\frac{b}{2} \end{cases}} = 0 \qquad \text{Eq. 4- 39 (Free)}$$

$$M_{xy}\Big|_{\begin{cases} (x=-\frac{a}{2}, y=\frac{-b}{2}) \\ (x=-\frac{a}{2}, y=\frac{b}{2}) \\ \left(x=\frac{a}{2}, y=\frac{-b}{2}\right) \\ (x=\frac{a}{2}, y=\frac{b}{2}) \end{cases}} = -2 \times (1-\nu) \times D\left(\frac{\partial^2 W}{\partial x \partial y}\right)\Big|_{\begin{cases} (x=-\frac{a}{2}, y=\frac{-b}{2}) \\ (x=-\frac{a}{2}, y=\frac{b}{2}) \\ \left(x=\frac{a}{2}, y=\frac{-b}{2}\right) \\ (x=\frac{a}{2}, y=\frac{b}{2}) \end{cases}} = 0 \qquad \text{Eq. 4- 40 (Free)}$$

The boundary condition on the clamped side only includes part of the structure's side limits to be (x= -a/2, -c/2≤y≤c/2). The q(x,y) is the force density over the surface top. In the analysis, we need to calculate this force based on the original source orientation, tire load, and dimensions of the structure (top face). In general, exact solutions for cantilever plates using plate theory required extensive works. Therefore, additional assumptions for special solution cases were investigated. Some of these cases can be found at:

I. An expansion of Young beam model solution[35]:

$$W(x,y) = \sum_{m=1}^{p} \sum_{n=1}^{q} A_{mn} X_m(x) Y_n(y) \qquad \text{Eq. 4- 41}$$

$$X_i(x) = \cosh\frac{\lambda_i \times x}{a} - \csc\frac{\lambda_i \times x}{a} - \alpha_i\left(\sinh\frac{\lambda_i \times x}{a} - \sin\frac{\lambda_i \times x}{a}\right) \qquad \text{Eq. 4- 42}$$

$$Y_i(y) = \cosh\frac{\mu_i \times y}{b} + \csc\frac{\mu_i \times y}{b} - \beta_i\left(\sinh\frac{\mu_i \times y}{b} + \sin\frac{\mu_i \times y}{b}\right) \qquad \text{Eq. 4- 43}$$

II. Reissner and Stein provide a theory that cantilever plate transverse displacement field formulation is [36]:

$$W(x,y) = W_x(x) + y \times \theta_x(x) \qquad \text{Eq. 4- 44}$$

III. Gupta and Khanna solutions to corresponding two-term defection function is [37]:

$$W(x,y) = \left[\frac{x}{a} \times \frac{y}{b}\left(1-\frac{x}{a}\right) \times \left(1-\frac{y}{b}\right)\right]^2 \times \left[A_1 + A_2 \times \frac{x}{a} \times \frac{y}{b}\left(1-\frac{x}{a}\right) \times \left(1-\frac{y}{b}\right)\right] \qquad \text{Eq. 4- 45}$$

IV. B. Tian, Y. Zhong and R. LI analyses [34] for rectangular thin cantilever plate analysis is:

$$W(x,y) = \frac{2}{a\times b} \times \left(\sum_{m=1,3,..}^{\infty} W_{m0} \times \sin\frac{(a_m \times x)}{2}\right) + \frac{4}{a\times b} \times \left(\sum_{m=1,3,..}^{\infty}\sum_{n=1,2,..}^{\infty} W \times \sin\frac{(a_m\times x)}{2} \times \csc(\beta_n \times y)\right) \quad \text{Eq. 4- 46}$$

V. Yin Zhang and Ya-pu Zhao solution is based on Stoney's formula expansion [38]. The formulations for a cantilever structure with a clamp support are:

$$W(x) = \begin{cases} -\frac{K_1}{2\times K_4\,\mathrm{csch}(\beta\times a)\times\beta^2}\left[\mathrm{csch}\left(\beta\times x+\frac{\beta\times a}{2}\right)-1\right], & \epsilon_0 > 0 \\ \frac{K_1}{2\times K_4\,\csc(\beta\times a)\times\beta^2}\left[\csc\left(\beta\times x+\frac{\beta\times a}{2}\right)-1\right], & \epsilon_0 < 0 \\ \frac{K_1}{4\times K_4}\left(x^2 + a\times x - \frac{3}{4}\times a^2\right) & \epsilon_0 = 0 \end{cases} \quad \text{Eq. 4- 47}$$

$$\beta = \sqrt{\left|\frac{K_2}{K_4}\right|} \quad \text{Eq. 4- 48}$$

$$\begin{cases} W(x) = 0\,,\ \frac{\partial W}{\partial x} = 0, & x = 0 \\ K_1 + 2\times K_4 \times \frac{\partial^2 W}{\partial x^2} = 0, & x = a \\ K_2 \times \frac{\partial W}{\partial x} - K_4 \times \frac{\partial^2 W}{\partial x^2} = 0, & x = a \end{cases} \quad \text{Eq. 4- 49 (Boundry conditions)}$$

Where: ϵ_0 is the uniform in-plane strain due to stretching the plate.

For measuring the microstructure plate displacement, we developed several 3D micro structure models with a finite element analysis in the Comsol environment. A three capacitor layer structure is shown in Fig. 4- 17 Electrostatic micro structure with three moving plates. The displacement of each layer depends on the position of the layer in the structure support. Higher displacement will occur at the top layer. In addition, the displacement is a factor of the vehicle tire force. This force reacts to the pavement surface. By using the pavement response models described in this Chapter, the effective force at the microstructure surface is estimated. The results of the three moving layers of the structure are shown in Fig. 4- 18. The main assumptions and results for the simulation of this model are summarized as follows:

- Three capacitors layers with three moveable plates. The capacitors are parallel.

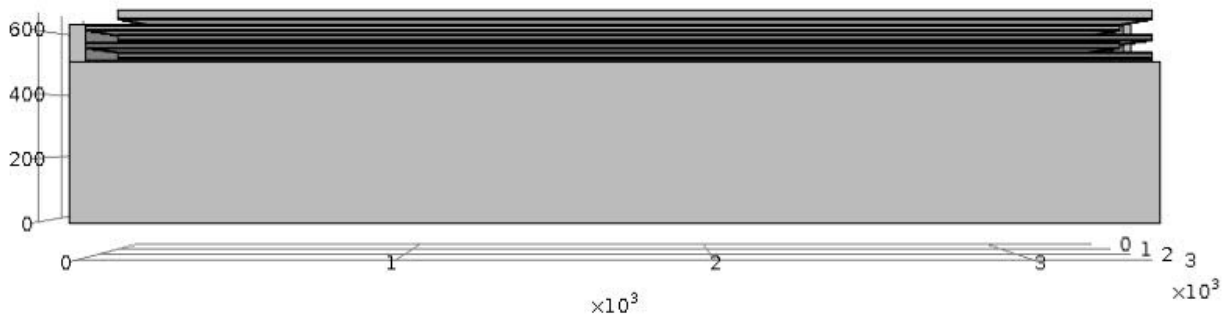

Fig. 4- 17 Electrostatic micro structure with three moving plates

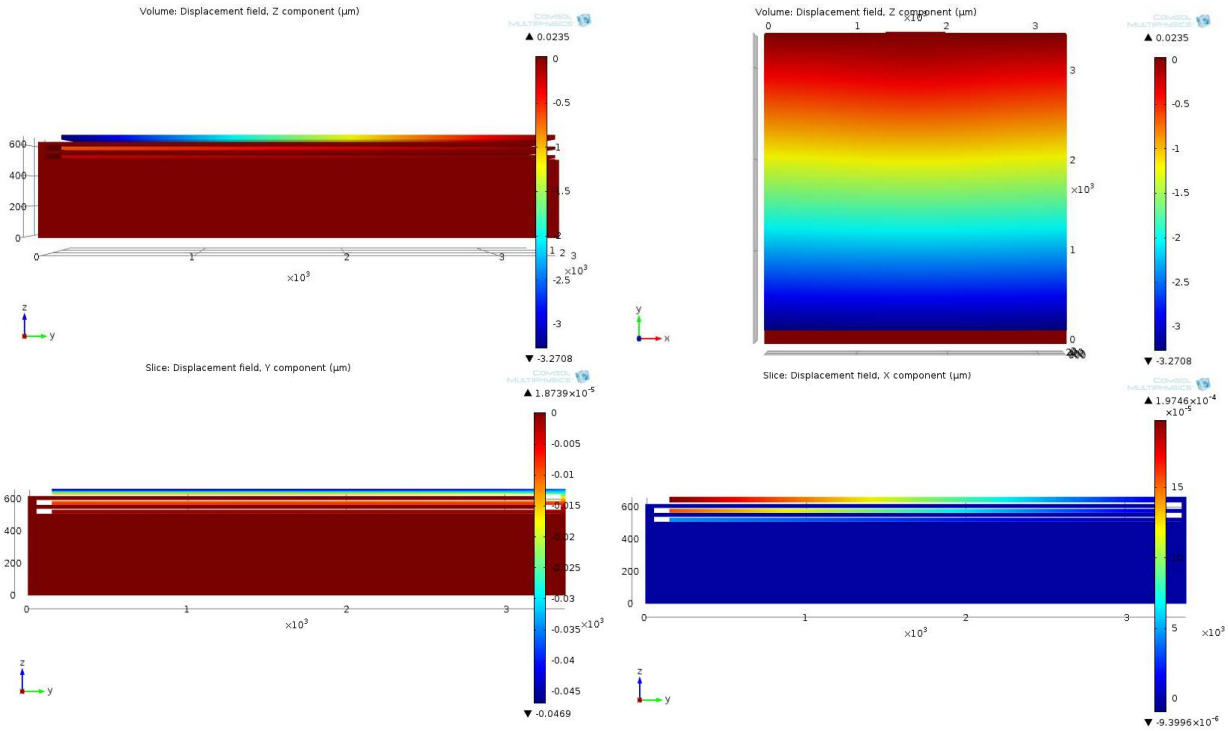

Fig. 4- 18 Micro structure displacement results

- Single support with free boundaries at other sides.
- The capacitor dielectric gap varied depending on the capacitor position. A higher gap will be in the top layer. This model has the following thicknesses: $C_{\text{Top thickness}}$ = 10 µm, $C_{\text{Middle thickness}}$ = 5 µm and $C_{\text{Bottom thickness}}$ = 5 µm.

- Maximum displacement at the top layer is in the Z direction and at the top moveable plate.
- Different vehicle classes/tire loading results in different forces to the moveable structure. Based on the P-Models' simulation of base units, a range of 20 to 75 N/ m^2 are considered.
- The maximum displacement in Z direction at top moveable layer is less than 9 μm.
- The maximum displacement in Z direction at middle layer is less than 3 μm.
- The maximum displacement in Z direction at bottom layer is less than 1 μm.
- The displacement at X direction can be neglected for all layers.
- Average thickness change at top layer is 1.53 μm (15.3%), under class one tire load.
- Average thickness change at top layer is 3.08 μm (30.8%), under class two tire loads.
- Average thickness change at top layer is 4.18 μm (41.8%), under class three tire loads.
- Average thickness change at middle layer is 0.33 μm (6.6%), under class one tire load.
- Average thickness change at middle layer is 0.70 μm (14%), under class two tire loads.
- Average thickness change at middle layer is 1.38 μm (27.6%), under class three tire loads.
- Average thickness change at bottom layer is 0.09 μm (1.8%), under class one tire load.
- Average thickness change at bottom layer is 0.23 μm (4.6%), under class two tire loads.
- Average thickness change at bottom layer is 0.41 μm (8.2%), under class three tire loads.

The thickness change with the details of the model data including the geometry and material parameters are included in Appendix 13: Micro Structure Model Data. The graphs of the movable plates under three loads are shown in Fig. 4- 19.

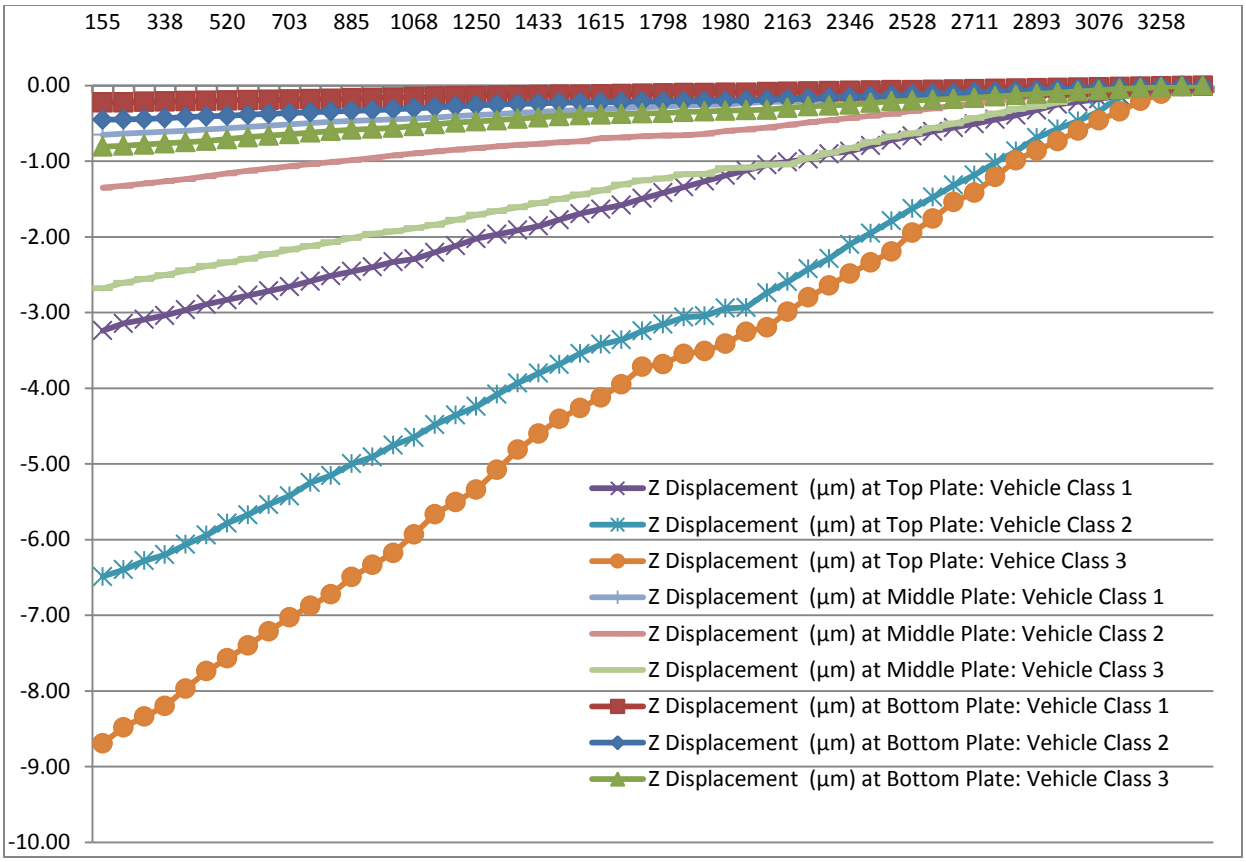

Fig. 4- 19 Moveable plates Z displacement Graphs vs. plate length in Y direction

Because a truck with heaviest tire loads will be a possible case, the thickness of the top layer should be higher to avoid the capacitor plate connection. Thus, 12 µm will be the thickness for the top capacitor. The thicknesses of the lower capacitors also can be adjusted to 3.5 µm and 1.5 µm.[35] These changes will be addressed in the design. The electrostatic charger microstructure information is shown in Table 4- 5.

Table 4- 5 Micro structure layers information

Layer	$C_{Thickness}$ (µm)	Min. Capacitance change	Max. Capacitance change
Top	12	14.6%	53.4%
Middle	3.5	10.4%	65%
Bottom	1.5	6.3%	37.6%

[35] Extend Comsol modeling results.

For each capacitor layer, the power storage capacity can be estimated as:

$$\Delta W = 0.5 \times \Delta C \times V^2 \qquad \text{Eq. 4- 50}$$

The voltage is the voltage source initiated by the embedded on-chip battery. Having a larger initial voltage source will result in generating higher energy, but fabrication or assembly of larger batteries will be required. Additionally, in order to achieve a low power consumption circuit design, it is desirable to use a lower voltage source on the chip. We used three options of 3, 5 and 10 VDC.

Appendix 14: Micro Electrostatic Generator – Power Estimate discusses the details of the micro generator power estimate. The analyses calculations are for two cases of three and ten layer cantilever structures. The estimates are based on a freeway that was simulated in the M-Model studies.[36] Both of these structures are bounded in an area of 12 x 12 mm^2. The effect of different dielectric material alternated in the calculation and three permittivity values (1, 10 and 1000) were considered. The results showed:

i- Three layers structures cannot satisfy the minimum power generating threshold of SPM (50 μw).

ii- Multi-layer capacitor structures are optimized with different capacitor thicknesses. The minimum thickness maintains non-capacitors metal contact under heavy activation. Different vehicle loads were tested in the micro-structure simulation.

iii- Instead of one large capacitor at each layer, the structure divided into a matrix of smaller structures. This increased the complexity of the generator assembly to the SPM core chip, but overall capacitors were increased in comparison to one big structure.

iv- The smaller structure plate is structured with 330 x 330 μm area and height less than 250 μm. The microgenerator matrix has a size of 33 x 33. This structure with a high permittivity dielectric value, 1000, will generate 57 μw at 5 VDC initial voltages or 230 μw at 10 VDC initial voltages.

The ten layers electrostatic micro structure details are shown in Fig. 4- 20. As discussed, variable capacitor thickness and structure support plates are proposed. We use this description to estimate the structure movement and capacitors' changes. This structure is a base plan. Other

[36] Henry Hudson Parkway North Bound

versions with larger height, materials, and thickness can be considered in the future prototyping stage.

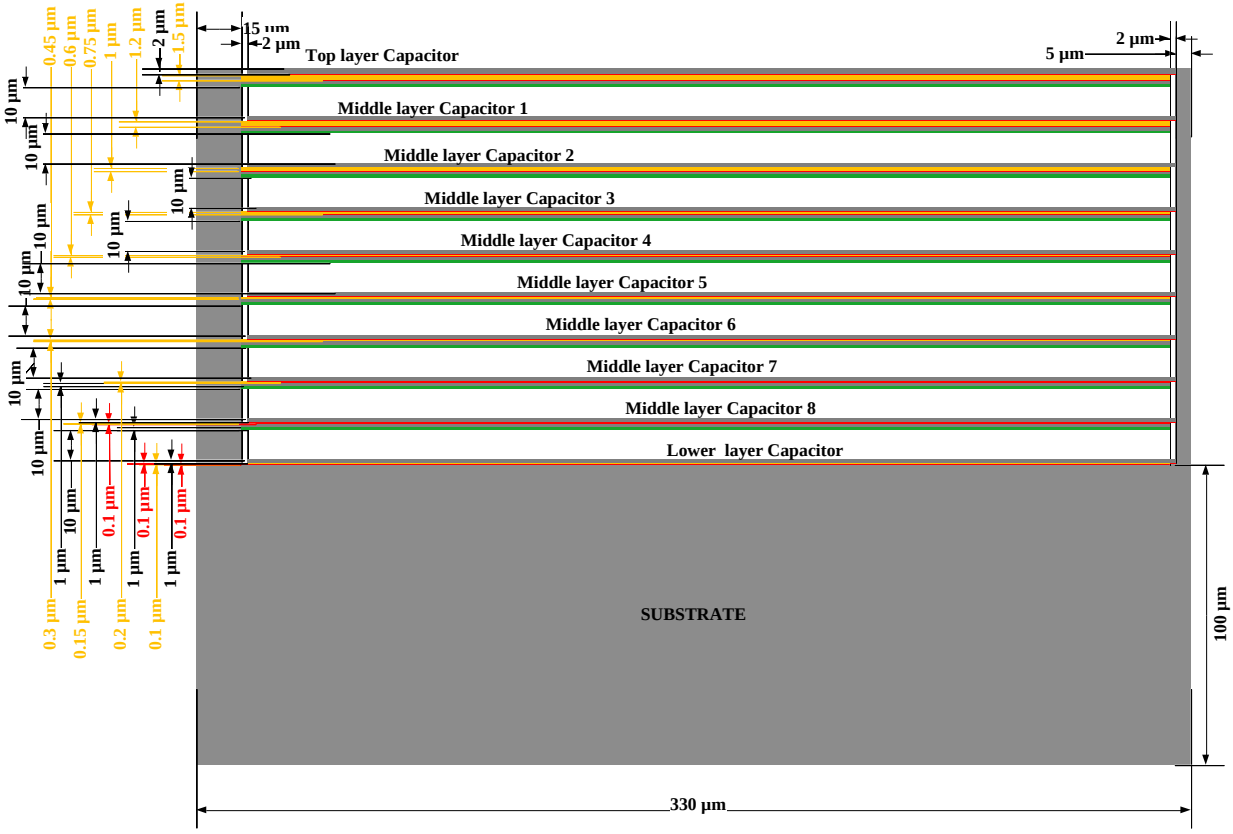

Fig. 4- 20 Electrostatic 10 layers Micro generator structure

A similar analysis can be applied for piezoelectric micro structure for the piezo material dimension changes. A piezoelectric micro-generator also will require a larger volume of piezo material. The piezo layer number also is a factor in the generator structure design that will affect the complexity of the fabrication (additional masks and material deposing) and control circuit implementation. The mode of piezo polarization, d31 or d33, also affects the generator structure. Two considered micro structure types for piezoelectric chargers are cantilever and a mono layer structure. Fig. 4- 21 and Fig. 4- 1, and Fig. 4- 22 show the example of these structural types. In this work, several structure types including mono layer piezo structure and multi layers cantilever cases are simulated by using Comsol multi physic tools. A mono layer piezo structure

is shown in Fig. 4- 22 . The piezo layer area is 6600^2 μm^2. The outer diameter of a symmetric SPM (6 generators one at each side) will be 10 mm.

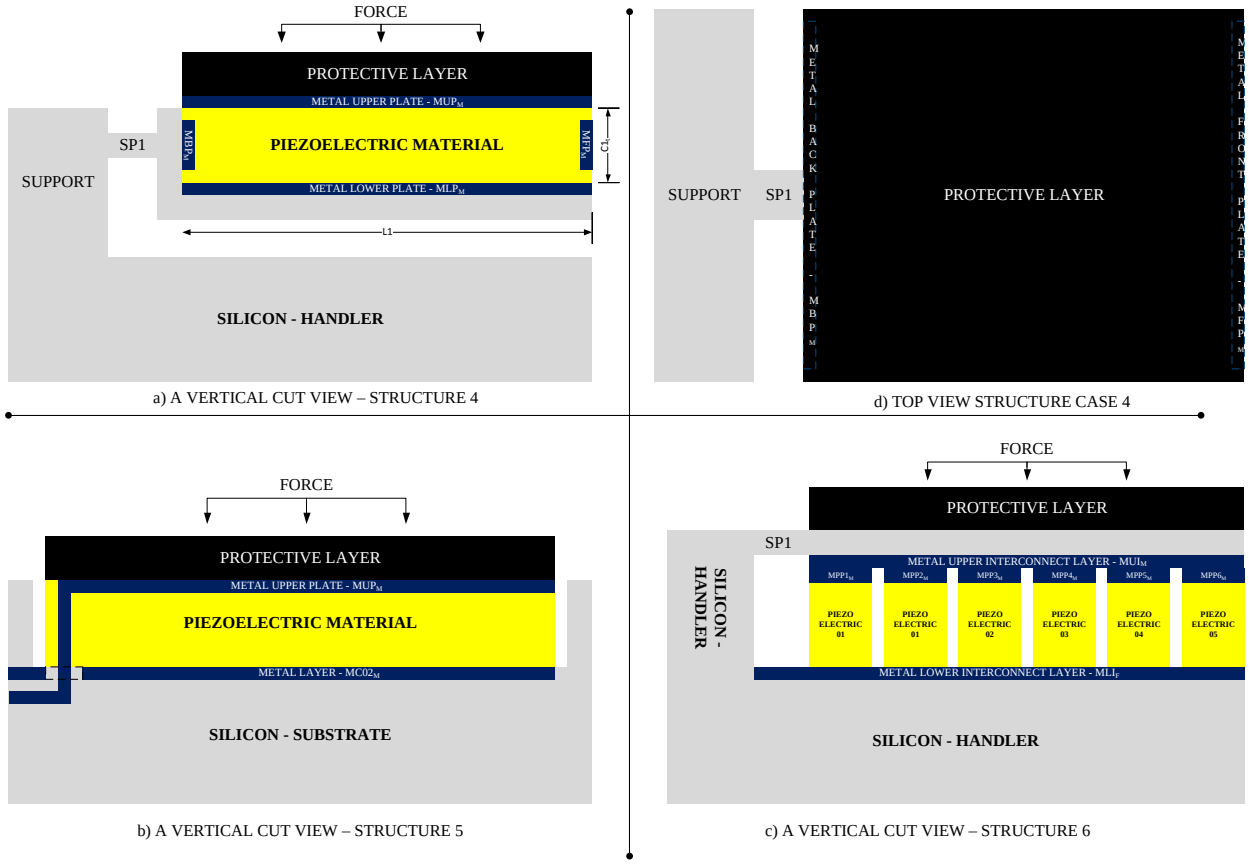

Fig. 4- 21 Simple Cantilever and press structures with Piezoelectric

For the first structure case, a mono layer structure in two modes of polarization, d31 and d33, are studied. Fig. 4- 22 shows the potential of the piezo layer in the mode of operation, d31. The detail data reports of this structure's case are summarized in Appendix 15: Micro Piezoelectric Generator - Power Estimate. The potential and current density along Y direction are measured. The average current density is -1.1×10^{-4} A/m^2 and the voltage is 7.2 V.

The power generation for this single layer structure can be estimated as:

$$P = \iint_{\beta=0,\gamma=0}^{\beta=p_l,\gamma=p_t} I_\alpha \times d\beta \times d\gamma \times \Delta V \qquad \text{Eq. 4- 51}$$

Where p_l is the piezo layer length and p_t is the piezo layer thickness, I_α is the current density in polarization direction and β and γ are the dimensions of a normal plan.

Study of the above structure, in d31 mode, calculated the power at 1.06 10^{-10} W. A similar study was conducted for d33 mode. The potential and displacement results are presented in Fig. 4- 23. This structure also results in I_α = Iz =-2.8 10^{-3} A/m^2, with the injected voltage ΔV= 1.70 10^{-2} V and P= 4.77 10^{-10} W. Both of the power ratings cannot be acceptable SPM generators.

The next analyzed structure is a cantilever structure. The models of single and multi-plate structures were analyzed. The analyses also included the effect of the cantilever support, sizes, and piezo layers or layers' placements. The main investigated scenarios include:

- A single plate cantilever with a size from 300 μ m x 300 μ m (30 x 30 generator modules) to 3300 μ m x 3300 μ m (3 x 3 generator modules). In this case, the thickness of the piezo layer material varied from a range of 20 μ m to 200 μ m. A structure with 3000 μm x 30 μm dimensions, 45 μ m piezo thickness, and contact plates of 5 μ m is presented in Appendix 15.
- A single plate cantilever with partial support with a size of 300 μ m x 300 μ m (30 x 30 generator modules). The structure support length varied from plate length of 300 μ m, to one third, 100 μ m.

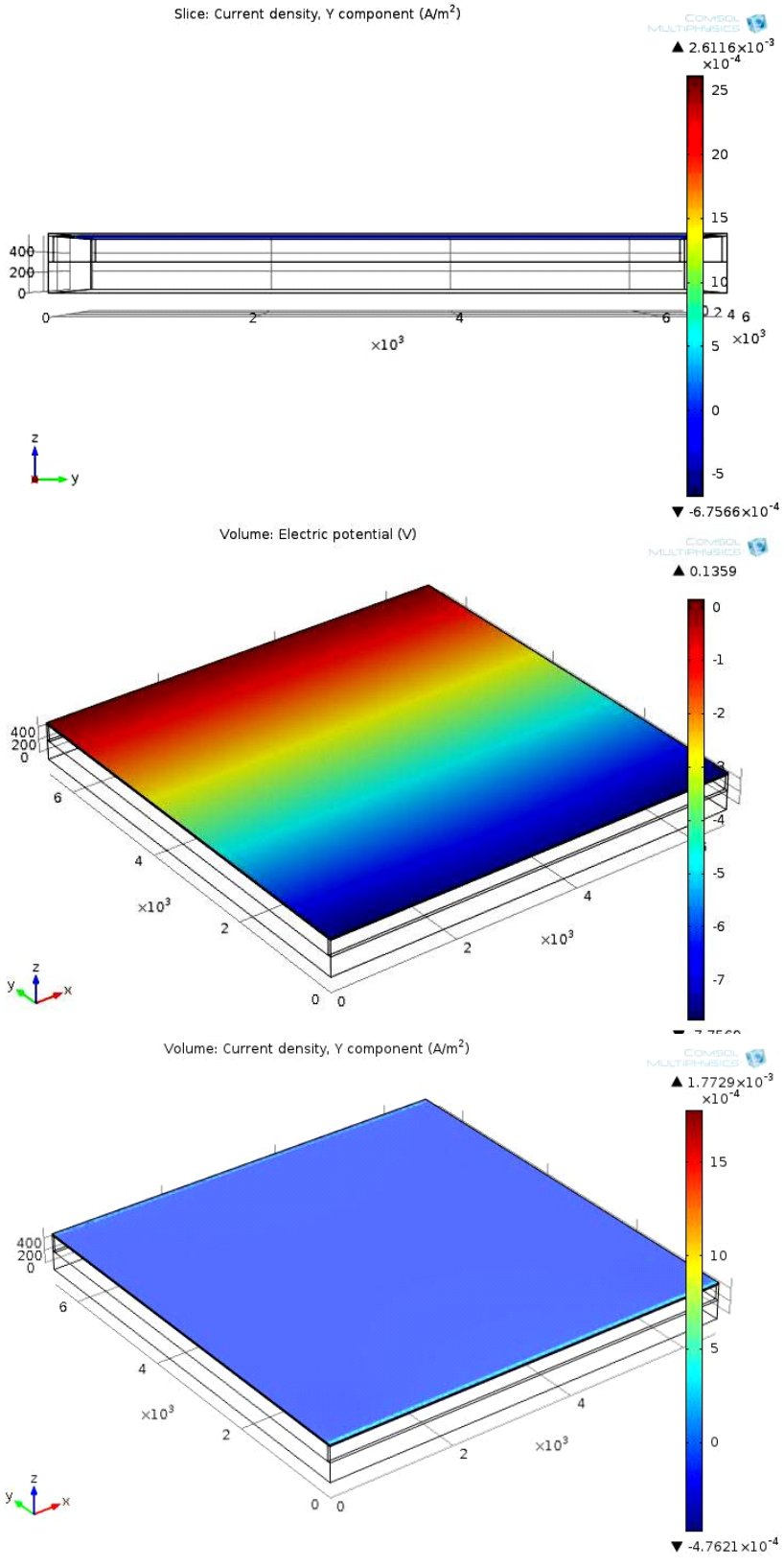

Fig. 4- 22 Mono layer piezoelectric structure geometry and electric potential (d31 mode)

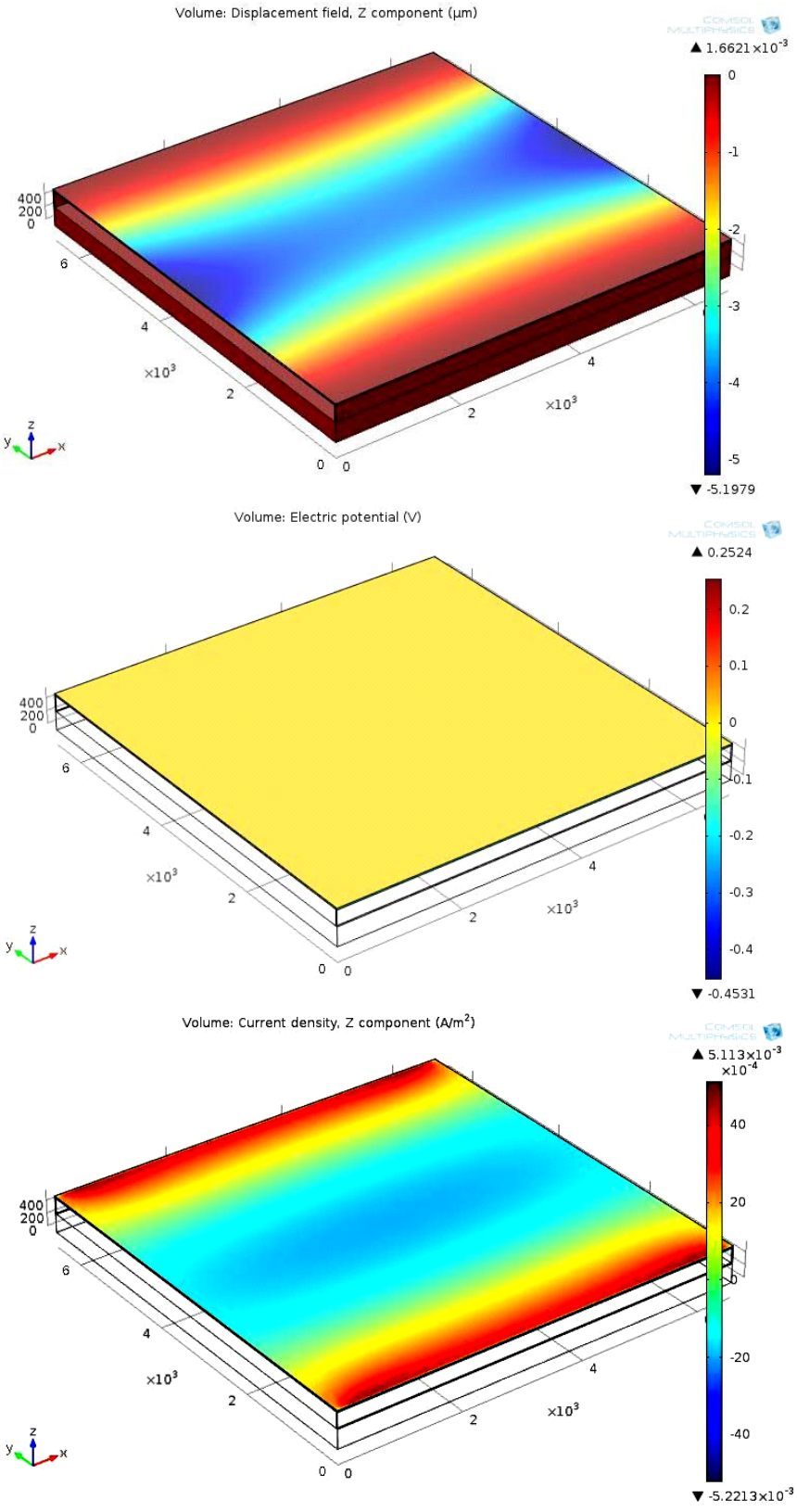

Fig. 4- 23 Mono layer piezoelectric structure geometry and electric potential (d33 mode)

- A single plate cantilever with stacking piezo layers with a size of 3300 μ m x 3300 μ m (3 x 3 generator modules). The multi layers of piezo materials (deleted space 2 to 5 in) were over each and were sandwiched between the connector plates.
- A triple plate cantilever with a size 300 μ m x 300 μ m (30 x 30 generator modules). A more complicated structure with additional plates was also simulated but no significant improvement was observed. The plate gaps adapted, based on the vertical arrangement of the plates.

With these scenarios, the effects of the geometries, thicknesses, lengths, connections and materials were analyzed. A summary of the results regarding the power generation study are included in Appendix 15. As we can see, the outcomes for these scenarios and the extension of other scenarios do not comply with our power generating target. The maximum expected generating rate is for case 1which provides for a 14 mV voltage at maximum current density of 80 μ A/m^2. These simulation results are based on a passenger car activation force and an ideal condition for the micro generator packaging. The detailed results can be found in Appendix 15. Therefore, we did not consider the piezo electric approach as the prime generating alternative. In this case, the thickness of the piezo layer material varied from a range of 20 μ m to 200 μ m.

A conclusion regarding these generators shows they will not be able to deliver the SPM minimum power requirements of 50 μW. However, the electrostatic cantilever structure with support piezo layers can be used.

A hybrid with a multilayer cantilever structure with piezo material overlay can be an alternative solution. However, the efficiency of the lower layers will not be optimum. A simulation of a three layer cantilevers structure with PZT 5 H materials is shown in Appendix 15. The polarization of the piezo materials is in Z direction (D_{33} operation mode).

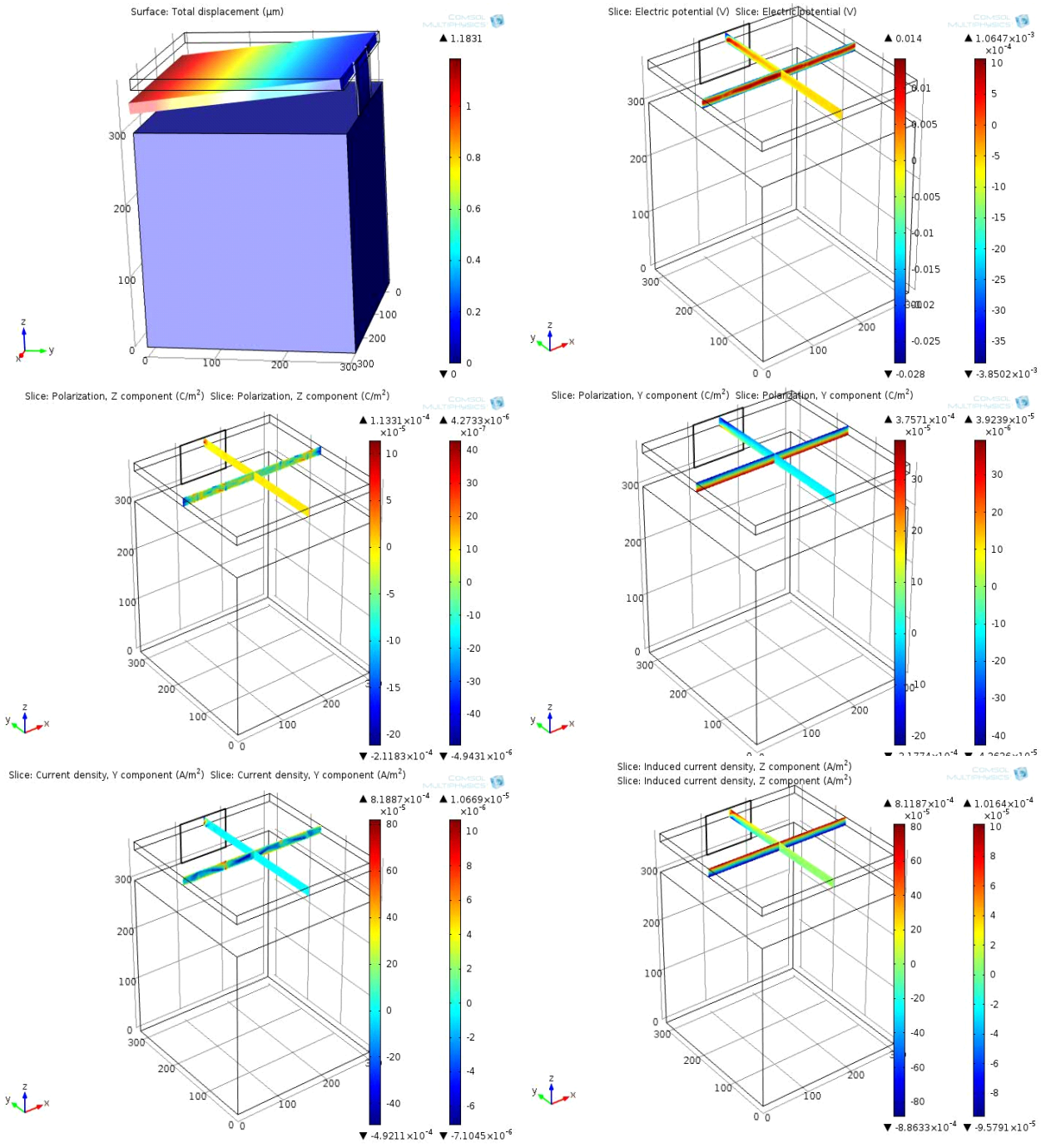

Fig. 4- 24 Single layer cantilever Piezo structure model- mode of d33 , 3D total displacement, plan views of potential (V), plan views of current density (IY), plan views of polarization Z component, plan views of polarization Y component, current density (IZ)

4.4 SPM MODULE PLACEMENT

In this Section, we discuss the assembly and packaging of the SPM micro-generator modules in the SPM node. The orientation of the SPM node in the pavement bed may be in a random or directional placement. Random placement will be easy and constructed in a fast installation process; however, it may not predetermine the faces of the SPM node which will be faced with vehicle load forces. Two cases of the SPM packaging structures are directional and symmetric packaging and were investigated in this research. The directional SPM required its placement on the pavement in a specific direction with the generator structure surface parallel to the pavement surface. Directional SPM will have maximum loading force affect to the generator. Directional SPM will require more installation time or the designing of the specific machine's automation installation. Either of these requirements will increase the cost of the SPM implementation and its operation significantly.

The second SPM assembly option is a symmetrical package that allows it to have interchangeable placement. Symmetric function allows for six or more orientations. The SPM package housing requires protection of the SPM generator, chips, and other circuits and it must be interfaced for mechanical force transfer to the micro-generator.

The generator module is defined as a micro-generator structure unit at a specific orientation. Examples of orientations are that of an orientation in SPM disk package (Directional SPM case), six orientations, a Cartesian coordinate, or a Dodecahedron[37] package with 12 orientations, one for each face. The symmetric SPM package will have one or more generator modules, each a face of the SPM housing. The generator modules will be at each face of the SPM node and will be covered with an outside jacket layer.

[37] Dodecahedron is any polyhedron with twelve flat faces (regular or non-regular).

SPM size is a design criteria that will affect the cost of material, fabrication process, and installation on the existing pavement. The original target plan for the SPM size was 1 cm diameter or a cubic length. The amount of the energy resource in the pavement is dependent on the roadway traffic volume/roadway class and the size of the generator. Therefore, to conceive of a solution for more roadway classes, we need to increase the size of the SPM in the range of 1.00 to 2.00 cm. Therefore, a default size for the SPM will set to 1.50 cm which will be adjusted by other parameters, such as fabrication packaging assembly limits. For final package and SPM housing, a scaling process will be included for all geometry. The scaling shall comply with minimum feature length and assembly tools.

Besides the generator modules, SPM's sensors and micro antennas also will be placed at the outer layer of the SPM housing for interfacing with the outside. Other circuit modules of the SPM will be placed at SPM core or inner layers. Fig. 1- 2 SPM On-Chip Components shows the block diagram of these modules. The connection between outer layer modules and the core will be a 3D coupling connection. It should be emphasized that all SPM modules and interconnections shall be designed to be ultra-low power components. Four examples of the SPM module placements are shown in Fig. 4- 25.

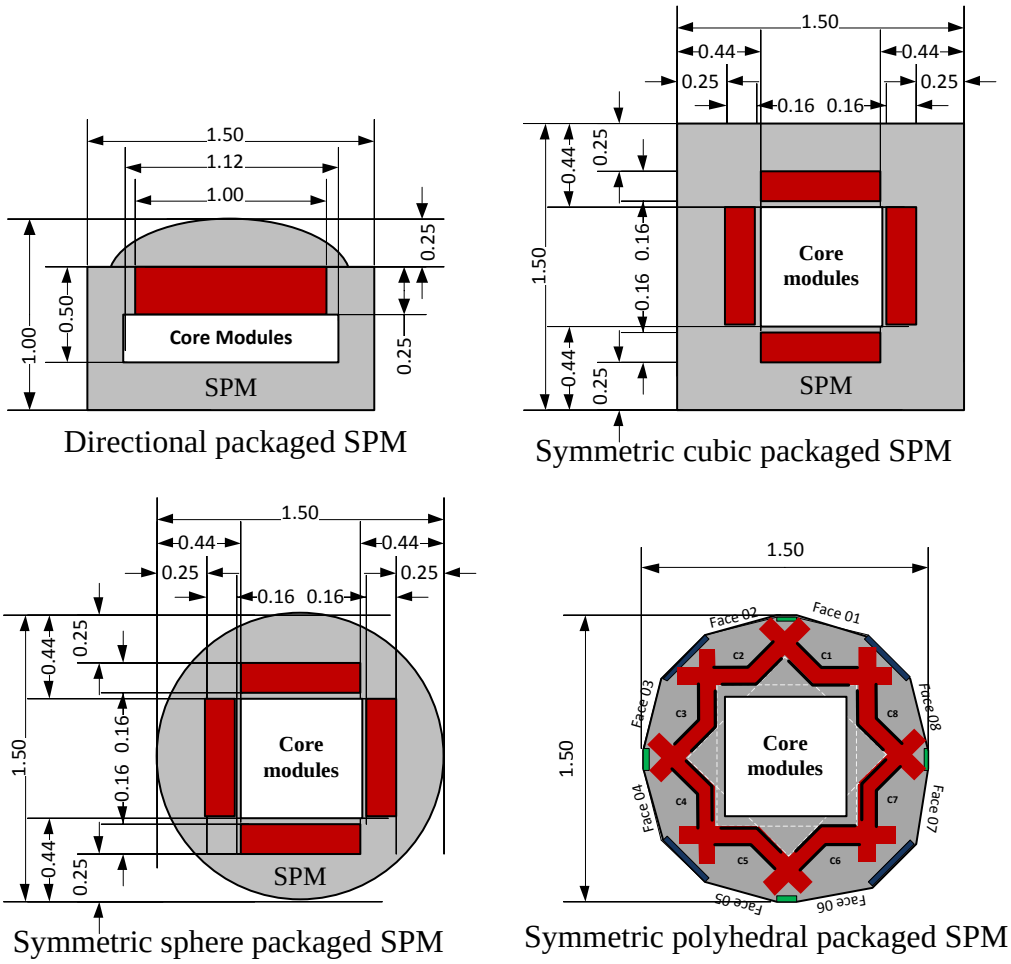

Fig. 4- 25 Examples of SPM modules placements

CHAPTER 5 – PAVEMENT ON-CHIP MICRO GENERATOR DESIGN

Chapters 2, 3 and 4 presented the conceptual planning study of the SPM micro-generator which presents the results of the SPM energy resource, optimum placement, harvesting approach, and the generator structure. In this Chapter, the design of the proposed SPM is presented. The Chapter includes description details of the proposed SPM, estimation of the power generated, generator control circuitry, fabrication and packaging. The design only includes the generator modules and core. Other SPM modules will be considered in future work.

5.1 SPM MICROGENERATOR DESIGN DESCRIPTION

The proposed micro-generator is an electrostatic alternative with a 10 layered microstructure in symmetrical packaging. In addition to the electrostatic approach, a piezo material was also used as a sensor for detection of tire/force. This sensor will be used in the generator control circuit. The information of this SPM is:

A. General

- Charging Concept: Electrostatic
- Packaging: Cubic Symmetric Shape
- Number of generator modules: 6 x 10 =60 (10 per each face)
- Structure type: Multi plate Cantilever , 10 plates

B. Geometry

- Outer length: 15.5 mm
- Generator module sizes: 4.85 (W) x 1.82 (D) x 0.4 (H) mm
- Substrate height: 200 µm
- Package protection layer (max): 1.5 mm
- Structure support: full support edge

- Structure plate thicknesses: SPT-01(2 µm); SPT-02 (1 µm); SPT-03 (1 µm); SPT-04 (1 µm); SPT-05 (1 µm); SPT-06 (1 µm); SPT-07 (1 µm); SPT-08 (1 µm); SPT-09 (1 µm); SPT-10 (1 µm)
- Charger capacitor gaps: CCG-01 (10 µm); CCG-02 (8 µm); CCG-03 (6 µm); CCG-04 (4.5 µm); CCG-05 (3.5 µm); CCG-06 (3 µm); CCG-07 (2.5 µm); CCG-08 (2 µm); CCG-09 (1.75 µm); CCG-10 (1.5 µm)
- Dielectric thicknesses: DT-01 (103 µm); DT-02 (10 µm); DT-03 (8 µm); DT-04 (5 µm); DT-05 (2 µm); DT-06 (1.3 µm); DT-07 (1.0 µm); DT-08 (0.8 µm); DT-09 (0.5 µm); DT-10 (0.5 µm)
- Metal layer thickness: 0.1 µm
- Free space between structure plates: 10 µm
- Isolation layer thickness: 1 µm
- Outer protection coating thickness: 2mm
- Adhesive layer thickness: 33.25 µm

C. Materials

- Wafer-Substrate: Silicon , Si

  Properties: Atomic number 14, energy gap Eg = 1.12 eV - indirect band-gap; crystal structure - diamond, lattice constant 0.543 nm; atomic concentration 5x1022 atoms/cm-3, index of refraction 3.42;density 2.33 g/cm3; dielectric constant 11.7; intrinsic carrier concentration 1.02 x 10^{10} cm-3, mobility of electrons and holes at 300 K: 1450 and 500 cm2/V-s; thermal conductivity 1.31 W/cm-^{o}C, thermal expansion coefficient 2.6 x 10^{-6} 1/^{o}C, melting point 1414^{o} C

Diameter: 300mm; Orientation: <100>, TTV: <5um; STIR: <2um Notch: SEMI Standard; Double Side Polished (DSP); DEVICE Layers: Type/ Doping: N/P types; Resistivity: 0-100 ohm-cm; Thickness: up to 725+/-20um; Orientation <100>.[38]

- Adhesive: EP3RRLV

  Properties: One Part, Lower Viscosity, Thermally Conductive Epoxy System for High Performance Potting, Encapsulation and Under-fill Applications Featuring Exceptional Dimensional Stability and Rapid Curing at 230-250°F.[39]

- Metal layer: Gold, Au

  Properties: Melting Point: 1063 °C; Density: 3 19.3 g/cm; Lattice Constant (@20 °C): 4.079 x10 $^{-10}$ m (Å); Lattice Structure: FCC; Specific Heat (@20 °C): 0.126 J/g K; Thermal Conductance: 31.1 kW/m ^{2} K; Coefficient of Linear Thermal Expansion: 14.2 ppm/K; Electrical Resistivity (@20 °C): 2.2 x 10 $^{-8}$ Ω m; Electrical Conductivity (@20 °C): 4.55 x 10 ^{7} / Ω m; Vickers Hardness: 216 MN/m ^{2} ; Young's Modulus: 78 GPa; Modulus of Elasticity: 79 GPa ; Tensile Strength: 120-220 N/mm ^{2} .[40]

- Dielectric: Strontium Titanate, $SrTiO_3$

  Properties: Nano Powder, 99.95%, cubic phase; Sr:Ti atomic ratio 0.998-1.002; average particle size ~100 nm (SEM & BET); BET specific surface area (SSA) > 10 m2/g, cubic phase (XRD); m.p. 2080 ^{o}C; density 5.12 g/cm^{3}. [41] ; Dielectric constant: 300; Thermal expansion coefficient: 9 x 10^{-6} K^{-1}; thermal conductivity: 120 milliwatts/cm °C at 100 °C; Dielectric loss tangent (10GRz): 2 x 10^{-2} ; Electrical character: Para-electric above 45°K

[38] http://www.svmi.com/default.aspx
[39] http://www.masterbond.com/tds/ep3rrlv
[40] http://heraeus-contactmaterials.com/en/home/contactmaterials.aspx
[41] http://www.advancedmaterials.us/3822-ON1.htm

and Ferroelectric below 45°K; Specific resistivity: > 10^7 Ohm/cm; hardness: 6 - 6.5 (Mohs).[42]

- Piezoelectric: Lead Zirconate Titanate (PZT-5H)[43]

  Properties: Crystal symmetry class: Uniaxial; density 7.5 g/cm^3 ;

  Compliance:

$$\mathbf{s_E} = \begin{bmatrix} 16.5 & -4.78 & -8.45 & 0 & 0 & 0 \\ -4.78 & 16.5 & -8.45 & 0 & 0 & 0 \\ -8.45 & -8.45 & 20.7 & 0 & 0 & 0 \\ 0 & 0 & 0 & 43.5 & 0 & 0 \\ 0 & 0 & 0 & 0 & 43.5 & 0 \\ 0 & 0 & 0 & 0 & 0 & 42.6 \end{bmatrix} *10^{-12} \ \frac{m^2}{N}$$

  Piezoelectric Coupling:

$$\mathbf{d} = \begin{bmatrix} 0 & 0 & 0 & 0 & 741 & 0 \\ 0 & 0 & 0 & 741 & 0 & 0 \\ -274 & -274 & 593 & 0 & 0 & 0 \end{bmatrix} *10^{-12} \ \frac{C}{N}$$

  Relative Permittivity

$$\frac{\boldsymbol{\varepsilon_T}}{\varepsilon_0} = \begin{bmatrix} 3130 & 0 & 0 \\ 0 & 3130 & 0 \\ 0 & 0 & 3400 \end{bmatrix}, \quad \varepsilon_0 = 8.854 *10^{-12} \ \frac{F}{m}$$

  Lead Zirconate Titanate (PZT) powder: density[44]: 7.7 to 8 g/cm^3 ; Young's module: 5.8

[42] http://www.surfacenet.de/html/strontium_titanate.html
[43] http://www.efunda.com/materials/piezo/material_data/matdata_output.cfm?Material_ID=PZT-5H

to 9 GPa; Curie temperature: 170- 360 °C ; relative dielectric constant : 1000 to 4000.[45] [46]

- Isolator : Silica, SiO2

  Properties: Atomic Volume (average): 0.009 to 0.0095 m^3/kmol; density: 2.17-2.65 Mg/m^3; bulk module: 33.5 to 36.8 GPa; Compressive Strength: 1100 to 1600 MPa; Elastic Limit: 45 to155 MPa; Hardness: 4500-9500 MPa; loss coefficient: 8e-006 to 2e-005; Poisson's Ratio: 0.15 to 0.19; Shear Modulus: 27.9 to 33.2 GPa; Tensile Strength: 45 to 155 MPa; Young's Modulus: 66.3 to 4.8 GPa; Maximum Service Temperature: 1170 to 1670 K; Thermal Conductivity: 1.3 to 1.5 W/m.K; Thermal Expansion: 0.55 to 0.75 10^{-6}/K; Breakdown Potential: 25 to 40 MV/m; Dielectric Constant: 3.6 to 4.2; resistivity: 1e+023 to 1e+027 10^{-8} ohm. [47]

- Interconnection: Cooper

- Soldering: Lead free solder: Sn on Cu; Sn1.5Ag on Cu; Sn3.0Ag on Cu

  Properties: Lead free and tin lead solder wire & solder bar,

D. SPM packaging layout

The SPM modules will be designed or chosen to provide acceptable levels of the desired attributes. The SPM interconnection and joining structure must provide a geometric and spatial translation from the micro-generator modules to the SPM core module. Thermo mechanical expansion shall be considered between the package modules' physical interfaces. In case a significant thermal coefficient difference between two coupling parts, the thermal expansion may result in package structure failure. However, the

---

[44] http://www.ecertec.com/uap.htm
[45] http://www.reade.com/products/41-titanate-compounds-powder/284-lead-zirconate-titanate-powder-pzt-lead-zirconate-titanate-lead-zirconium-titanate-lead-titanate-zirconate-plumbum-zirconate-titanate-cas-12626-81-2
[46] http://www.piezo.com/prodmaterialprop.html
[47] http://www.azom.com/properties.aspx?ArticleID=1114

thermal expansion will be less critical in an ultra-low power SPM. The SPM package shall provide high performance on the fabrication (assembly, handling, and interconnections), uniformity/standard, testing and verification, and the construction cost. SPM 3-dimensional structures and elements are special cases of systems on package (SOP) that include different SPM modules on the package. Fig. 5- 1 shows the proposed cross section layout of an SPM package. This 3-D package required a 3-D interconnection, or bonding between the micro generator modules and the core chip. The SPM device might also require thermal isolation within the package and a mounting method that optimizes the mechanical stress on the generator modules.

E. Interconnection

Wire bounding between generator modules to the Core SPM module. These connections include:

Contact 1. Vi: initial voltage controlled by generator charging control circuit

Contact 2. Gnd: ground from Core module

Contact 3. Vc: Charger output voltage to Core module

Contact 4. C1: Charger control signal to Core module

Contact 5. C2: Charger control signal to Core module

Contact 6. C3: Charger control signal to Core module

Contact 7. C4: Charger control signal to Core module

Contact 8. C5: Charger control signal to Core module

Contact 9. C6: Charger control signal to Core module

Contact 10. A1: Antenna RF signal to Core module

Contact 11. A2: Antenna RF signal to Core module

Contact 12. A3: Antenna RF signal to Core module

Contact 13. A4: Antenna RF signal to Core module

Contact 14. S1: Sensor signal to Core module

Contact 15. S2: Sensor signal to Core module

Contact 16. S3: Sensor signal to Core module

Contact 17. S4: Sensor signal to Core module

Contact 18. S5: Sensor signal to Core module

Contact 19. S6: Sensor signal to Core module

Contact 20. S7: Sensor signal to Core module

Contact 21. S8: Sensor signal to Core module

Contact 22. S9: Sensor signal to Core module

Contact 23. S10: Sensor signal to Core module

Contact 24. S11: Sensor signal to Core module

Contact 25. S12: Sensor signal to Core module

Contact pad sizes: 50 µm x 50 µm

F. SPM on package battery

SPM battery will be the source of the initial voltage of the charger and the storage of the charging energy. The initial voltage is a subject of the charger system and in the case of the electrostatic system; the charging capacity depends on that value. Two initial voltages of 5 VDC and 10 VDC can provide charges of more than 50 µW. The voltage storage can be a different voltage from the initial charging source, but it will require a voltage conversion module.

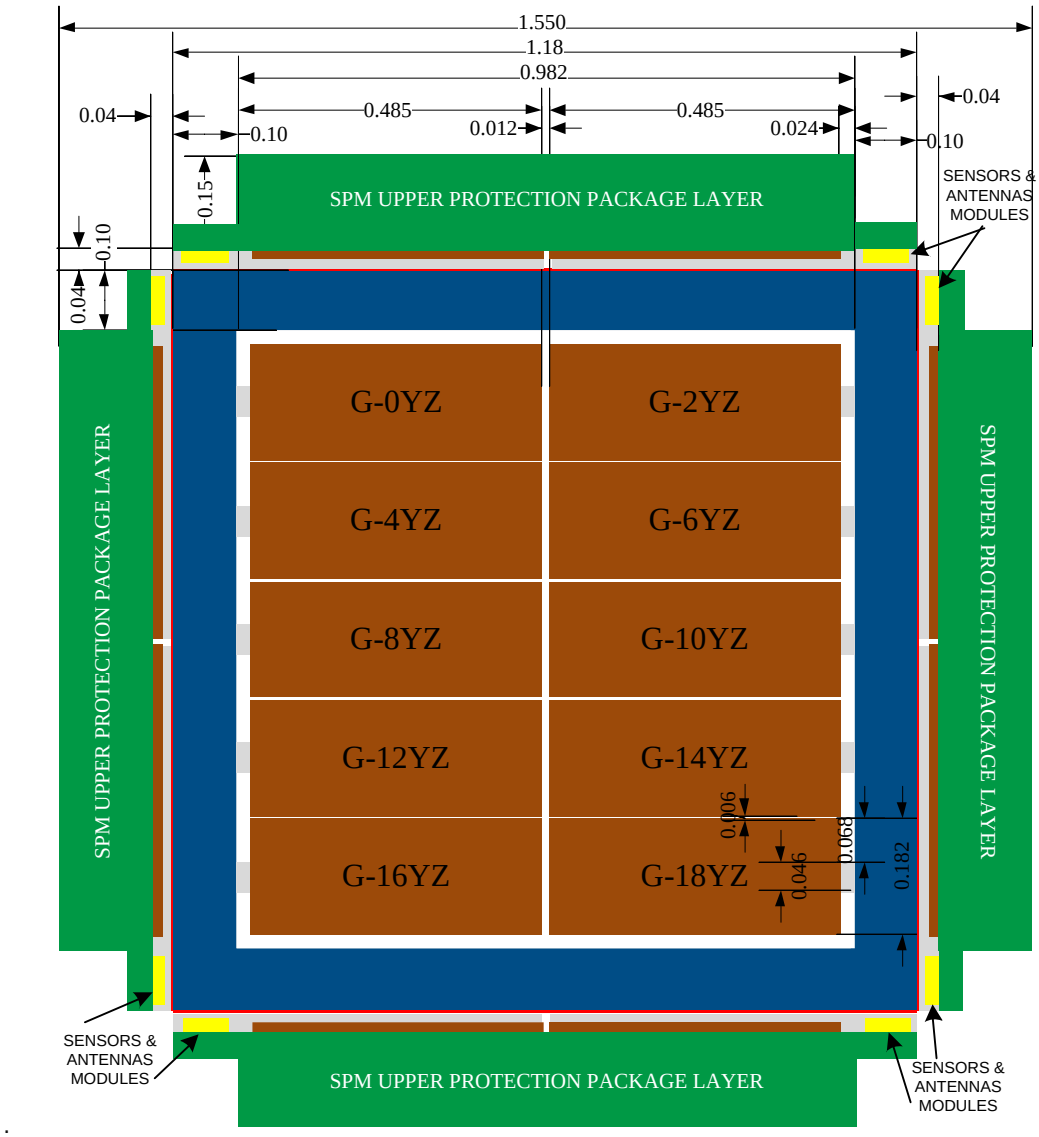

Fig. 5- 1 A SPM Packaging Layout

A DC-to-DC converter could utilize some of the residual energy of the system but this would add to the fabrication cost and introduce a 10 to 15 percent energy loss (converter loss). The lower V_{dd} voltage is preferable for the low power IC design. The performance of typical CMOS logic circuits drops off more slowly than power consumption does as V_{dd} is reduced. The power consumption drops linearly with the circuit frequency and quadratically with voltage so that the power reduction rate is roughly cubic with the

voltage drop when the consequential reduction in frequency is included. [39] SPM micro-generators and core circuits design use this fact to establish low V_{dd} of the on package battery with lower power, but the performance and the operating frequency of the core circuits will be compromised.

SPM on package battery can be an on-chip module fabricated battery (micro-battery) or a prepackaged miniature battery. In either of these cases, the battery will be placed as a part of the central core of the SPM. The functional requirements of the SPM battery are:

- Battery Operation Modes: SPM will operate in three functional modes, M1-full functional mode (sense, detection, listen and transmission), M-2-partial functional mode (listen and transmission) and M-3-sleeping mode. The power consumption for each mode is capped at 50, 30 and 10 μW. This power limits the design fact for the SPM core module design.
- Battery C-rate: The maximum operational time period between two charging cycles (vehicle passing) will be less than two hours for a freeway or expressway. This long period is matched to off peak traffic time. The simulation results of the M-modeling cases show this time to be in the range of (5400 to 5800 seconds). However, to include the wider class of the highway traffic classes, 7200 seconds is considered for that time period. A C-rate is a measure of the rate at which a battery is discharged relative to its maximum capacity. A 1C rate means that the discharge current will discharge the entire battery in one hour. Based on the SPM mode of the operation, the C-rate will be different. The sleeping mode and the definition above 0.5C rate will be used.

- Battery End of Discharge: The maximum battery discharge rate will be the factor of the battery fabrication, materials and its chemistry. As examples, the end-of-discharge voltage for lead acid is 1.75V/cell; for a nickel-based system, it is 1.00V/cell; and for most Li-ion it is 3.00V/cell. At this level, roughly 95 percent of the energy is spent and the voltage would drop rapidly if the discharge were to continue [40]. In an SPM battery, it is recommended that the maximum energy discharge rate be 90% the battery capacity. This rate will be used for sizing the battery capacity.
- Battery Depth of Discharge (DOD): DOD is the percentage of battery capacity discharge over the maximum capacity. SPM's battery will operate in DOD more than 80% in most typical times (deep discharge) which need to be considered in the selection of the standalone miniature/micro battery type.
- Battery's voltage: Higher voltage is preferred for the charger circuit as discussed in a previous Section. 10 and 5 Vdc are target voltages for the SPM battery, but a 3 Vdc is also being considered because of the availability of lower voltage miniature/micro batteries.
- Battery capacity: The total micro-amp-hours available when the battery is discharged at a certain discharge current, decrease the capacity by an increasing C-rate. Table 5-1 presents a summary of the SPM battery capacity calculation. A minimum capacity for the SPM battery is calculated at 72 mW.
- Maximum battery charging cycle: This is the number of discharge-charge cycles the battery can experience before it fails to meet lower voltage. Life time requirements for the SPM operation determine the maximum charging cycle for the SPM battery. As far as the charger, the lower the voltage, its charging energy will be decreased.

The SPM battery charge/discharge cycle is a daily cycle and it is more complicated because of the discrete charging/activating process.

Table 5- 1 SPM Battery minimum capacity

SPM power consumption (µW)			Operating mode rates				Operate time (s)
Full	Partial	Sleeping	Full	Partial	Sleeping	Total	
50	30	10	26.2%	44.3%	30%	100.0%	86400
SPM activation rate			Energy consumption				Discharge time (s)
Min.	Ave.	Max.	Full	Partial	Sleeping	Total	
5.0%	6.3%	9.5%	1130400	1148256	255168	2.53E+06	7200
DOD	C- rate	Voltage- Vdc	Current- µA	Capacity µAh	Capacity (mWh)		
90%	0.8	1.5	6.67E+00	1.33E+01	7.20E+01		
90%	0.8	5	2.00E+00	4.00E+01	7.20E+01		
90%	0.8	10	1.00E+00	2.00E+00	7.20E+01		

A typical traffic pattern can be a factor for grouping the individual activations. This typical pattern will have two peak periods when most of charging will happen. Therefore, a minimum of two daily cycles should be considered. In our assessment, we considered three daily cycles. If a minimum life time of SPM is 10 years, the total expected SPM battery life cycle is 11,000. This cycle number is high/not applicable for several battery technologies such as Lead Acid, NiCd, and NiMH, all of which support maximum life cycle less than 1000 years. The battery life cycle is affected by the operating C-rate and depth of cycles and by other conditions such as temperature and humidity. Higher the DOD will have lower the cycle life.

SPM battery implementation can be an on-package rechargeable stand-alone battery or an on-chip fabricated battery module. The stand-alone battery will comply with the minimum requirements, above. An example of a stand-alone battery from Seiko is shown in Fig. 5- 2. This Lithium battery has sizes, voltage, current and capacity that

comply with SPM battery needs, but the life cycle of the battery is a 1000 year cycle. However, we considered it for the SPM prototype deployment. The battery with a higher life cycle requires a customized order and should be provided.

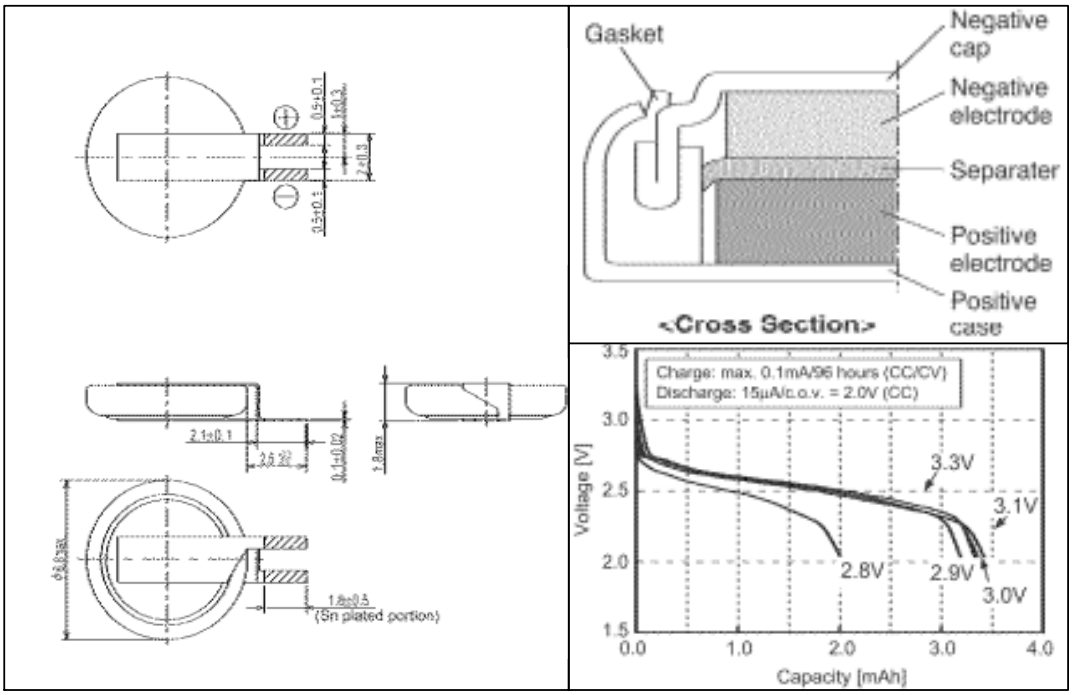

Fig. 5- 2 Seiko MS614SE: Lithium rechargeable battery [41]

The specifications of the Seiko battery are: nominated voltage: 3 Vdc, charge/discharge voltage: 2.8 to 3.3 Vdc, capacity: 3.4 mAh, internal impedance: 80 ohm, standard charge/discharge current: 15 μA, maximum charge/discharge current: 250 μA, life cycle at 20% DOD: 1000, diameter: 6.8 mm, thickness: 1.4 mm and weight: 0.17 grams. Two series batteries will connect to each other and will be placed on the SPM package (total voltage 6 Vdc).

A layout of the SPM core modules with the stand-alone batteries is shown in Fig. 5-3. The core module requires a 3D interconnection between the core chip to the battery and to the PCB's. The PCB's are connection interfaces at different orientations. The

interconnections will be a flex interconnect type, such as DuPont™ Pyralux® AP-*PLUS*, an all-polyimide thick copper-clad laminate[48] or Coining Rolled Narrow Ribbon [49]. This core layout is symmetrical for micro generators connecting to it. Using MS614SE batteries in series, we built a 9 Vdc initial voltage source. The outside dimensions of the core module are the same as specified in Fig. 5- 1 A SPM Packaging Layout. The internal dimension will be the subject of an adjustment based on the details of the fabrication equipment. The connector pads are sized at 50 x 50 $(\mu m)^2$ and 100 x 100 $(\mu m)^2$ as shown in the layout. The flexible wire interconnect thickness is 12.5 μm to 25 μm based on the selected flex interconnect. The size of the SPM core chip in this layout is 7.82 x 7.82 x 4.00 $(mm)^3$.

The second option for the SPM battery is an on-chip battery module. This means the battery will be fabricated as a compatible IC substrate, such as silicon or silicon oxide. This module can be combined with a micro-generator module with a die to die bonding such as Cu-Cu which should be considered for a mass production of SPM. The existing on-chip micro scale battery technologies are available in research and commercial markets.

[48] http://www2.dupont.com/Pyralux/en_US/products/laminate/AP_PLUS/pyralux_ap-plus.html
[49] http://www.coininginc.com/gold_wire_and_ribbon.asp

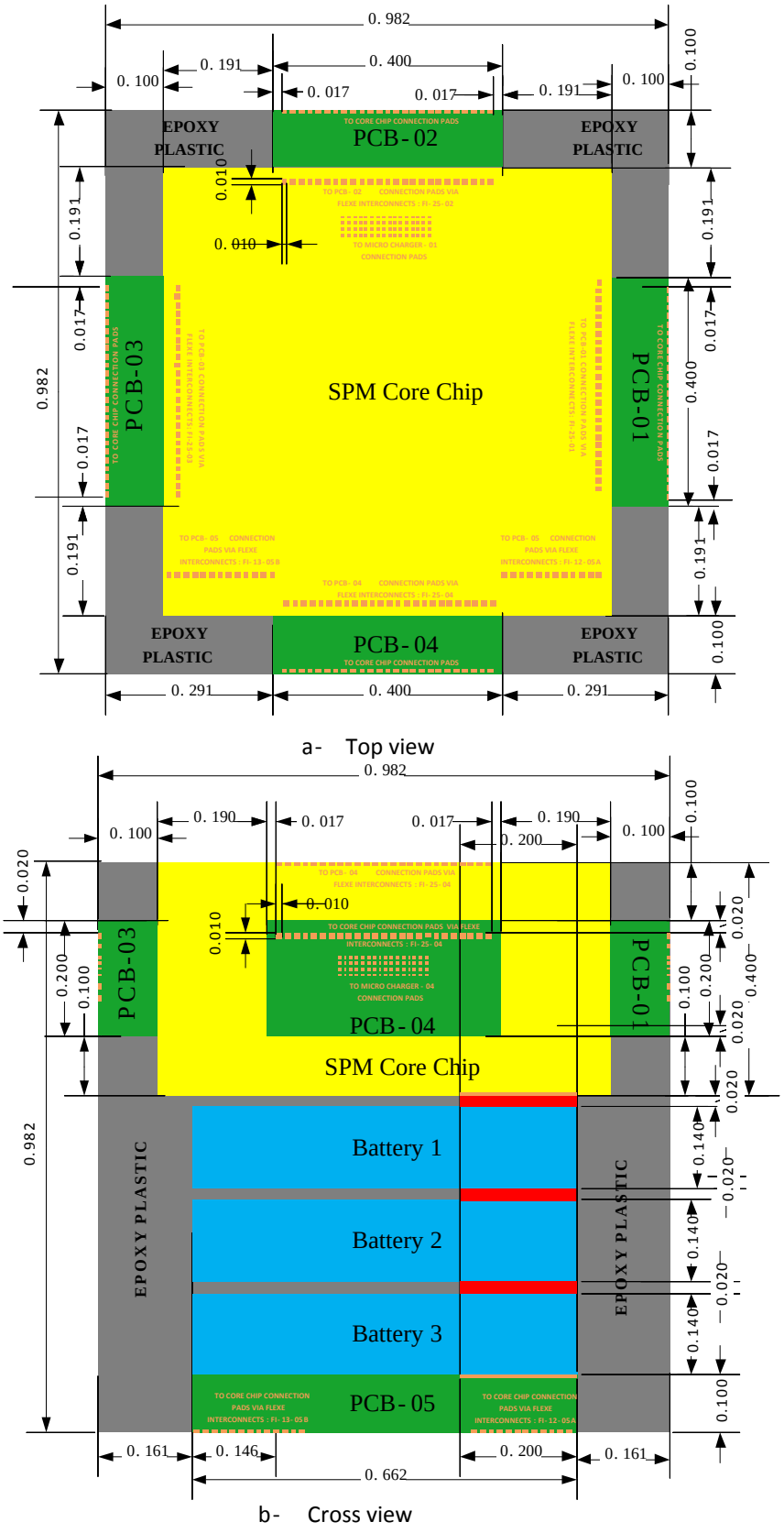

Fig. 5- 3 SPM core modules with the stand-alone batteries (unit is cm)

The available categories for these batteries are a thin film battery and a high capacitor. A micro scale lithium battery is an on-chip battery that has been used in MEMS or NEMS devices since the last decade. Examples of such thin batteries designed by Bates with a thickness less than 15 μm consist of cathodes that are crystalline or nano-crystalline oxide-based lithium intercalation compounds such as $LiCoO_2$ and $LiMn_2O_4$, and anodes of lithium metal and inorganic compounds such as silicon-tin oxynitrides, Sn_3N_4 and Zn_3N_2, or metal films such as Cu in which the anode is formed by lithium plating on the initial charge [42]. Jie Song, et al [43] proposed a micro-fabrication process for a single micro-battery with active size of 500 μm × 500 μm and thickness of1.5 μm. Their proposed process had $LiCoO_2$ films prepared by RF sputtering and annealed at moderate temperature (500 °C), were employed as a cathode electrode, and LiPON and Al films were used as a solid electrolyte and an anode electrode, respectively. The single micro-battery delivers a capacity of about 17 nAh at a current of 5 nA at the initial cycles and can be operated at as high as a 40 nA discharge current [43].

W. C. West, J. F. Whitacre, V. White, B. V. Ratnakumar from the California Institute of Technology implemented a microbattery for a MEMS space micro system application [44]. They developed a micro-fabrication process to prepare thin film solid-state lithium batteries as small as 50 μm × 50 μm. Individual cells operate nominally at 3.9 Vdc with 10 μA h cm^{-2} for a 0.25 μm thick cathode film. The cells are easily fabricated in a series and parallel arrangement to yield batteries with higher voltage and/or capacity. Multiple charge/discharge cycles are possible, though an apparent reaction of the *in situ* plated Li film with water or oxygen decreases cycle

life several orders of magnitude from expected results [44]. A schematic process for on chip battery is shown in Fig. 5- 4.

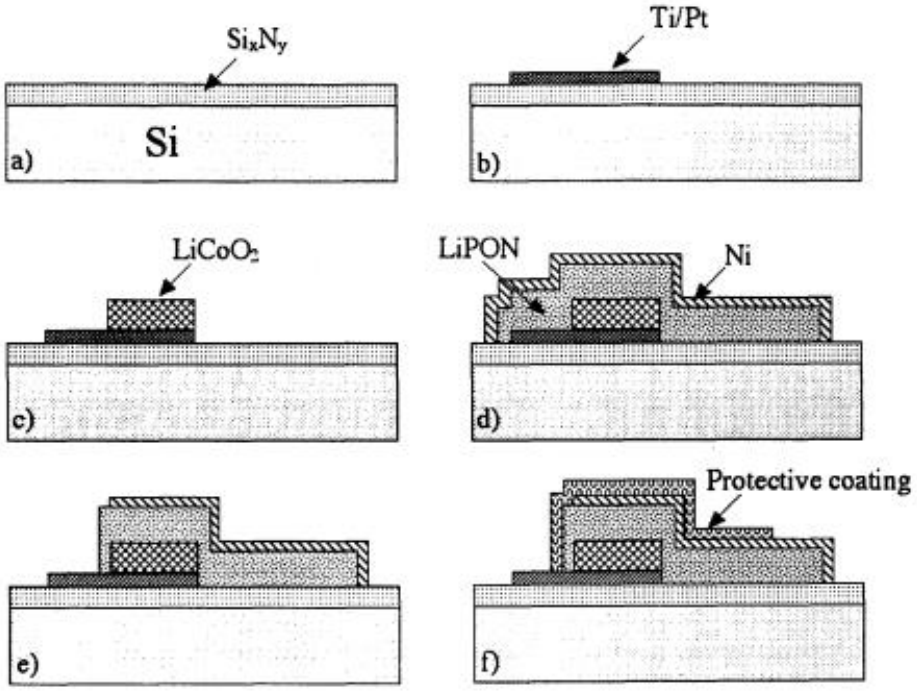

Fig. 5- 4 Schematic process flow for microfabricated batteries [44]

N. J. Dudney, B. J. Neudecker, and J. B. Bates presented key performance results achieved by ORNL[50]'s thin film batteries as a micro-power source [45]. This research indicated batteries fabricated using the crystalline LiCoO 2 cathode consistently provided the maximum power levels up to 30 mW/cm^2 and long cycle life with rapid charge rates. Lithium - $cLiCoO_2$ thin film batteries have been cycled many thousands of times with only small losses in capacity, typically ~0.2 $nAh/(cm)^2$/cycle at 25°C. Long term cycling of Li-$nLi_xMn_{2-y}O_4$ cells is likewise very stable for more than 1000 cycles. Mixed results have been found for cells with $cLiMn_2O_4$ cathodes. Several have achieved 1000's of cycles with less than $1nAh/(cm)^2$/cycle loss rates, while

[50] Oak Ridge National Laboratory (ORNL)

others exhibit capacity fades of 30 nAh/cycle over at least part of the cycle life. These variations are only partially attributable to differences in the cathode film compositions [45].

Therefore, Lithium – a $cLiCoO_2$ on chip battery is considered as an alternative SPM on chip battery. This process will be compatible with solid state fabrication; however, the life cycle of the battery shall be the main criteria on the design and material selection to maintain a high life cycle value, 11,000, for the SPM operation life time. This will involve future research work on the SPM core module development.

The last consideration for the on chip energy storage is high capacity capacitors. Super capacitors are of a new research field for battery alternatives in different application scales. Fast energy discharge and long energy holding are main parameters. Because capacitors store charges only on the surface of the electrode plates rather than within the entire electrode, they will have lower energy storage capability and lower energy densities in comparison with a battery. The charge/discharge reaction is not limited by ionic conduction into the electrode bulk, so capacitors can be run at high rates and provides very high specific powers but only for a very short period. The life cycle of a power storage capacitor is extremely longer than a battery. Using a super-capacitor alternative for the SPM energy storage will involve future study research for SPM core module designs.

G. Micro generator control circuit

Three primary methods for a micro-generator require a low current rectifier circuit with high efficiency and simple deployment. In addition, the generator requires a control or switching circuit to assist the efficiency and optional operation control of multi micro

generator modules in the node. The circuit design depends on the harvesting approach. In this Section, the proposed circuits for each approach are presented in a conceptual plan. The circuit is not complex for implementation on an integrated circuit; however, these proposals are fabricated by the generator micro structure which will be a custom MEMS process. Alternative solutions may include the rectifier and the control circuit to be part of the main SPM controller chip or sensor chip. Section 5.3 provides the description of the control circuit.

5.2 SPM MICROGENERATOR POWER ESTIMATE

In this Section, a power generation calculation of the proposed SPM micro power generator is provided. This estimate is based on the energy resource, generator structure efficiency, and placement or position of the SPM node on the pavement. The major facts in this calculation are:

- The micro-generator will be a 10 layer electrostatic generator as shown in Fig. 4- 20. The geometries of the generator parts are included in Table 5- 2. This generator has a multi plate cantilever structure. This micro-generator will have 10 variable charging capacitors. The capacitor gaps range from 1.5 μm to 0.1 μm.
- The generator is a 2 x 5 matrix array of micro-generator modules. The modules' area is 4850 x 1820 $(\mu m)^2$. The total micro generator area is 9.7 x 9.7 $(mm)^2$.
- The selected materials are described in Section 5.1.
- The calculations include 12 scenarios based on the generator's initial voltage (1, 5 and 9 Vdc) and relative permittivity as 1, 28, 300, and 2,800. The alternative represents with labels ESG-01 to ESC-12.

- The charging/mechanical conversion efficiency is considered in the calculation. The efficiency will depend on the SPM;s laying orientation on a pavement.
- Vehicle loads are estimated from the P- models.
- The traffic distribution data are from the M-Model simulation of the Henry Hudson Parkway.
- Traffic distribution is generated from M-Models. For simplicity, the passenger vehicle class is presented in the tables. The SPM node with maximum tire crossing will have a 9.2% activation rate.
- Micro structure movement is estimated from S-models. The maximum plate displacement is estimated at 1.4 μm (at top layer) and the minimum at 0.05 μm (at lower layer).
- The default capacitors value is 3.86 μF.
- The alternative case, ESG-12 shows the maximum power which is 345 μW. ESG-12 has the initial voltage at 9 Vdc and capacitor with a high relative permittivity of 2800.
- Alternative ESG-11 also can be acceptable for SPM application. ESG-11 power generation rate is 106 μW. ESG-11 has the initial voltage at 5 Vdc and capacitor with a high relative permittivity at 2800.
- Alternative ESG-09 is not acceptable for a full SPM operation case. However as a sensor, the base can be functional. This operation mode will be considered as a partial SPM operation which requires lower power consumption.

Table 5- 2 Electrostatic multi layers, 10, micro-generator power calculation

	DESIGN PARAMETERS	UNIT	ESG-01	ESG-02	ESG-03	ESG-04	ESG-05	ESG-06
P-01	Capacitor X Size	µm	4850	4850	4850	4850	4850	4850
P-02	Capacitor Y Size	µm	1820	1820	1820	1820	1820	1820
P-03	Capacitor Gap Thickness- Top Layer	µm	1.5	1.5	1.5	1.5	1.5	1.5
P-04	Capacitor Gap Thickness- Layer 01	µm	1.2	1.25	1.25	1.25	1.25	1.25
P-05	Capacitor Gap Thickness- Layer 02	µm	1	1	1	1	1	1
P-06	Capacitor Gap Thickness- Layer 03	µm	0.75	0.75	0.75	0.75	0.75	0.75
P-07	Capacitor Gap Thickness- Layer 04	µm	0.6	0.6	0.6	0.6	0.6	0.6
P-08	Capacitor Gap Thickness- Layer 05	µm	0.45	0.45	0.45	0.45	0.45	0.45
P-09	Capacitor Gap Thickness- Layer 06	µm	0.3	0.3	0.3	0.3	0.3	0.3
P-10	Capacitor Gap Thickness- Layer 07	µm	0.2	0.2	0.2	0.2	0.2	0.2
P-11	Capacitor Gap Thickness- Layer 08	µm	0.15	0.15	0.15	0.15	0.15	0.15
P-12	Capacitor Gap Thickness- Lower Layer	µm	0.1	0.1	0.1	0.1	0.1	0.1
P-13	Capacitor Support Plate Thickness Top	µm	2	2	2	2	2	2
P-14	Capacitor Support Plate Thickness 01	µm	1	1	1	1	1	1
P-15	Capacitor Support Plate Thickness 02	µm	1	1	1	1	1	1
P-16	Capacitor Support Plate Thickness 03	µm	1	1	1	1	1	1
P-17	Capacitor Support Plate Thickness 04	µm	1	1	1	1	1	1
P-18	Capacitor Support Plate Thickness 05	µm	1	1	1	1	1	1
P-19	Capacitor Support Plate Thickness 06	µm	1	1	1	1	1	1
P-20	Capacitor Support Plate Thickness 07	µm	1	1	1	1	1	1
P-21	Capacitor Support Plate Thickness 08	µm	1	1	1	1	1	1
P-22	Capacitor Support Plate Thickness Lower	µm	1	1	1	1	1	1
P-23	Capacitor Isolation Layer Plate Thickness	µm	1	1	1	1	1	1
P-44	Load Cl. 2-Capacitor Gap Change Top	µm	1.41	1.41	1.41	1.41	1.41	1.41
P-45	Load Cl. 2-Capacitor Gap Change Layer 01	µm	1.17	1.17	1.17	1.17	1.17	1.17
P-46	Load Cl. 2-Capacitor Gap Change Layer 02	µm	0.93	0.93	0.93	0.93	0.93	0.93
P-47	Load Cl. 2-Capacitor Gap Change Layer 03	µm	0.7	0.7	0.7	0.7	0.7	0.7
P-48	Load Cl. 2-Capacitor Gap Change Layer 04	µm	0.56	0.56	0.56	0.56	0.56	0.56
P-49	Load Cl. 2-Capacitor Gap Change Layer 05	µm	0.42	0.42	0.42	0.42	0.42	0.42
P-50	Load Cl. 2-Capacitor Gap Change Layer 06	µm	0.28	0.28	0.28	0.28	0.28	0.28
P-51	Load Cl. 2-Capacitor Gap Change Layer 07	µm	0.19	0.19	0.19	0.19	0.19	0.19
P-52	Load Cl. 2-Capacitor Gap Change Layer 08	µm	0.13	0.13	0.13	0.13	0.13	0.13
P-53	Load Cl. 2-Capacitor Gap Change Lower	µm	0.05	0.05	0.05	0.05	0.05	0.05
P-54	Capacitor Isolation Layer Plate Thickness	µm	1	1	1	1	1	1
P-55	Plate Thickness	µm	0.1	1	1	1	1	1
P-56	A Free Space	µm	10	10	10	10	10	10
P-57	A column Capacitor Thickness	µm	129.25	147.3	147.3	147.3	147.3	147.3
P-58	Substrate Thickness	µm	100	100	100	100	100	100
P-59	Charger Structure Thickness	µm	229.25	247.3	247.3	247.3	247.3	247.3
P-60	Permittivity		0	0	0	0	0	0
P-61	Relative Permittivity	NA	1	1	1	28	28	28
P-62	NO. Of Capacitors Per Layer	NO	1	1	1	1	1	1

P-63	NO OF Capacitor per Column Layers	NO	10	10	10	10	10	10
P-64	NO. OF Capacitor Column (2 x 5)	NO	10	10	10	10	10	10
P-65	Capacitor Value- Top Layer	µF	0	0	0	0	0	0
P-66	Capacitor Value- Layer 1	µF	0	0	0	0	0	0
P-67	Capacitor Value- Layer 2	µF	0	0	0	0	0	0
P-68	Capacitor Value- Layer 3	µF	0	0	0	0	0	0
P-69	Capacitor Value- Layer 4	µF	0	0	0	0	0	0
P-70	Capacitor Value- Layer 5	µF	0	0	0	0	0	0
P-71	Capacitor Value- Layer 6	µF	0	0	0	0.01	0.01	0.01
P-72	Capacitor Value- Layer 7	µF	0	0	0	0.01	0.01	0.01
P-73	Capacitor Value- Layer 8	µF	0	0	0	0.01	0.01	0.01
P-74	Capacitor Value- Lower Layer	µF	0	0	0	0.02	0.02	0.02
P-75	Initial Column Capacitor Value	µF	0	0	0	0.07	0.07	0.07
P-76	Initial Capacitor Value	µF	0.03	0.03	0.03	0.72	0.72	0.72
P-101	Load Cl. 2- Capacitor Change Top	µF	0	0	0	0	0	0
P-102	Load Cl. 2- Capacitor Change Layer 1	µF	0	0	0	0.01	0.01	0.01
P-103	Load Cl. 2- Capacitor Change Layer 2	µF	0	0	0	0.01	0.01	0.01
P-104	Load Cl. 2- Capacitor Change Layer 3	µF	0	0	0	0.01	0.01	0.01
P-105	Load Cl. 2- Capacitor Change Layer 4	µF	0	0	0	0.01	0.01	0.01
P-106	Load Cl. 2- Capacitor Change Layer 5	µF	0	0	0	0.01	0.01	0.01
P-107	Load Cl. 2- Capacitor Change Layer 6	µF	0	0	0	0.02	0.02	0.02
P-108	Load Cl. 2- Capacitor Change Layer 7	µF	0	0	0	0.03	0.03	0.03
P-109	Load Cl. 2- Capacitor Change Layer 8	µF	0	0	0	0.03	0.03	0.03
P-110	Load Cl. 2- Capacitor Change Lower	µF	0	0	0	0.03	0.03	0.03
P-111	Load Cl. 3-Column Capacitor Value	µF	0.01	0.01	0.01	0.17	0.17	0.17
P-112	Load Cl. 2-Total Capacitor Value	µF	0.06	0.06	0.06	1.65	1.65	1.65
P-113	Initial Voltage Source	VDC	3	5	9	3	5	9
P-114	Average Daily Traffic per lane (HHP)		27250	27250	27250	27250	27250	27250
P-117	Daily Activation -Vehicle Cl. 1 (HHP)	NO/Day	98100	98100	98100	98100	98100	98100
P-118	Max Activation Rate nodes(4 Nodes)	%	0.1	0.1	0.1	0.1	0.1	0.1
P-119	2nd Activation rate nodes (4 nodes)	%	0.07	0.07	0.07	0.07	0.07	0.07
P-120	3rd Max Activation rate nodes (2 nodes)	%	0.05	0.05	0.05	0.05	0.05	0.05
P-121	4th Max Activation rate nodes (4 nodes)	%	0.03	0.03	0.03	0.03	0.03	0.03
P-122	Other Activation Rate nodes (8 Nodes)	%	0.01	0.01	0.01	0.01	0.01	0.01
CH-01	Capacitance Default Energy	µJ	0.12	0.32	1.03	3.22	8.94	28.96
CH-04	Activation Charge per Vehicle Cl. 2 load	µJ	0.15	0.42	1.36	4.23	11.75	38.07
CH-07	Daily Charge Per Vehicle Cl. 2 Vehicle	µJ	1.5E+03	4.10E+03	1.3E+04	4.1E+04	1.20E+05	3.7E+05
CH-08	Daily Total Charge	µJ	1.5E+03	4.10E+03	1.3E+04	4.1E+04	1.20E+05	3.7E+05
CH-09	Generator Efficiency	NA	0.8	0.8	0.8	0.8	0.8	0.8
CH-10	Generator Power	µW	0.01	0.04	0.12	0.38	1.07	3.46
	DESIGN PARAMETERS	UNIT	**ESG-07**	**ESG-08**	**ESG-09**	**ESG-10**	**ESG-11**	**ESG-12**
P-01	Capacitor X Size	µm	4850	4850	4850	4850	4850	4850
P-02	Capacitor Y Size	µm	1820	1820	1820	1820	1820	1820
P-03	Capacitor Gap Thickness- Top Layer	µm	1.5	1.5	1.5	1.5	1.5	1.5
P-04	Capacitor Gap Thickness- Layer 01	µm	1.25	1.25	1.25	1.25	1.25	1.25

P-05	Capacitor Gap Thickness- Layer 02	µm	1	1	1	1	1	1
P-06	Capacitor Gap Thickness- Layer 03	µm	0.75	0.75	0.75	0.75	0.75	0.75
P-07	Capacitor Gap Thickness- Layer 04	µm	0.6	0.6	0.6	0.6	0.6	0.6
P-08	Capacitor Gap Thickness- Layer 05	µm	0.45	0.45	0.45	0.45	0.45	0.45
P-09	Capacitor Gap Thickness- Layer 06	µm	0.3	0.3	0.3	0.3	0.3	0.3
P-10	Capacitor Gap Thickness- Layer 07	µm	0.2	0.2	0.2	0.2	0.2	0.2
P-11	Capacitor Gap Thickness- Layer 08	µm	0.15	0.15	0.15	0.15	0.15	0.15
P-12	Capacitor Gap Thickness- Lower Layer	µm	0.1	0.1	0.1	0.1	0.1	0.1
P-13	Capacitor Support Plate Thickness Top	µm	2	2	2	2	2	2
P-14	Capacitor Support Plate Thickness 01	µm	1	1	1	1	1	1
P-15	Capacitor Support Plate Thickness 02	µm	1	1	1	1	1	1
P-16	Capacitor Support Plate Thickness 03	µm	1	1	1	1	1	1
P-17	Capacitor Support Plate Thickness 04	µm	1	1	1	1	1	1
P-18	Capacitor Support Plate Thickness 05	µm	1	1	1	1	1	1
P-19	Capacitor Support Plate Thickness 06	µm	1	1	1	1	1	1
P-20	Capacitor Support Plate Thickness 07	µm	1	1	1	1	1	1
P-21	Capacitor Support Plate Thickness 08	µm	1	1	1	1	1	1
P-22	Capacitor Support Plate Thickness Lower	µm	1	1	1	1	1	1
P-23	Capacitor Isolation Layer Plate Thickness	µm	1	1	1	1	1	1
P-44	Load Cl. 2-Capacitor Gap Change Top	µm	1.41	1.41	1.41	1.41	1.41	1.41
P-45	Load Cl. 2-Capacitor Gap Change Layer 01	µm	1.17	1.17	1.17	1.17	1.17	1.17
P-46	Load Cl. 2-Capacitor Gap Change Layer 02	µm	0.93	0.93	0.93	0.93	0.93	0.93
P-47	Load Cl. 2-Capacitor Gap Change Layer 03	µm	0.7	0.7	0.7	0.7	0.7	0.7
P-48	Load Cl. 2-Capacitor Gap Change Layer 04	µm	0.56	0.56	0.56	0.56	0.56	0.56
P-49	Load Cl. 2-Capacitor Gap Change Layer 05	µm	0.42	0.42	0.42	0.42	0.42	0.42
P-50	Load Cl. 2-Capacitor Gap Change Layer 06	µm	0.28	0.28	0.28	0.28	0.28	0.28
P-51	Load Cl. 2-Capacitor Gap Change Layer 07	µm	0.19	0.19	0.19	0.19	0.19	0.19
P-52	Load Cl. 2-Capacitor Gap Change Layer 08	µm	0.13	0.13	0.13	0.13	0.13	0.13
P-53	Load Cl. 2-Capacitor Gap Change Lower	µm	0.05	0.05	0.05	0.05	0.05	0.05
P-54	Capacitor Isolation Layer Plate Thickness	µm	1	1	1	1	1	1
P-55	Plate Thickness	µm	1	1	1	1	1	1
P-56	A Free Space	µm	10	10	10	10	10	10
P-57	A column Capacitor Thickness	µm	147.3	147.3	147.3	147.3	147.3	147.3
P-58	Substrate Thickness	µm	100	100	100	100	100	100
P-59	Charger Structure Thickness	µm	247.3	247.3	247.3	247.3	247.3	247.3
P-60	Permittivity		0	0	0	0	0	0
P-61	Relative Permittivity	NA	300	300	300	2800	2800	2800
P-62	NO. Of Capacitors Per Layer	NO	1	1	1	1	1	1
P-63	NO OF Capacitor per Column Layers	NO	10	10	10	10	10	10
P-64	NO. OF Capacitor Column (2 x 5)	NO	10	10	10	10	10	10
P-65	Capacitor Value- Top Layer	µF	0.02	0.02	0.02	0.15	0.15	0.15
P-66	Capacitor Value- Layer 1	µF	0.02	0.02	0.02	0.17	0.17	0.17
P-67	Capacitor Value- Layer 2	µF	0.02	0.02	0.02	0.22	0.22	0.22
P-68	Capacitor Value- Layer 3	µF	0.03	0.03	0.03	0.29	0.29	0.29

P-69	Capacitor Value- Layer 4	µF	0.04	0.04	0.04	0.36	0.36	0.36
P-70	Capacitor Value- Layer 5	µF	0.05	0.05	0.05	0.49	0.49	0.49
P-71	Capacitor Value- Layer 6	µF	0.08	0.08	0.08	0.73	0.73	0.73
P-72	Capacitor Value- Layer 7	µF	0.12	0.12	0.12	1.09	1.09	1.09
P-73	Capacitor Value- Layer 8	µF	0.16	0.16	0.16	1.46	1.46	1.46
P-74	Capacitor Value- Lower Layer	µF	0.23	0.23	0.23	2.19	2.19	2.19
P-75	Initial Column Capacitor Value	µF	0.77	0.77	0.77	7.15	7.15	7.15
P-76	Initial Capacitor Value	µF	7.66	7.66	7.66	71.5	71.5	71.5
P-101	Load Cl. 2- Capacitor Change Top Layer	µF	0.05	0.05	0.05	0.44	0.44	0.44
P-102	Load Cl. 2- Capacitor Change Layer 1	µF	0.05	0.05	0.05	0.5	0.5	0.5
P-103	Load Cl. 2- Capacitor Change Layer 2	µF	0.07	0.07	0.07	0.63	0.63	0.63
P-104	Load Cl. 2- Capacitor Change Layer 3	µF	0.09	0.09	0.09	0.83	0.83	0.83
P-105	Load Cl. 2- Capacitor Change Layer 4	µF	0.11	0.11	0.11	1.04	1.04	1.04
P-106	Load Cl. 2- Capacitor Change Layer 5	µF	0.16	0.16	0.16	1.45	1.45	1.45
P-107	Load Cl. 2- Capacitor Change Layer 6	µF	0.22	0.22	0.22	2.08	2.08	2.08
P-108	Load Cl. 2- Capacitor Change Layer 7	µF	0.34	0.34	0.34	3.13	3.13	3.13
P-109	Load Cl. 2- Capacitor Change Layer 8	µF	0.37	0.37	0.37	3.42	3.42	3.42
P-110	Load Cl. 2- Capacitor Change Lower	µF	0.32	0.32	0.32	3.03	3.03	3.03
P-111	Load Cl. 3-Column Capacitor Value	µF	1.77	1.77	1.77	16.55	16.55	16.55
P-112	Load Cl. 2-Total Capacitor Value	µF	17.73	17.73	17.73	165.49	165.49	165.49
P-113	Initial Voltage Source	VDC	3	5	9	3	5	9
P-114	Average Daily Traffic per lane (HHP)		27250	27250	27250	27250	27250	27250
P-117	Daily Activation -Vehicle Cl. 1 (HHP)	NO/Day	98100	98100	98100	98100	98100	98100
P-118	Max Activation Rate nodes(4 Nodes)	%	0.1	0.1	0.1	0.1	0.1	0.1
P-119	2nd Activation rate nodes (4 nodes)	%	0.07	0.07	0.07	0.07	0.07	0.07
P-120	3rd Max Activation rate nodes (2 nodes)	%	0.05	0.05	0.05	0.05	0.05	0.05
P-121	4th Max Activation rate nodes (4 nodes)	%	0.03	0.03	0.03	0.03	0.03	0.03
P-122	Other Activation Rate nodes (8 Nodes)	%	0.01	0.01	0.01	0.01	0.01	0.01
CH-01	Capacitance Default Energy	µJ	34.47	95.76	310.27	321.76	893.77	2895.81
CH-04	Activation Charge per Vehicle Cl. 2 Load	µJ	45.32	125.88	407.86	422.96	1174.89	3806.65
CH-07	Daily Charge Per Vehicle Cl. 2 Vehicle	µJ	4.40E+05	1.20E+06	4.00E+06	4.1E+06	1.20E+07	3.70E+07
CH-08	Daily Total Charge	µJ	4.40E+05	1.20E+06	4.00E+06	4.1E+06	1.20E+07	3.70E+07
CH-09	Generator Efficiency	NA	0.8	0.8	0.8	0.8	0.8	0.8
CH-10	Generator Power	µW	4.12	11.43	37.05	38.42	106.72	345.77

5.3 SPM MICRO-GENERATOR RECTIFIER AND CONTROL CIRCUIT

The rectifier and control circuit is the circuit that detects, multiplies and rectifies the generator outputs. The circuit will control this process in a manner of efficiency to respond to the input force to the system. The generating voltage may have a high range that will require a micro transformer. A micro transformer with a milivolts voltage, high efficiency, full CMOS compatibility, and area are some factors for such micro transformer designs. Section 4.2.1 described the voltage and charge constrain methods for the electrostatic generating. In a charge constrain generator, the capacitor will change with a range of 1- 100. The voltage also follows the similar changing rate[51].

A general circuit is a voltage constrains circuit. Torres and Rincón-Mora [46] presented a circuit with a control cycle for an electrostatic voltage constrain generator that we used for our proposed electrostatic voltage constrain generator shown in Fig. 5- 5. The Torres and Rincón-Mora analysis and simulation showed the efficiency of harvesting of 71.8% for their circuits. This circuit includes the following cycle:

Stage 01- Study State: There will be no vehicle activation. There is no charging at the electrostatic variable capacitor.

Stage 02- Pre-Charging: Switches S1 and S3 will be activated by the C1 control signal. The internal battery will energize the inductance L. The energizing period will be a fixed time and depends on the pre-charging required for the system. A C1 signal will be activated via a piezo sensor in a top later of the SPM that maintains a leading time required for Stages 02 and 03. Switches S2, S4, and S5 are open in this Stage. The pre-charging will have a time constant of $\tau =$

[51] : q=C x V

L/ R_{LOSS}. R_{LOSS} is the inductance resistance that attempts to be low for losing the energy in the pre-charging stage. The inductance current will be:

$$\boldsymbol{I_L = \frac{V_i}{R_{LOSS}} \times \left(1 - e^{\frac{-t \times R_{LOSS}}{L}}\right)} \quad \text{Eq. 5- 1}$$

The approximate amount of pre-charging energy can be estimated with:

$$\boldsymbol{E = \frac{1}{2} \times C_{MAX} \times V_i^{\,2} = \frac{1}{2} \times L \times I_L^{\,2}} \quad \text{Eq. 5- 2}$$

Based on the pre-charging period time, current and inductance parameters can be verified for the implementation.

Stage 03- Charging: Switches S2 and S4 will be activated by the C2 control signal. The electrostatic capacitor will be charged. The C2 signal is a delay signal from C1. The variable capacitance will be in a maximum value as the force has not activated the variable capacitor. Switches S1, S3, and S5 are open in this stage.

Stage 04- Discharging: Switch S5 will be activated by the C3 control signal. During this stage, the voltage of the electrostatic capacitor will approximately be constant because we assume the battery's impedance will be very small. Therefore, reducing the capacitance by mechanical force generates the current charging to the battery as:

$$\boldsymbol{I_{CHARGING} = \frac{d(VC)}{dt} \cong V_i \times \frac{d(C)}{dt} \cong \frac{V_i \times (C_{MAX} - C_{MIN})}{\Delta T}} \quad \text{Eq. 5- 3}$$

Stage 05- Reverse: Reverse action of Stage 3 discharges the capacitor and energizes the inductance. Switches S2 and S4 will be activated by the C4 control signal. The electrostatic capacitor will be discharged. The C4 signal will be activated at an edge point when the tire passes the touch point. The variable capacitance will reach its minimum gap and maximum value.

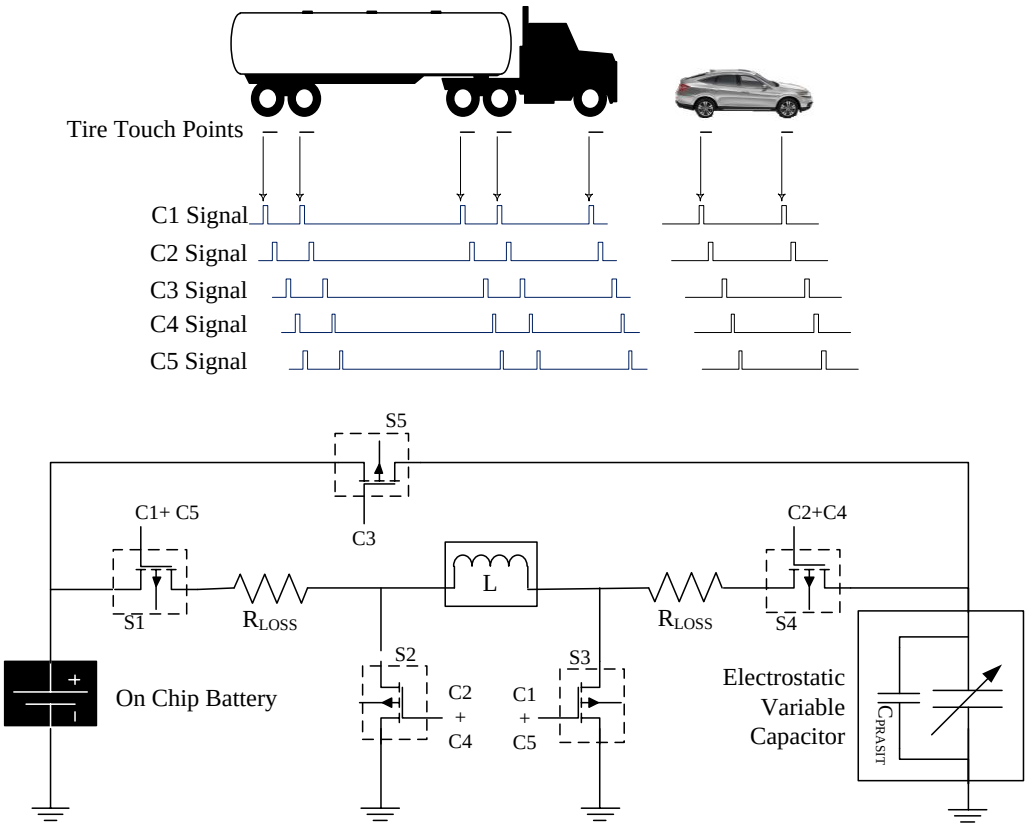

Fig. 5- 5 SPM Electrostatic Micro Generator Control Circuit (Adapted from 46)

Stage 06- Recovery: By activating the circuit path via S1 and S3, the inductor energy will be returned to the battery.

5.4 PAVEMENT ON-CHIP MICRO GENERATOR LAYOUT AND FBRICATION DESIGN

The micro-generator fabrication process shall be compatible with IC fabrication. The proposed SPM nodes, with a complete set of micro generators and core modules, will be non-planar, 3D devices. Fabrication of non-planar devices uses the same methods as fabrication of planar devices, but the processing of vertical surfaces and/or deep etched features are emphasized in 3D device processing. In an SPM fabrication process, with the addition of a non-planar device process, we also require a 3D packaging process. The 3D packaging will be constructed with connections and bonding processes between core modules and micro generator modules. A

layout of such packaging was shown in Fig. 5- 1. Before describing the layout and details of the micro-generator module, a short description of how the fabrication process works and some non-customary processes are referenced.

5.4.1 FABRICATION PROCESS

The fabrication process for the micro-generator is a similar process used in MEMS construction. The micro-generator is built on standard silicon wafers. A unit or array module of the micro generator will be built on the wafer with a photographic-like process.

Deposition process: The basic building block in the SPM micro-generator processing is the ability to deposit thin films of material. The thickness of the film will be in size from submicron to hundreds of micron. Several chemical and physical deposition reaction processes can be used for the SPM implementation. These processes are:

- Chemical Vapor Deposition (CVD): In this process, the substrate is placed inside a reactor to which a number of gases are supplied and chemical reaction will take place and solid material will deposit onto the substrata surface. Two CVD technologies are: (a) Low Pressure CVD (LPCVD) with excellent uniformity but requiring high temperature processing with a slow deposition rate and (b) Plasma Enhanced CVD (PECVD) with lower processing temperature but with lower layer quality. Consideration for this method application on SPM is a problem for piezo material (PZT) because hazardous by-products form during the process.
- Electro-Deposition or Electroplating: Typically this is restricted to electrically conductive materials. Two Electro-Deposition technologies for plating are (a) Electroplating and (b) Electro-less plating. The electro-deposition process is well suited to make films of metals

with any thickness from ~1µm to greater than 100µm. Therefore, it is not the primary choice for the SPM metal layer deposition where a sub-micron thickness layer is proposed. It will be applicable in the SPM prototype cases where higher thickness is desirable. In the electro-deposition process, the surface of the substrate must have an electrically conducted coating before the deposition can be done.

- Epitaxy: This technology is quite similar to what happens in CVD processes, however, if the substrate is an ordered semiconductor crystal (i.e. silicon, gallium arsenide), it is possible with this process to continue building on the substrate with the same crystallographic orientation with the substrate acting as a seed for the deposition. If an amorphous/polycrystalline substrate surface is used, the film will also be amorphous or polycrystalline. In the case of growing a piezo material over the silicon substrate, the orientation of the piezo layer and the mode of the operation of the piezo layer (d31, d33) can be controlled.
- Physical Vapor Deposition (PVD): This method comprises the standard technologies for deposition of metals. It is far more common than CVD for metals since it can be performed at a lower process risk and is at a less expensive cost for materials. But, the qualities of the films are inferior to CVD and additionally, its step coverage is also not as good as CVD. Two PVD technologies are (a) Evaporation, which includes e-beam and resistive heating methods and (b) Sputtering.

Lithography process: Lithography for an SPM fabrication is the typical lithography used in an integrated circuit design. Its context is typically the transference of a pattern to a photosensitive material by selective exposure to a radiation source such as light. Lithography is the principal mechanism for pattern definition in micromachining. Photosensitive compounds are primarily

organic and do not encompass the spectrum of material properties of interest to micro-machinists. Lithography is the first stage of the pattern definition in semiconductor fabrication. The second part of the pattern definition is the etching process. Optical lithography is the most common process which uses UV light. Non-optical lithography uses electron beam (EBL) or X-ray radiation. Optical lithography will be used for the SPM micro-generator process.

Etching process: Etching is a subtractive process during which desired material is removed from the surface of the wafer. This etching can be implemented either in the liquid-phase (wet etching) or in the gas-phase (dry etching). Wet etching is a simple process but has some issues including not dissolving the mask or the different etching rates in different crystal directions. Three different dry etching technologies are reactive ion etching (RIE), sputter etching, and vapor phase etching. Dry etching will be a more expensive process and based on the minimum size of the SPM micro-generator structure, it may not be considered as the primary process for etching.

Wire bonding process: Chip-to-substrate interconnections provide the electrical paths for power and signal distribution. The most common interconnect technology is wire bonding for low density of the connection. A special method for wire bonding is ball bonding. In our SPM design, the interconnection between core module and some micro-generators will be a wire bonding method (see Fig. 5- 1). In our proposed design, the contact pad is sized at 50 x 50 μm and 100 x 100 μm [47].

Through Silicon Vias (TSV) process: TSV is an important developing technology that utilizes short vertical interconnections or “vias” that pass through a silicon wafer in order to achieve greater space efficiencies and higher interconnecting densities. A simple TSV process for interconnection between layers of micro-generators is proposed. This will simplify the overall

process of the micro-generator. Two TSV technologies are Mid-End-of-Line (MEOL) or Back-End-of-Line (BEOL) assembly processes. Using TSV shall be considered for a large production of an SPM node with service from TSV assembly service manufacturing [48].

Flip chip process: Flip Chip assembly is the direct electrical connection of face-down (flipped) electronic die onto organic or ceramic circuit boards by means of generating conductive bumps on the chip bond pads. This process is quickly gaining popularity over traditional face-up wire bonding due to its advantages in circuit board real-estate reductions, performance, reliability, density of the connections, and cost over other packaging methods[49].

5.4.2 SPM MICRO-GENERATOR PROTOTYPE LAYOUT DESIGN

The layout design of an SPM multilayer electrostatic micro-generator is shown in Fig. 5- 6 to Fig. 5- 21. These figures show the process of lithography, etching, deposition, and vias processes. Additional standard processes such as cleaning are not specified and will be determined based on the manufacturing facility. The generator mask patterns are specified in Fig. 5- 22 to Fig. 5- 26. This design includes additional piezo layers which are designated as sensors and also for testing proposes. This design is proposed for the prototype micro-generator case. This prototype layout is designed for performance testing of the embedded micro-generator in a test bed. This prototype has:

- Three electrostatic capacitors layers and two piezo sensor layers
- Unidirectional generator packaging (see Fig. 4- 25 Examples of SPM modules placements)
- Vias used for connections of the layers
- A total of nine masks designed for this layout

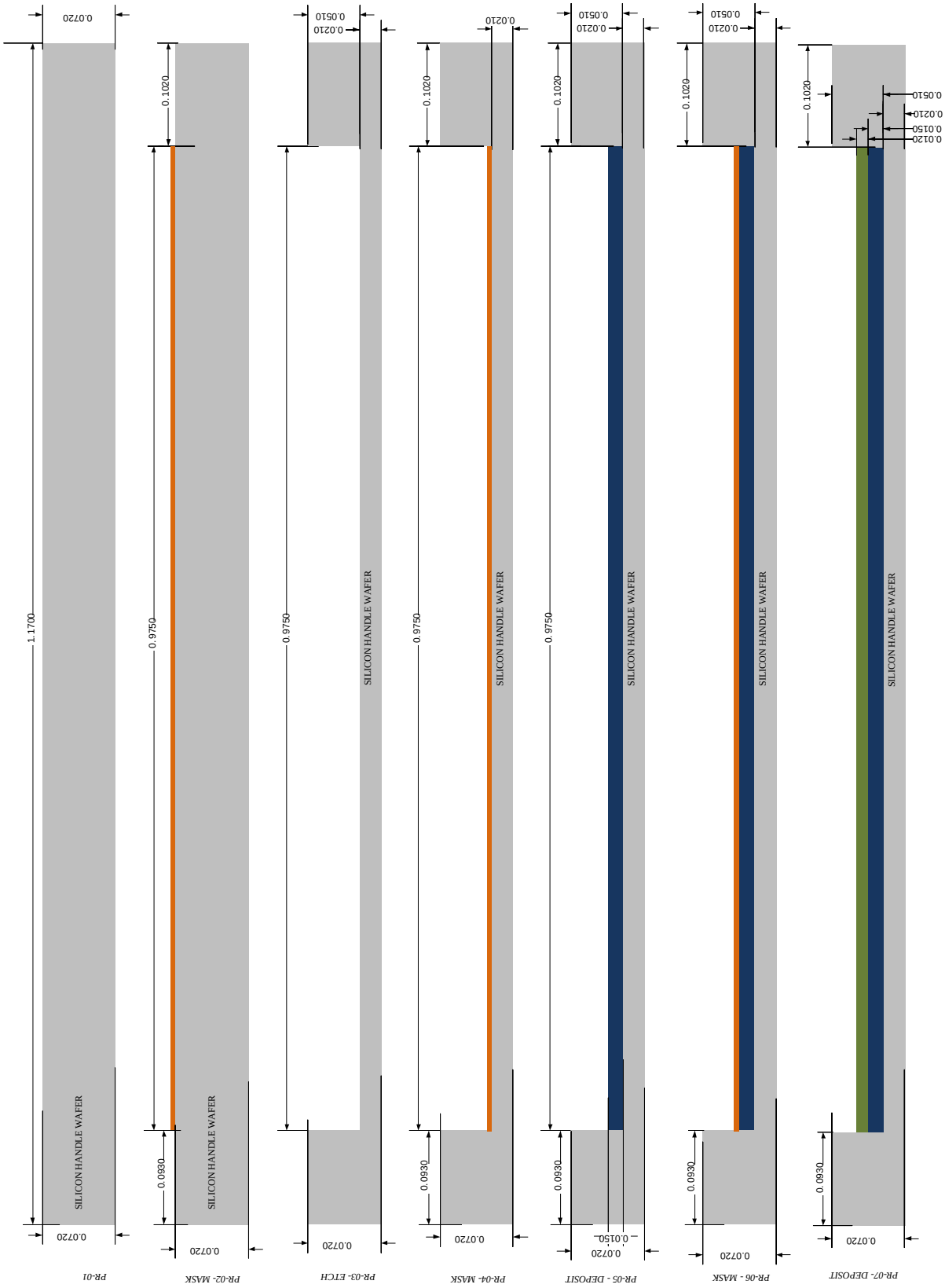

Fig. 5- 6 SPM micro generator prototype fabrication process layout 1

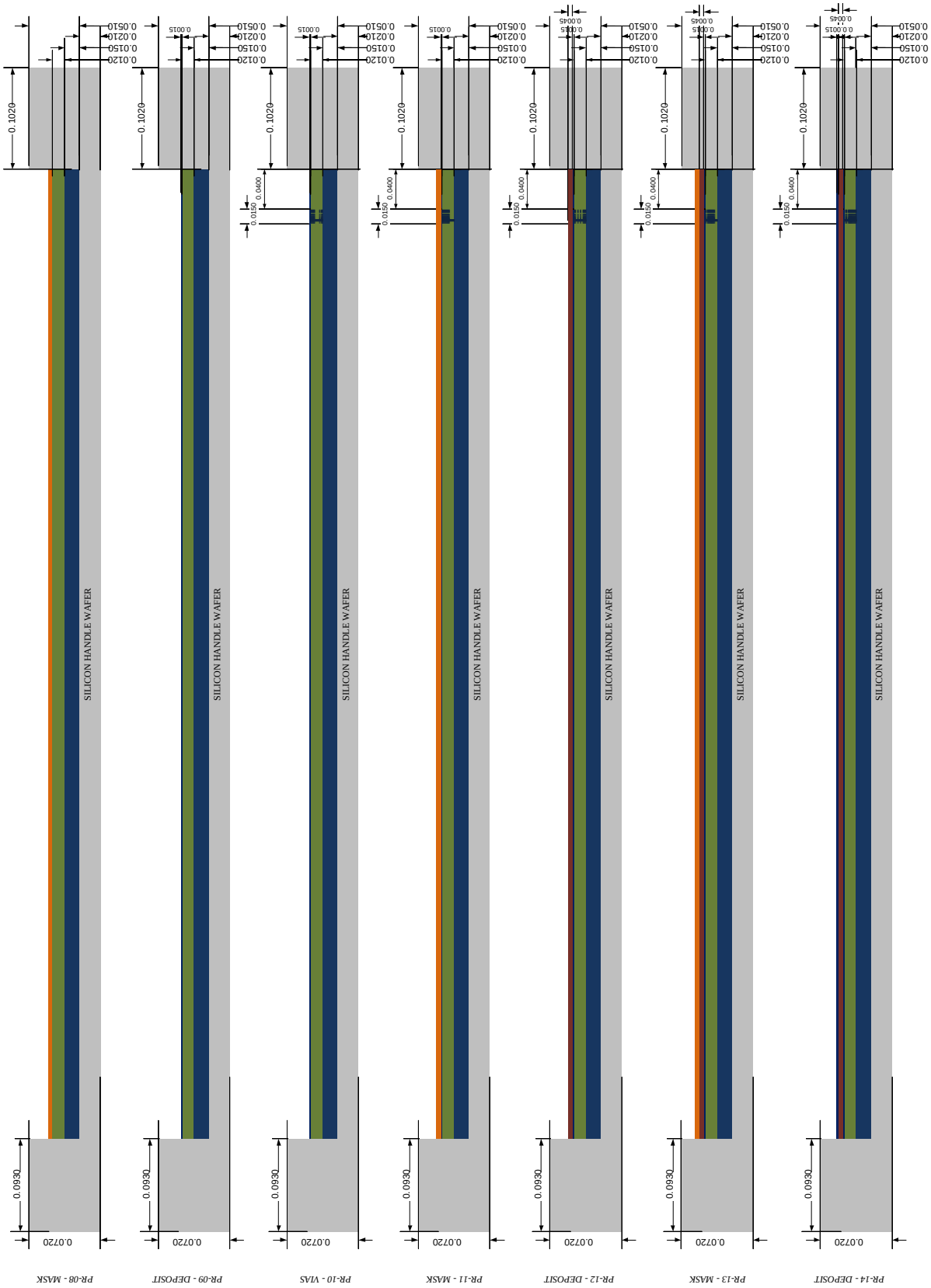

Fig. 5- 7 SPM micro generator prototype fabrication process layout 2

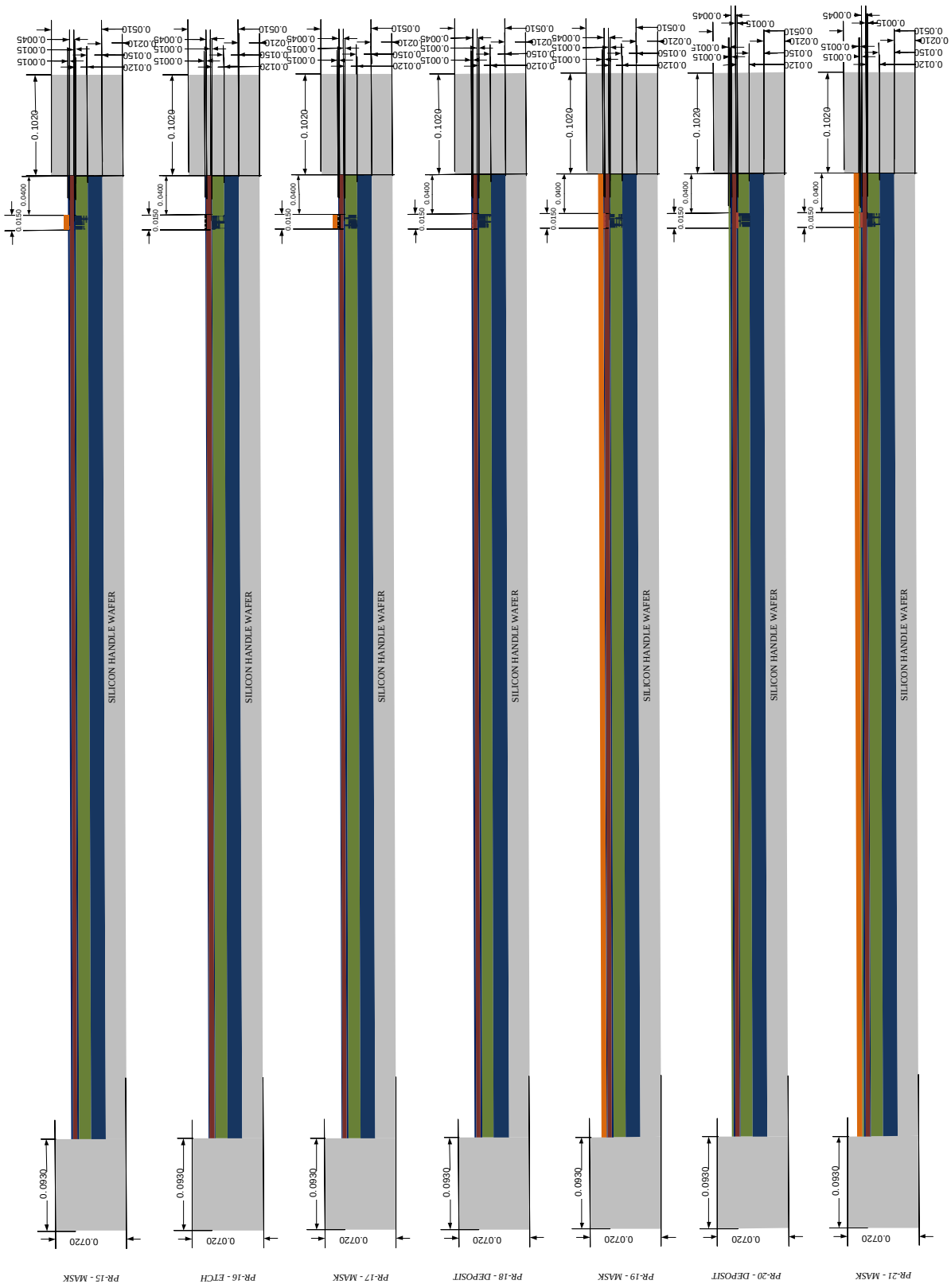

Fig. 5- 8 SPM micro generator prototype fabrication process layout 3

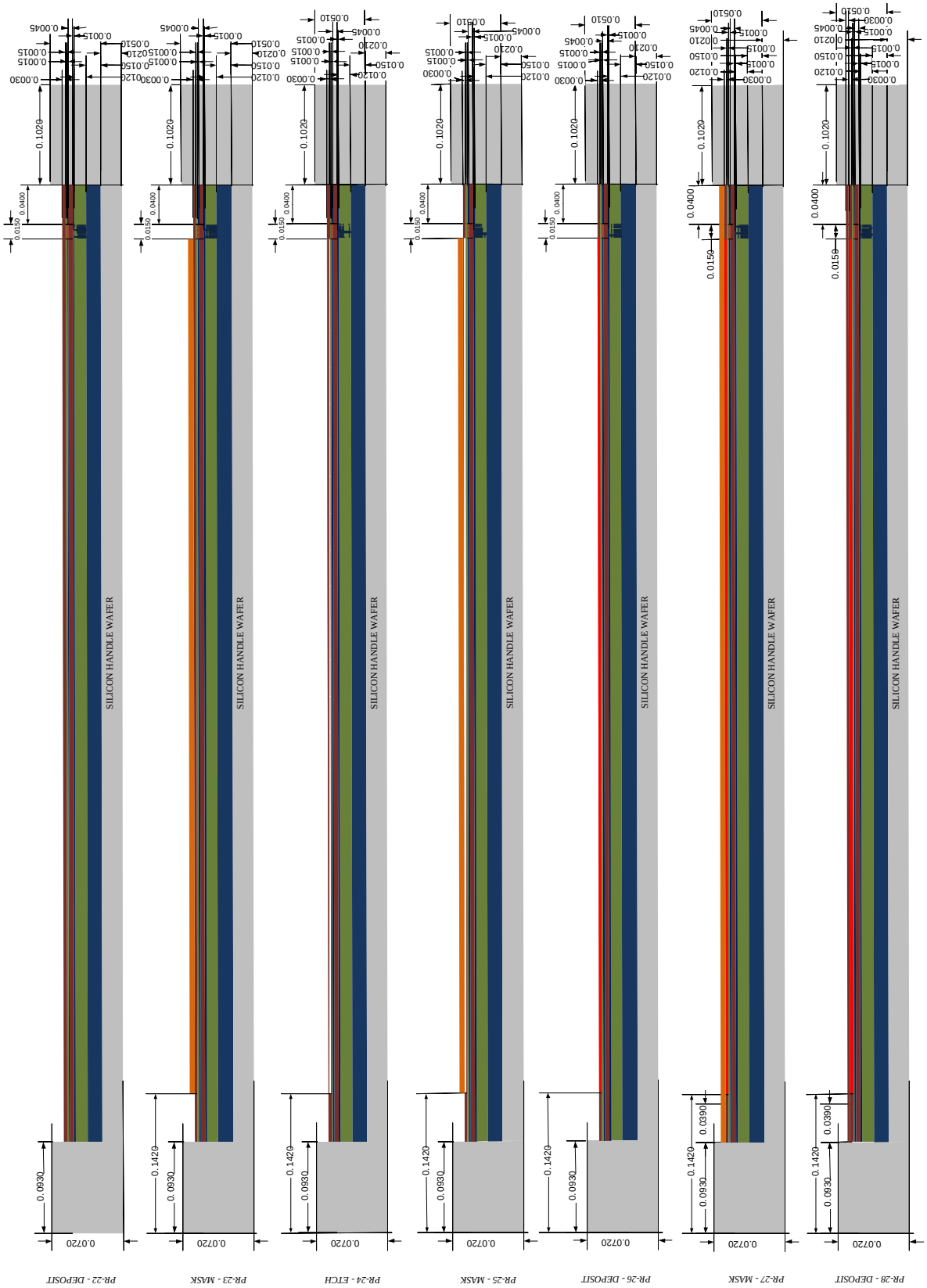

Fig. 5- 9 SPM micro generator prototype fabrication process layout 4

Fig. 5- 10 SPM micro generator prototype fabrication process layout 5

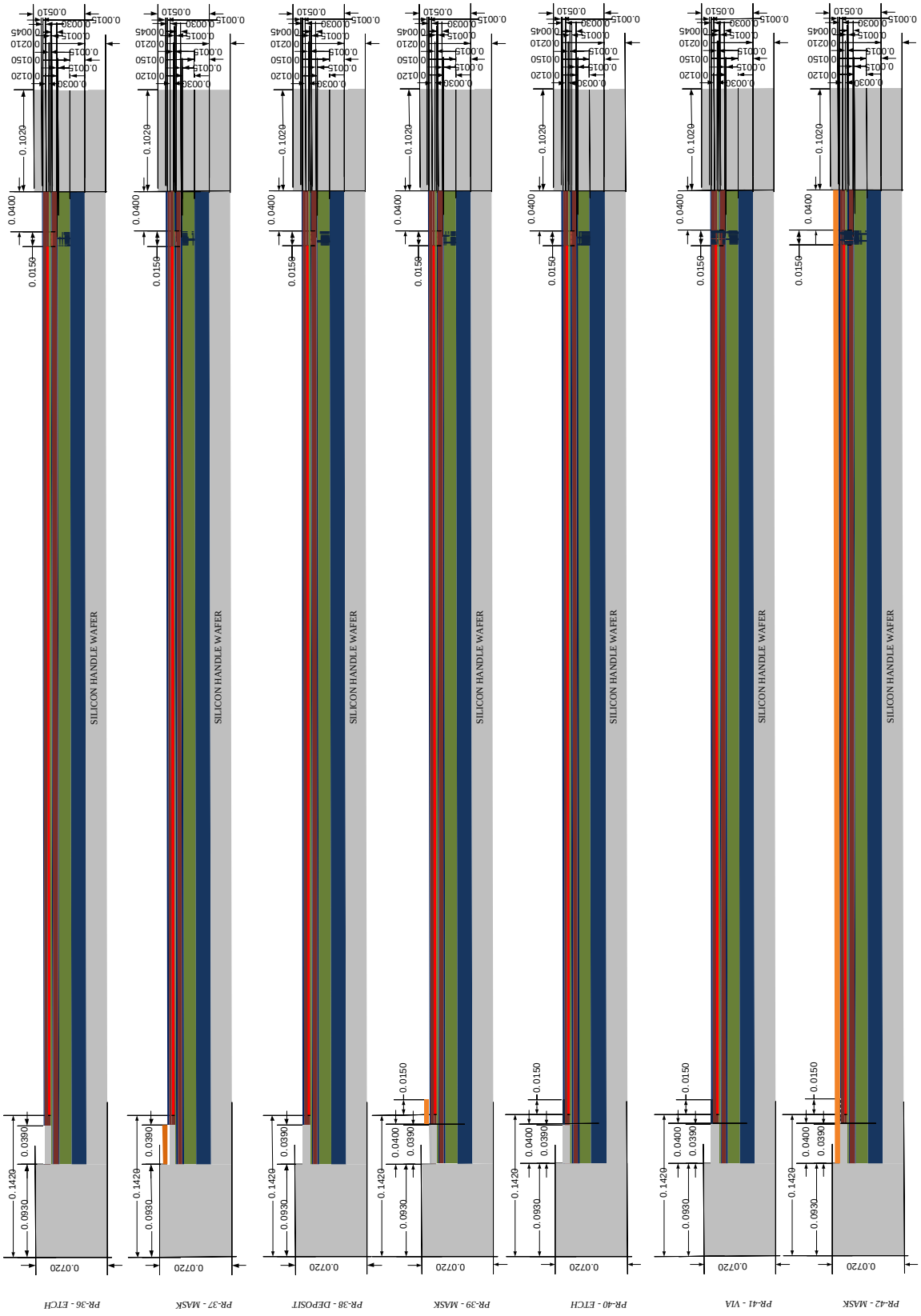

Fig. 5- 11 SPM micro generator prototype fabrication process layout 6

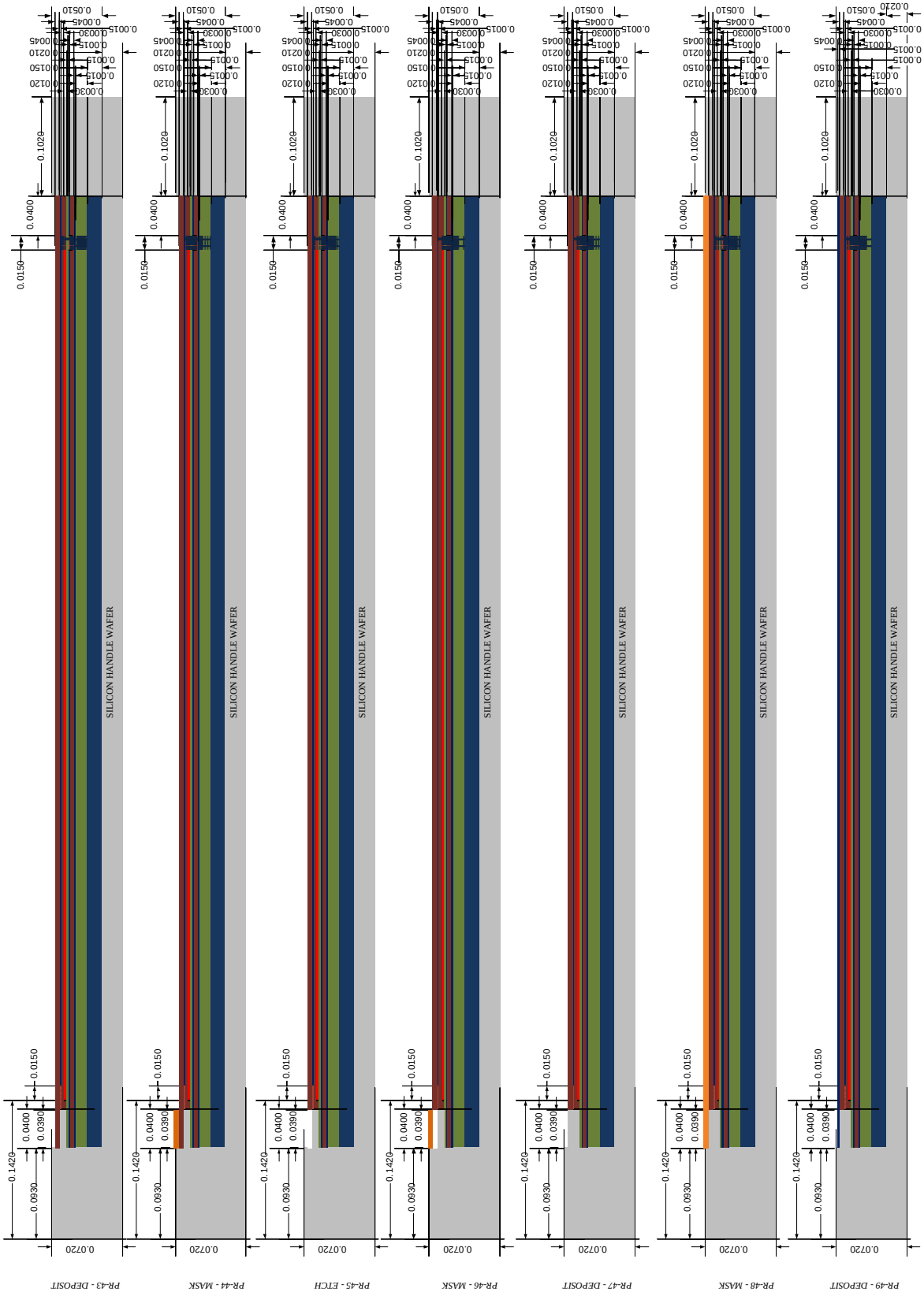

Fig. 5- 12 SPM micro generator prototype fabrication process layout 7

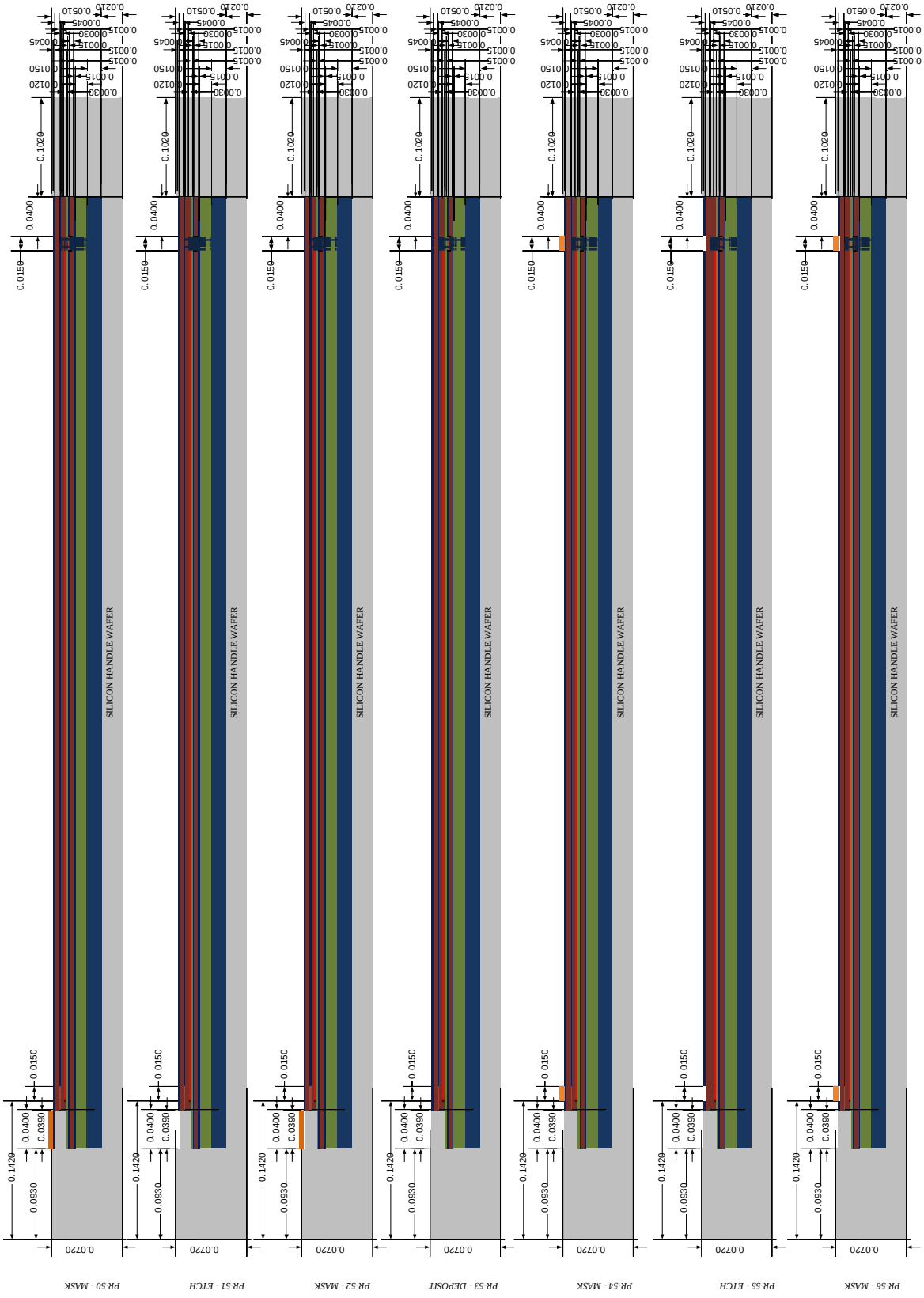

Fig. 5- 13 SPM micro generator prototype fabrication process layout 8

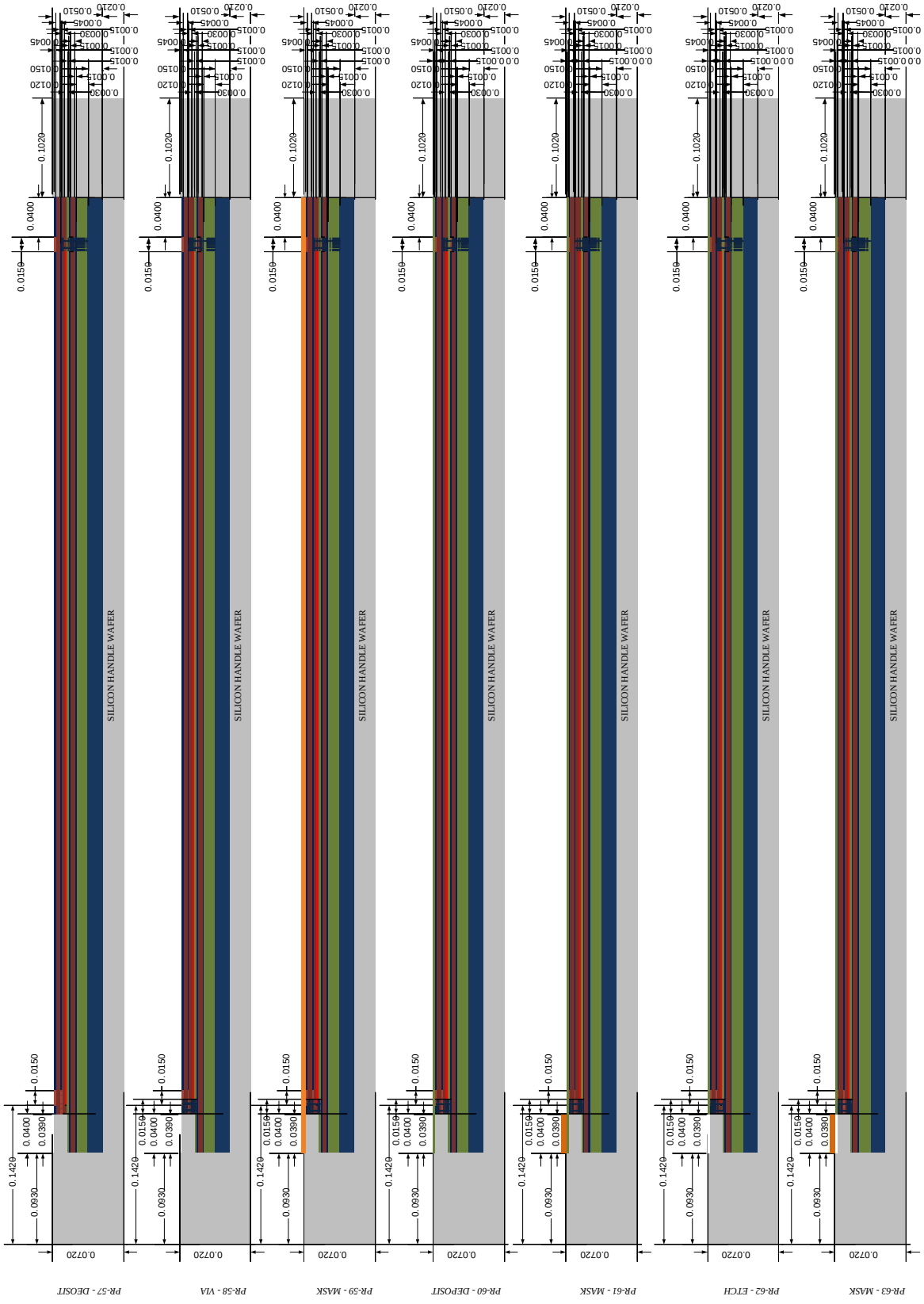

Fig. 5- 14 SPM micro generator prototype fabrication process layout 9

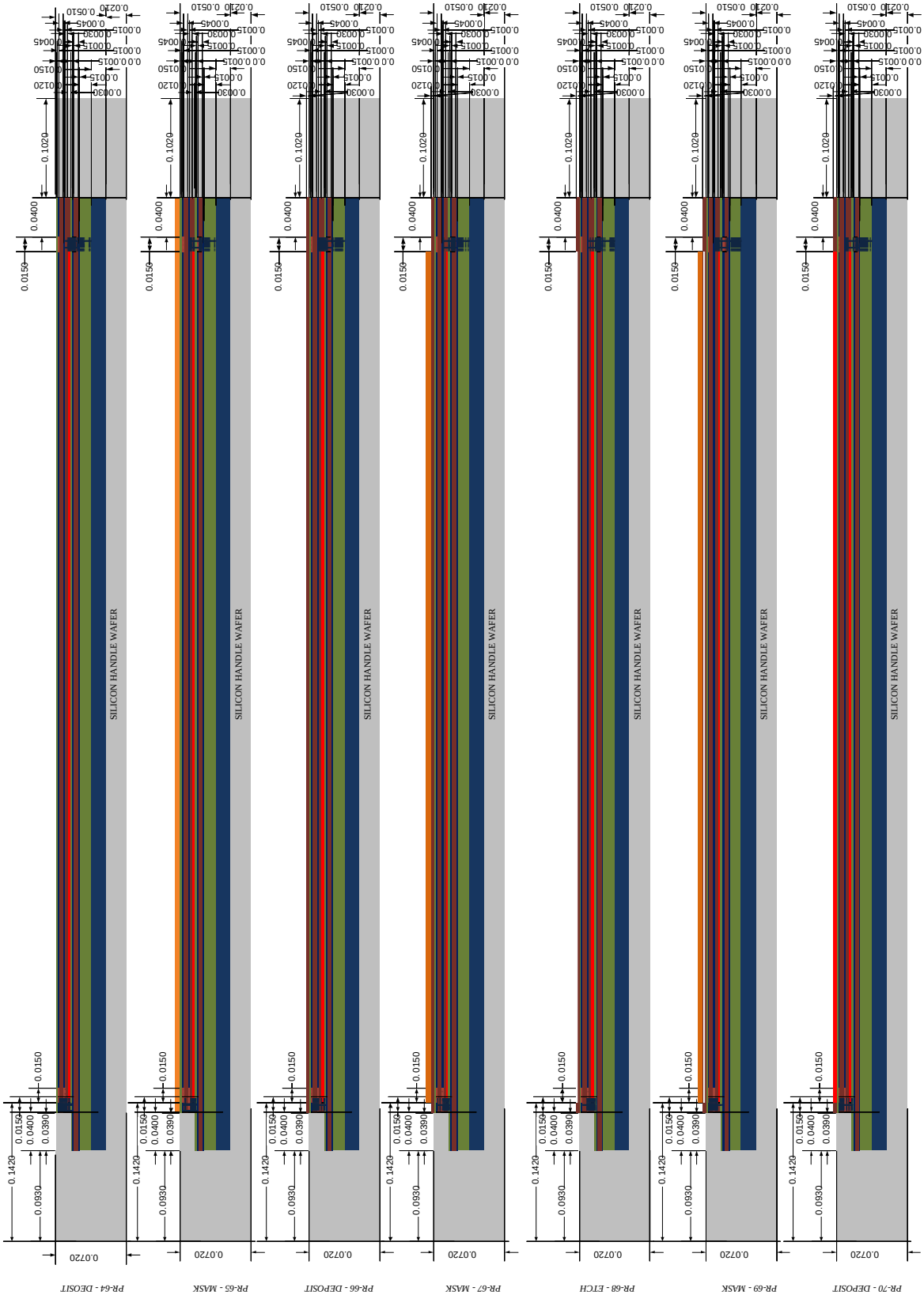

Fig. 5- 15 SPM micro generator prototype fabrication process layout 10

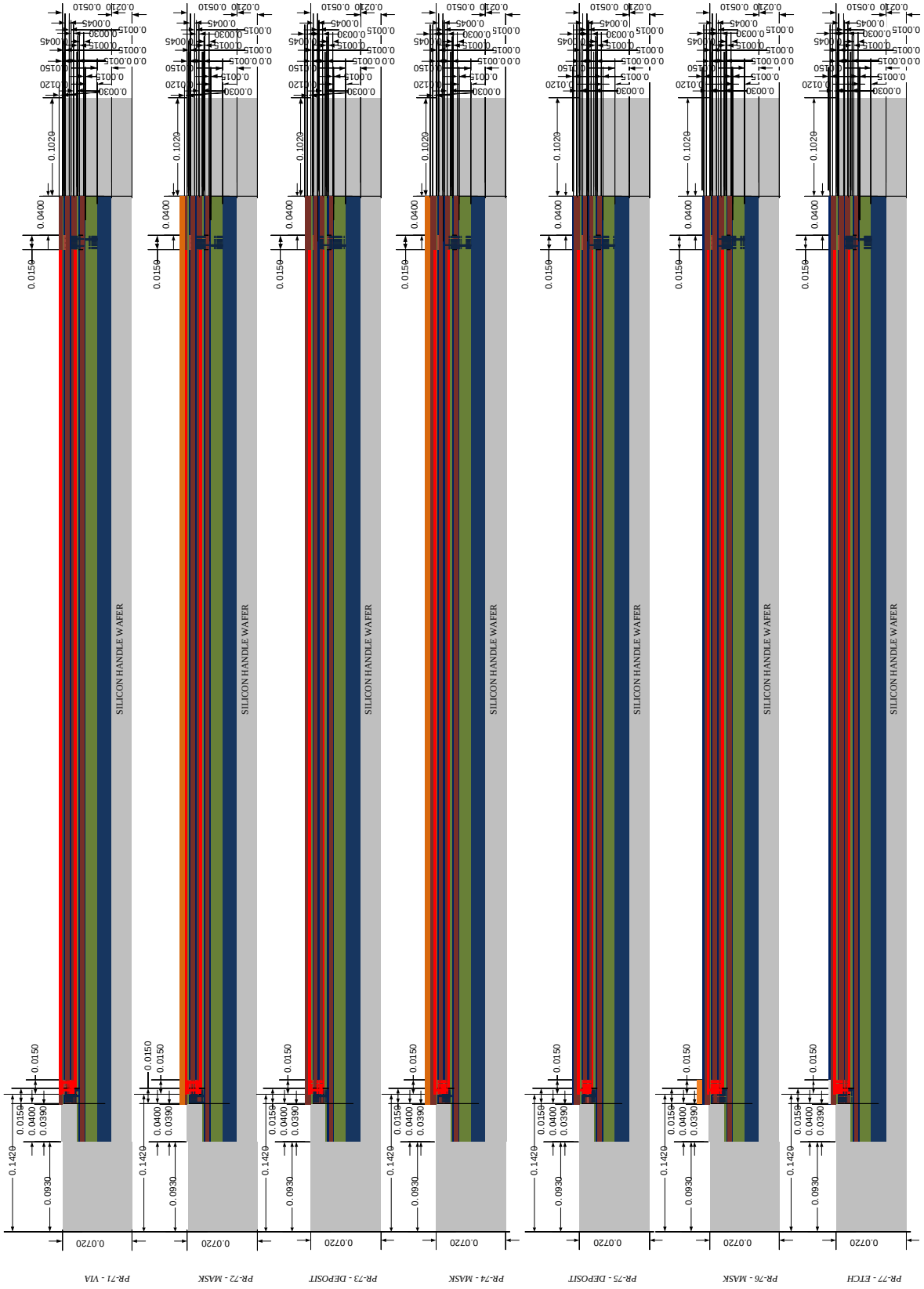

Fig. 5- 16 SPM micro generator prototype fabrication process layout 11

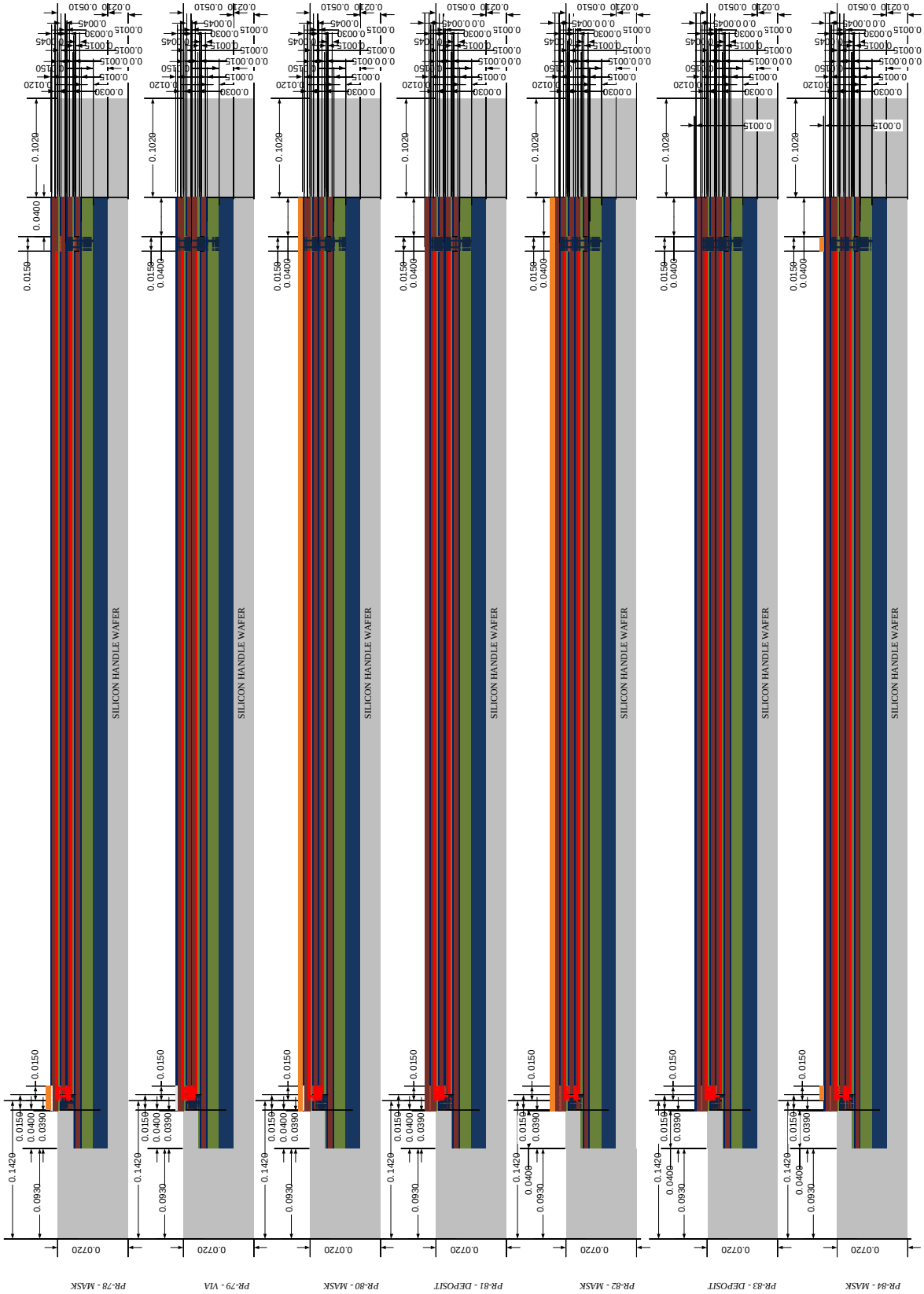

Fig. 5- 17 SPM micro generator prototype fabrication process layout 12

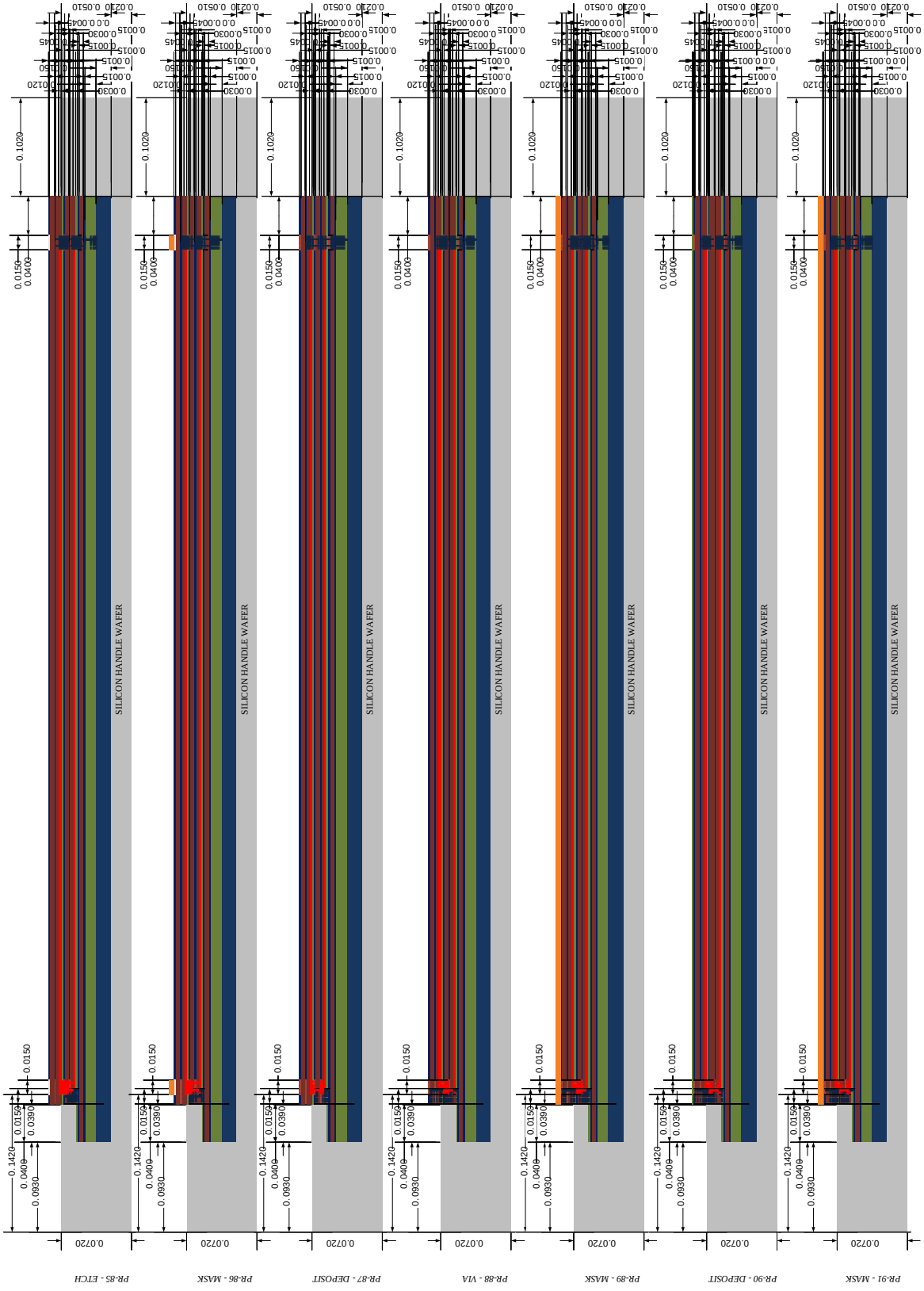

Fig. 5- 18 SPM micro generator prototype fabrication process layout 13

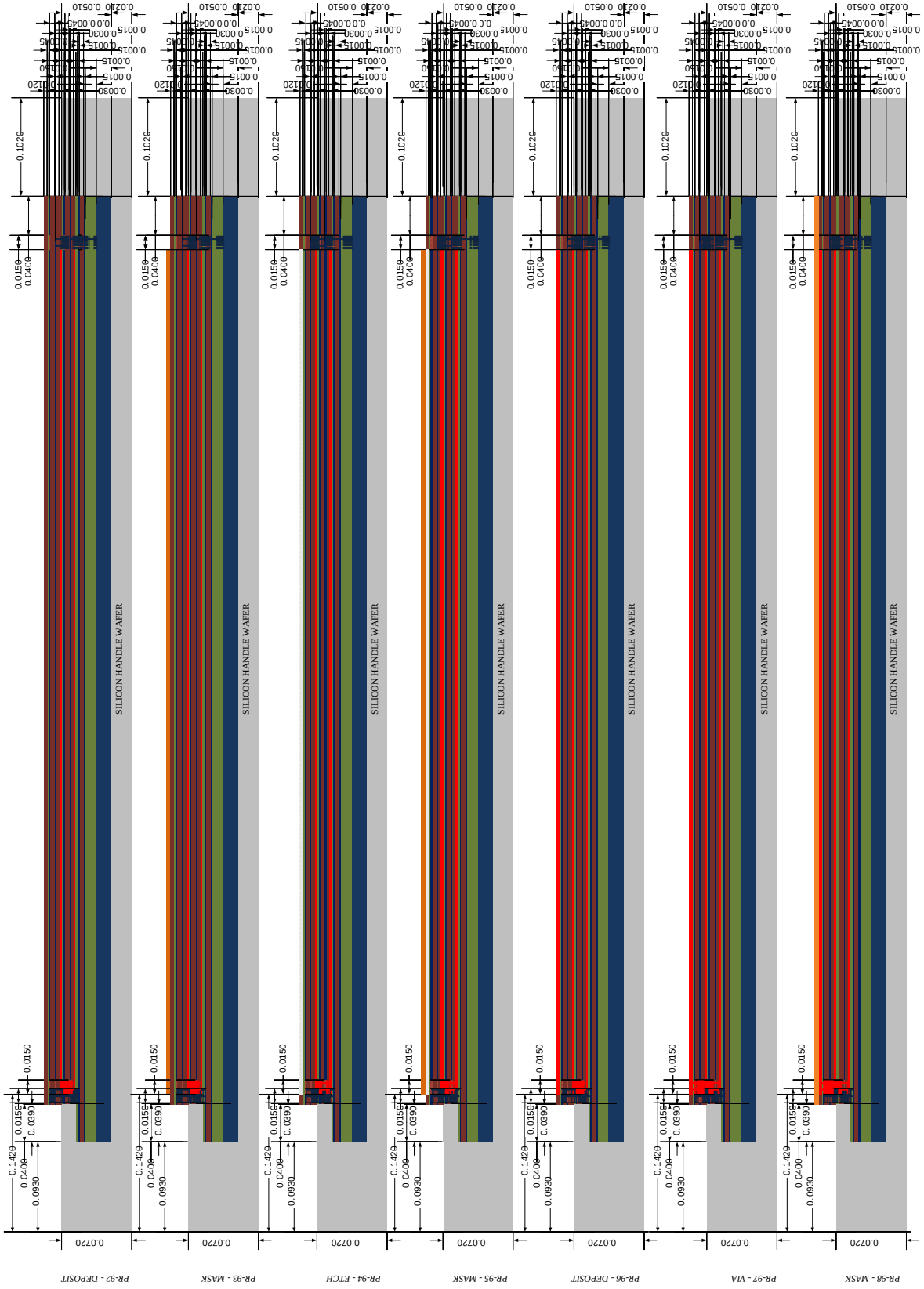

Fig. 5- 19 SPM micro generator prototype fabrication process layout 14

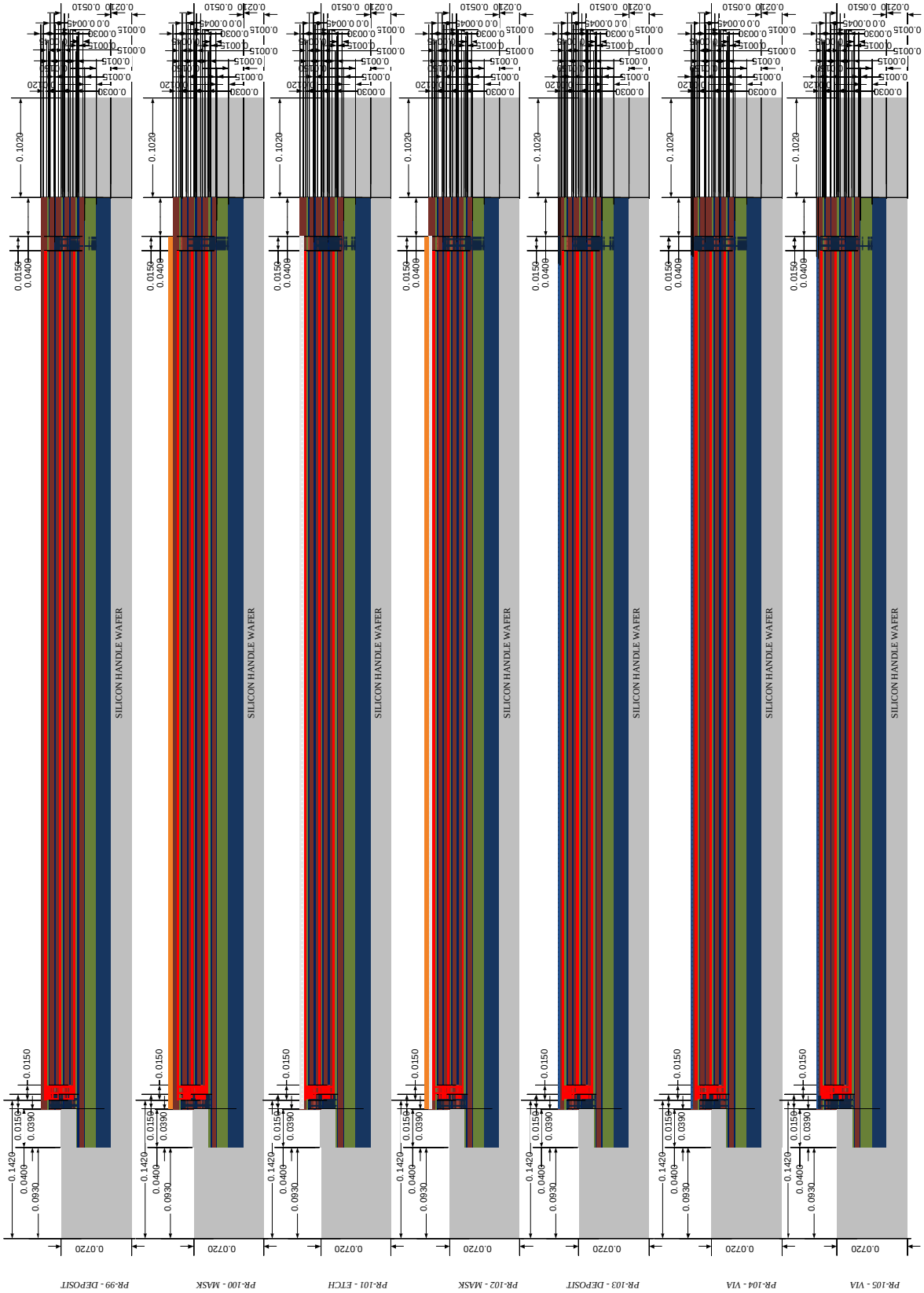

Fig. 5- 20 SPM micro generator prototype fabrication process layout 15

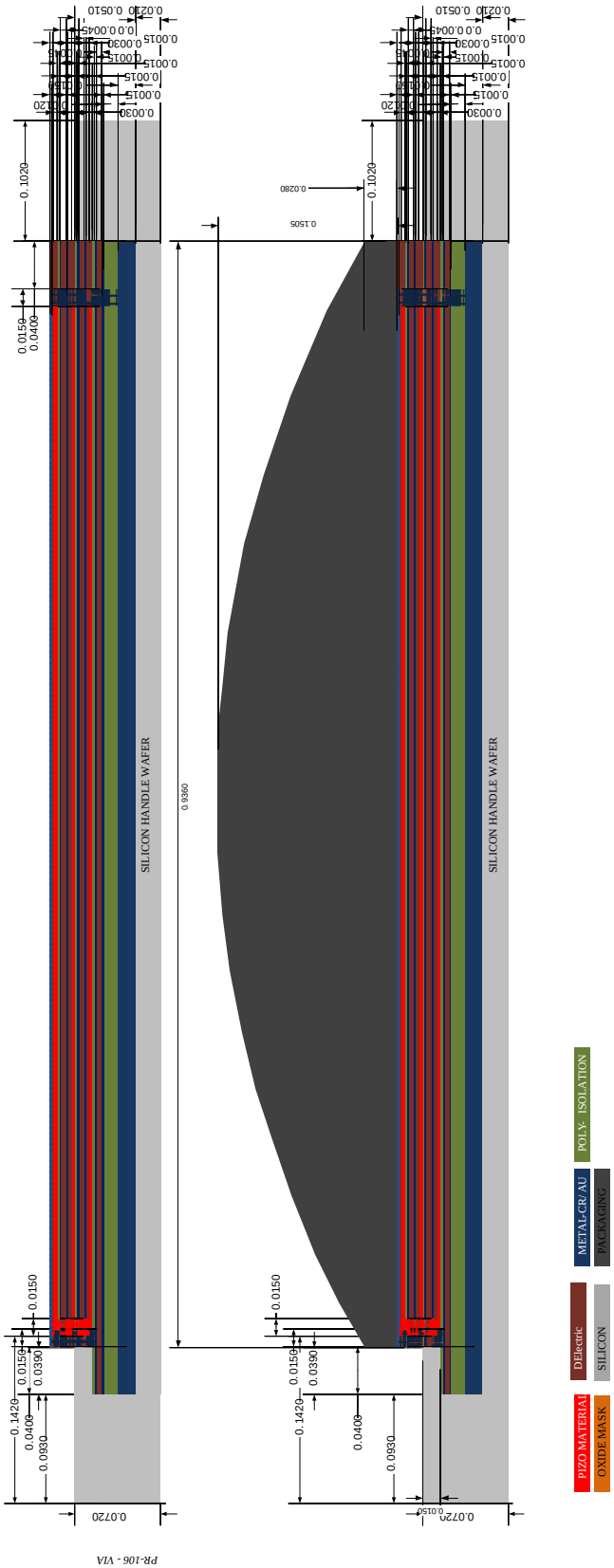

Fig. 5- 21 SPM micro generator prototype fabrication process layout 16

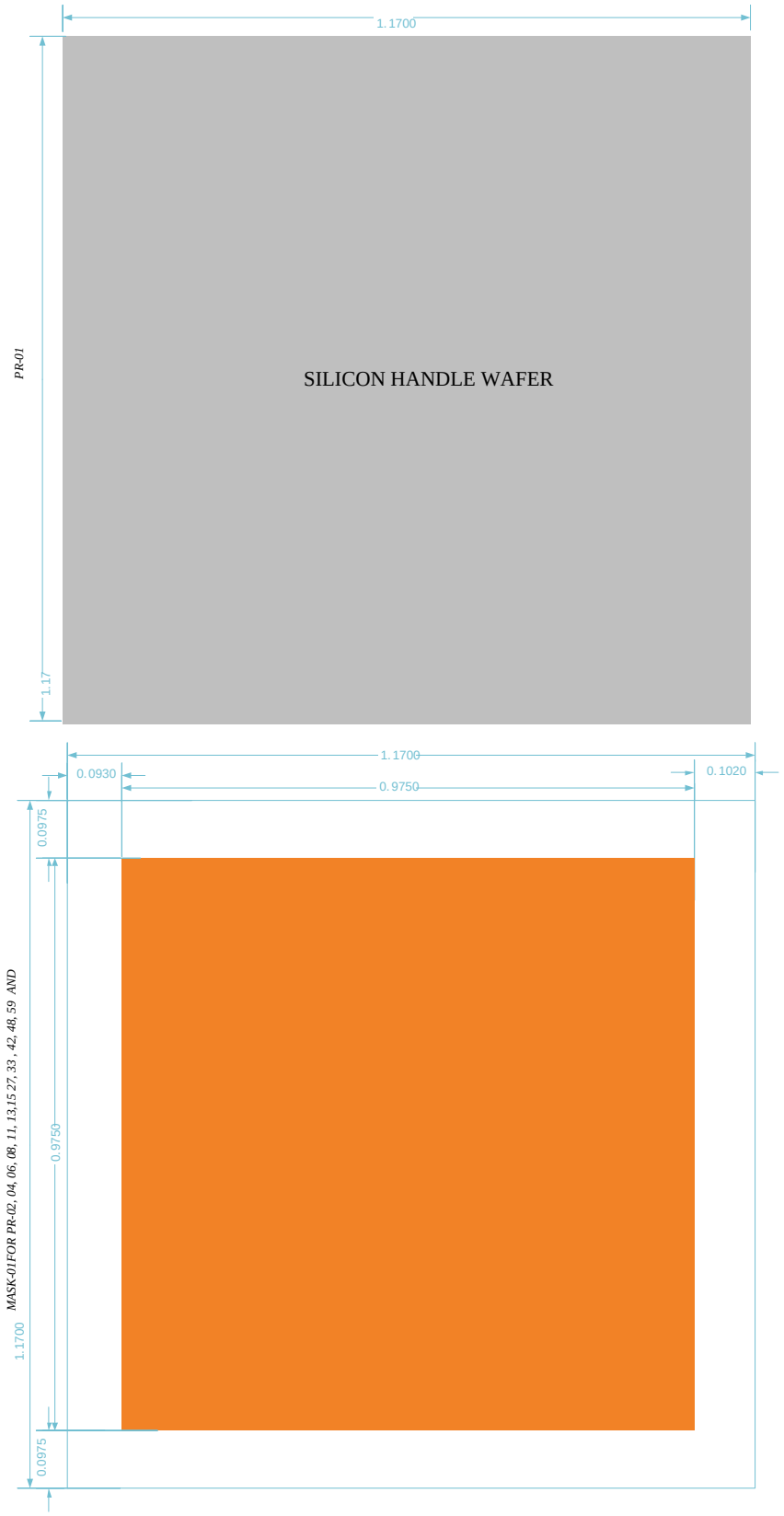

Fig. 5- 22 SPM micro generator prototype fabrication Masks plan 1

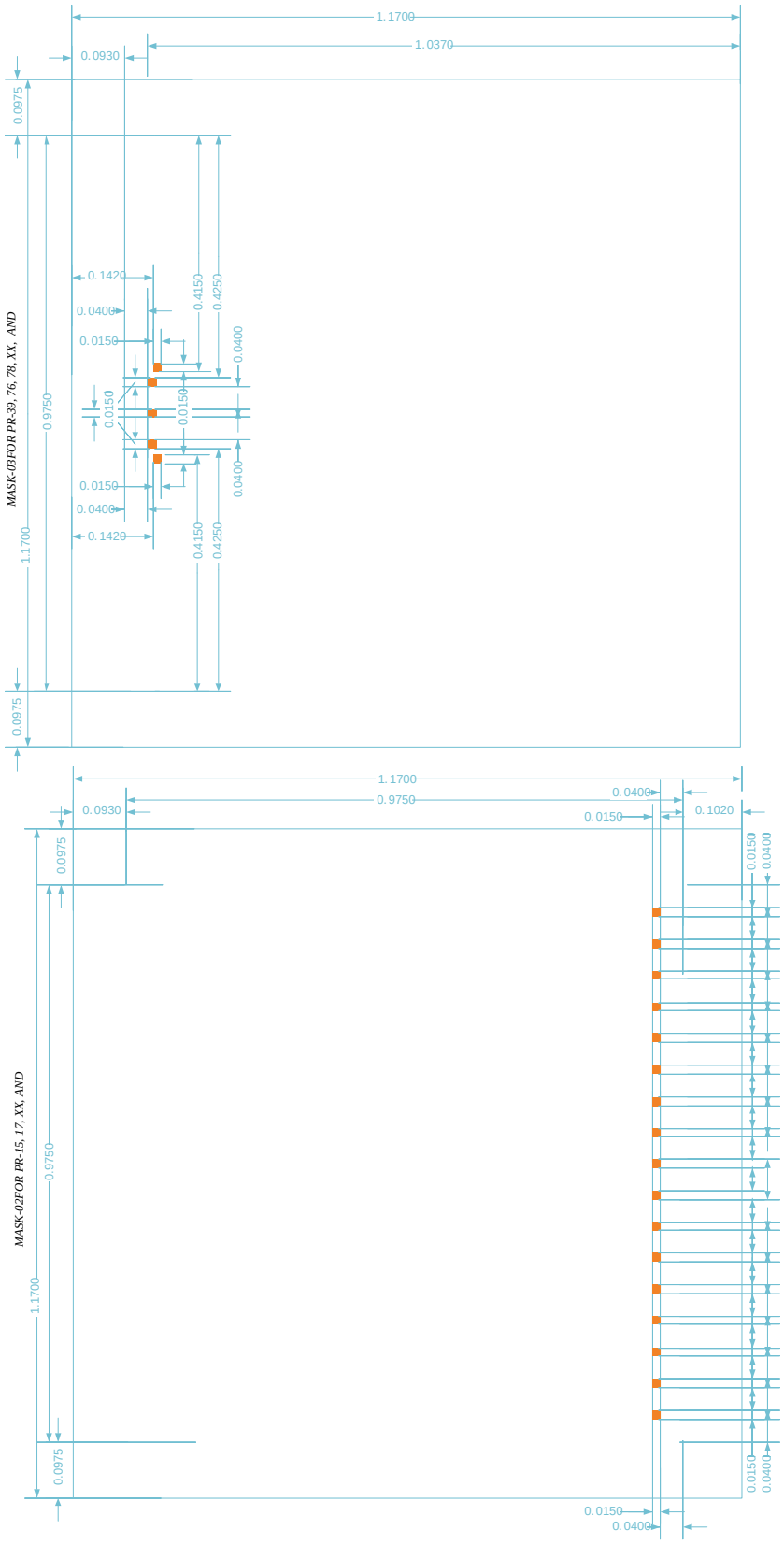

Fig. 5- 23 SPM micro generator prototype fabrication Masks plan 2

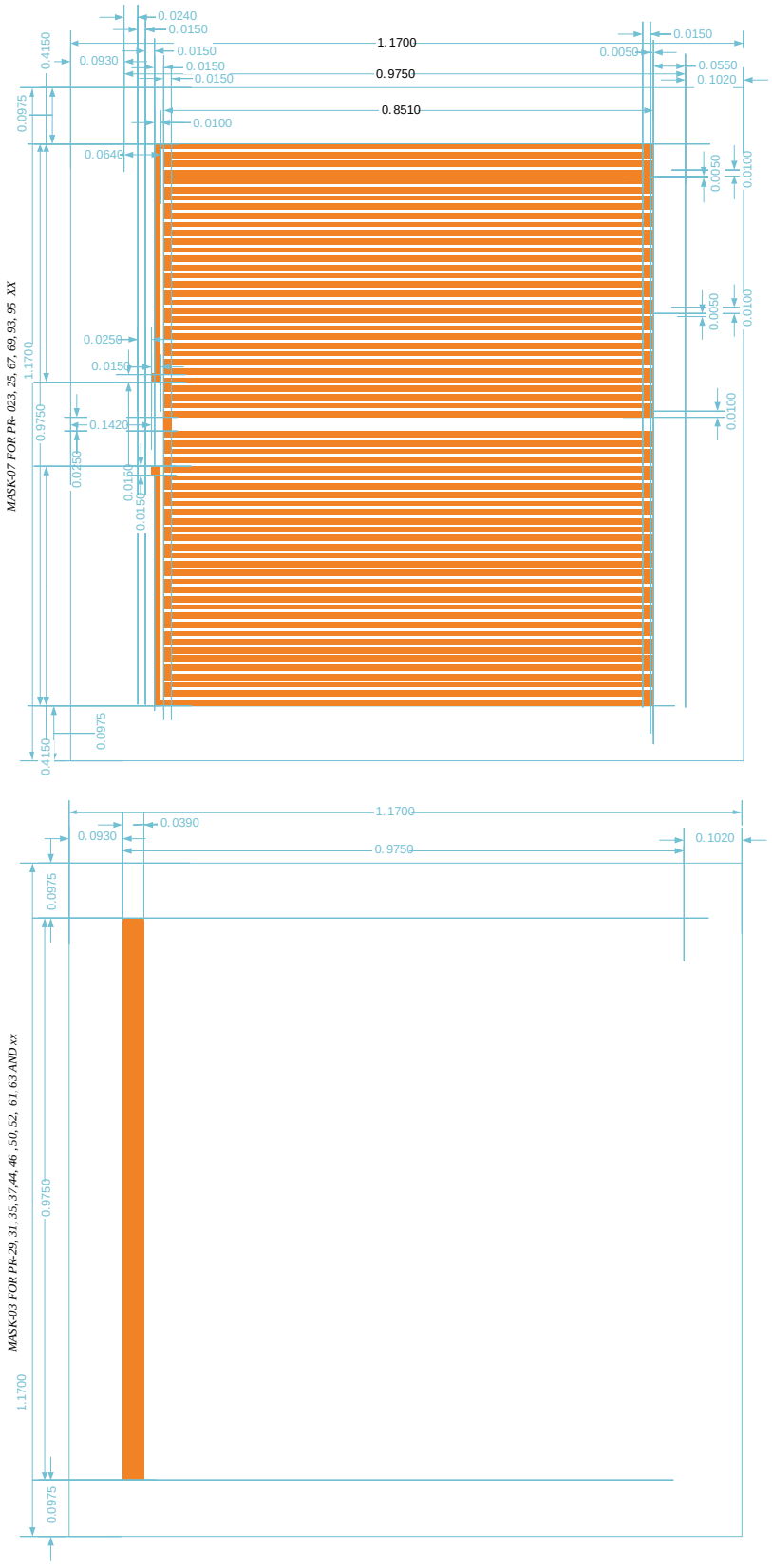

Fig. 5- 24 SPM micro generator prototype fabrication Masks plan 3

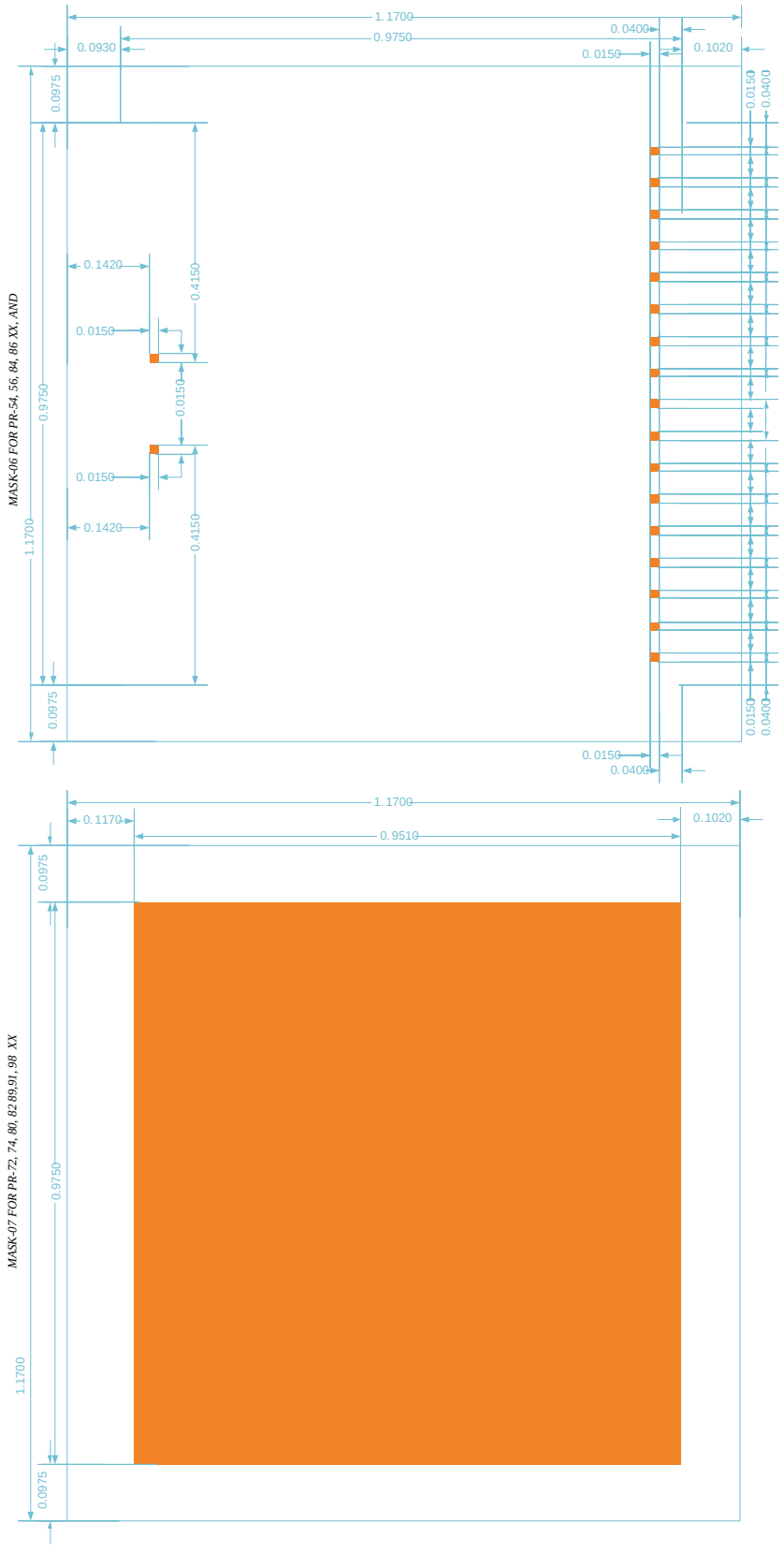

Fig. 5- 25 SPM micro generator prototype fabrication Masks plan 4

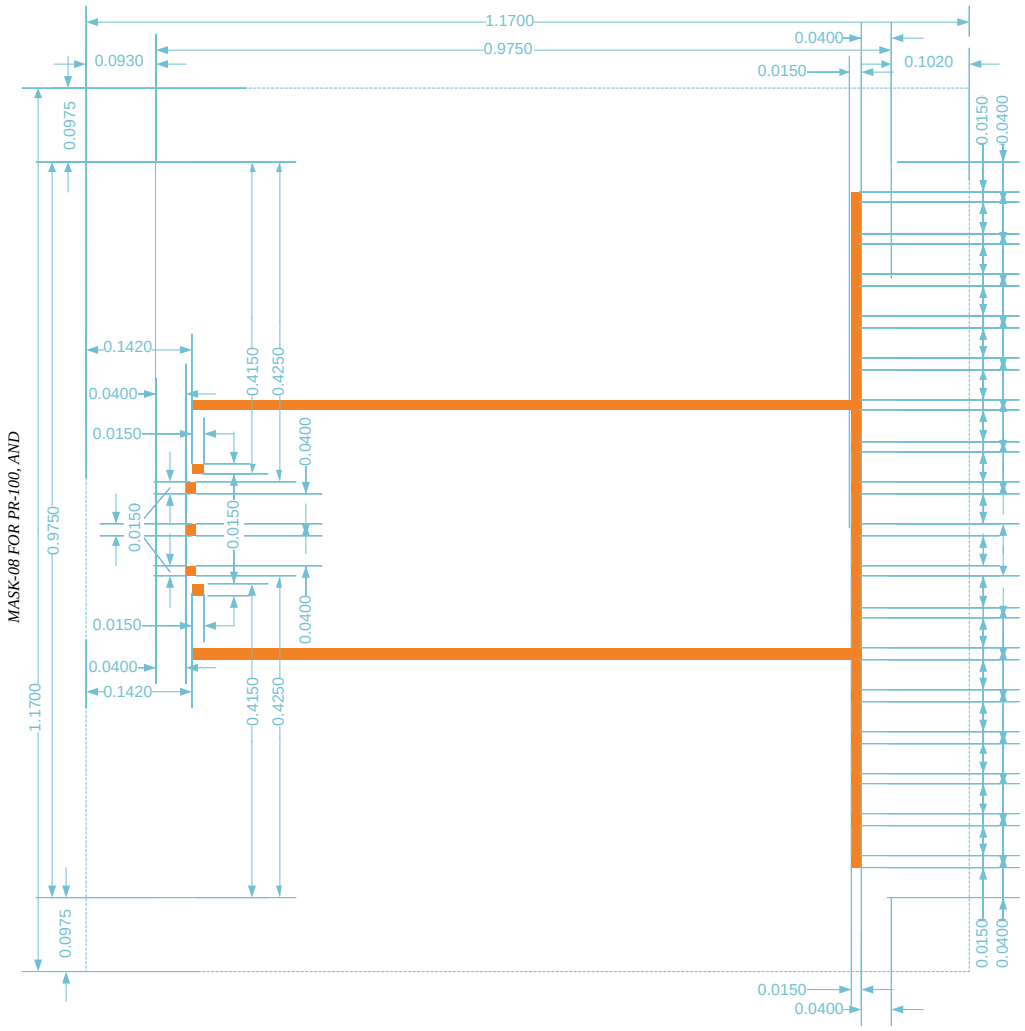

Fig. 5- 26 SPM micro generator prototype fabrication Masks plan 5

CHAPTER 6 CONCLUSION

6-1 SMART PAVEMENT MATERIAL (SPM)

Intelligent transportation systems (ITS) are a collection of technologies on transportation systems for improving the system efficiency and safety. Smart Pavement Material (SPM) is proposed as a new ITS system for the highway network. SPM is an embedded element on the roadway with sensing, processing, wireless communication and micro power generator capabilities. This research covers the feasibility, conception, and design of the SPM micro power generator. The feasibility assessment of the SPM power consumption was studied and as a result, minimum power consumption for an SPM node was estimated.. SPM as a node and as a network will be capable for several applications for roadway transportation systems such as pavement management, traffic monitoring and surveillance, incident and collision avoidance, dynamic navigating, vehicle to vehicle communication, vehicle to roadside communication, and roadway operation and maintenance. The functionality of the SPM for supporting the applications depends on the power resource or its micro power generator modules. In addition, power consumption of the SPM modules and ultralow power design concepts are also effective in the functionality of SPM and its application deployment. The feasibility analysis estimates the minimum power generation of 50 μw is needed for a full operation of the SPM for application of pavement management and traffic surveillance systems.

6-2 ON PAVEMENT MICRO POWER GENERATOR FEASIBILITY

This research started with a feasibility study for the SPM micro power generator. The feasibility study included an SPM power consumption estimate, energy resource and energy conversion alternatives. The main operational module for the SPM node includes a processor/

microcontroller, wireless communication and sensor elements. The technologies, such as Pico power or other ultralow power have been reduced significantly by the power consumption of the integrated circuit. The research feasibility reviews such technologies for determination of SPM core microcontroller power usage. The study estimated this power consumption as 30 µw. That power is equivalent to a power consumption of a microcontroller (16 bit) with the following conditions;

- Clock:500 KHz
- Voltage: 1 Vdc
- Typical power consumption at 9% daily running time period: 180 µA
- Typical power consumption at 1.5µs waiting time period: 5.9 µA
- Typical power consumption at 1.5µs return time period: 3.1 µA
- Typical power consumption at 20µs sleep switching time period: 1870 µA
- Typical power consumption at 90% backup time period: 1.5 µA

The SPM wireless module provides communication between SPM nodes. Multiple antennas are considered for directional point to point coverage to reduce the transmission's power consumption. These antennas will be assembled/fabricated in an SPM 3D package. The study estimated the power consumption of the wireless module is power consumption as low as 10 µw. This low power system will be achievable. An example of the existing low power wireless system is the Nordic, µBlue™ Series of Bluetooth low energy chips with 32-pin 5 by 5mm QFN packaging incorporating a fully embedded radio, link controller, and host subsystem. This is suitable for watches, sensors and remote controls, among other applications. This chip has a typical current consumption of 12.5 µA [50].

The last section of the feasibility study included the energy conversion methods/harvesting methods, and feasibility of them for highway pavement application. Most of the micro energy harvesting methods have application with vibration as the energy input source. Several experimental and research works reported the micro harvesting elements have the energy conversion density from a few micro watts to hundreds of micro watts per cubic centimeter. In regard to a roadway pavement system, the available energy resource is dependent on roadway class, traffic type, traffic volume and distribution, and the pavement structure and materials' properties. The feasibility study specified electrostatic, piezoelectric and electromagnetic as possible options for the pavement harvesting methods. These methods were considered in the work and the design.

6-3 SPM MICROGENERATOR MODELING AND SIMULATION

The research work developed three modeling and simulation methods for the SPM design and implementation. These methods are M, P, and S series modeling. M-models are developed for simulation of the traffic micro distribution along a roadway. The M series provide the details of vehicle movement, including the tire location and the load assignment as a function of time. The M-models were implemented with the following main models and algorithms:

- Vehicle Dynamic Motion Model simulates the total dynamic forces
- Vehicle Traffic Generation Model-Vehicles Generator Module involves the generation of the vehicle input to the simulation segment. The generation input is the Average Annual Daily Traffic volume and the output will be the individual vehicle entrance time to the simulation segment.

- Vehicle Traffic Generation Model-Vehicle Classification Module assigns vehicle class type for each vehicle entry. The assignment is based on the FHWA vehicle classification and seeding data from average annual class rates.
- Vehicle Traffic Generation Model-Vehicle Distribution Module simulates the traffic distribution to roadway segments.
- Vehicle Traffic Generation Model-Vehicle Traffic Platoon Module, define the platoon scenarios and recognition.
- Vehicle Traffic Generation Model- Vehicle Lane Use Module involves lane assignment algorithms.
- Vehicle Traffic Generation Model-Vehicle Lane Change/ Passing Module involves passing or lane change behavior algorithms.
- Vehicle Traffic Generation Model- Vehicle Platoon Module involves traffic platoon assignment algorithms.
- Vehicle Weight Distribution Model distributes dynamic vehicle loading.
- Vehicle Lane Offset Model determines vehicle tires from the center of the lane.
- Vehicle Tire Contact Model simulates a tire contact area on touch with the surface of the pavement.

The M-Models were implemented and several roadways in the New York area, such as Henry Hudson River Parkway, Hutchinson River Parkway, and Major Deegan Expressway were simulated. As a result, the pavement surface activation/loading effect was simulated. In freeway cases, the maximum activation rates were more than 9.2%. These activation rates had been used in P and S models. In Chapter 2, the results of the M-Models were presented.

P-modes series are a set of macro and micro pavement response models. These models were designed and developed for simulation of the energy in the pavement layers. Two approaches of the macro and micro modeling were investigated and a combination of them was implemented. The SPM macro model emulates a small pavement element, which is called pavement unit (PU), with a Kelvin-Voiget or Maxwell stress-strain model. This model block representative will be used for each PU but with different parameters. The parameters are randomly variable dependent on the pavement material distribution (mostly aggregate material size and shapes). A segment of roadway is defined with large 2D or 3D arrays of the PU units. Pavement micro simulation has been developed for applications such as pavement design or operation and maintenance. SPM micro simulation was exercised, but because of the large scale of the models' simulator memory and CPU, our work was limited. Therefore, we used the micro simulation for PU and confirmed the stress-strain model parameters. Simulation results of P-Models were presented in Chapter 3.

The third simulation work developed in this study was a microgenerator system and structure model called the S-Model. In this model, energy harvesting methods and their operation on the pavement were analyzed. Three micro harvesting methods were reviewed and based on the SPM concept, were analyzed. These methods are Electrostatic, Piezo and Electromagnetic microgenerator. The Electrostatic microgenerator acts as variable capacitor, with its capacitance changed by mechanical forces to the generator. In pavement, the mechanical source is vehicle load force. The capacitor charging will be used in charging circuitry and will be stored in an SPM on package battery. An SPM electrostatic generator required a movable microstructure that could be in different types regarding the number of layers or supporting points. This research analyzed and modeled several structure types and a concision multi plate cantilever structure was proposed. The criteria for the structure's selection were the power production and generator

fabrication process. S-Model results for different electrostatic micro structures presented and the displacement, capacity changes and charging rate were calculated. A ten layer micro structure can generate power, which complies with SPM minimum power need of (50 μW).

S-Modeling also included piezo electric micro generator studies and several piezo microstructures were simulated. A multi plates cantilever structure was simulated and it was concluded that the number of plates should be increased significantly in comparison with an electrostatic generator. This will require a longer and more complex fabrication process.

Electromagnetic micro generator alternatives were also reviewed and evaluated for an SPM application. The charging energy, after a direct activation, showed a maximum of 2 mW, but the average of this charge is 2 μW. Therefore, that alternative was not considered for design. Further research on an SPM electromagnetic method will be proposed for future work.

6-4 SPM MICROGENERATOR DESIGN

In Chapter 5, the design process and details of the proposed micro-generator were presented. This design was based on an electrostatic generator with a multi plates cantilever structure. The proposed SPM is in symmetric cubic shape with overall diameters of 15.5 mm. An array of 2 x 5 micro-generator elements was placed at each face of the SPM. The design process and details included:

- Architecture/Structure: An array of 2 by 5 generator elements were placed in a common substrate and held on each face of the SPM. Each element has a size of 3.3 x 1.82 $(mm)^2$. The elements are in parallel connection. (See Fig. 5- 1 A SPM Packaging Layout.)
- Material selection: Integrated circuit/CMOS compatible material for the generator components was determined. The main properties of the material and references are included.

- Micro-generator Control Circuit: The circuit plan for management and control of the operation cycle was proposed. The operation cycle included steady state, pre-charging, charging, discharging, and energy storing stages. The control circuit was distributed in each SPM generator array/SPM face or was to be designated as part of the SPM core module. (See Fig. 5- 1 A SPM Packaging Layout.)
- The energy storage and alternatives are described in the design. An on-package battery or on-chip battery are main alternatives to be used in the SPM. The capacity, life cycle, cost, sizes of a fabricated process (for on-chip battery option) are the design criteria for this battery. The SPM energy storage battery is part of the core module and will serve/charge by all generator arrays and feed all SPM circuits. The design criteria for the battery are specified as: Capacity: min 7.2 mWh, Life Cycle: min 11000, Voltage: 2.8-3.3 Vdc (modular), Diameter: < 7 mm, Thickness < 1.5 mm. (See Fig. 5- 3.)
- The micro generator fabrication process was compatible with IC fabrication. The proposed SPM nodes, complete set of micro generators and core modules, were a non-planar, 3D device. Fabrication of non-planar devices used the same methods as fabrication of planar devices, but the processing of vertical surfaces and/or deep etched features were emphasized in 3D device processing. In the SPM fabrication process, in addition to a non-planar device process, we also required a 3D packaging process. The typical fabricating processes used were: Deposition Process (Chemical Vapor deposition (CVD), Electro Deposition (ED), Epitaxy, and Physical Vapor deposition (PVD).
- Estimating Power Generating Rate: A calculation of the expecting power rate for the proposed generator was included in the design. The calculations included 12 scenarios based on the generator initial voltage (1, 5 and 9 Vdc) and the relative permittivity of selected

dielectric (1, 28, 300 and 2,800). The alternative was called ESG-01 to ESC-12. The traffic data was generated from an M-Model for a freeway case (Henry Hudson Parkway) and SPM maximum activation was 9.2% of total traffic activation. The alternative case ESG-12 (Vcc=9 Vdc and ε_r=2800) showed the maximum power, which was 345 μW. Alternative ESG-11 also can be acceptable for SPM application. ESG-11 power generation rate was 106 μW. ESG-11 had its initial voltage as 5 Vdc and its capacitor with a high relative permittivity as 2800. Other ESG cases can be used conditionally or partially, which means SPM will be operational with limited application or functional service or be operational at specific periods of the day for 12 or 16 hours per day. (See Table 5- 2 for the calculation)

- SPM microgenerator prototype layouts were designed. This design included the fabrication process sequences and the required masks for the construction of the element. The design layouts showed the process of lithography, etching, deposition, and vias. In additional, standard processes such as cleaning and cutting shall be used for fabrication of the prototype generator chip based on the manufacturing facility. For the propose of the assessment of piezoelectric as a generator and as a sensor for SPM, two piezo layers were also included in the design to be used during the testing and post prototype analysis. This prototype layout is designed for performance testing of the embedded micro-generator in a test bed. (See Fig. 5- 6 to Fig. 5- 26)

6-5 SPM ON CHIP MICROGENERATOR RESEARCH ACCOMPLISH AND FUTURE WORKS

This research included a new investigation, analysis and design for an embedded micro-generator for pavement application. Micro energy harvesting has been developed for a variety of application ranges, such as human wearing market or the automobile industry, but was not studied for pavement application. In this work, three new models and analyzing tools were

proposed and developed for traffic mobility/loading (M-Model), pavement response (P-Model) and micro structure assessment (S-Model). These models were used for pavement energy estimation, determination of the optimum location for SPM placement, and determination of the microstructure type and the harvesting methods to be used. In addition to an SPM application for these models, M-Models can be used for other applications that require the detail of the traffic distribution on roadway surface. M-Model applications may be expanded for traffic measurement and management applications. One of the sub-topics in this project was roadway energy patterning in response to the traffic. Study of such patterning will be achievable by using M-Model detail traffic distribution placement data.

By design, part of this research involved the design requirements for an SPM micro-generator and detail layout and materials were specified. This design also included battery and control circuits that were specifically proposed for SPM applications.

For future works and a general road work for SPM research and development, the following items/projects are proposed. These plans include full SPM implementation and include the core modules and SPM networking (See Fig. 1- 2 SPM On-Chip Components). Some important soft projects and, application developments are also included here, but other applications should be considered on a longer term.

SPM On-Chip Generator (SPM-OCG) Prototype Fabrication and Testing -Project 1: Under this effort, the proposed SPM microgenerator will be fabricated in a minimum of two prototype stages. The first prototype will be a planar element fabrication for testing in a pavement lab facility and a roadside test bed. Results of this test will revise engineering and modification of the generator design will be conducted. The second prototype will include the revised design layouts and also fabrication in a 3D package. This generator also will be tested in a pavement lab

and in a field test bed. The assessment and measurement of the generating power will be an expected outcome of the project. .

SPM in–Pavement Wireless Communication (SPM-IPWC) Sub-Project 2: In this research, a low power wireless transmission system/network inside the pavement material will be studied, designed and prototyped. This ultra-low power RF system will support an adaptive micro antenna and transmission power management circuits. The transmission throughput of this system will be a dynamic rate related to the SPM node power capacity and will be varied in a range specified with minimum and maximum SPM sensor network operation functions.

SPM Off–Pavement Wireless Communication (SPM-OPWC) Project 3: To access the SPM network information in a stationary node outside of the pavement, a separate wireless transmission system with alternative of RF charging capability will be investigated, researched, designed, and prototyped. This project is mainly proposed for Vehicle to Vehicle communication applications. The SPM-OPWC will be separate from SPM-OPWC, but for mobile node interfaces (vehicle), they will operate in a synchronized and common network.

SPM On-Chip Sensors (SPM-OCS) Project 4: Based on the SPM application needs of different type, size and network, sensing will be studied, designed and prototyped in this work. The purpose of this design will be the development of new sensor devices and sensor network data for operating at ultra-low power consumption. The sensors are specified with SPM functions in the transportation systems and vehicle industry.

SPM Network (SPM-NET) Project 5: SPM low power support data transmission protocol, SPM data coding and SPM network dynamic architecture are the research topics in this sub-project. As part of this study, a simulation of the proposed solution and a small scale SPM network Test Bed will be investigated, designed and implemented.

SPM Application Development-Dynamic Pavement Management System (DPMS) Project 6: This research will include investigating and the design of software and high level PMS applications based on SPM dynamic information.

SPM Application Development-Advanced Traffic Monitoring System (ATMS) Project 7: This research will include investigating and the design of software and high level ATMS applications based on SPM dynamic information.

SPM Application Development-Advanced Traveler Information System (ATIS) Project 8: This research will include investigating and design of software and high level ATIS applications based on SPM dynamic information.

SPM Application Development-Advanced Incident Detection System (AIDS) Project 9: This research will include investigating and design of software and high level AIDS applications based on SPM dynamic information

SPM Application Development-Vehicle Navigation System (VNS) Project 10: This research will include investigating and design of in-vehicle hardware and software and high level VNS applications based on SPM dynamic information.

SPM Application Development-Vehicle Awareness System (VAS) Project 11: This research will include investigating and design of in-vehicle hardware and software and high level VAS applications based on SPM dynamic information.

SPM Application Development-Vehicle to Vehicle Communication System (V2V) Project 12: This research will include investigating and design of in-vehicle hardware and software and high level V2V applications based on SPM dynamic information.

Appendix 1- VMM Modeling Program

1- **MODEL-00-MASTER MODEL**

MAIN MASTER MACRO

2- **MODEL-11B-VDMEM_DEF**

M - MODEL 01-:VDMEM-DFC: VEHICLE DYNAMIC MOTION EFFECT MODEL DYNAMIC

% FORCE CALCULATION REVISION A- (MEMORY CUT)

3- **M_MODEL_21_DTGM_VTP**

M-MODEL 02-1: M21-DTGM-VTP:

4- **M_MODEL_22_DTGM_VCD**

M-MODEL 02-2: M22-DTGM-VCD

5- **M_MODEL_23_DTGM_VLU**

M-MODEL 02-3: M23-DTGM-VLU

6- **M_MODEL_24_DTGM_VG**

M-MODEL 02-4: M24-DTGM-VG

7- **M_MODEL_24_DTGM_VG**

M-MODEL 02-5: M25-DTGM-VP

8- **M_MODEL_26_DTGM_VLC/P1**

M - MODEL 02-6:M26-DTGM-VLC/P1

9- **M_MODEL_27_DTGM_VLC/P2**

M - MODEL 02-7:M27-DTGM-VLC/P2

10- **M_MODEL_28_DTGM_VLA**

M - MODEL 28-:M28-DTGM-VLA

M- MODEL-02-08: DTGM-VLA - DYNAMIC TRAFFIC GENERATION MODEL-VEHICLE LANE ASSEMBLY

11- **M_MODEL_29_DTGM_VRA**

M - MODEL 29-:M29-DTGM-VRA

M- MODEL-02-09: DTGM-VRA - DYNAMIC TRAFFIC GENERATION MODEL-VEHICLE ROAD ASSEMBLY

12- **M_MODEL_30_VWDM**

M - MODEL 03-6:VWDM

M - MODEL-03: VEHICLE WEIGHT DISTRIBUTION MODEL

13- **M_MODEL_40_VILM**

M - MODEL 04-:VILM

M - MODEL-04: VEHICLE IN LANE MODEL

14- **M_MODEL_50_VPIFM**

M - MODEL 05-:VPIFM

M - MODEL-05: VFIP - VEHICLE PAVEMENT INTERFACING FORCE MODEL

15- **M_MODEL_60_VDPAM**

M - MODEL: M-06: M60-VDPAM - VEHICLE DYNAMIC PARAMETERS ANALYZING MODEL

Complete MATLAB Program codes are available at:

Appendix Materials\Appendix 1\VMM Modeling Program.docx

Appendix 2- VMM Case Study Model Input and Outputs Data

2005 Screen Line Volumes- Bronx – Westchester[52]

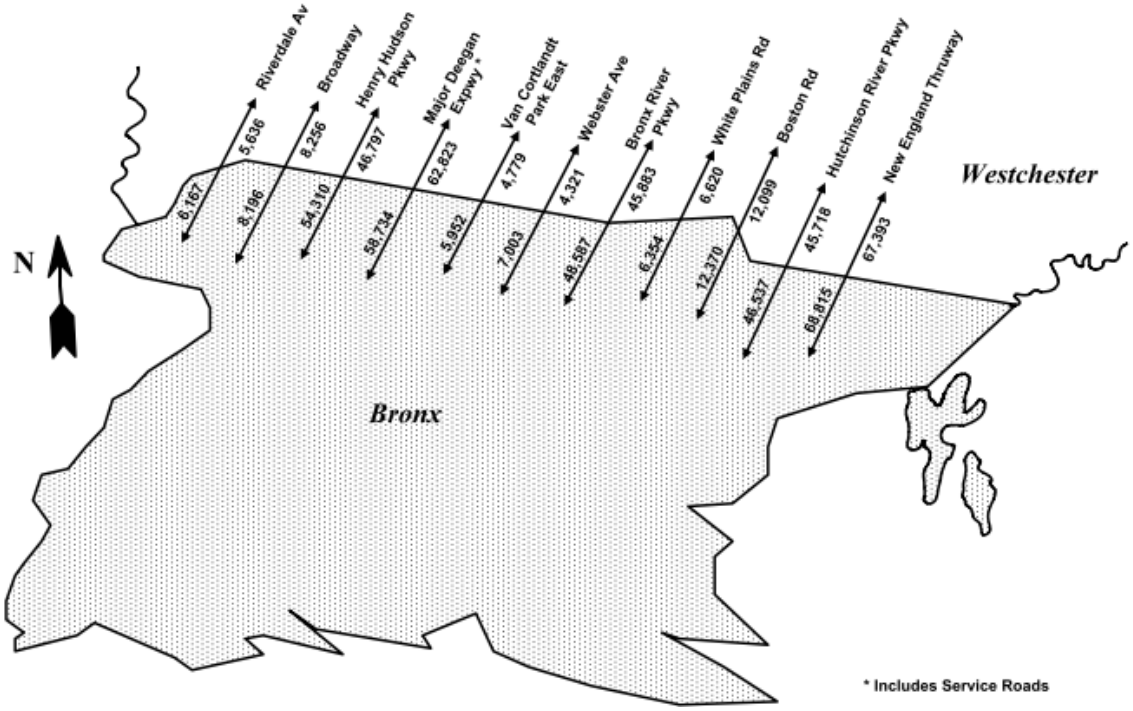

[52] Reference: New York City Screen line Traffic Flow 2005, NYCDOT

	Boston Rd		Broadway		Bronx River Parkway		Henry Hudson Parkway		Hutchinson River Parkway		Major Deegan Expressway		Majo (Ser
	S/B*	N/B	S/B*	N/B	S/B*	N/B	S/B*	N/B	S/B*	N/B	S/B*	N/B	S/B*
Mid-1am	124	99	100	155	473	472	379	781	425	333	713	1,079	48
1-2am	55	57	64	100	210	245	193	350	239	162	455	634	29
2-3am	43	43	49	58	158	186	131	227	128	126	386	428	25
3-4am	42	67	36	47	172	174	113	163	125	204	413	397	28
4-5am	87	61	67	58	352	238	267	180	346	773	746	526	35
5-6am	200	169	169	116	1,178	680	1,075	417	1,156	2,237	1,893	1,025	106
6-7am	407	436	417	238	3,372	2,015	3,591	1,388	2,416	3,198	3,968	2,156	283
7-8am	769	765	725	383	4,528	3,248	5,202	2,595	3,247	2,985	4,359	3,147	440
8-9am	731	838	621	462	3,480	3,303	4,373	2,909	3,320	2,497	3,766	3,186	329
9-10am	652	665	427	389	2,677	2,055	3,502	1,964	2,714	2,102	3,042	2,556	272
10-11am	610	597	355	377	2,184	1,720	2,792	1,619	2,157	2,159	2,516	2,419	221
11-Noon	677	708	359	381	2,012	1,751	2,477	1,734	2,093	2,131	2,390	2,561	211
Noon-1	770	717	381	390	2,042	1,851	2,401	1,954	2,201	2,328	2,442	2,578	211
1-2pm	758	739	432	411	2,035	2,053	2,299	2,206	2,357	2,910	2,510	2,738	220
2-3pm	789	887	457	414	2,371	2,930	2,624	2,765	2,728	3,066	2,609	3,045	240
3-4pm	851	901	515	516	2,826	4,091	3,242	3,572	3,037	2,856	2,836	3,745	250
4-5pm	864	897	515	540	3,243	3,833	3,615	3,510	3,183	2,873	3,060	4,061	260
5-6pm	893	856	494	594	3,586	4,082	4,023	3,629	3,163	2,888	3,250	4,311	267
6-7pm	824	738	519	644	3,226	3,142	3,750	3,433	3,005	2,617	3,174	3,931	243
7-8pm	688	639	452	596	2,374	2,409	2,750	3,128	2,672	2,130	2,589	3,304	190
8-9pm	527	444	336	461	1,880	1,740	1,949	2,514	2,031	1,792	2,225	2,719	149
9-10pm	415	345	283	367	1,804	1,499	1,574	2,094	1,607	1,523	2,037	2,309	142
10-11pm	331	271	242	311	1,415	1,274	1,209	1,953	1,313	1,132	1,741	2,032	110
11-Mid	263	160	181	248	989	892	779	1,712	874	696	1,223	1,641	82
24 hr Total	12,370	12,099	8,196	8,256	48,587	45,883	54,310	46,797	46,537	45,718	54,343	56,528	4,391
6-10am	2,559	2,704	2,190	1,472	14,057	10,621	16,668	8,856	11,697	10,782	15,135	11,045	1,324
10am-1pm	2,057	2,022	1,095	1,148	6,238	5,322	7,670	5,307	6,451	6,618	7,348	7,558	643
1-3pm	1,547	1,626	889	825	4,406	4,983	4,923	4,971	5,085	5,976	5,119	5,783	460
3-7pm	3,432	3,392	2,043	2,294	12,881	15,148	14,630	14,144	12,388	11,234	12,320	16,048	1,020
6am-7pm	9,595	9,744	6,217	5,739	37,582	36,074	43,891	33,278	35,621	34,610	39,922	40,434	3,447

* To Bronx

Based on the above cases and data, the VMM Traffic and Static input files are prepared in the following files:

STATIC_DATA.xls

TRAFFIC_DATA.xls

Typical Daily Traffic Pattern for a Freeway and Arterial Highway in New York City

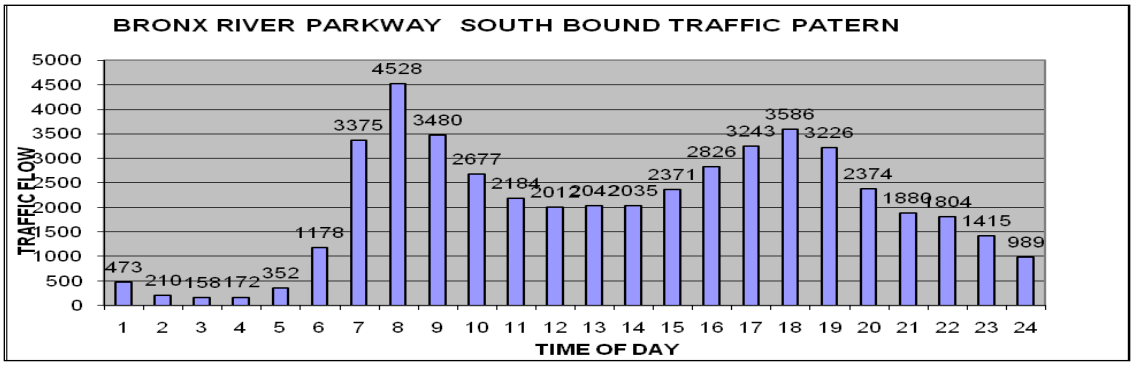

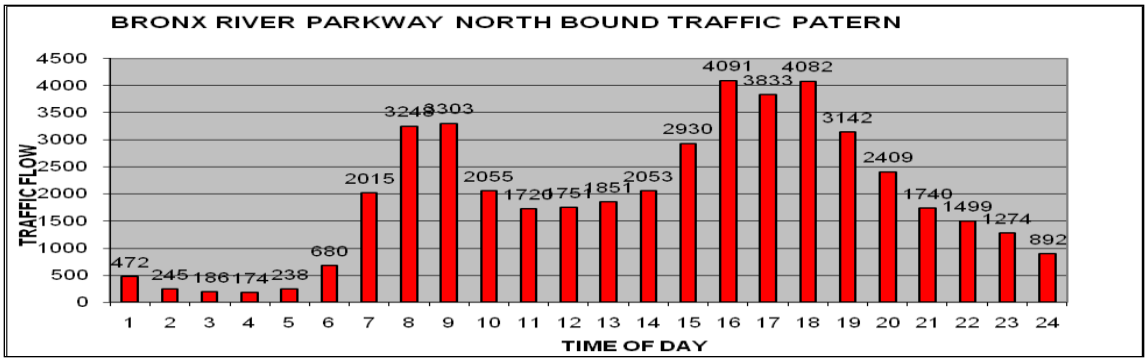

Typical Traffic Pattern, Bronx River Parkway, New York City

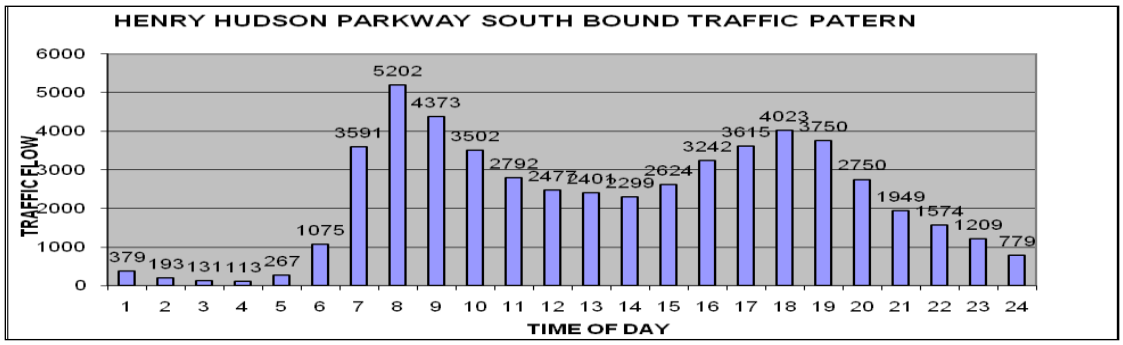

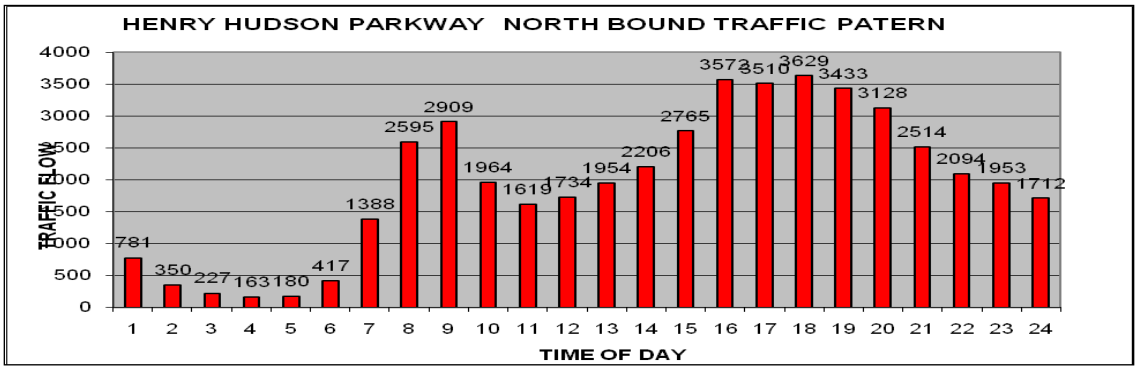

Typical Traffic Pattern, Henry Hudson Parkway, New York City

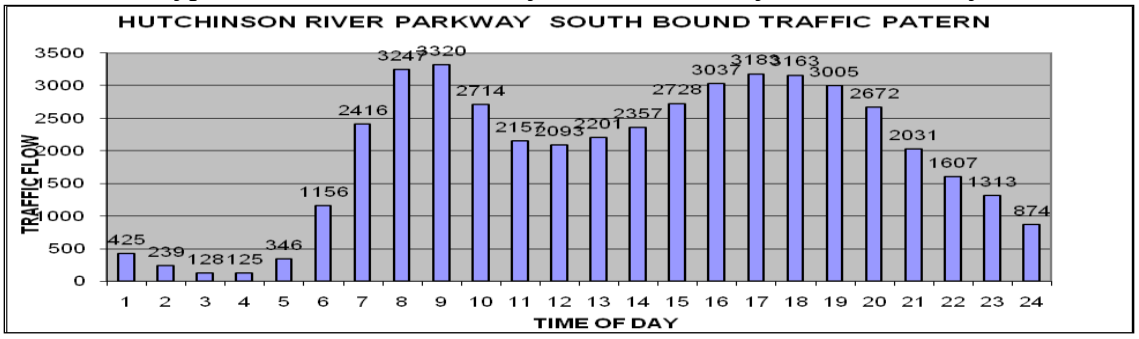

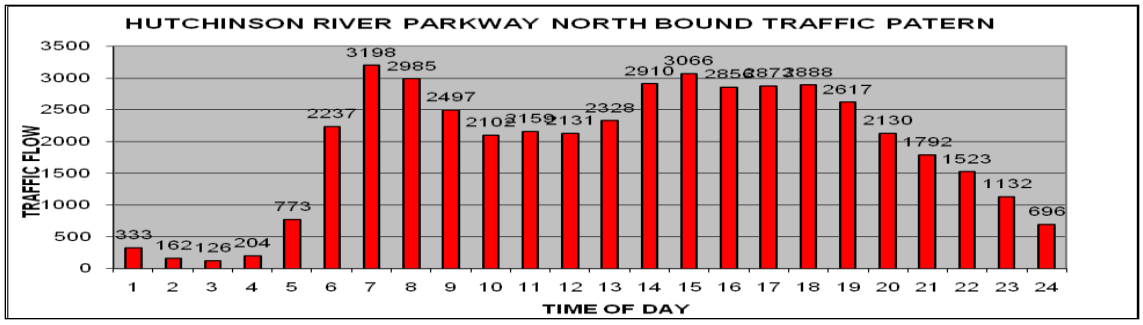

Typical Traffic Pattern, Hutchinson River Parkway, New York City

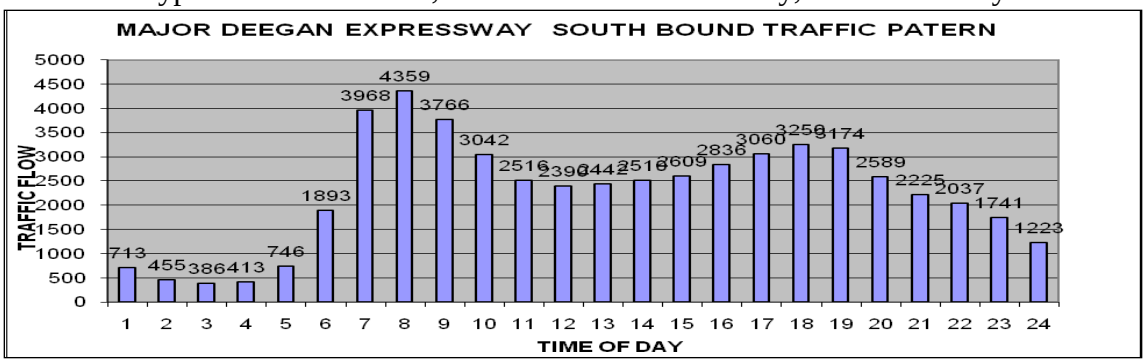

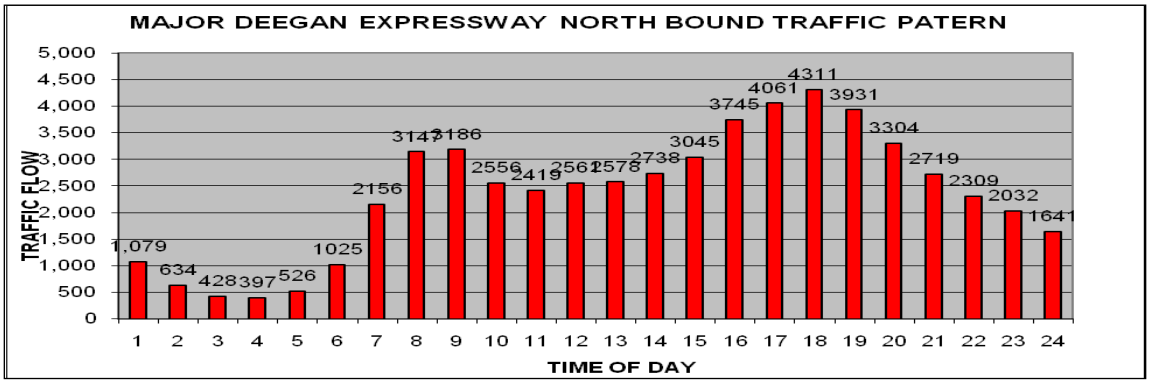

Typical Traffic Pattern, Major Deegan Expressway, New York City

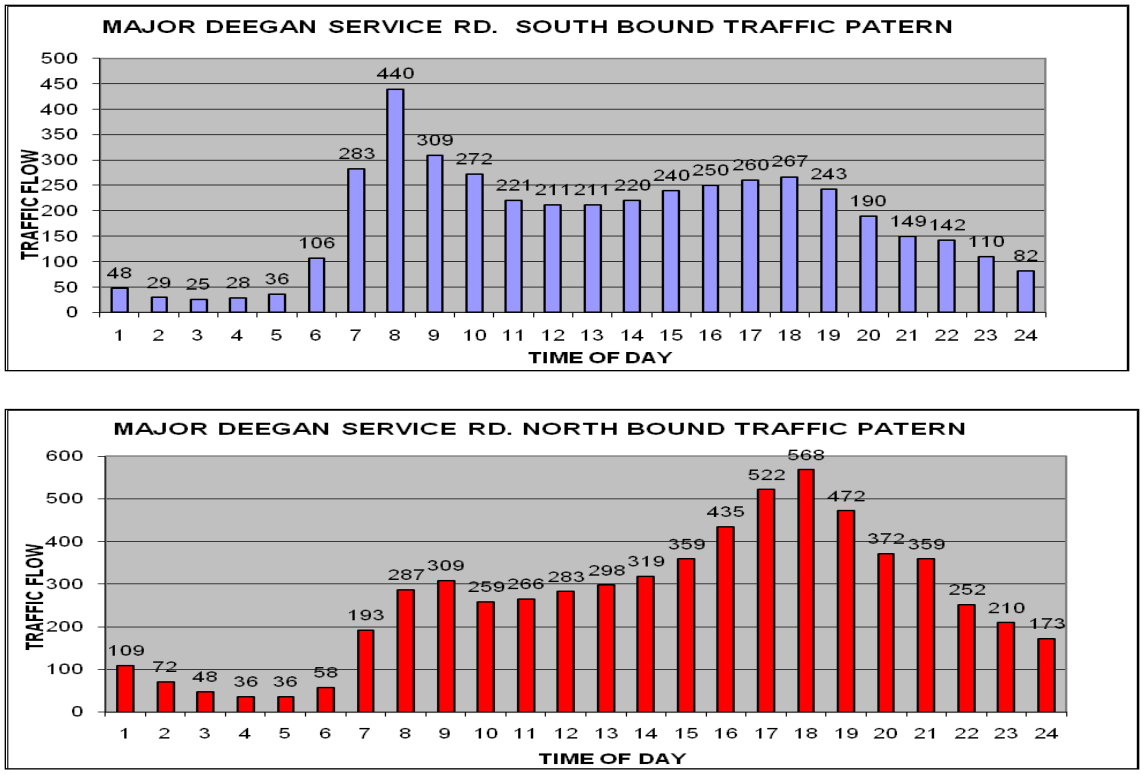

Typical Traffic Pattern, Major Deegan Service Road, New York City

Appendix 3 VMM Output Results

The results of the VMM modeling outputs are with the following files:

- BOSTON-VMM-OUT.xls
- BROADWAY-VMM-OUT.xls
- BRP-VMM-OUT.xls
- HHP-VMM- Out.xlsx
- HRP-VMM-OUT.xls
- MDE-VMM-OUT.xls
- MDS-VMM-OUT.xls

Appendix 4 Vehicle Mobility Model Parameters

The VMM Roadway and Traffic Inputs Parameters and Variables are with the following file:

Appendix Materials\Appendix 4\VMM Roadway-Traffic Inputs Parameters-Variables.xlsx

Appendix 5 - Material and Field Testing Methods

A- Materials- List of Appropriate Bituminous Mixture Tests[53]

I. Asphalt Cements

- AASHTO M-20 Penetration Graded Asphalt Cement
- AASHTO M-140 Emulsified Asphalt
- AASHTO M-208 Cationic Emulsified Asphalt
- AASHTO M-226 Viscosity Graded Asphalt Cement
- AASHTO MP1-93 Specification for Performance Graded Asphalt Binder
- AASHTO PP1-93 Practice for Accelerated Aging of Asphalt Binder Using a Pressurized Aging Vessel
- AASHTO PP2-93 Practice for Short and Long Term Aging of Hot Mix Asphalt (HMA)
- AASHTO PP6-93 Practice for Grading or Verifying the Performance Grade of an Asphalt Binder
- AASHTO T-48 Flash and Fire Points by Cleveland Open Cup
- AASHTO T-49 Penetration of Bituminous Materials
- AASHTO T-51 Ductility of Bituminous Materials
- AASHTO T-59 Testing Emulsified Asphalts
- AASHTO T-179 Effect of Heat and Air on Asphalt Materials (Thin-Film Oven Test)
- AASHTO T-201 Kinematic Viscosity of Asphalts (Bitumen){135C}
- AASHTO T-202 Viscosity of Asphalts by Vacuum Capillary Viscometer {60C}
- AASHTO T-240 Effect of Heat and Air on a Moving Film of Asphalt

[53] http://www.fhwa.dot.gov/pavement/materials/matnote47.cfm

- Rolling Thin Film Oven Test
- AASHTO TP1-93 Test Method for Determining the Flexural Creep Stiffness of Asphalt Binder Using the Bending Beam Rheometer (BBR)
- AASHTO TP3-93 Test Method for Determining the Fracture Properties of Asphalt Binder in Direct Tension (DT)
- AASHTO TP5-93 Test Method for Determining the Rheological Properties of Asphalt Binder Using a Dynamic Shear Rheometer (DSR)

II. **Aggregates**

A. **Quality/Qualification**

- AASHTO M-17 Mineral Filler for Bituminous Paving Mixtures
- AASHTO M-29 Fine Aggregate for Bituminous Paving Mixtures
- AASHTO T-96 Resistance to Degradation of Small-Size Course Aggregate by Abrasion and Impact in the Los Angeles Machine
- AASHTO T-103 Soundness of Aggregates by Freezing and Thawing
- AASHTO T-104 Soundness of Aggregate by Use of Sodium Sulfate or Magnesium Sulfate
- AASHTO T-112 Clay Lumps and Friable Particles in Aggregate
- AASHTO T-113 Lightweight Pieces in Aggregate
- AASHTO T-176 Plastic Fines in Graded Aggregates and Soils by the Use of the Sand Equivalent Test

B. **Design/Control Testing**

- AASHTO T-11 Materials Finer than 75μm (No. 200) Sieve in Mineral Aggregates by Washing

- AASHTO T-19 Unit Weight and Voids in Aggregate
- AASHTO T-27 Sieve Analysis of Fine and Coarse Aggregates
- AASHTO T-84 Specific Gravity and Absorption of Fine Aggregate
- AASHTO T-85 Specific Gravity and Absorption of Coarse Aggregate
- AASHTO T-255 Total Moisture Content of Aggregate by Drying

Bituminous Mixture

. **Design Mixture**

- AASHTO PP19-93 Practice for Volumetric Analysis of Compacted Hot Mix Asphalt (HMA)
- AASHTO T-165 Effect of Water on Cohesion of Compacted Bituminous Mixtures
- AASHT0 T-182 Coating and Stripping of Bitumen-Aggregate Mixtures
- AASHT0 T-209 Maximum Specific Gravity of Bituminous Paving Mixtures
- AASHTO T-245 Resistance to Plastic Flow of Bituminous Mixtures Using Marshall Apparatus
- AASHTO T-246 Resistance to Deformation and Cohesion of Bituminous Mixtures by Means of Hveem Apparatus
- AASHTO T-283 Resistance of Compacted Bituminous Mixture to Moisture Induced Damage (Lottman Test)
- AASHTO TP4-93 Method for Preparing and Determining the Density of Hot Mix Asphalt (HMA) Specimens by Means of the SHRP Gyratory Compactor

- AASHTO TP7-94 Test Method for Determining the Permanent Deformation and Fatigue Cracking Characteristics of Hot Mix Asphalt (HMA) Using the Simple Shear Test (SST) Device
- AASHTO TP9-94 Test Method for Determining the Creep Compliance and Strength of Hot Mix Asphalt (HMA) Using the Indirect Tensile Test Device

A. **Field Control**

- AASHT0 T-166 Bulk Specific Gravity of Compacted Bituminous Mixtures Using Saturated Surface-Dry Specimens
- AASHT0 T-164 Quantitative Extraction of Bitumen from Bituminous Paving Mixtures
- AASHT0 T-195 Determining Degree of Particle Coating of Bituminous-Aggregate Mixtures
- AASHTO T-269 Percent Air Voids in Compacted Dense and Open Bituminous Paving Mixtures
- ASTM D2950 Density of Bituminous Concrete in Place by Nuclear Method

(NOTE: TESTS IN italics ARE PROVISIONAL STANDARDS)

B- Field Sampling and Testing Procedure

- AASHTO T 2 Sampling of Aggregates
- AASHTO T 11 Materials Finer than No. 200 Sieve in Mineral Aggregates by Washing
- AASHTO T 23 Making and Curing Concrete Test Specimens in the Field
- AASHTO T 27 Sieve Analysis of Fine and Coarse Aggregates

- AASHTO T 84 Specific Gravity and Absorption of Fine Aggregate
- AASHTO T 85 Specific Gravity and Absorption of Coarse Aggregate
- AASHTO T 87 Dry Preparation of Disturbed Soil and Soil Aggregate Samples for Test
- AASHTO T 89 Determining the Liquid Limit of Soils
- AASHTO T 90 Determining the Plastic Limit and Plasticity Index of Soils
- AASHTO T 99/T 180 Moisture-Density Relations of Soils
- AASHTO T 113 Lightweight Pieces in Aggregate
- AASHTO T 119 Slump of Hydraulic Cement Concrete
- AASHTO T 121 Density (Unit Weight), Yield, and Air Content (Gravimetric) of Concrete
- AASHTO T 141 Sampling Freshly Mixed Concrete
- AASHTO T 152 Air Content of Freshly Mixed Concrete by the Pressure Method
- AASHTO T 166 Bulk Specific Gravity of Compacted Hot Mix Asphalt Mixtures Using Saturated Surface-Dry Specimens
- AASHTO T 176 Plastic Fines in Graded Aggregates and Soils by Use of the Sand Equivalent Test
- AASHTO T 191 Density of Soil In-Place by the Sand-Cone Method
- AASHTO T 209 Theoretical Maximum Specific Gravity and Density of Hot Mix Asphalt (HMA)
- AASHTO T 217 Determination of Moisture in Soils by Means of a Calcium Carbide Gas Pressure Moisture Tester (Speedy)
- AASHTO T 224 Correction for Coarse Particles in the Soil Compaction Test AASHTO T 245 Resistance to Plastic Flow of Bituminous Mixtures Using Marshall Apparatus

- AASHTO T 248 Reducing Samples of Aggregate to Testing Size
- AASHTO T 255 Total Evaporable Moisture Content of Aggregate by Drying
- AASHTO T 265 Laboratory Determination of Moisture Content of Soils
- AASHTO T 304 Uncompact Void Content of Fine Aggregate
- AASHTO T 309 Temperature of Freshly Mixed Hydraulic Cement Concrete
- AASHTO T 312 Preparing and Determining Density of Hot Mix Asphalt (HMA) Specimens by Means of the Superpave Gyratory Compactor
- AASHTO T 318 Water Content of Freshly Mixed Concrete Using Microwave Oven Drying
- ASTM D 2167 Density and Unit Weight of Soil in Place by the Rubber-Balloon Method
- ASTM D 4643 Microwave Method of Drying Soils
- ASTM D 4791 Flat Particles, Elongated Particles, or Flat and Elongated Particles in Coarse Aggregate
- NDDOT 1 Sampling of Bituminous Materials
- NDDOT 2 Contractor Coring
- NDDOT 3 Shale, Iron Oxide Particles, Lignite and Other Coal, Soft Particles, Thin or Elongated Pieces
- NDDOT 4 Percentage of Fractured Particles in Coarse Aggregate
- NDDOT 5 Sampling and Splitting Field Verification Hot Mix Asphalt (HMA) Samples
- NDDOT 6 Settlement Test for Liquid Membrane Curing Compound

C- Aggregate Sizes Chart[54]

Size Number	Total Percent Passing																
	100m (4")	90mm (3½")	63mm (2½")	50mm (2")	37.5m (1½")	25mm (1")	19 (¾")	12.5m (½")	9.5mm (⅜")	4.75m (No.4)	2.36 (No.8)	2.0m (No. 10)	1.18m (No.16)	850µ (No.20)	425µ (No.40)	150µ (#100)	75µm (#200)
AASHTO 1	100	90-100	25-60		0-15		0-5										
AASHTO 3			100	90-100	35-70	0-15		0-5									
AASHTO 467				100	95-100		35-70		10-30	0-5							
AASHTO 5					100	90-100	20-55	0-10	0-5								
AASHTO 57					100	95-100		25-60		0-10	0-5						
AASHTO 67						100	90-100		20-55	0-10	0-5						
AASHTO 7							100	90-100	40-70	0-15	0-5						
AASHTO 8								100	85-100	10-30	0-10		0-5				
AASHTO 10									100	85-100						10-30	
PennDOT 2A				100			52-100		36-70	24-50	16-38		10-30				0-10
PennDOT OGS				100			52-100		36-65	8-40			0-12				0-5
MDSHA CR-6				100	90-100		60-90			30-60							0-15
MDSHA Bank Run Gravel - Subbase			100			90-100		60-100				35-90			20-55		5-25
MD GAB				100	95-100		70-92		50-70	35-55							0-8
DelDOT "RICE"									100	70-100		0-10			0-10		0-5
DelDOT Type A CR-1			100			50-80				20-50				10-30		2-20	
DelDOT Type B Crusher Run					100		50-95			20-50		15-40				2-20	

[54] http://independenceconstructionmaterials.com/products.aspx

Appendix 6 – PEM Micro Simulation Reports

Appendix Materials\Appendix 6\PEM Report Run 1.docx

Appendix Materials\Appendix 6\PEM Report Run 2.docx

Appendix Materials\Appendix 6\PEM Report Run 3.docx

Appendix Materials\Appendix 6\PEM Report Run 4.docx

Appendix Materials\Appendix 6\PEM Report Run 5.docx

Appendix Materials\Appendix 6\PEM Report Run 6.docx

Appendix Materials\Appendix 6\PEM Report Run 7.docx

Appendix Materials\Appendix 6\PEM Report Run 8.docx

Appendix Materials\Appendix 6\PEM Report Run 9.docx

Appendix Materials\Appendix 6\PEM Report Run 10.docx

Appendix 7 – Piezoelectric Materials Film Typical Properties

Symbol	Parameter	PVDF	Copolymer	Units
t	Thickness	9, 28, 52, 110	<1 to 1200	μm (micron, 10^{-6})
d_{31}	Piezo Strain Constant	23	11	10^{-12} $\frac{m/m}{V/m}$ *or* $\frac{C/m^2}{N/m^2}$
d_{33}		-33	-38	
g_{31}	Piezo Stress constant	216	162	10^{-3} $\frac{V/m}{N/m^2}$ or $\frac{m/m}{C/m^2}$
g_{33}		-330	-542	
k_{31}	Electromechanical Coupling Factor	12%	20%	
k_t		14%	25-29%	
C	Capacitance	380 for 28μm	68 for 100μm	pF/cm^2 @ 1KHz
Y	Young's Modulus	2-4	3-5	10^9 N/m^2
V_0	Speed of Sound stretch:	1.5	2.3	10^3 m/s
	thickness:	2.2	2.4	
p	Pyroelectric Coefficient	30	40	10^{-6} C/m^2 °K
ε	Permittivity	106-113	65-75	10^{-12} F/m
$\varepsilon/\varepsilon_0$	Relative Permittivity	12-13	7-8	
ρ_m	Mass Density	1.78	1.82	10^3kg/m
ρ_e	Volume Resistivity	$>10^{13}$	$>10^{14}$	Ohm meters
$R_\square$	Surface Metallization Resistivity	<3.0	<3.0	Ohms/square for NiAl
$R_\square$		0.1	0.1	Ohms/square for Ag Ink
tan δ_e	Loss Tangent	0.02	0.015	@ 1KHz
	Yield Strength	45-55	20-30	10^6 N/m^2 (stretch axis)
	Temperature Range	-40 to 80...100	-40 to 115...145	°C
	Water Absorption	<0.02	<0.02	% H_2O
	Maximum Operating Voltage	750 (30)	750 (30)	V/mil(V/μm), DC, @ 25°C
	Breakdown Voltage	2000 (80)	2000 (80)	V/mil(V/μm), DC, @ 25°C

Source: Measurement Specialties, Inc., Sensor Products Division, 950 Forge Avenue, Norristown, PA 19403, Tel: 610.650.1500, FAX: 610.650.1509, Internet: www.msiusa.com

Appendix 8 – Piezoelectric Parameters Description

Parameter Definitions

Permittivity ε

The **permittivity**, or relative dielectric constant, ε is a measure of the polarizability of the material.

The directionality of the permittivity is expressed by tensor components, whereby the same component indexes are used as for th electric field and dielectric displacement.

For example,

ε_{33}^{T} describes the permittivity value in the polarization direction (direction 3) when an electric field is applied also in the polarization direction, under conditions of constant mechanical stress ($T = 0$: "free" permittivity)

ε_{11}^{S} is the electric field and dielectric displacement in direction 1, perpendicularto to the polarization direction at constant deformation ($S = 0$: clamped permittivity)

Piezoelectric charge constant d_{ij}

The **piezoelectric charge or strain constant d** is a measure of the electric charge induced in response to a mechanical stress, or the achievable mechanical strain when an electric field is applied (T = constant).

For example,

d_{31} is the charge density developed per mechanical stress, or, alternatively, strain developed per unit of electric field strength, all in the polarization direction.

Piezoelectric voltage constant g_{ij}

The **piezoelectric voltage constant g** defines the ratio of the electric field strength E to the effective mechanical stress T. If one divides the respective piezoelectric charge constants d_{ij} by the corresponding permittivity value one gets the corresponding g_{ij} constant.

For example,

g_{31} describes the electric field induced in direction 3 by a mechanical stress acting in direction 1.

Elastic constant s_{ij}

The **elastic constant or compliance** s_{ij} is a measure of the ratio of the relative deformation S to the mechanical stress T. Because it depends on the interaction of mechanical and electrical energy, the electrical boundary conditions must be taken into consideration.

For example,

s_{11}^{E} describes the ratio of the mechanical strain in direction 3 to the mechanical stress in direction 3, with constant electric field (for $E = 0$: short circuit)

s_{55}^{D} is the ratio of a shear strain to the effective shear stress with constant dielectric displacement (for $D = 0$: open circuit)

Note:

Young's modulus Y, which is often used in the English-speaking world, is the reciprocal of the compliance constant.

Frequency constant N_i

The **frequency constant N** corresponds to half the speed of the sound wave propagating in the ceramic body (with the exception N_p, the planar oscillation). The indexes identify the corresponding direction of oscillation, for which the respective dimension A determines the (series) resonant frequency f_n: $N = f_n \cdot A$.

For example,

N_t describes the frequency constant for the longitudinal oscillation of a slim rod polarized in the longitudinal direction

N_1 is the frequency constant for the transverse oscillation of a slim rod polarized direction 3

N_p is the frequency constant of the surface (planar) oscillation of a round disk

N_s is the frequency constant of the thickness oscillation of a thin disk polarized in the thickness direction.

Mechanical quality factor Q_m

The **mechanical quality factor** Q_m characterizes the "sharpness of the resonance" of a piezoelectric body (resonator) and is primarily determined from the 3 dB bandwidth of the series resonance of the resonating system. The reciprocal value of the Q-factor is the ratio of resistance to reactance, the mechanical loss factor, tan .

Coupling factor k

The **coupling factor k** is a measure of the effectiveness of the piezoelectric effect (not the efficiency, as it is frequently incorrectly called!). It describes the ability of a piezoelectric material to transform electrical energy into mechanical energy and vice versa. Mathematically, the size of the coupling factor is determined by the square root of the ratio of stored mechanical energy to the total energy applied. At resonance, k is a function of the form of oscillation of the piezoelectric body.

For example,

k_{33} is the coupling factor for the longitudinal oscillation

k_{31} is the coupling factor for the transverse longitudinal oscillation

k_p is the coupling factor for the radial oscillation (planar) of a round disk

K_s is the coupling factor for the thickness oscillation of a plate

k_{15} is the coupling factor for the thickness shear oscillation of a plate

Source: PI Ceramic PmbH , Piezoelectric Ceramic Product, www.piceramic.com

Appendix 9 US Truck Configuration

Single-Unit Trucks

Truck-Trailer Combinations

Tractor-Semitrailer Combinations

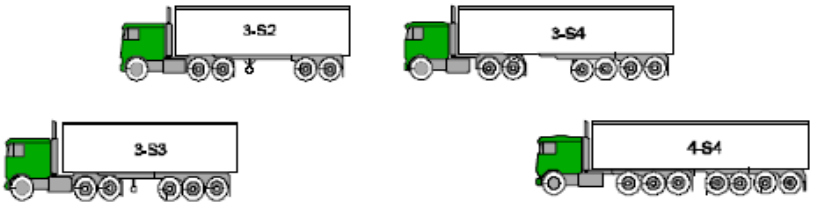

STAA Double-Trailer Combination

LCVs

Double-Trailer Combinations

Triple-Trailer Combination

Appendix 10 Tire Contact Interface

One interesting discovery in Europe by the Transportation Research Laboratory, UK, shows that some of the highest dynamic tire forces were generated by vehicles with (so called) 'road-friendly' air suspensions. The reason for this apparently anomalous result is that air suspensions require well maintained shock absorbers to provide their damping, otherwise, their bouncing motion can be lightly damped and they can generate very high dynamic loads.

Existing European Commission regulations for road-friendly suspensions encourage the use of air suspensions by providing a one tone payload incentive to operators. However, the regulations do not control their in-service dynamic loading performance or suspension and damper maintenance. It seems, therefore, that current regulations have the opposite effect to that intended by the European Commission. In a significant proportion of cases, they increase rather than decrease dynamic loads and the resulting road damage. [51]

The vertical forces consist of a static component, the static tire force, and due to vehicle weight and a fluctuating component, the dynamic tire force, causes vibration of the vehicle in response to road roughness. Dynamic tire forces typically occur in the frequency range of 1 Hz to 15 Hz, due to road roughness features with wavelengths of 0.5 m to 15 m, depending on the speed. They are a function of the roughness of the road, the speed of the vehicle, and the dynamic characteristics of the suspension and tires. The main tire parameter influencing dynamic tire forces is the overall vertical stiffness.

Tire damping is generally small and can be ignored in predictions of vehicle response to road roughness. Wide single tires have lower vertical stiffness than dual tires which generally results

in lower dynamic tire forces. However, they also generate considerably higher contact pressures than dual tires, and this has been implicated in increased [11].

In this study, it is assumed that the normal component of the contact pressure between tire and road surface is uniform. For example, pressures are observed to increase around the edges of the contact area, particularly in the 'shoulder' areas at either side, due to the stiffness of the side walls and at the front and rear, due to bending of the tread band [11]. This assumption will be different from actual field conditions. However, we ignored that error.

The model is developed based on a tire dynamic model with modifications regarding the model parameters' estimate and model integration to other M-Models. Here is a summary of the tire modeling plans which are presented originally in a math worksmodel[55]. A tire model describes the tire contact with the road. By calculating the vertical load F_z and providing the vehicle speed (longitudinal velocity) V_x , the model provides the longitudinal force F_x on the vehicle.

The tire is a flexible body in contact with the road surface and is subject to slip. When a torque is applied to the wheel axle, the tire deforms, pushes on the ground (while subject to contact friction), and transfers the resulting reaction as a force back on the wheel, pushing the wheel forward or backward.

At full speed, the tire acts like a damper and the longitudinal force F_x is determined mainly by the slip. At low speeds, when the tire is starting up from a stop, or slowing down to a stop, the tire behaves more like a deformable, circular spring. The effective rolling radius r_e (a radius, at which the longitudinal force is transferred to the wheel as a torque) is normally slightly less than

---

55 http://www.mathworks.com/access/helpdesk/help/toolbox/physmod/drive/index.html?/access/helpdesk/help/toolbox/physmod/drive/longitudinalvehicledynamics.html&http://www.google.com/search?q=VEHICLE+DYNAMIC+MOTION+EFFECT&hl=en&start=10&sa=N

the nominal tire radius because the tire deforms under its vertical load. The tire relaxation length σ_κ (length that determines the transient response of the tire force F_x at the tire's rated load) is the ratio of the slip stiffness to longitudinal force stiffness. It determines the transient response of F_x to slip as in Table A10. 1, which shows the tire model variables. This figures display the forces from the ground on the tire. The normal convention for F_z is positive downward, representing the vertical load on the tire and the force from the tire on the ground. If the tire was rigid and did not slip, it would roll and translate as $V_x = r_e\Omega$, with Ω as the angular velocity. In reality, even a rigid tire slips, and a tire develops a longitudinal force F_x only in response to slip. The wheel slip velocity V_{sx} and slip κ are described in Eq. A10.1 and Eq.A10.4.

$$V_{sx} = V_x - r_e\Omega \neq 0 \qquad \text{(Wheel Slip Velocity)} \quad \text{Eq. A10. 1}$$

$$k = -V_{sx} / |V_x| \qquad \text{(Wheel Slip)} \quad \text{Eq. A10. 2}$$

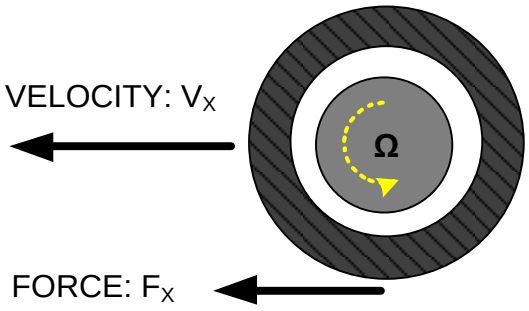

Fig. A10. 1 Tire Model Variables

(Note: For a locked, sliding tire, $\kappa = -1$, For perfect rolling, $\kappa = 0$:)

$$k' = -V'_{sx} / |V_x| \qquad \text{(Contact Point Slip)} \quad \text{Eq. A10. 3}$$

$$V'_{sx} = V_{sx} - r_e\Omega' \qquad \text{(Contact Point Slip Velocity)} \quad \text{Eq. A10. 4}$$

Table A10. 1 Tire Model Variables and Constants

Symbol	Meaning and Unit
r_e	Effective rolling radius (m)
I_w	Wheel-tire assembly inertia (kg·m^2)
τ_{drive}	Torque applied by the axle to the wheel (N·m)
V_x	Wheel center longitudinal velocity (m/s)
Ω	Wheel angular velocity (rad/s)
Ω'	Contact point angular velocity (rad/s)
$V_{sx} = V_x - r_e\Omega$	Wheel slip velocity (m/s)
$V'_{sx} = V_x - r_e\Omega'$	Contact point slip velocity (m/s)
$\kappa = -V_{sx}/\lvert V_x\rvert$	Wheel slip
$\kappa' = -V'_{sx}/\lvert V_x\rvert$	Contact patch slip
u	Tire longitudinal compliance or deformation (m)
F_z	Vertical load on tire (N)
$F_x = f(\kappa', F_z)$	Longitudinal force exerted by the tire on the wheel at the contact point (N). Also a characteristic function f of the tire.
$C_{Fx} = (\partial F_x/\partial u)_0$	Tire longitudinal stiffness (N/m)
$\sigma_\kappa = (\partial F_x/\partial \kappa')_0/(C_{Fx})$	Tire relaxation length (m)

The tire is also flexible. Because it deforms, the contact point turns at a slightly different angular velocity Ω' from the wheel. The tire deformation u directly measures the difference of wheel and contact point slip and satisfies Eq. A10.5. The model inputs are vertical load F_z and the contact slip κ'. The tire characteristic function specifies this relationship in the steady state is described in Eq. A10.6.

$$\frac{du}{dt} = V'_{sx} - V_{sx} \qquad \text{Eq. A10. 5}$$

$$F_x = f(k', F_z) \qquad \text{Eq. A10. 6}$$

The contact slip κ' in turn depends on the deformation u. The longitudinal force F_x is approximately proportional to the vertical load because F_x is generated by contact friction and the normal force F_z. (The relationship is somewhat non-linear because of tire deformation and slip.) The dependence on F_x on κ' is more complex. The tire model incorporates transient as well as steady-state behavior and is thus appropriate for starting from, and coming to, a stop. Because

a rolling, stressed tire is not in a steady state, the contact slip κ′ and deformation u are not constant. Before they can be used in the characteristic function, for which their time evolution must be accounted. In this model, u and κ′ are moderate to small. The relationships of F_x to u and u to κ′ are then linear as formulated in Eq. A10.7 These properties are taken from empirical tire data. The deformation u evolves according to Eq.A10.10

$$F_x = C_{F_x}.u = C_{F_k}.k' \qquad \text{Eq. A10. 7}$$

$$C_{F_x} = \left(\frac{\partial F_x}{\partial u}\right)_{u=0} \qquad \text{Eq. A10. 8}$$

$$C_{F_k} = \left(\frac{\partial F_x}{\partial k'}\right)_{k'=0} \qquad \text{Eq. A10. 9}$$

$$u = \sigma_k.k' \qquad \text{Eq. A10. 10}$$

$$\sigma_k = \left(\frac{\partial F_x}{\partial k'}\right)_{k'=0} \Big/ \left(\frac{\partial F_x}{\partial k'}\right)_{u=0} = C_{F_k} \Big/ C_{F_x} \qquad \text{Eq. A10. 11}$$

$$\frac{du}{dt} + \left(\frac{1}{\sigma_k}\right).|V_x|.u = -V_{sx} \qquad \text{Eq. A10. 12}$$

The slip κ′ follows from σ_κ and u. The tire behaves like a driven damper of damping rate $|V_x|/\sigma_\kappa$. At low speeds, the slip remains finite, and the tire behaves more like a circular spring of stiffness C_{Fx}. In this limit, the linear approximation relating contact slip κ′ and deformation *u* becomes singular if damping is not explicitly included. This relationship can be modified as:

$$k' = \frac{u}{\sigma_k} \rightarrow k' = \left(\frac{u}{\sigma_k} - \frac{k_{V,low}}{C_{F_K}} V_{sx}\right) \qquad \text{Eq. A10. 13}$$

Where smooth transition from zero speed is provided by:

$$k_{V,low} = \begin{cases} \frac{1}{2} k_{V,low}(0)\left\{1+\cos\left(\pi \frac{|V_x|}{V_{low}}\right)\right\} & \forall \left(|V_x| \le V_{low}\right) \\ 0 & \forall \left(|V_x| \ge V_{low}\right) \end{cases} \qquad \text{Eq. A10. 14}$$

Manifestly nonsingular forms of the tire evolution valid at vanishing speeds are:

$$\left(\frac{1}{C_{F_x}}\right).\frac{dF_x}{dt} + |V_x|.k' = -V_{sx} \qquad \text{Eq. A10. 15}$$

$$\left(\frac{1}{C_{F_x}}\right).\frac{\partial F_x}{\partial k'}\frac{dk'}{dt} + |V_x|.k' = -V_{sx} - \left(\frac{1}{C_{F_x}}\right).\frac{\partial F_x}{\partial F_z}\frac{dF_z}{dt} \qquad \text{Eq. A10. 16}$$

The second form explicitly shows the dependence on a varying vertical load F_z. Finding the wheel and vehicle motion, with the tire characteristic function $f(\kappa', F_z)$, the vertical load F_z, and the evolved u and κ', you can find the longitudinal force F_x and wheel velocity Ω. From these, the equations of motion determine the wheel angular motion (the angular velocity Ω) and longitudinal motion (the wheel center velocity V_x) as:

$$I_\omega.\frac{d\Omega}{dt} = \tau_{drive} - r_e F_x \qquad \text{Eq. A10. 17}$$

$$m\frac{dV_x}{dt} = F_x - mg.\sin\beta \qquad \text{Eq. A10. 18}$$

Where β is the slope of the incline upon which the vehicle is traveling (positive for uphill), and *m* and *g* are the wheel load mass and the gravitational acceleration, respectively. τ_{drive} is the drive shaft torque applied to the wheel axis.

Appendix 11 PAVEMENT GEOMETRY PARAMETERS

TABLE 12A -01P -MODELS ROADWAY VARIABLES AND PARAMETERS					
	SYMBOL	PAVEMENT GEOMETRY AND (PG_{VECTOR})	UNIT	FROM	TO
PR-101	RSN	ROADWAY SEGMENT NUMBER	NA	SEG-01	SEG-100
PR-102	RPW	ROADWAY PAVEMENT WIDTH	M	6	40
PR-103	RPL	ROADWAY PAVEMENT LENGTH	M	150	1500
PR-104	NOL	NUMBER OF LANES	NA	1	12
PR-105	RSA	ROADWAY VERTICAL SLOPE ANGEL	PERCENT	0	5%
PR-106	V_{SAF}	ROADWAY HORIZENTAL SLOPE ANGEL	PERCENT	0	2%
PR-107	PT	PAVEMENT TYPE	NA	FP	RP
PR-108	RVCD	ROADWAY VERTICAL CURVE-DEGREE	DEGREE		
PR-109	RVCR	ROADWAY VERTICAL CURVE-RADIUS	M		
PR-110	RHCD	ROADWAY HORIZENTAL CURVE-DEGREE	DEGREE		
PR-111	RHCR	ROADWAY HORIZENTAL CURVE-RADIUS	M		

TABLE 12-02 P -MODELS PAVEMENTSTRUCTURE VARIABLES AND PARAMETERS					
	SYMBOL	PAVEMENT STRUCTURE GEOMETRY ($PSG-_{VECTOR}$)	TYPE	UNIT	VALUE
PR-112	$PSID_{THICKNESS}$	FLEXIBLE PAVEMENT SURFACE COURSE THICKNESS	SCALER	NA	50
PR-113	$FPS_{THICKNESS}$	FLEXIBLE PAVEMENT SURFACE COURSE THICKNESS	SCALER	MM	50
PR-114	$FPB_{THICKNESS}$	FLEXIBLE PAVEMENT BASE COURSE MIX THICKNESS	SCALER	MM	75
PR-115	$FPSB1_{THICKNESS}$	FLEXIBLE PAVEMENT SUBBASE LAYER 1, ASPHALT TREAT DRAINAGE COURSE THICKNESS	SCALER	MM	
PR-116	$FPSB2_{THICKNESS}$	FLEXIBLE PAVEMENT SUBBASE LAYER 2, CENTER STABLIZER BASE COURSE THICKNESS	SCALER	MM	
PR-117	$FPSB3_{THICKNESS}$	FLEXIBLE PAVEMENT SUBBASE LAYER 3, AGGREGATE SUBBASE COURSE THICKNESS	SCALER	MM	300
PR-118	$FPSB4_{THICKNESS}$	FLEXIBLE PAVEMENT SUBBASE LAYER 4, SELECTED LAYER SUBBASE COURSE THICKNESS	SCALER	MM	
PR-119	$FPSG_{THICKNESS}$	FLEXIBLE PAVEMENT SUBGRADE COURSE THICKNESS	SCALER	MM	500
PR-120	$RPS_{THICKNESS}$	RIGID PAVEMENT SURFACE COURSE THICKNESS	SCALER	MM	100
PR-121	$RPB_{THICKNESS}$	RIGID PAVEMENT BASE COURSE MIX THICKNESS	SCALER	MM	100
PR-122	$RPSB_{THICKNESS}$	RIGID PAVEMENT SUBBASE COURSE THICKNESS	SCALER	MM	100
PR-123	$RPSG_{THICKNESS}$	RIGID PAVEMENT SUBGRADE COURSE THICKNESS	SCALER	MM	100
PR-124	$FPRS1_{THICKNESS}$	FLEXIBLE PAVEMENT RE-SURFACE LAYER - THICKNESS 1	SCALER	MM	15
PR-125	$FPRS2_{THICKNESS}$	FLEXIBLE PAVEMENT RE-SURFACE LAYER - THICKNESS 2	SCALER	MM	20
PR-126	$FPRS3_{THICKNESS}$	FLEXIBLE PAVEMENT RE-SURFACE LAYER - THICKNESS 3	SCALER	MM	25
PR-127	$FPRS4_{THICKNESS}$	FLEXIBLE PAVEMENT RE-SURFACE LAYER - THICKNESS	SCALER	MM	30

		4			

PAVEMENT UNIT TYPE FP1 GEOMETRY MODELING PARAMETERS						
TABLE 12A-03A -P -MODELS PAVEMENTSTRUCTURE VARIABLES AND PARAMETERS						
		FLEXIBLE PAVEMENT MESH GEOMETRY (FPMG-$_{VECTOR}$)	**LAYER NO.**	**PU GEOMETRY**		
	SYMBOL			**C_X**	**C_Y**	**C_Z**
PR-127	**TYPE 1-FP$_{SURFACE}$**	FLEXIBLE PAVEMENT SURFACE COURSE VECTOR	1	50	50	25
PR-128	**TYPE 1-FP$_{BASE}$**	FLEXIBLE PAVEMENT BASE COURSE MIX VECTOR	2	50	50	25
PR-129	**TYPE 1-FP$_{SUBBASE1}$**	FLEXIBLE PAVEMENT SUBBASE LAYER 1, ASPHALT TREAT DRAINAGE COURSE VECTOR 1	3--1	50	50	50
PR-130	**TYPE 1-FP$_{SUBBASE2}$**	FLEXIBLE PAVEMENT SUBBASE LAYER 2, CENTER STABLIZER BASE COURSE VECTOR 1	3--2	50	50	50
PR-131	**TYPE 1-FP$_{SUBBASE3}$**	FLEXIBLE PAVEMENT SUBBASE LAYER 3, AGGREGATE SUBBASE COURSE VECTOR 1	3--3	50	50	50
PR-132	**TYPE 1-FP$_{SUBBASE4}$**	FLEXIBLE PAVEMENT SUBBASE LAYER 4, SELECTED LAYER SUBBASE COURSE VECTOR 1	3--4	50	50	50
PR-133	**TYPE 1-FP$_{SUBGRADE}$**	FLEXIBLE PAVEMENT SUBGRADE COURSE VECTOR 1	4	50	50	100
PR-134	**TYPE 1-FP$_{SUBGRADE}$**	FLEXIBLE PAVEMENT RE-SURFACE LAYER - THICKNESS 1 VECTOR	1	50	50	15
PR-135	**TYPE 1-FP$_{SUBGRADE}$**	FLEXIBLE PAVEMENT RE-SURFACE LAYER - THICKNESS 2 VECTOR	1	50	50	20
PR-136	**TYPE 1-FP$_{SUBGRADE}$**	FLEXIBLE PAVEMENT RE-SURFACE LAYER - THICKNESS 3 VECTOR	1	50	50	25
PR-137	**TYPE 1-FP$_{SUBGRADE}$**	FLEXIBLE PAVEMENT RE-SURFACE LAYER - THICKNESS 4 VECTOR	1	50	50	30

PAVEMENT UNIT TYPE FP1 GEOMETRY MODELING PARAMETERS										
TABLE 12A -03 B P -MODELS PAVEMENTSTRUCTURE VARIABLES AND PARAMETERS										
MESHE DENSITY KG/M3	**NO. MESHE LAYERS**	**NO. PAVEMENT UNITES**	**PMAS**	**PNAS**	**POISSON RATIOS**			**ELASTIC MODULES (GPA)**		
					AGR.	**ASP.**	**EQ.**	**AGR.**	**ASP.**	**EQ.**
2082.0	2	4	19	13	0.4	0.3	0.3	0.15	5	3.4
1842.0	2	8	26	20	0.35	0.35	0.25	0.5	0.25	5.2
1842.0	1.5	8	52	40	0.4	0.35	0.2	0.5	0.25	6
1842.0	1	8	52	40	0.3	0.35	0.2	0.75	0.25	6
1842.0	2	8	52	40	0.3	0.35	0.2	0.5	0.25	6
1842.0	6	8	52	40	0.35	0.35	0.2	0.4	0.25	6
1600	0	8	52	40	0.42	0.25	0.42	0.15	0.2	7
2082.0	10	4	6.5	5	0.4	0.3	0.3	0.15	5	3.10
2082.0	2	4	6.5	5	0.4	0.3	0.3	0.15	5	3.10
2082.0	2	4	9.1	7	0.4	0.3	0.3	0.15	5	3.10
2082.0	2	4	9.1	7	0.4	0.3	0.3	0.15	5	3.10

PAVEMENT UNIT TYPE FP1 GEOMETRY MODELING PARAMETERS								
TABLEA12A -03 C (PU1)P -MODELS PAVEMENTSTRUCTURE VARIABLES AND PARAMETERS								
MMD_1			MVD_1				MGF_1	MDF_1
AGGREGATE	FILLER	BINDER	AGR.	FILLER	ASP.	AIR VOID		
75%	18%	7%	65%	7%	22%	6%	1	1
75%	25%		88%	7%		5%	1	1
75%	25%		88%	7%		5%	1	1
75%	25%		88%	7%		5%	1	1
80%	20%		88%	7%		5%	1	1
80%	20%		88%	7%		5%	1	1
90%	10%		90%	5%		5%	1	1
75%	15%	10%	65%	7%	19%	9%	1	1
75%	15%	10%	65%	7%	20%	9%	1	1
75%	15%	10%	65%	7%	20%	8%	1	1
75%	15%	10%	65%	7%	21%	8%	1	1

PAVEMENT UNIT TYPE RP1 GEOMETRY MODELING PARAMETERS						
P -MODELS PAVEMENTSTRUCTURE VARIABLES AND PARAMETERS TABLE -04A						
		FLEXIBLE PAVEMENT MESH GEOMETRY ($FPMG_{-VECTOR}$)	LAYER NO.	PU GEOMETRY		
	SYMBOL			C_X	C_Y	C_Z
PR-138	**TYPE 1-$RP_{SURFACE}$**	RIGID PAVEMENT SURFACE COURSE VECTOR 1	8	50	50	50
PR-139	**TYPE 1-RP_{BASE}**	RIGID PAVEMENT BASE COURSE MIX VECTOR 1	9	50	50	50
PR-140	**TYPE 1-$RP_{SUBBASE}$**	RIGID PAVEMENT SUBBASE COURSE VECTOR 1	10	50	50	50
PR-141	**TYPE 1-$RP_{SUBGRAD}$**	RIGID PAVEMENT SUBGRADE COURSE VECTOR 1	11	50	50	50

PAVEMENT UNIT TYPE RP1 GEOMETRY MODELING PARAMETERS										
TABLE A12 -04 B P -MODELS PAVEMENTSTRUCTURE VARIABLES AND PARAMETERS										
MESHE DENSITY KG/M3	NO. MESHE LAYERS	NO. PAVEMENT UNITES	PMAS	PNAS	POISSON RATIOS			ELASTIC MODULES (GPA)		
					AGR.	PCC.	FINE.	PCC	PCC	FINE
2000	10	4	9.1	7	0.25	0.15	0.35	0.20	27.57	0.13
1500	2	8	13	10	0.25	0.35	0.35	0.21	**0.4**	0.13
1500	2	4	13	10	0.22	0.35	0.35	0.21	**0.4**	0.13

1500	2	4	13	10	0.22	0.2	0.35	0.21	**0.2**	0.13

PAVEMENT UNIT TYPE RP1 GEOMETRY MODELING PARAMETERS								
TABLE A12 -04 C (PU1)P -MODELS PAVEMENTSTRUCTURE VARIABLES AND PARAMETERS								
MMD_1			MVD_1					
AGGREGATE	CEMENT	FINE A.	AGGREGATE	PCC	FINE A.	AIR	MGF_1	MDF_1
0.408	0.267	0.325	0.3	0.3	0.3	99.0	1	1
0.408	0.267	0.325	0.3	0.3	0.3	99.0	1	1
0.415	0.261	0.324	0.3	0.3	0.3	99.0	1	1
0.415	0.261	0.324	0.3	0.3	0.3	99.0	1	1

MMD :	*PAVEMENT UNIT - MESH MASS DENSITY*
MVD :	PAVEMENT UNIT - MESH VOLUME DENSITY
MGF :	PAVEMENT UNIT - MESH GEOMETRY FACTOR
MDF :	PAVEMENT UNIT - MESH DISTRIBUTION FACTOR
PMAS :	PAVEMENT LAYER: MAXIMUM AGGREGATE SIZE, The smallest sieve through which 100 percent of the aggregate sample particles pass. SuperPave defines the maximum aggregate size as "one sieve larger than the nominal maximum size.”
PNAS :	PAVEMENT LAYER: NOMINAL AGGREGATE SIZE, The largest sieve that retains some of the aggregate particles but generally not more than 10 percent by weight. Super-pave defines nominal maximum aggregate size as "one sieve size larger than the first sieve to retain more than 10 percent of the material aggregate size” as "one sieve larger than the nominal maximum size.”

Appendix 12 M MODELS VEHICLE MOBILITY PARAMETERS

Table A12. 1 VMM General Vector

M -MODELS VARIABLES AND PARAMETERS				
NO	***SYMBOL***	***DYNAMIC MATRIX ($D_{MATRIXS}$)***	***TYPE***	***UNIT***
PR-001	VW_{CN}	VEHICLE WEIGHT DISTRIBUTION CASE NUMBER	SCALER	1 TO 5
PR-002	VG_{CN}	VEHICLE GENERATION CASE NUMBER	SCALER	1 TO 4
PR-003	VTP_{CN}	VEHICLE TIRE PRESURE CASE NUMBER	SCALER	1 OR 2
PR-004	$VDPA_{CN}$	VEHICLE DYNAMIC PARAMETER ANALYSING CASE NUMBER	SCALER	0 OR 1
PR-005	$THRESHOLD_1$	TRAFFIC FLOW RATE DIFFERENTIAL THRESHOLD 1	SCALER	5%
PR-006	$THRESHOLD_2$	TRAFFIC FLOW RATE DIFFERENTIAL THRESHOLD 2	SCALER	7 %
PR-007	$THRESHOLD_3$	TRAFFIC DENSITY RATE LANE DISTRIBUTION THRESHOLD 3	SCALER	500%
PR-008	$THRESHOLD_4$	PLATOON ASSIGNMENT THRESHOLD	SCALER	15%
PR-009	VMSR	VEHICLE MOVEMENT SIMULATION RESULOTION	SCALER	5

Table A12. 2 VMM- Dynamic Vehicle Matrix

M -MODELS VARIABLES AND PARAMETERS				
NO	***SYMBOL***	***DYNAMIC MATRIX ($D_{MATRIXS}$)***	***TYPE***	***UNIT***
VR-001	$V_{TN}(G,I)$	VEHICLE TRACKING NUMBER MATRIX (LANE, CLASS)	MATRIX	8 x 14
VR-002	$L_{TN}(G)$	VEHICLE TRACKING NUMBER VECTOR (LANE)	VECTOR	8
VR-003	t	TIME START FROM FIRST VEHICLE PASS THE X_0 LINE	SCALAR	SEC
VR-004	V_{DW}	VEHICLE DYNAMIC WEIGHT	SCALAR	KG
VR-005	V_{TH}	VEHICLE HEARWAY SPACE	SCALAR	M
VR-006	T_{HW}	VEHICLE HEADWAY TIME	SCALAR	SEC
VR-007	A_{COUNT}	TOTAL NO. OF AXELS ON A LANE DURING THE SIMULATION	SCALAR	NA
VR-008	$M_{PATTERN}$	MATRIX OF TRAFFIC PATERN	MATRIX	96 x 12
VR-009	$M_{PATTERN-C}$	MATRIX OF TRAFFIC PATERN FOR CLASS I ONLY, I FROM 1 TO 14	MATRIX	96 x 12
VR-010	$M_{PATTERN(L-C)}$	TRAFFIC PATERN FOR CLASS I ONLY,(I= 1 TO 14) & G = 1 TO R_{LN}	MATRIX	96

Table A12. 3 VMM- Force Vector

M -MODELS VARIABLES AND PARAMETERS				
	SYMBOL	***FORCE VECTOR (F_{VECTOR})***	***TYPE***	***UNIT***
VR-011	$F_z(x,y,0,t)$	VEHICLE VERTICAL LOAD FORCE AT THE GROUND CONTACT POINT	SCALAR	NEWTON
VR-012	$F_z(x,y,z,t)$	VEHICLE VERTICAL LOAD FORCE AT TIME "t" AND POINT (X, Y, Z)	SCALAR	NEWTON

VR-013	F_x (x,y,0,t)	VEHICLE LONGITUNAL LOAD FORCE AT THE GROUND CONTACT POINT	SCALAR	NEWTON
VR-014	F_x (x,y,z,t)	VEHICLE LONGITUNAL LOAD FORCE AT TIME t AND POINT (X,Y,Z)	SCALAR	NEWTON
VR-015	F_z(x,y, 0)	AVERAGE VERTICAL FORCE AT PLANE (X, Y); AT PAVEMENT SURFACE Z=0	SCALAR	NEWTON
VR-016	FD_x (x,y,0,t)	AERODYNAMIC DRAG FORCE	SCALAR	NEWTON

Table A12. 4 VMM- Traffic Matrix

M -MODELS VARIABLES AND PARAMETERS					
	SYMBOL	***TRAFFIC VECTOR (T_{VECTOR})***	***TYPE***	***UNIT***	***VALUE***
VR-018	VP_{NUMBER}	NUMBER OF TIME WINDOWS, TRAFFIC PATTERN, IN THE PROFILES	SCALAR	NA	4 TO 24
VR-019	ADT	AVERAGE DAILY TRAFFIC	SCALAR	VEH/DAY	
PR-081	V_F	TRAFFIC FLOW RATE (TIME WINDOW VECTOR)	VECTOR	Veh./Hrs.	INPUT
PR-082	V_S=V_X (t)	VEHICLE SPEED (X DIRECTION)	VECTOR	M/S	INPUT
PR-083	V_A (t)	VEHICLE ACCELERATION	VECTOR	M/S^1	INPUT
PR-084	V_D (t)	VEHICLE ROAD DENSITY	SCALAR	Veh/KM . Ln	85
PR-085	H_{MAX}	HEADWAY AT MINIMUM DENCITY	SCALAR	M	50
PR-086	H_{MIN}	HEADWAY AT MAXIMUM DENCITY	SCALAR	M	100
PR-087	TSP	TRAFFIC SAMPLE PERIOD	SCALAR	Hr	1/4 TO 1

Table A12. 5 Roadway Vector

M -MODELS VARIABLES AND PARAMETERS					
	SYMBOL	***ROADWAY VECTOR (R_{VECTOR})***	***TYPE***	***UNIT***	***VALUE***
PR-088	R_N	ROADWAY NAME	TEXT	NA	INPUT
PR-089	R_{ID}	ROADWAY ID	SCALAR	NA	8 DIGITS
PR-090	R_C	ROADWAY CLASS	SCALAR	NA	1 TO 5
PR-091	R_{LN}	ROADWAY LANE NUMBER	SCALAR	NA	INPUT
PR-092	R_S	ROADWAY SLOP	SCALAR	%	INPUT
PR-093	R_{LW}	ROADWAY LANE WIDTH	SCALAR	M	3.6
PR-094	R_{HC}	ROAD HORIZENTAL CARVE	SCALAR	%	INPUT
PR-095	$OFFSET_{MAX}$	MAXIMUM OFFSET VALUE	SCALAR	CM	50

Table A12. 6 Vehicle Classification Vector

M -MODELS VARIABLES AND PARAMETERS							
NO	***SYMBOL***	***VEHICLE CLASS VECTOR (VC_{VECTOR})***	***TYPE***	***UNIT***	***VALUE CLASS-01***	***VALUE CLASS-02***	***VALUE CLASS-03***
PR-010	V_{CN}	VEHICLE CLASS NUMBER	SCALAR	NA	1	2	3
PR-011	T_W	TIRE WIDE	SCALAR	CM	15	20	25

PR-012	T_P	TIRE PRESSURE	SCALAR	Pascal	30	40	45
PR-013	V_{NA}	VEHICLE NO. OF AXELS	SCALAR	NA	2	3	4
PR-014	V_{NT}	VEHICLE NO. OF TRAILER/ TRACTOR	SCALAR	NA	0	0	0
PR-015	V_L	VEHICLE LENGTH	SCALAR	M	4	6	12
PR-016	V_W	VEHICLE WIDE (A VEHICLE CLASS FACTOR)	SCALAR	M	2	2.2	2.2
PR-017	V_M	VEHICLE MASS	SCALAR	KG	1500	21560	37300
PR-018	V_{FLM}	VEHICLE FULL LOADED MASS	SCALAR	KG	2400	34496	59680
PR-019	V_{EFA}	VEHICLE EFFECTIVE FRONTAL CROSS-SECTION AREA	SCALAR	M^2	3	4.4	6
PR-020	CG	VEHICLE CENTER OF GRAVITY POINT	SCALAR	NA			
PR-021	h	VEHICLE CG HEIGHT (A VEHICLE CLASS FACTOR)	SCALAR	M	0.5	1	1.5
PR-022	a	VEHICLE CG DISTANCE TO FRONT TIRE	SCALAR	M	1.4	3	5
PR-023	b	VEHICLE CG DISTANCE TO REAR TIRE	SCALAR	M	1.6	1	3
PR-024	c	VEHICLE CG DISTANCE TO SECOND AXEL	SCALAR	M	NA	2	2
PR-025	d	VEHICLE CG DISTANCE TO THIRD AXEL	SCALAR	M	NA	NA	2
PR-026	e	VEHICLE CG DISTANCE TO FOURTH AXEL	SCALAR	M	NA	NA	1
PR-027	C_d	AERODYNAMIC DRADG COEFFICENT	SCALAR	N•s2/KG•m	0.35	0.45	0.5
PR-028	ρ	MASS DENSITY OF AIR	SCALAR	kg/m^3	1.2	1.2	1.2
PR-029	V_{PI}	VEHICLE PASSING INDEX	SCALAR	NA	35%	20%	10%
PR-030	V_{LCI}	VEHICLE LANE CHANGE INDEX	SCALAR	NA	15%	10%	2%
PR-031	$V_{MIN-HEADWAY}$	VEHICLE MINIMUM HEARWAY	SCALAR	S	1.5	3	5
PR-032	$V_{LUF}(1)$	VEHICLE LANE UTILIZATION FACTOR FOR LANE 1	SCALAR	NA	1	1	1
PR-033	$V_{LUF}(2)$	VEHICLE LANE UTILIZATION FACTOR FOR LANE 2	SCALAR	NA	1	1	1
PR-034	$V_{LUF}(3)$	VEHICLE LANE UTILIZATION FACTOR FOR LANE 3	SCALAR	NA	1	0.85	0.8
PR-035	$V_{LUF}(4)$	VEHICLE LANE UTILIZATION FACTOR FOR LANE 4	SCALAR	NA	0.95	0.8	0.75
PR-036	$V_{LUF}(5)$	VEHICLE LANE UTILIZATION FACTOR FOR LANES 5, 6, 7 AND 8	SCALAR	NA	0.92	0.75	0.7
PR-037	V_{CDF}	VEHICLE CLASS DISTIBUTION FACTORS	VECTOR	14	75%	20%	5%
PR-038	V_{CSF}	VEHICLE CLASS SPEED FACTORS	VECTOR	14	1.25	0.75	0.50
PR-039	V_{CSF}	VEHICLE CLASS ACCELARATOR FACTORS	VECTOR	14	1.00	0.80	0.50
PR-040	CA	CONSTANT A	SCALAR	NA	7200	206976	596800
PR-041	CB	CONSTANT B	SCALAR	NA	500	3593.333	3730
PR-042	μ_{OFFSET}	AVERAGE OF VEHICLE MOVEMENT OFFSET	SCALAR	CM	0	0	0
PR-043	o_{ffset}	VARRIANCE OF VEHICLE MOVEMENT OFFSET	SCALAR	CM^2	100	400	625

PR-044	μ_{TPV}	AVERAGE OF VEHICLE TIRE PAVEMENT CONTACT LENGHT	SCALAR	CM	10	20	25
PR-045	σ_{TPV}	VARRIANCE OF VEHICLE TIRE PAVEMENT CONTACT LENGHT	SCALAR	CM^2	100	160	160
PR-046	μ_{VDW}	DAILY AVERAGE OF VEHICLE DYNAMIC WEIGHT	SCALAR	KG	525	7546	13055
PR-047	σ_{VDW}	DAILY VARRIANCE OF VEHICLE DYNAMIC WEIGHT	SCALAR	KG^2	2500	4900	6400
PR-048	$LOAD_{AXCEL0}$	VEHICLE LOAD AT AXCEL 0 (FOR CLASS 2 OR HIGHER VEHICLE)	SCALAR	KG	NA	7000	8180
PR-049	$LOAD_{AXCEL1}$	VEHICLE LOAD AT AXCEL 1 (FOR CLASS 2 OR HIGHER VEHICLE)	SCALAR	KG	NA	7280	7280
PR-050	$LOAD_{AXCEL2}$	VEHICLE LOAD AT AXCEL 2 (FOR CLASS 2 OR HIGHER VEHICLE)	SCALAR	KG	NA	7280	7280
PR-051	$LOAD_{AXCEL3}$	VEHICLE LOAD AT AXCEL 3 (FOR CLASS 2 OR HIGHER VEHICLE)	SCALAR	KG	NA	NA	7280
PR-052	$LOAD_{AXCEL4}$	VEHICLE LOAD AT AXCEL 4 (FOR CLASS 2 OR HIGHER VEHICLE)	SCALAR	KG	NA	NA	7280
PR-053	$LOAD_{AXCEL5}$	VEHICLE LOAD AT AXCEL 5 (FOR CLASS 2 OR HIGHER VEHICLE)	SCALAR	KG	NA	NA	NA
PR-054	$LOAD_{AXCEL6}$	VEHICLE LOAD AT AXCEL 6 (FOR CLASS 2 OR HIGHER VEHICLE)	SCALAR	KG	NA	NA	NA

Appendix 13: Micro Structure Model Data


MS 11 Report.html


MS 11 Parameters.txt


MS 10 Report.html


MS 10 Prameters.txt


MS 9 Report.html


MS 9 Parameters.txt

Appendix 14: Micro Electrostatic Generator – Power Estimate

Case 1- Three Layers Micro Structure

ELECTROSTATIC

SCENARIOS ESG-

3-01 TO ESG-3-09

Multi-Layer Parallel

Capacitors

Capacitors Gap

1.5µm to 0.1µm

ε_r = 1, 10 and 1000

	DESIGN PARAMETERS	UNIT	ESG-01	ESG-02	ESG-03	ESG-04	ESG-05	ESG-06	ESG-07	ESG-08	ESG-09
P-01	Capacitor X Size	µm	3300	3300	3300	3300	3300	3300	3300	3300	3300
P-02	Capacitor Y Size	µm	3300	3300	3300	3300	3300	3300	3300	3300	3300
P-03	Capacitor Gap Thickness-Top Layer	µm	10	10	10	10	10	10	10	10	10
P-04	Capacitor Gap Thickness-Mid. Layer 01	µm	3.5	3.5	3.5	3.5	3.5	3.5	3.5	3.5	3.5
P-05	Capacitor Gap Thickness-Mid. Layer 02	µm	0.00	0.00	0.00	0.00	0.00	0.00	0.00	0.00	0.00
P-06	Capacitor Gap Thickness-Mid. Layer 03	µm	0.00	0.00	0.00	0.00	0.00	0.00	0.00	0.00	0.00
P-07	Capacitor Gap Thickness-Mid. Layer 04	µm	0.00	0.00	0.00	0.00	0.00	0.00	0.00	0.00	0.00
P-08	Capacitor Gap Thickness-Mid. Layer 05	µm	0.00	0.00	0.00	0.00	0.00	0.00	0.00	0.00	0.00
P-09	Capacitor Gap Thickness-Mid. Layer 06	µm	0.00	0.00	0.00	0.00	0.00	0.00	0.00	0.00	0.00
P-10	Capacitor Gap Thickness-Mid. Layer 07	µm	0.00	0.00	0.00	0.00	0.00	0.00	0.00	0.00	0.00
P-11	Capacitor Gap Thickness-Mid. Layer 08	µm	0.00	0.00	0.00	0.00	0.00	0.00	0.00	0.00	0.00
P-12	Capacitor Gap Thickness-Lower Layer	µm	1.50	1.50	1.50	1.50	1.50	1.50	1.50	1.50	1.50
P-13	Capacitor Support Plate Thickness Top Layer	µm	25	25	25	25	25	25	25	25	25
P-14	Capacitor Support Plate Thickness Mid. Layer 01	µm	10	10	10	10	10	10	10	10	10
P-22	Capacitor Support Plate Thickness Lower Layer	µm	10	10	10	10	10	10	10	10	10
P-23	Capacitor Isolation Layer Plate Thickness	µm	5	5	5	5	5	5	5	5	5
P-44	Load Class 1-Capacitor Gap Change Top Layer	µm	8.36	8.36	8.36	8.36	8.36	8.36	8.36	8.36	8.36
P-45	Load Class 1Capacitor Gap Change Mid. Layer 01	µm	2.76	2.76	2.76	2.76	2.76	2.76	2.76	2.76	2.76
P-53	Load Class 1Capacitor Gap Change Lower Layer	µm	0.81	0.81	0.81	0.81	0.81	0.81	0.81	0.81	0.81

P-54	Capacitor Isolation Layer Plate Thickness	µm	5	5	5	5	5	5	5	5	5
P-55	A Plate Thickness	µm	5	5	5	5	5	5	5	5	5
P-56	A Free Space	µm	5	5	5	5	5	5	5	5	5
P-57	A Column Capacitor Thickness	µm	155	155	155	155	155	155	155	155	155
P-58	Substrate Thickness	µm	200	201	202	203	204	205	206	207	208
P-59	Charger Structure Thickness	µm	355	356	357	358	359	360	361	362	363
P-60	PERMITIVITY		8.85E-12	8.85E-12	8.85E-12	8.85E-12	8.85E-12	8.85E-12	8.85E-12	8.85E-12	8.85E-12
P-61	Relative Permittivity	NA	1	1	1	1	1	1	1	1	1
P-62	NO. of Capacitors Per Layer	NO	1	1	1	1	1	1	1	1	1
P-63	NO of Capacitor per Column	NO	3	3	3	3	3	3	3	3	3
P-64	NO. OF Capacitor Column (33 x 33)	NO	9	9	9	9	9	9	9	9	9
P-65	Capacitor Value- Top Layer	µF	9.64E-06	9.64E-06	9.64E-06	9.64E-06	9.64E-06	9.64E-06	9.64E-06	9.64E-06	9.64E-06
P-66	Capacitor Value- Mid. Layer 1	**µF**	2.75E-05	2.75E-05	2.75E-05	2.75E-05	2.75E-05	2.75E-05	2.75E-05	2.75E-05	2.75E-05
P-74	Capacitor Value- Lower Layer	**µF**	6.43E-05	6.43E-05	6.43E-05	6.43E-05	6.43E-05	6.43E-05	6.43E-05	6.43E-05	6.43E-05
P-75	Initial Column Capacitor Value	**µF**	1.01E-04	1.01E-04	1.01E-04	1.01E-04	1.01E-04	1.01E-04	1.01E-04	1.01E-04	1.01E-04
P-76	Initial Total Capacitor Value	**µF**	9.13E-04	9.13E-04	9.13E-04	9.13E-04	9.13E-04	9.13E-04	9.13E-04	9.13E-04	9.13E-04
P-101	Load Class 1- Capacitor Change Top Layer	**µF**	2.08E-05	2.08E-05	2.08E-05	2.08E-05	2.08E-05	2.08E-05	2.08E-05	2.08E-05	2.08E-05
P-102	Load Class 1- Capacitor Change Middle Layer 1	**µF**	5.43E-05	5.43E-05	5.43E-05	5.43E-05	5.43E-05	5.43E-05	5.43E-05	5.43E-05	5.43E-05
P-110	Load Class 1- Capacitor Change Lower Layer	**µF**	9.24E-05	9.24E-05	9.24E-05	9.24E-05	9.24E-05	9.24E-05	9.24E-05	9.24E-05	9.24E-05
P-111	Load Class 1-Column Capacitor Value	**µF**	1.67E-04	1.67E-04	1.67E-04	1.67E-04	1.67E-04	1.67E-04	1.67E-04	1.67E-04	1.67E-04
P-112	Load Class 1-Total Capacitor Value	**µF**	1.51E-03	1.51E-03	1.51E-03	1.51E-03	1.51E-03	1.51E-03	1.51E-03	1.51E-03	1.51E-03
P-113	Initial Voltage Source	VDC	3	5	10	3	5	10	3	5	10
P-114	Average Daily Traffic per lane (HHP)		27250	27250	27250	27250	27250	27250	27250	27250	27250
P-117	Daily Activation -Vehicle Class 1 (Freeway: HHP)	NO/Day	98100	98100	98100	98100	98100	98100	98100	98100	98100
P-118	Max Activation Rate nodes(4 Nodes)	%	10%	10%	10%	10%	10%	10%	10%	10%	10%
P-119	Second Activation Rate nodes (4 Nodes)	%	7%	7%	7%	7%	7%	7%	7%	7%	7%
P-120	Third Max Activation Rate nodes (2 Nodes)	%	5%	5%	5%	5%	5%	5%	5%	5%	5%
P-121	Forth d Max Activation Rate nodes (4 Nodes)	%	3%	3%	3%	3%	3%	3%	3%	3%	3%
P-122	Min d Max Activation Rate nodes (8 Nodes)	%	1%	1%	1%	1%	1%	1%	1%	1%	1%
	DESIGN VARIABLES	**UNIT**	**ESG-01**	**ESG-02**	**ESG-03**	**ESG-04**	**ESG-05**	**ESG-06**	**ESG-07**	**ESG-08**	**ESG-09**
CH-01	CAPACITANCE DEFAULT ENERGY	µJ	4.11E-03	1.14E-02	4.56E-02	4.11E-03	1.14E-02	4.56E-02	4.11E-03	1.14E-02	4.56E-02
CH-04	Activation Charge per Vehicle Class 1 Axel Load	µJ	2.68E-03	7.43E-03	2.97E-02	2.68E-03	7.43E-03	2.97E-02	2.68E-03	7.43E-03	2.97E-02
CH-05	Daily Charge Per Vehicle Class3Vehicle	µJ	0.00E+00	0.00E+00	0.00E+00	0.00E+00	0.00E+00	0.00E+00	0.00E+00	0.00E+00	0.00E+00
CH-06	Daily Charge Per Vehicle Class 2 Vehicle	µJ	0.00E+00	0.00E+00	0.00E+00	0.00E+00	0.00E+00	0.00E+00	0.00E+00	0.00E+00	0.00E+00
CH-07	Daily Charge Per Vehicle Class 1 Vehicle	µJ	2.63E+01	7.29E+01	2.92E+02	2.63E+01	7.29E+01	2.92E+02	2.63E+01	7.29E+01	2.92E+02

CH-08	Daily Total Charge	µJ	2.63E+01	7.29E+01	2.92E+02	2.63E+01	7.29E+01	2.92E+02	2.63E+01	7.29E+01	2.92E+02
CH-09	GENERATOR EFFICENCY	NA	8.00E-01	8.00E-01	8.00E-01	8.00E-01	8.00E-01	8.00E-01	8.00E-01	8.00E-01	8.00E-01
CH-10	GENERATION POWER PER SECOND	µW	2.43E-04	6.75E-04	2.70E-03	2.43E-04	6.75E-04	2.70E-03	2.43E-04	6.75E-04	2.70E-03

Case 2- Ten Layers Micro Structure

ELECTROSTATIC SCENARIOS ESG-10-01 TO ESG-10-09

Multi-Layer Parallel Capacitors, Capacitors Gap 1.5µm to 0.1µm, εr = 1, 10 and 1000

	DESIGN PARAMETERS	**UNIT**	**ESG-01**	**ESG-02**	**ESG-03**	**ESG-04**	**ESG-05**	**ESG-06**	**ESG-07**	**ESG-08**	**ESG-09**
P-01	Capacitor X Size	µm	3.3E+02	3.3E+02	3.3E+02	3.3E+02	3.3E+02	3.3E+02	3.3E+02	3.3E+02	3.3E+02
P-02	Capacitor Y Size	µm	3.3E+02	3.3E+02	3.3E+02	3.3E+02	3.3E+02	3.3E+02	3.3E+02	3.3E+02	3.3E+02
P-03	Capacitor Gap Thickness- Top	µm	1.5E+00	1.5E+00	1.5E+00	1.5E+00	1.5E+00	1.5E+00	1.5E+00	1.5E+00	1.5E+00
P-04	Capacitor Gap Thickness- 01	µm	1.2E+00	1.3E+00	1.3E+00	1.3E+00	1.3E+00	1.3E+00	1.3E+00	1.3E+00	1.3E+00
P-05	Capacitor Gap Thickness- 02	µm	1.0E+00	1.0E+00	1.0E+00	1.0E+00	1.0E+00	1.0E+00	1.0E+00	1.0E+00	1.0E+00
P-06	Capacitor Gap Thickness- 03	µm	7.5E-01	7.5E-01	7.5E-01	7.5E-01	7.5E-01	7.5E-01	7.5E-01	7.5E-01	7.5E-01
P-07	Capacitor Gap Thickness- 04	µm	6.0E-01	6.0E-01	6.0E-01	6.0E-01	6.0E-01	6.0E-01	6.0E-01	6.0E-01	6.0E-01
P-08	Capacitor Gap Thickness- 05	µm	4.5E-01	4.5E-01	4.5E-01	4.5E-01	4.5E-01	4.5E-01	4.5E-01	4.5E-01	4.5E-01
P-09	Capacitor Gap Thickness- 06	µm	3.0E-01	3.0E-01	3.0E-01	3.0E-01	3.0E-01	3.0E-01	3.0E-01	3.0E-01	3.0E-01
P-10	Capacitor Gap Thickness- 07	µm	2.0E-01	2.0E-01	2.0E-01	2.0E-01	2.0E-01	2.0E-01	2.0E-01	2.0E-01	2.0E-01
P-11	Capacitor Gap Thickness- 08	µm	1.5E-01	1.5E-01	1.5E-01	1.5E-01	1.5E-01	1.5E-01	1.5E-01	1.5E-01	1.5E-01
P-12	Capacitor Gap Thickness- Lower	µm	1.0E-01	1.0E-01	1.0E-01	1.0E-01	1.0E-01	1.0E-01	1.0E-01	1.0E-01	1.0E-01
P-13	Capacitor Support Plate Thickness Top	µm	2.0E+00	2.0E+00	2.0E+00	2.0E+00	2.0E+00	2.0E+00	2.0E+00	2.0E+00	2.0E+00
P-14	Capacitor Support Plate Thickness- 01	µm	1.0E+00	1.0E+00	1.0E+00	1.0E+00	1.0E+00	1.0E+00	1.0E+00	1.0E+00	1.0E+00
P-15	Capacitor Support Plate Thickness- 02	µm	1.0E+00	1.0E+00	1.0E+00	1.0E+00	1.0E+00	1.0E+00	1.0E+00	1.0E+00	1.0E+00
P-16	Capacitor Support Plate Thickness- 03	µm	1.0E+00	1.0E+00	1.0E+00	1.0E+00	1.0E+00	1.0E+00	1.0E+00	1.0E+00	1.0E+00
P-17	Capacitor Support Plate Thickness- 04	µm	1.0E+00	1.0E+00	1.0E+00	1.0E+00	1.0E+00	1.0E+00	1.0E+00	1.0E+00	1.0E+00
P-18	Capacitor Support Plate Thickness- 05	µm	1.0E+00	1.0E+00	1.0E+00	1.0E+00	1.0E+00	1.0E+00	1.0E+00	1.0E+00	1.0E+00
P-19	Capacitor Support Plate Thickness- 06	µm	1.0E+00	1.0E+00	1.0E+00	1.0E+00	1.0E+00	1.0E+00	1.0E+00	1.0E+00	1.0E+00
P-20	Capacitor Support Plate	µm	1.0E+00	1.0E+00	1.0E+00	1.0E+00	1.0E+00	1.0E+00	1.0E+00	1.0E+00	1.0E+00

	Thickness- 07										
P-21	Capacitor Support Plate Thickness- 08	µm	1.0E+00	1.0E+00	1.0E+00	1.0E+00	1.0E+00	1.0E+00	1.0E+00	1.0E+00	1.0E+00
P-22	Capacitor Support Plate Thickness Lower	µm	1.0E+00	1.0E+00	1.0E+00	1.0E+00	1.0E+00	1.0E+00	1.0E+00	1.0E+00	1.0E+00
P-23	Capacitor Isolation Layer Plate Thickness	µm	1.0E+00	1.0E+00	1.0E+00	1.0E+00	1.0E+00	1.0E+00	1.0E+00	1.0E+00	1.0E+00
P-44	Load Class 1- Capacitor Gap Change Top	µm	1.4E+00	1.4E+00	1.4E+00	1.4E+00	1.4E+00	1.4E+00	1.4E+00	1.4E+00	1.4E+00
P-45	Load Class 1- Capacitor Gap Change- 01	µm	1.2E+00	1.2E+00	1.2E+00	1.2E+00	1.2E+00	1.2E+00	1.2E+00	1.2E+00	1.2E+00
P-46	Load Class 1- Capacitor Gap Change- 02	µm	9.3E-01	9.3E-01	9.3E-01	9.3E-01	9.3E-01	9.3E-01	9.3E-01	9.3E-01	9.3E-01
P-47	Load Class 1- Capacitor Gap Change- 03	µm	7.0E-01	7.0E-01	7.0E-01	7.0E-01	7.0E-01	7.0E-01	7.0E-01	7.0E-01	7.0E-01
P-48	Load Class 1- Capacitor Gap Change- 04	µm	5.6E-01	5.6E-01	5.6E-01	5.6E-01	5.6E-01	5.6E-01	5.6E-01	5.6E-01	5.6E-01
P-49	Load Class 1- Capacitor Gap Change- 05	µm	4.2E-01	4.2E-01	4.2E-01	4.2E-01	4.2E-01	4.2E-01	4.2E-01	4.2E-01	4.2E-01
P-50	Load Class 1- Capacitor Gap Change- 06	µm	2.8E-01	2.8E-01	2.8E-01	2.8E-01	2.8E-01	2.8E-01	2.8E-01	2.8E-01	2.8E-01
P-51	Load Class 1- Capacitor Gap Change- 07	µm	1.9E-01	1.9E-01	1.9E-01	1.9E-01	1.9E-01	1.9E-01	1.9E-01	1.9E-01	1.9E-01
P-52	Load Class 1- Capacitor Gap Change- 08	µm	1.3E-01	1.3E-01	1.3E-01	1.3E-01	1.3E-01	1.3E-01	1.3E-01	1.3E-01	1.3E-01
P-53	Load Class 1- Capacitor Gap Change Lower	µm	5.0E-02	5.0E-02	5.0E-02	5.0E-02	5.0E-02	5.0E-02	5.0E-02	5.0E-02	5.0E-02
P-54	Capacitor Isolation Layer Plate Thickness	µm	1.0E+00	1.0E+00	1.0E+00	1.0E+00	1.0E+00	1.0E+00	1.0E+00	1.0E+00	1.0E+00
P-55	A Plate Thickness	µm	1.0E-01	1.0E+00	1.0E+00	1.0E+00	1.0E+00	1.0E+00	1.0E+00	1.0E+00	1.0E+00
P-56	A Free Space	µm	1.0E+01	1.0E+01	1.0E+01	1.0E+01	1.0E+01	1.0E+01	1.0E+01	1.0E+01	1.0E+01
P-57	A Column Capacitor Thickness	µm	1.2E+02	1.2E+02	1.2E+02	1.2E+02	1.2E+02	1.2E+02	1.2E+02	1.2E+02	1.2E+02
P-58	Substrate Thickness	µm	1.0E+02	1.0E+02	1.0E+02	1.0E+02	1.0E+02	1.0E+02	1.0E+02	1.0E+02	1.0E+02
P-59	Charger Structure Thickness	µm	2.2E+02	2.2E+02	2.2E+02	2.2E+02	2.2E+02	2.2E+02	2.2E+02	2.2E+02	2.2E+02
P-60	Permittivity		8.9E-12	8.9E-12	8.9E-12	8.9E-12	8.9E-12	8.9E-12	8.9E-12	8.9E-12	8.9E-12
P-61	Relative Permittivity	NA	1.0E+00	1.0E+00	1.0E+00	1.0E+01	1.0E+01	1.0E+01	1.0E+03	1.0E+03	1.0E+03
P-62	NO OF CAPACITORS Per Layer	NO	1.0E+00	1.0E+00	1.0E+00	1.0E+00	1.0E+00	1.0E+00	1.0E+00	1.0E+00	1.0E+00
P-63	NO OF Capacitor per Column Layers	NO	1.0E+01	1.0E+01	1.0E+01	1.0E+01	1.0E+01	1.0E+01	1.0E+01	1.0E+01	1.0E+01
P-64	NO. OF Capacitor Column (33 x 33)	NO	1.2E+03	1.2E+03	1.2E+03	1.2E+03	1.2E+03	1.2E+03	1.2E+03	1.2E+03	1.2E+03

P-65	Capacitor Value- Top Layer	µF	6.4E-07	6.4E-07	6.4E-07	6.4E-06	6.4E-06	6.4E-06	6.4E-04	6.4E-04	6.4E-04
P-66	Capacitor Value- Middle Layer 1	**µF**	8.0E-07	7.7E-07	7.7E-07	7.7E-06	7.7E-06	7.7E-06	7.7E-04	7.7E-04	7.7E-04
P-67	Capacitor Value- Middle Layer 2	**µF**	9.6E-07	9.6E-07	9.6E-07	9.6E-06	9.6E-06	9.6E-06	9.6E-04	9.6E-04	9.6E-04
P-68	Capacitor Value- Middle Layer 3	**µF**	1.3E-06	1.3E-06	1.3E-06	1.3E-05	1.3E-05	1.3E-05	1.3E-03	1.3E-03	1.3E-03
P-69	Capacitor Value- Middle Layer 4	**µF**	1.6E-06	1.6E-06	1.6E-06	1.6E-05	1.6E-05	1.6E-05	1.6E-03	1.6E-03	1.6E-03
P-70	Capacitor Value- Middle Layer 5	**µF**	2.1E-06	2.1E-06	2.1E-06	2.1E-05	2.1E-05	2.1E-05	2.1E-03	2.1E-03	2.1E-03
P-71	Capacitor Value- Middle Layer 6	**µF**	3.2E-06	3.2E-06	3.2E-06	3.2E-05	3.2E-05	3.2E-05	3.2E-03	3.2E-03	3.2E-03
P-72	Capacitor Value- Middle Layer 7	**µF**	4.8E-06	4.8E-06	4.8E-06	4.8E-05	4.8E-05	4.8E-05	4.8E-03	4.8E-03	4.8E-03
P-73	Capacitor Value- Middle Layer 8	**µF**	6.4E-06	6.4E-06	6.4E-06	6.4E-05	6.4E-05	6.4E-05	6.4E-03	6.4E-03	6.4E-03
P-74	Capacitor Value- Lower Layer	**µF**	9.6E-06	9.6E-06	9.6E-06	9.6E-05	9.6E-05	9.6E-05	9.6E-03	9.6E-03	9.6E-03
P-75	Initial Column Capacitor Value	**µF**	3.2E-05	3.2E-05	3.2E-05	3.2E-04	3.2E-04	3.2E-04	3.2E-02	3.2E-02	3.2E-02
P-76	Initial Total Capacitor Value	**µF**	3.9E-02	3.9E-02	3.9E-02	3.9E-01	3.9E-01	3.9E-01	3.9E+01	3.9E+01	3.9E+01
P-101	Load Class 1- Capacitor Change Top	**µF**	1.9E-06	1.9E-06	1.9E-06	1.9E-05	1.9E-05	1.9E-05	1.9E-03	1.9E-03	1.9E-03
P-102	Load Class 1- Capacitor Change- 1	**µF**	2.9E-06	2.2E-06	2.2E-06	2.2E-05	2.2E-05	2.2E-05	2.2E-03	2.2E-03	2.2E-03
P-103	Load Class 1- Capacitor Change- 2	**µF**	2.8E-06	2.8E-06	2.8E-06	2.8E-05	2.8E-05	2.8E-05	2.8E-03	2.8E-03	2.8E-03
P-104	Load Class 1- Capacitor Change- 3	**µF**	3.7E-06	3.7E-06	3.7E-06	3.7E-05	3.7E-05	3.7E-05	3.7E-03	3.7E-03	3.7E-03
P-105	Load Class 1- Capacitor Change- 4	**µF**	4.6E-06	4.6E-06	4.6E-06	4.6E-05	4.6E-05	4.6E-05	4.6E-03	4.6E-03	4.6E-03
P-106	Load Class 1- Capacitor Change- 5	**µF**	6.4E-06	6.4E-06	6.4E-06	6.4E-05	6.4E-05	6.4E-05	6.4E-03	6.4E-03	6.4E-03
P-107	Load Class 1- Capacitor Change- 6	**µF**	9.2E-06	9.2E-06	9.2E-06	9.2E-05	9.2E-05	9.2E-05	9.2E-03	9.2E-03	9.2E-03
P-108	Load Class 1- Capacitor Change- 7	**µF**	1.4E-05	1.4E-05	1.4E-05	1.4E-04	1.4E-04	1.4E-04	1.4E-02	1.4E-02	1.4E-02
P-109	Load Class 1- Capacitor Change- 8	**µF**	1.5E-05	1.5E-05	1.5E-05	1.5E-04	1.5E-04	1.5E-04	1.5E-02	1.5E-02	1.5E-02
P-110	Load Class 1- Capacitor Change Lower	**µF**	1.3E-05	1.3E-05	1.3E-05	1.3E-04	1.3E-04	1.3E-04	1.3E-02	1.3E-02	1.3E-02
P-111	Load Class1- Column Capacitor Value	**µF**	7.4E-05	7.3E-05	7.3E-05	7.3E-04	7.3E-04	7.3E-04	7.3E-02	7.3E-02	7.3E-02
P-112	Load Class 1- Total Capacitor	**µF**	9.0E-02	8.9E-02	8.9E-02	8.9E-01	8.9E-01	8.9E-01	8.9E+01	8.9E+01	8.9E+01

	Value										
P-113	Initial Voltage Source	VDC	3.0E+00	5.0E+00	1.0E+01	3.0E+00	5.0E+00	1.0E+01	3.0E+00	5.0E+00	1.0E+01
P-114	Average Daily Traffic per lane (HHP)		2.7E+04	2.7E+04	2.7E+04	2.7E+04	2.7E+04	2.7E+04	2.7E+04	2.7E+04	2.7E+04
P-117	Daily Activation -Vehicle Class 1 (HHP)	Days	9.8E+04	9.8E+04	9.8E+04	9.8E+04	9.8E+04	9.8E+04	9.8E+04	9.8E+04	9.8E+04
P-118	Max Activation Rate nodes(4 Nodes)	%	1.0E-01	1.0E-01	1.0E-01	1.0E-01	1.0E-01	1.0E-01	1.0E-01	1.0E-01	1.0E-01
P-119	2nd Activation Rate nodes (4 Nodes)	%	7.0E-02	7.0E-02	7.0E-02	7.0E-02	7.0E-02	7.0E-02	7.0E-02	7.0E-02	7.0E-02
P-120	3rd Max Activation Rate nodes (2 Nodes)	%	5.0E-02	5.0E-02	5.0E-02	5.0E-02	5.0E-02	5.0E-02	5.0E-02	5.0E-02	5.0E-02
P-121	4rd Max Activation Rate nodes (4 Nodes)	%	3.0E-02	3.0E-02	3.0E-02	3.0E-02	3.0E-02	3.0E-02	3.0E-02	3.0E-02	3.0E-02
P-122	Other Activation Rate nodes (8 Nodes)	%	1.0E-02	1.0E-02	1.0E-02	1.0E-02	1.0E-02	1.0E-02	1.0E-02	1.0E-02	1.0E-02
	DESIGN VARIABLES	**UNIT**	**ESG-01**	**ESG-02**	**ESG-03**	**ESG-04**	**ESG-05**	**ESG-06**	**ESG-07**	**ESG-08**	**ESG-09**
CH-01	CAPACITANCE DEFAULT ENERGY	µJ	1.7E-01	4.8E-01	1.9E+00	1.7E+00	4.8E+00	1.9E+01	1.7E+02	4.8E+02	1.9E+03
CH-04	Activation Charge per Vehicle Class 1 Axle	µJ	2.3E-01	6.3E-01	2.5E+00	2.3E+00	6.3E+00	2.5E+01	2.3E+02	6.3E+02	2.5E+03
CH-05	Daily Charge Per Vehicle Class 3	µJ	0.0E+00	0.0E+00	0.0E+00	0.0E+00	0.0E+00	0.0E+00	0.0E+00	0.0E+00	0.0E+00
CH-06	Daily Charge Per Vehicle Class 2	µJ	0.0E+00	0.0E+00	0.0E+00	0.0E+00	0.0E+00	0.0E+00	0.0E+00	0.0E+00	0.0E+00
CH-07	Daily Charge Per Vehicle Class 1	µJ	2.3E+03	6.2E+03	2.5E+04	2.2E+04	6.2E+04	2.5E+05	2.2E+06	6.2E+06	2.5E+07
CH-08	Daily Total Charge	µJ	2.3E+03	6.2E+03	2.5E+04	2.2E+04	6.2E+04	2.5E+05	2.2E+06	6.2E+06	2.5E+07
CH-09	GENERATOR EFFICENCY	NA	8.0E-01	8.0E-01	8.0E-01	8.0E-01	8.0E-01	8.0E-01	8.0E-01	8.0E-01	8.0E-01
CH-10	GENERATION POWER PER SECOND	µW	2.1E-02	5.8E-02	2.3E-01	2.1E-01	5.8E-01	2.3E+00	2.1E+01	5.8E+01	2.3E+02

Appendix 15: Micro Piezoelectric Generator - Power Estimate

The results of the Micro Piezoelectric generator simulation and calculation are included in the following files:

BIBLIOGRAPHY

[1] H. Homami, D. Crouse, N. Moini "SMART PAVEMENT MATERIAL (SPM) PRE-FEASIBILITY STUDY" TRB Annual meeting 2008

[2] Erick O. Torres, Gabriel A. Rincón-Mora, Electrostatic Energy Harvester and Li-Ion Charger Circuit for Micro-Scale Applications. Georgia Tech Analog and Power IC Design Lab.

[3] J. A. Paradiso and T. Starner "Energy Scavenging for Mobile and Wireless Electronics" Pervasive Computing IEEE COS 2005

[4] B. A. Warneke, Ultra- Low Energy Arch. & Circuits for Cubic Millimeter distributed wireless sensor Net., UC Berkeley

[5] A. Perrig, et al, SPINS: security protocols for sensor networks, ACM MobiCom'01, Rome Italy, 2001

[6] E. Shih, S. Cho, N. Ickes, R. Min, A. Sinha, A. Wang, A. Chandrakasan, Physical layer driven protocol and algorithm design for energy-efficient wireless sensor networks, Proceedings of ACM MobiCom'01, Rome, Italy, July 2001.

[7] I.F. Akyildiz, W. Su*, Y. Sankarasubramaniam, E. Cayirci, wireless sensor networks: a survey, Computer Networks, 02

[8] Telos: Enabling Ultra-Low Power Wireless Research, 4th inter. Symposium on Info. Processing in sensor networks.

[9] I.F. Akyildiz, W. Su*, Y. Sankarasubramaniam, E. Cayirci, wireless sensor networks: a survey, Computer Networks, 02

[10]http://www.monroe.com/en-US/support/Technical-Training/Understanding-Vehicle-Dynamics

[11] DJ Cole and D. Cebon; TRUCK TIRES, SUSPENSION DESIGN AND ROAD DAMAGE; Cambridge University Engineering Department, Trumpington St, Cambridge, CB2 1PZ

[12] Yong K. Cho, Thaddaeus Bode, Yong-Rak Kim, "Infrared Thermography-Driven Flaw Detection and Evaluation of Hot Mix Asphalt Pavements" 2010.

[13] Martin H. Sadd, Qingli Dai, Venkit Parameswaran, Arun Shukla, "Simulation of Asphalt Materials using a Finite Element Micromechanical Model with Damage Mechanics: TRB Annual meeting 2003.

[14]Francisco Thiago Sacramento Aragão, "Computational Microstructure Modeling of Asphalt Mixtures Subjected to Rate-Dependent Fracture" University of Nebraska-Lincoln, Dissertation 2011.

[15] David Cebon, Handbook of Vehicle- Road Interaction, Swets & Zeitlinger Publishers

[16] http://www.nra.co.za

[17] http://training.ce.washington.edu

[18] http://www.tfhrc.gov

[19] ACPA-Associated Construction Publications, 7/2/2008

[20] Australian Pavement Asphalt Institute, Advisory Note 2, 2003

[21] Asphalt Binders, Dave Anderson, Jack Youtcheff, Mike Zupanick, TRB

[22] U. Pfeiffer, "Miniaturized Thermal Generators" International Newsletter on Micro-Nano Integration Vol. 4/05.

[23] Yen Kheng Tan and Sanjib Kumar Panda, "Review of Energy Harvesting Technologies for Sustainable Wireless Sensor Network", www. intechopen.com

[24] http://www.customthermoelectric.com/powergen/pdf/1261G-7L31-04CL_spec_sht.pdf

[25] Brian K. Diefenderfer, " Moisture Content Determination and Temperature Profile Modeling of Flexible Pavement Structures" Dissertation Report University of Virginia

[26]http://www.micropelt.com/products/thermogenerator.php

[27] Loreto Mateu and Francesc Moll "Review of Energy Harvesting Techniques and Applications for Micro Electronics" Proceedings of the SPIE Micro Technologies for the New Millennium, 2005

[28] S. Meninger, J. Mur-Miranda, R. Amirtharajah, A. P. Chandrasakan, and J. H. Lang, "Vibration to electric energy conversion," IEEE Trans. on VLSI 9, February 2001.

[29] http://en.wikipedia.org/wiki/Piezoelectricity

[30] Rajeevan Amirtharajah and Anantha P. Chandrakasan, "Self-Powered Signal Processing Using Vibration-Based Power Generation" IEEE Journal of Solid State, 1998

[31] V. Longo, N. Leick, F. Roozeboom and W. M. M. Kessels, "Plasma-Assisted Atomic Layer Deposition of $SrTiO_3$: Stoichiometry and Crystallinity Studied by Spectroscopic Ellipsometry" ECS J. Solid State Sci. Technology 2013, Volume 2, Issue 1.

[32] http://en.wikipedia.org/wiki/Plate_theory

[33] L. B. Freund, J. A. Floro, and E. Chason, "Extensions of the Stoney formula for substrate curvature to configurations with thin substrates or large deformations", Appl. Phys. Let. 74**,** 1987

[34] B, Tian, Y. Zhong, R. Li, "Analytic bending solutions of rectangular cantilever thin plates", Archives of Civil and Mechanical Engineering, Vol. XI, No. 4, 2011

[35] Timothy Eggborn, "Analytical Models to Predict Power Harvesting with Piezoelectric Materials", Virginia Polytechnic Institute and State University MSME Dissertation, 2003

[36] E. Reissner and M. Stein "Torsion and transverse bending of cantilever plates" Technical Note 2369, National Advisory Committee for Aeronautics, Washington, 1951.

[37] A. K. Gupta, A. Khanna, D. V. Gupta, Free vibration of clamped viscoelastic rectangular plate having bi-direction exponentially thickness variations " Journal of Theoretical and Applied Machine 2009

[38] Yin Zhang and Ya-pu Zhao, "Applicability range of Stoney's formula and modified formulas for a film/substrate bi-layer" Journal of the Applied Physics 2006

[39] A. Chandrakasan, W. J. Bowhill and F. Fox" Design of high- performance microprocessor circuits" IEEE Press 2001.

[40] http://batteryuniversity.com/learn/article/discharge_methods

[41] http://www.allelectronics.com/mas_assets//spec/LBAT-518.pdf

[42] J. B. Bates, N. J. Dudney, B. Neudecker, A. Ueda, and C. D. Evans "Thin-Film Lithium and Lithium-Ion Batteries" Solid State Division, Oak Ridge National Laboratory, Oak Ridge, Tennessee 37831-6030, 1999.

[43] Jie Song, Xi Yang, Shuang-Shuang Zeng, Min-Zhen Cai, Liang-Tang Zhang, Quan-Feng Dong, Ming-Sen Zheng, Sun-Tao Wu and Qi-Hui Wu "Solid-state micro-scale lithium batteries prepared with micro-fabrication processes" Journal of Micro Electronics and Micro Engineering, Volume 19, issue 4, 2009

[44] W. C. West, J. F. Whitacre, V. White, B. V. Ratnakumar;" Fabrication and Testing of All Solid-State Micro-Scale Lithium Batteries for Microspacecraft Applications" Journal of Micromechanics and Micro engineering, Vol. 12 No. 1, 2011.

[45] N. J. Dudney, B. J. Neudecker, and J. B. Bates; “Rechargeable Thin-Film Batteries with $LiMn_2O_4$ and $LiCoO_2$ Cathodes” ; Solid State Division, Oak Ridge National Laboratory, Oak Ridge, TN 37831.

[46] Erick O. Torres and Gabriel A. Rincón-Mora “Electrostatic Energy Harvester and Li-Ion Charger Circuit for Micro-Scale Applications”; 49th IEEE International Midwest Symposium on Circuits and Systems, 2006.

[47] IVY WEI QIN “Wire Bonding Tutorial” Solid State Technology, Volume 14 Issue 7, 2005

[48] Stats Chip Pac “Through silicon via” statschippac.com

[49] Quick-Pack “ Flip Chip Packaging and Advanced Assembly Services” http://www.icproto.com

[50] Nordic Semiconductor “Bluetooth low energy wireless technology backgrounder” Version 4: Updated 22 March 2011

[51] G. Centa, Motor “Vehicle Dynamics Modeling and Simulation” Singapore, World Scientific, 1997.

[52] Paul Enquist and Chris Sanders;” 3D IC Technology: Interconnect for the 21 Century” Ziptronix, Inc. 2010

[53] Xuejue Huang, Yu Cao; “3D-Solenoid MEMS RF Inductor Design in Standard CMOS Technology” Department of EECS, University of California, Berkeley

[54] Margery Conner ;” Advances in Energy Storage Technology for Power Wireless Devices” EDN 2011

[55] Erick O. Torres, Lucas A. Milner, and Gabriel A. Rincón-Mora;” Hybrid Supplies for Wireless Micro-Systems” The Electrochemical Society Interface 2008

[56] Jason Tollefson; “Why NanoAmps Matter in Low-Power Design” Microchip Technology Inc. 2010

[57] Ali Eftekhari; “Fabrication of 5 V lithium rechargeable micro-battery” Journal of Power Sources 2004.

[58] S. V. Ogrimov;” Generalized Theory of Multi Layers Plates” International Journal of Solid and Structure, 2001

[59] Đorđe Vuksanović, Marina Ćetković; “ANALYTICAL SOLUTION FOR MULTILAYER PLATES USING GENERAL LAYERWISE PLATE THEORY” FACTA UNIVERSITATIS Series: Architecture and Civil Engineering Vol. 3, No 2, 2005.

[60] Yin Zhang and Ya-pu Zhao; “Applicability range of Stoney’s formula and modified formulas for a film /substrate bilayer” JOURNAL OF APPLIED PHYSICS 2006.

[61] Seema Sharma, U. S. Gupta, Prag Singhal; “Vibration Analysis of Non-Homogeneous Orthotropic Rectangular Plates of Variable Thickness Resting on Winkler Foundation” Journal of Applied Science and Engineering 2012

[62] Thomas von Büren, Paul D. Mitcheson, Tim C. Green, Eric M. Yeatman, Andrew S. Holmes, and Gerhard Tröster; “Optimization of Inertial Micropower Generators for Human Walking Motion” IEEE SENSORS JOURNAL 2006.

[63] Joseph A. Paradiso, Thad Starner;” Energy Scavenging for Mobile and Wireless Electronics” IEEE PERVASIVE computing 2005.

[64] P. Glynne-Jones, M.J. Tudor, S.P. Beeby, N.M. White; “An electromagnetic, vibration-powered generator for intelligent sensor systems” Elsevier- Sensor and Actuator A 2003.

[65] S. P. Beeby et al, “DESIGN AND PERFORMANCE OF A MICROELECTROMAGNETIC VIBRATION-POWERED GENERATOR” Solid-State Sensors, Actuators and Microsystems, 2005.

[66] Jiabin Wang et al, “Design of a Miniature Permanent-Magnet Generator and Energy Storage System” IEEE TRANSACTIONS ON INDUSTRIAL ELECTRONICS 2005.

[67] Jiabin Wang, A Low-Power, Linear, Permanent-Magnet Generator/Energy Storage System” IEEE TRANSACTIONS ON INDUSTRIAL ELECTRONICS 2002

[68] S. P. Beeby, M. J. Tudor, E. Koukharenko, N. M. White, T. O’Donnell, C. Saha, S. Kulkarni*, S. Roy; “DESIGN, FABRICATION AND SIMULATIONS OF MICRO ELECTROMAGNETIC VIBRATION-POWERED GENERATOR FOR LOW POWER MEMS” Montreux, Switzerland, 01-03 June 2005.

[69] Paul D. Mitcheson, et al; “Architectures for Vibration-Driven Micropower Generators” JOURNAL OF MICROELECTROMECHANICAL SYSTEMS 2004.

[70] Scott Meninger, Jose Oscar Mur-Miranda, Rajeevan Amirtharajah, Anantha P. Chandrakasan, and Jeffrey H. Lang, “Vibration-to-Electric Energy Conversion” IEEE TRANSACTIONS ON VERY LARGE SCALE INTEGRATION (VLSI) SYSTEMS 2001.

[71] E.P. James, M.J. Tudor, S.P. Beeby, N.R. Harris, P. Glynne-Jones, J.N. Ross, N.M. White; “An investigation of self-powered systems for condition monitoring applications” Elsevier- Sensor and Actuator A 2004.

[72] P.D. Mitcheson, P. Miao, B.H. Stark, E.M. Yeatman, A.S. Holmes, T.C. Green; “MEMS electrostatic micro power generator for low frequency operation” Elsevier- Sensor and Actuator A 2004.

[73] Bolduc, L. ; Brissette, Y. ; Beaudin, D. ; Page, D. ; Berube, A. ; Savard, P. “A NEW POWER MEMS COMPONENT WITH VARIABLE CAPACITANCE” IEEE Transaction on Power Delivery 2004

[74] Invited Paper; “Micro fabrication Techniques for Chemical/Biosensors” Proceedings of the IEEE 2003.

[75] Shadrach Joseph Roundy;” Energy Scavenging for Wireless Sensor Nodes with a Focus on Vibration to Electricity Conversion” Ph. D dissertation University of California Berkeley 2003.

[76] Shad Roundy, et al; “Power Sources for Wireless Sensor Networks” University of California Berkeley 2004

[77] Shad Roundy;” Improving Power Output for Vibration-Based Energy Scavengers” IEEE PERVASIVE computing 2005

[78] P D Mitcheson, T C Green, E M Yeatman and A S Holmes; “Analysis of Optimized Micro-Generator Architectures for Self-Powered Ubiquitous Computers” Journal of Microelectromechanical System 2004.

[79] V. Schaefer, L. Stevens, D. White, H. Ceylan;” Design Guide for Improved Quality of Roadway Sub-grades and Sub-bases” Iowa Highway Research Board (IHRB Project TR-525) 2008.

[80] Y. Richard Kim, B. Underwood, M. Sakhaei Far, N. Jackson, and J. Puccinelli;” LTPP Computed Parameter: Dynamic Modulus” FHWA-HRT-10-035, 2011

[81] Tom V. Mathew and K V Krishna Rao; “ Introduction to Transportation Engineering” NPTEL 2006.

[82] Youn su Jung, Dan G. Zollinger, Moon Won, and Andrew J. Wimsatt; "SUBBASE AND SUBGRADE PERFORMANCE INVESTIGATION
FOR CONCRETE PAVEMENT" FHWA/TX-09/0-6037-1 , 2009.

[83] Joshua P. Ayers, David W. Greve, Irving J. Oppenheim; " Energy Scavenging for Sensor Applications using Structural Strains" Smart Structures and Materials 2003: Smart Systems and Nondestructive Evaluation for Civil Infrastructures, Shih-Chi Liu, Editor, Proceedings of SPIE 2003.

[84] Elizabeth K. Reilly, Eric Carleton, and Paul K. Wright; "Thin Film Piezoelectric Energy Scavenging Systems for Long Term Medical Monitoring" International Workshop on Wearable and Implantable Body Sensor Networks, 2006. BSN 2006.

[85] Y.B. Jeon, R. Sood , J.-h. Jeong , S.-G. Kim l; "MEMS power generator with transverse mode thin film PZT" Elsevier Journal of Sensor and Actuator A, 2005.

[86] Chih-Tang Peng, Kuo-Ning Chiang; "Overview of Multilayered Thin Film Theories for MEMS and Electronic Packaging application" The Eighth Intersociety Conference on Thermal and Thermomechanical Phenomena in Electronic Systems, 2002

[87] Rafael Reif, Chuan Seng Tan, Andy Fan, Kuan-Neng Chen, Shamik Das, and Nisha Checka; "3-D Interconnects Using Cu Wafer Bonding : Technology and Applications", NSF/SRC for Environment Bening Semiconductor Manufacturing Annual Meeting 2004

[88] Brian W. LeFevre; " INTEGRATED MICROBATTERY CHARGER FOR AUTONOMOUS SYSTEMS" MS Dissertation Brigham Young University 2003.

[89] Silke Salewski, Erich Barke; "An Upper Bound for 3D Slicing Floor plans" Design Automation Conference 2002